Dissertation

on

AIRGLOW STUDIES IN LOW LATITUDES

Presented

by

VITHALA RAMACHANDRA RAO

for

the degree of

DOCTOR OF PHILOSOPHY

of

THE GUJARAT UNIVERSITY

April 1971

PHYSICAL RESEARCH LABORATORY
AHMEDABAD - 9
(INDIA)

PREFACE

Airglow radiations in the visible portion of the electromagnetic spectrum have been studied in many aspects at middle and high latitude stations from ground based observations and also by rockets. Until recently the behaviour of these emissions in low and equatorial latitudes has received little attention. The emissions in the infrared region of the spectrum are almost not studied in low latitudes except for a few attempts at some places.

The thesis incorporates the results and conclusions of the night airglow studies made during 1966-69 at the Atmospheric Optics Observatory, Hill View, Mt.Abu (24.6°N, 72.7°E geographic); (15.4°N, 144.2°E geomagnetic) India. Night airglow observations on two hydroxyl bands OH (7-2) and OH (8-3) were taken. The three emissions at 6300 A, 5893 A and 5577 A were also observed, using two fixed and one automatic all-sky scanning, photoelectric photometers. Two other photometers were constructed and used for measuring the atmospheric extinction coefficients at wavelengths 6080 A, 5750 A and 5360 A.

The author, working at Physical Research Laboratory, Ahmedabad, India, under the guidance of Prof. P.V. Kulkarni and Prof. K.R. Ramanathan, has designed and constructed the different photometers and all the necessary electronic circuits. From time to time different modifications were done to improve

the quality of observations. The author has maintained the various photometers at Mt. Abu and taken the night airglow observations during 1966-1969. Scaling and the reduction of airglow data into absolute units, taking proper care of regular calibration with radioactive sources and the analysis and interpretation of the various results are done by the author. The computations were carried out with the IBM 1620 computer facility at the Physical Research Laboratory.

The thesis contains seven chapters. Two chapters describe the methods that were used to account for the passage of the night airglow emissions through the lower atmosphere and the absolute calibration of photometers. In the rest of the chapters the results obtained with the different photometers are critically examined with a view to understand some of the physical processes in the upper atmosphere. In the last chapter the conclusions of all the above night airglow studies are summarised.

K R Ramanathan — P V Kulkarni — V. Ramachandra Rao

Prof.K.R.Ramanathan** Prof.P.V.Kulkarni** V.Ramachandra Rao**

(Professors in-charge) (Author)

ACKNOWLEDGEMENTS

The author is extremely happy to express his deep gratitude and indebtedness to his guides Prof.K.R.Ramanathan and Prof.P.V.Kulkarni, for guidance, keen interest and encouragement at all stages of the work, for providing all the necessary facilities, and for the critical examination of the manuscript and help in preparation of the thesis.

The author expresses his heartiest gratitude to Prof. P.R.Pisharoty for the constant encouragement and advice.

The author is also grateful to Prof. R.P. Kane and Prof. R. Raghava Rao for helpful suggestions and encouragement.

It is with great pleasure that the author acknowledges his heartiest thanks to Dr. S.R.Pal for the enthusiastic help in the initial stages and useful discussions and encouragement in the course of this work.

The author also expresses his heartiest thanks in acknowledging the assistance he has received of these individuals.

Dr. P.D.Angreji, Dr. J.N.Desai and Dr. C.R.Reddy for many helpful suggestions.

Prof. R.G.Rastogi and Dr.S.S.Degaonkar for providing all the necessary ionograms of Ahmedabad and advice.

Mr.M.S.Narayanan, Mr. R.P.Sharma, Dr.Harish Chandra, Mr.S.C.Chakravarty and Mr. M.R. Sivaraman for many useful discussions in the ionospheric physics.

Mr. Dhanjibhai Mistry and Mr. A.J.Shroff for the help in the construction of the photometers.

Mr. P.K.Kikani for his active assistance in the observations. Miss U.G. Modi and Miss P.M. Shah for the unstinting help in the computational work and assistance in scaling the ionograms and the laborious task of plotting the isophote maps of the airglow observations.

Mr. P.S. Shah for the help in the programming.

Mr. E.Narayanan and Mrs. C.Antony for the careful painstaking job of the excellent typing of the dissertation.

Thanks are also due to the following staff of the Physical Research Laboratory,

Airglow department for their cooperative assistance in scaling the scanning photometer data.

Computing centre for the help in punching the data and running the programs and their kind cooperation.

Drafting and Photography section for their cooperative help.

The author acknowledges his grateful thanks to the Ministry of Education and the Department of Atomic Energy of Government of India for the financial support.

The airglow work at Mt.Abu has been assisted by a generous grant (No.62-399) from the Air Force Cambridge Research Laboratory, U.S.A. to Professor K.R. Ramanathan which is gratefully acknowledged.

CONTENTS

CHAPTER I

BRIEF REVIEW OF NIGHT AIRGLOW WORK

EXPERIMENTAL SET-UP AT MT. ABU

1.1 Introduction:

The word 'airglow' was introduced by ELVEY (1950) following a suggestion of O.Struve to designate the optical emissions (other than the polar aurora) originating in the earth's upper atmosphere by some of its constituents such as atomic oxygen (O), atomic hydrogen (H), sodium (Na), molecular oxygen (O_2), hydroxyl molecule (OH), nitric oxide (NO) etc. Depending on the time of the day, it is further classified as "day airglow", "twilight airglow" and "night airglow". Here in this brief survey the 'twilight airglow' and the 'day airglow' are excluded each of which is distinguished from 'night airglow' by the fact that direct sunlight is also operative in the former two cases.

1.1.1 Distinction between aurora and night airglow:

McCORMAC (1967) describes aurora as part of the overall interaction of the solar wind with the earth's magnetosphere, and of airglow as that of solar radiations with the earth's atmosphere. Although it is very difficult

to distinguish between aurora and airglow from a simple definition like the above, they can be distinguished to some extent from the regions of their occurrence and by their spectra. The characteristic feature of the auroral spectrum is the presence of strong N_2^+ bands (excitation energy 19 ev). These are very weak in the night airglow. However, in the night airglow, strong hydroxyl bands (excitation energy 3.23 ev) are always present. BARBIER (1958) found that there was a high correlation between 5577 A (OI) and O_2 Herzberg bands in nonpolar airglow and a lack of correlation of these emissions in aurora. It is advantageous to study night airglow emission in low latitudes as the observations are less contaminated by emissions due to particle bombardment than those at higher latitudes.

1.1.2 Spectrum of the night airglow:

Excellent reviews on various aspects of night airglow have been made by a number of authors from time to time.(MITRA, 1952; MASSEY and BOYD, 1958; BATES, 1960; CHAMBERLAIN, 1961 a; BARBIER, 1963; ROACH, 1963a; 1964; SILVERMAN, et al., 1965; SILVERMAN, 1965; 1968; ROACH and SMITH, 1967; ROACH et al., 1969; KRASSOVSKY et al., 1962a; KRASSOVSKY and SHEFOV, 1965; WEILL, 1967; CHAPMAN, 1967 etc.).

In Table 1-I A the various night airglow emissions are given with their wavelengths and the transition energy states and the excitation potentials. In Table 1-I B their approximate average zenith intensities and their emission heights together with the main reactions which are presently supposed to give a major contribution to these emissions are given. The intensity unit is rayleigh which is defined as 4π times the surface brightness measured in 10^6 quanta cm^{-2} $sec^{-1}sterad^{-1}$. It is to be emphasised that the exact reactions and their relative contributions are still not fully understood for these emissions. There are uncertainties about the particle concentrations and the dynamical processes taking place at the emission heights.

Night airglow is studied by spectroscopic or photoelectric photometry methods. These two methods have complementary roles, the former for making exact determination of wavelengths and the latter for rapid intensity measurements and for survey of rapid intensity variations.

Much work has been done at different latitudes regarding the nocturnal variations of the different emissions in the visible region by photoelectric techniques using interference filters. Long term variations together with the solar-terrestrial relations associated with the airglow emissions and their excitation mechanisms are studied at different latitudes.

TABLE 1 - I.A

The wavelengths, the transitions and the excitation potentials of the Night airglow Emissions.

SOURCE	WAVELENGTHS	TRANSITION	EXCITATION POTENTIAL
OH	0.38 μ to 4.5 μ	$X^2\Pi - X^2\Pi$ $v' = 9$ to 1 $v'' = 8$ to 0	3.23 ev
$O_2(0, 1)$	8645 A	$b\ ^1\Sigma_g^+ - X\ ^3\Sigma_g^-$	1.8 ev
HI(Hα)	6563 A	$^2D - ^2P$	12.04 ev
(OI)	6300,6364 A	$^1D_2 - ^3P_{1,0}$	1.96 ev
Na I	5890-5896 A	$^2P_{3/2} - ^2S_{1/2}$ $^2P_{1/2} - ^2S_{1/2}$	2.1 ev
(OI)	5577 A	$^1S_o - ^1D_2$	4.17 ev
HI (Hβ)	4861 A	$^2D - ^2P$	12.69 ev
O_2(Herzberg bands)	3000-4000 A	$A\ ^3\Sigma_u^+ - X\ ^3\Sigma_g^-$	4.6 ev
N_2^+	3914 A	$B\ ^2\Sigma_u^+ - X\ ^2\Sigma_g^+$	19 ev

TABLE 1 - I B

The emission heights, the average intensities and the main reactions of the night airglow emissions.

Source	Wavelengths	Emission height	Average intensity rayleighs	Main reactions
OH	0.38μ to 4.5μ	80 km	5×10^6	$O_3 + H \rightarrow O_2 + OH^*$ $O_2^* + H \rightarrow O + OH^*$
$O_2(0, 1)$	8645 A	100 km	500	$O(^3P) + O(^3P) + X \rightarrow O_2^* + X$
(OI)	6300, 6364 A	F region	200	$O_2^+ + e \rightarrow O^* + O^*$ $NO^+ + e \rightarrow N + O^*$
Na I	5890-5896 A	85 km	30	$Na\ O + O \rightarrow Na^* + O_2$ $Na\ H + O \rightarrow Na^* + OH$ $Na\ H + H \rightarrow Na^* + H_2$
(OI)	5577 A	100 km + F region	250	$O + O + O \rightarrow O_2 + O^*$ $O_2^+ + e \rightarrow O + O^*$
O_2(Herzberg bands)	3000-4000 A	90-100 km	1500	$N + O_3 \rightarrow NO + O_2(A\ ^3\Sigma_u^+)$
Continuum (Nightglow)	4000-7000 A	60-80 km	1500 (0.5R/A)	$NO + O \rightarrow NO_2 + h\nu$ $O + O \rightarrow O_2 + h\nu$ $O^+ + e \rightarrow O^- + h\nu$ $O + e \rightarrow O^- + h\nu$ $O_2^+ + e \rightarrow O_2^- + h\nu$

In the following, the work done in low latitudes is very briefly reviewed. Later, the need for further work on the nightglow emissions is emphasised.

1.1.3 Earlier night airglow studies in low latitudes:

The first measurements in low latitude airglow were made by RAYLEIGH (1928) and his associates who carried out a world wide program of visual photometry of the green line λ 5577 Å between 1924 and 1933. This early work was recently compiled and reanalysed by HERNANDEZ and SILVERMAN (1964).

The first spectra of night airglow in low latitudes were obtained by RAMANATHAN (1932) at Poona (India). KARANDIKAR (1933) at Poona (India) determined the nocturnal variation of green line by photographic photometry. He recorded (1934) about 25 lines and bands in the spectrum of the night sky. Taking advantage of the black-out conditions in the second world war years GHOSH (1943) at Calcutta (India) maintained photographic record of the nightsky intensity variation. CHIPLONKAR (1950) at Poona found the inter-nocturnal variation of the oxygen green line using a visual photometer. In the year of maximum solar activity around 1947-48 BAPPU (1950) took night airglow spectra from Hyderabad, 17^{o}N (India). He has reported the relative intensities of

the principal airglow emissions. By comparing his results with BABCOCK'S (1939), Bappu has shown that his intensity values were higher for all the airglow radiations at that place.

Airglow studies with new techniques of photoelectric photometers with narrow band interference filters were taken up at Poona from 1954 (KULKARNI, 1958) and at Mt.Abu since 1956 (DANDEKAR, 1961). WEILL (1967) and later KULKARNI (1969) listed the airglow observing stations in low latitudes which number to about twenty todate.

The IGY program and later the IQSY program have yielded much more knowledge about the night airglow emissions and their nocturnal variations at different latitudes, interrelationships between different emissions, their exact heights of emission and the dynamical features in their nocturnal variations etc. The results of some of these studies are reviewed in later chapters.

1.1.4 Need for further study of night airglow emissions:

Although observations were available for many years in the visible region and the gross features of these emissions were known at different latitudes, the absolute intensity measurements with an accuracy of 5 to 10% is

very difficult. It is because of the difficulties involved in sorting out the airglow component of the emission line from the measured total light transmitted by interference filters (which consists of star-light, zodiacal light, and airglow continuum, besides airglow emission line intensity) and also due to the calibration of the measured intensities into absolute units. Accurate intensity measurements are very necessary in establishing the long term variations to understand the solar terrestrial relations, quantitative study of the various excitation reactions and their relative importances. The emissions in the infra-red (i.e. OH bands) and in the ultra-violet region of the spectrum are not sufficiently studied in low latitudes except for a few attempts at some places. Temperature determinations of the emission regions can be made from the intensity measurements of the rotational lines of these bands. There are no low latitude measurements of OH rotational temperatures.

The exact nature of airglow movements and their latitude dependence is not well known which may throw light on the dynamical behaviour of the upper atmosphere. The study of the dependence of airglow variations with change in magnetic activity and with latitude should prove interesting if more data are collected. Continuous monitoring of airglow intensities and of their intensity variations will throw light on some of the dynamical

processes taking place at the height of that emission. Simultaneous measurements of different emissions will give the interrelation of the atmosphere at different heights. There are very few studies in this direction.

With a view to study some of the above mentioned problems, and understand some of the atmospheric physical processes, airglow observations are taken up and continued at Mt. Abu (India) with improved techniques of recording such as narrow band interference filters, good photomultipliers and due attention to regular calibration with radioactive calibrating sources. The results of these investigations are described in the following chapters.

1.1.5 Atmospheric optics observatory at Mt. Abu:

The photometry of night airglow requires a location free from city lights, dust and aerosols. The Physical Research Laboratory, Ahmedabad,(India) has maintained an airglow and ozone station at Mt. Abu (India) (Geog.Lat. 24.6°N, long. 72.7°E) since 1952. The observatory is at an altitude of 1219 m. on the eastern outskirts of the hill-station Mt.Abu on the Aravallis. The photometers are placed on the roof of a building located on a small hillock. There are hills all around the observatory, but they are below 10° in altitude. This is a great convenience for operating an 'all-sky scanning photometer'. At Mt.Abu,

the nights remain generally clear between October and June. Observations have to be closed down for about two to three months from July to September owing to cloud and rain.

The station was maintained from 1956 to 1959 including the IGY period in which airglow emissions at 5577 A, 5893 A and 6300-64 A were regularly monitored and studied by DANDEKAR (1961). The observations were revived in November 1964 with improved equipment in the same spectral regions. The results of these observations during 1964-67 are discussed in detail by PAL (1968) in his doctoral thesis. The observations are continued with improvements from time to time since then. Observations of two OH bands OH (7-2) and OH (8-3) are added since October 1966.

1.2 Instrumental set-up at Mt. Abu

The photoelectric photometers utilised for the present study of night airglow include Pole photometer, Red photometer and scanning photometer which can be turned both in altitude and azimuth. In the following, a brief description of these photometers and the filters used, is given.

1.2.1 Pole photometer:

One of the photometers used for the study of the night airglow is continually directed towards the celestial pole so that the star field included in the angular aperture of the photometer remained the same. The angle of the photometer is 7.5^{o}. The photometer uses an EMI 6095 photomultiplier with a head-on cathode of S-10 response. The high voltage D.C. of 1600 volts (negative) applied to the photomultiplier is from a regulated d.c. power supply.

The prominent wavelength emissions in the night airglow spectrum at 5577 A, 5893 A and 6300 A are isolated by interference filters with their transmission peaks at these wavelengths and half transmission widths 80 A, 97 A, 135 A (see Figure 1.1).

A filter with maximum transmission at 5350 A and half-width 45 A is used for estimating the background intensity. The filters are symmetrically mounted on a circular disc which can be rotated with a synchronous motor. A geneva rotation is arranged so that each filter in turn stays for one minute against the cathode of the photomultiplier and its characteristic light intensity is recorded. The zero level when there is no light incident on the photomultiplier is also recorded for

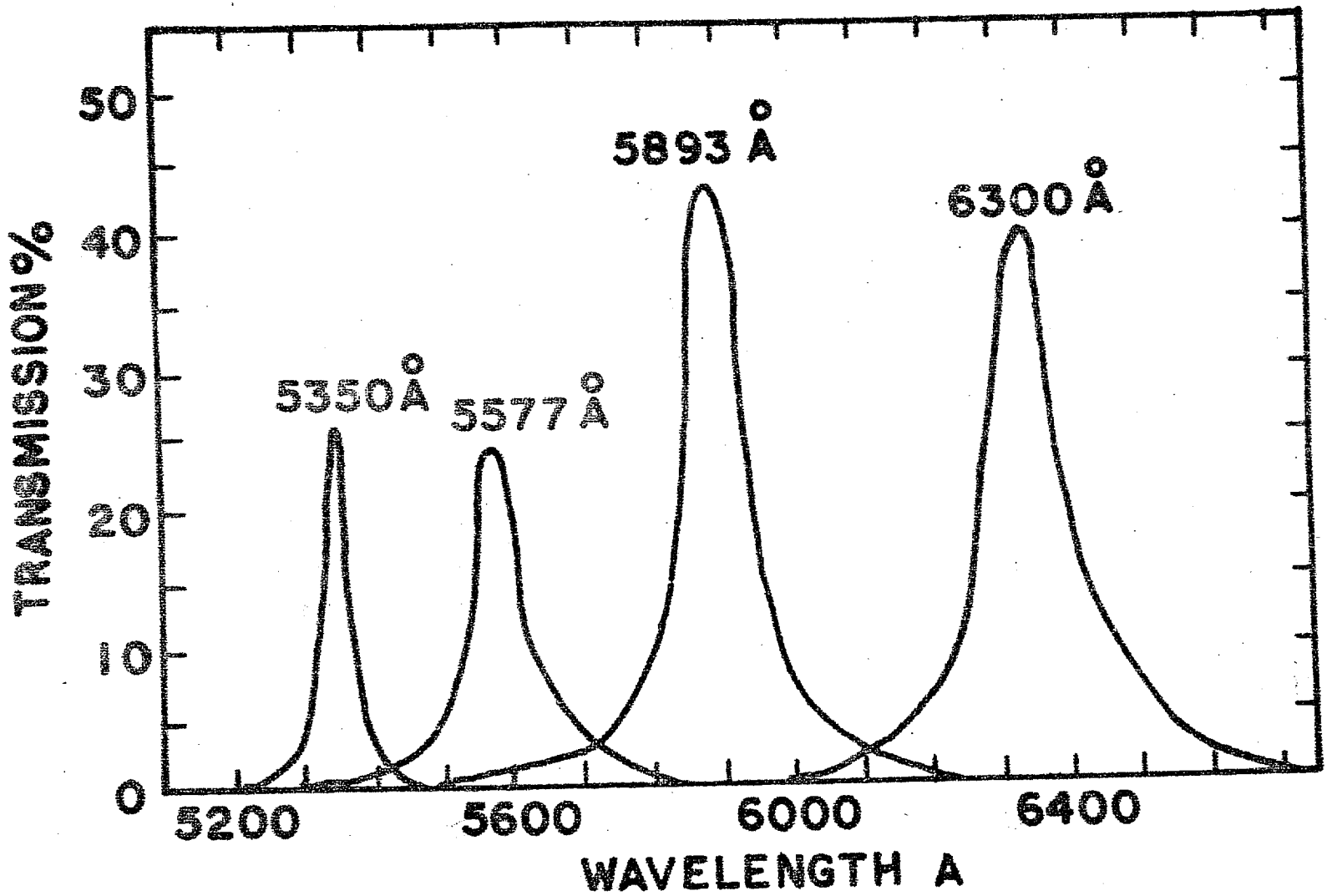

FIGURE 1.1 Transmission of the filters used on the Pole photometer.

one minute. Thus in five minutes, one complete set of intensities of all the transmitted wavelengths of the different filters is recorded. The photometer is provided with a shutter and is exposed to light only when the shutter is uncovered.

The output of the photomultiplier is fed to a Kipp and Zonen 'Micrograph' pen recorder. The recorder itself is of the balanced bridge type, with a transistorized low-drift d.c. amplifier. Its sensitivity is 10^{-9} amp/division. The chart is 21 cm wide and is linearly divided into 100 divisions. With the help of a single rotary switch, any of the six ranges from 0.1 μA to 5.0 μA can be utilised. The micrograph recorder has proved to be a very valuable asset for night airglow studies.

For Pole photometer, no inter-stage d.c.amplifier is needed, because the 1600 VDC applied to the tube is sufficient to record the nightglow signals on 0.1 μA and 0.25 μA ranges of the recorder, in all seasons of the year. The A.C. mains supply to all the units is regulated by a constant voltage transformer. Figure 1.2 shows a sample record obtained with this photometer.

1.2.2 Red photometer:

This photometer uses a high gain, S-20 response EMI 9558 B photomultiplier tube. Other constructional

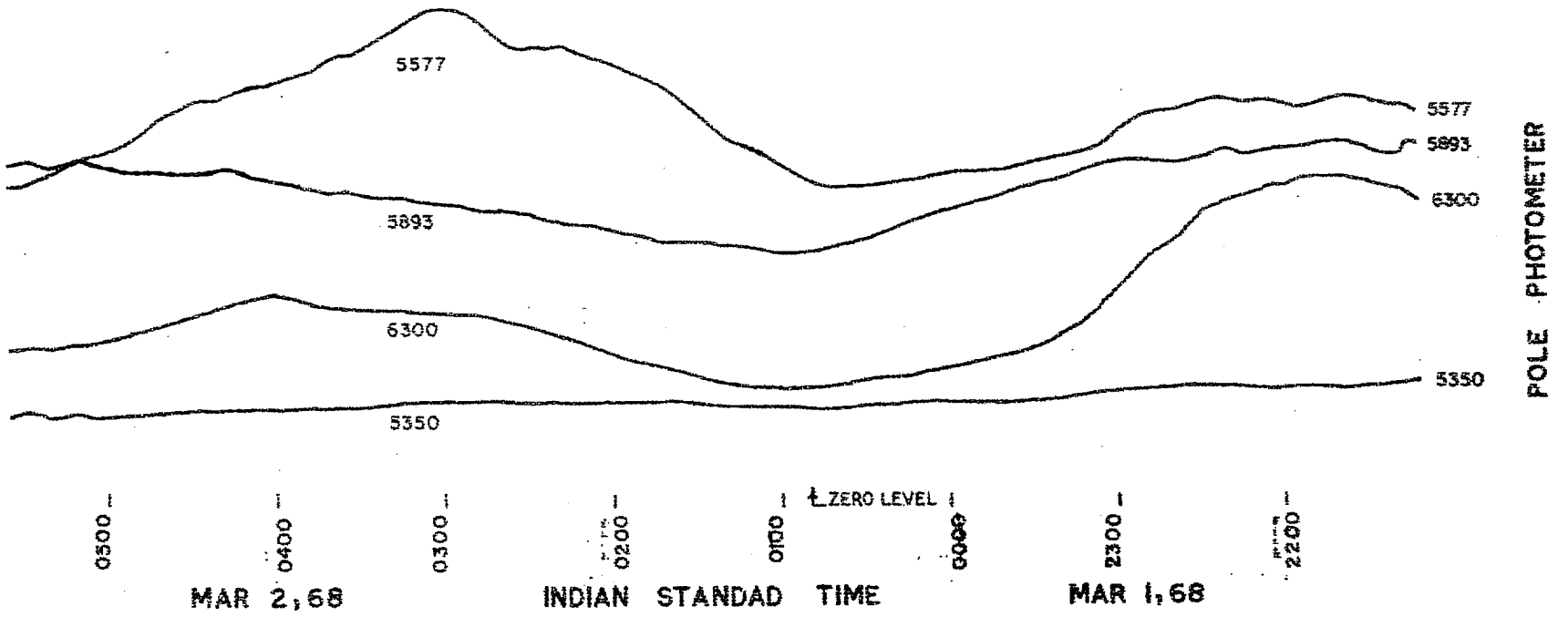

FIGURE 1.2 Sample record obtained with the Pole Photometer

details are the same as in the Pole photometer. The signal is recorded on an Evershed Vignoles milli-ammeter. As the output of the photomultiplier is insufficient to be recorded directly on the 0-1.0 mA range of the recorder, a d.c. amplifier is used to amplify the signals.

With the high sensitivity of the S-20 tube, it is possible to record OH (7-2) (band origin at 6862 A) and OH (8-3) (band origin at 7272 A) on this photometer. The rotational structure of these two bands are given in Figure 1.3. The relative total intensities of P branch ($\sum P$), Q branch ($\sum Q$) and R branch ($\sum R$) are given in the figure. The OH (7-2) and OH (8-3) filters have half transmission width 105 A and 90 A respectively. One of the other two filters transmits 6300 A and has a half transmission width 100 A. The other is a background filter centered around 6080 A with half transmission width 45 A. The angle of this photometer is about 4.5°. Figure 1.4 shows the transmission of the filters used on this photometer. Figure 1.5 shows the sample records obtained with this photometer.

1.2.3 All-sky scanning photometer

An RCA 7265, S-20 response photomultiplier is used in this photometer and interference filters

ROTATIONAL STRUCTURE OF OH (7-2) AND OH (8-3) BANDS.

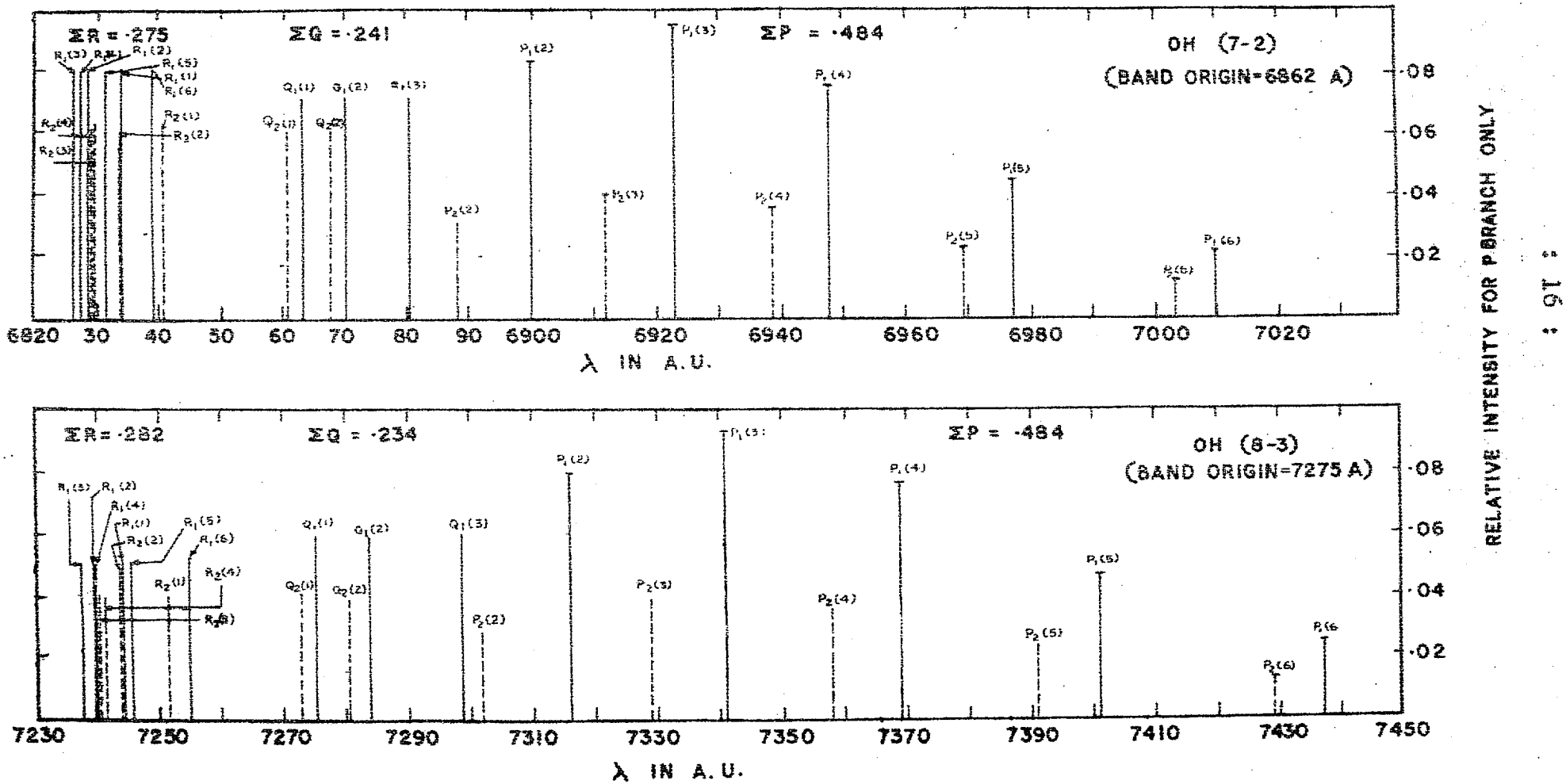

FIGURE 1.3 Rotational structure of OH (7-2) and OH (8-3) bands.

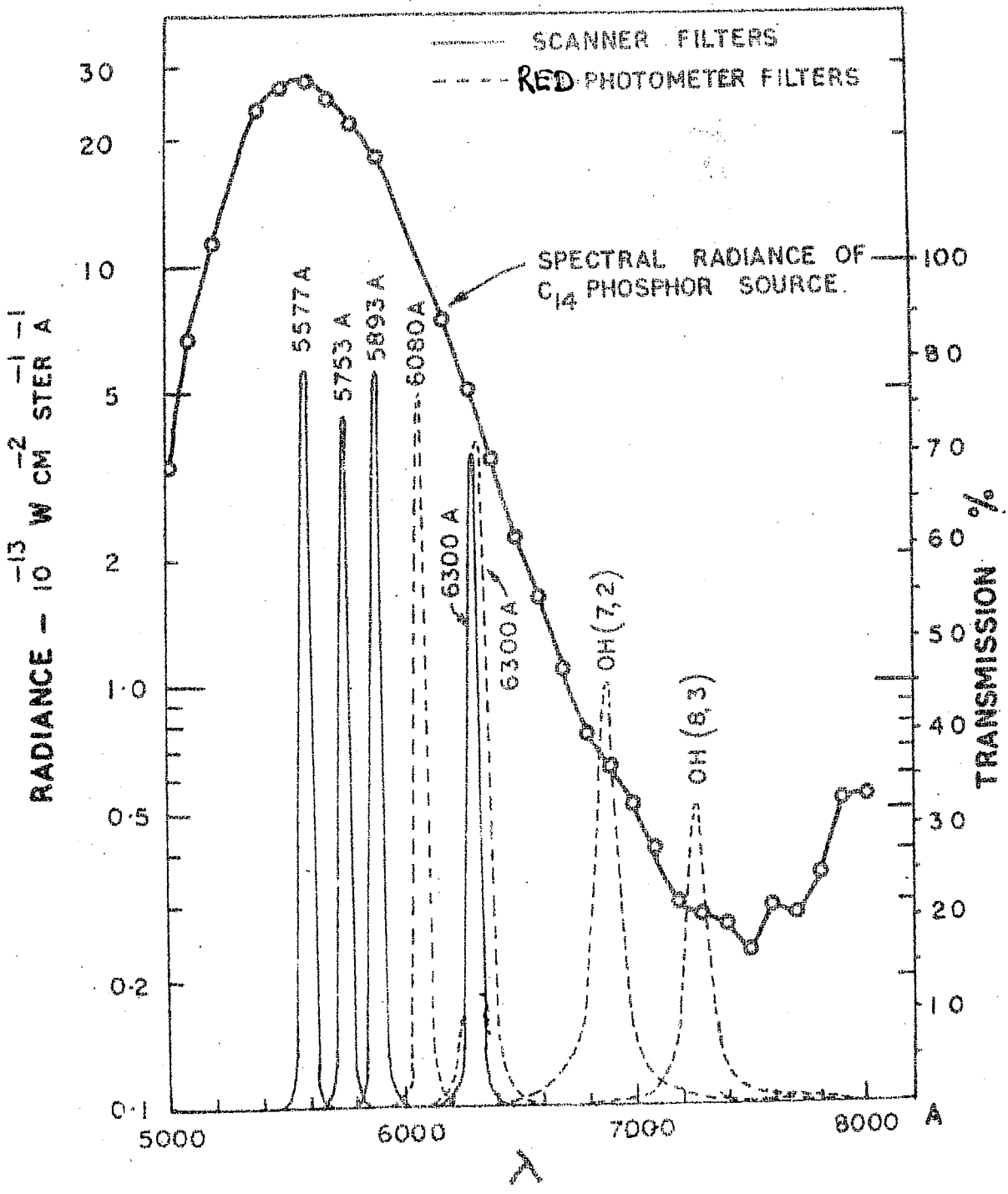

FIGURE 1.4 Transmission of filters used on the Red photometer and Scanning photometer.

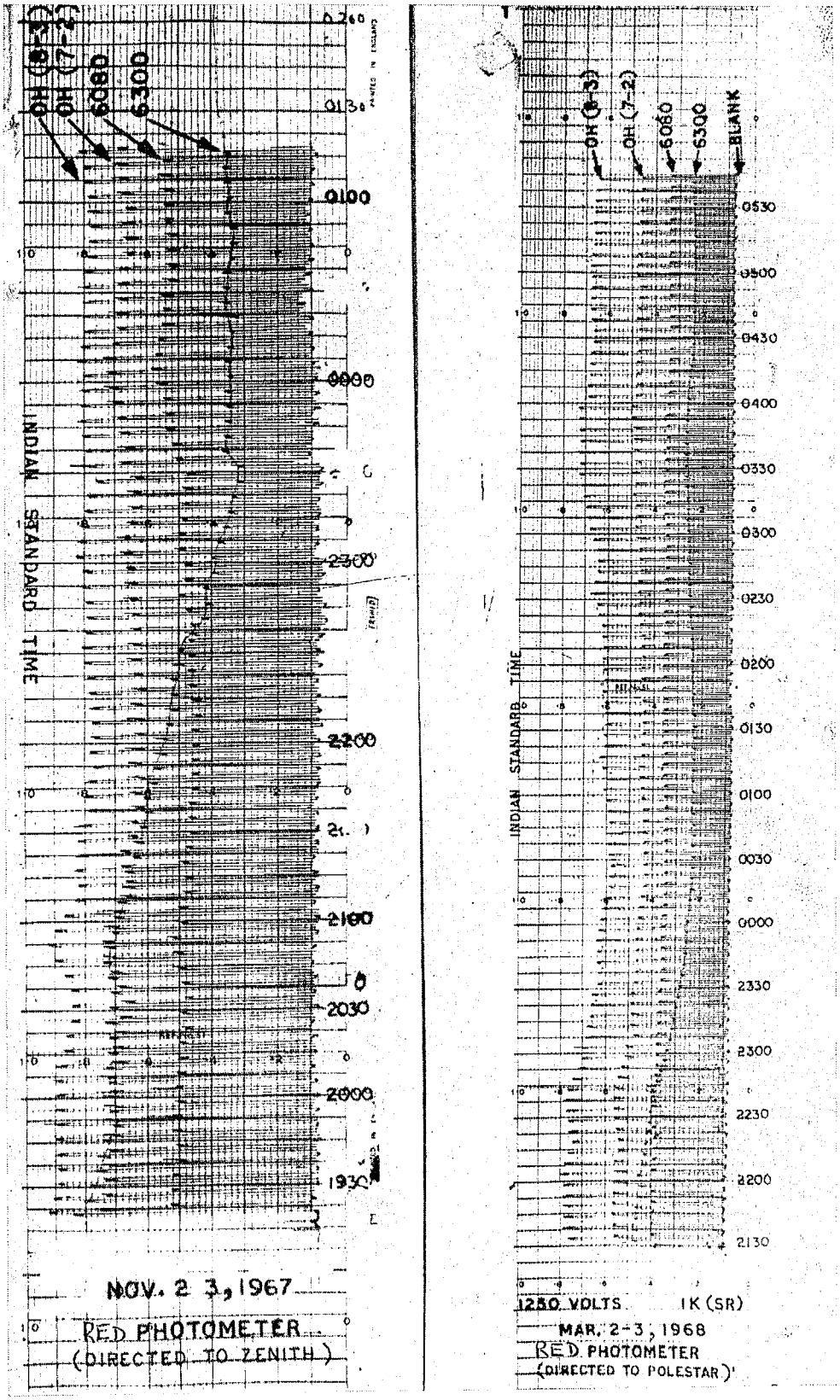

Figure 1.5 Sample records obtained with the Red Photometer

(type B10,Baird Atomic Inc.) centered at 6300 A, 5893 A, 5577 A, 5750 A/ 5300 A (background) having half widths of about 45 A are mounted on a circular disc, enclosed in a rectangular box.

Recording the intensities of light of the four wavelengths and of the zero-level takes 22.5 sec each filter staying on the photocathode for 4.5 sec. The angle of the photometer is about 5^{o}. The photomultiplier is given a negative D.C. voltage of 2500 volts from a regulated power supply. The output from the photometer is amplified with a drift free electrometer amplifier developed by SATYA PRAKASH and SUBBARAYA (1967), and is recorded on the chart of the micrograph recorder.

The photometer is mounted on an alta-azimuth frame (see Figure 1.6). The frame can be rotated round the vertical axis. The photometer looking in a defined altitude scans 360^{o} of azimuth in one rotation, taking 6 minutes. Using the four filters in succession, the photometer observes the sky at zenith angles of 75^{o}, 70^{o}, 60^{o}, 40^{o} and 0^{o}. The scanning of the whole sky at these five elevations and in all azimuths is completed in 30 minutes, taking six minutes for each zenith angle. These particular zenith angles were chosen to give roughly equal distances along the earth's surface. In Table 1-II the radii of the circles of observations with these zenith angles for the different emissions and the geographic latitudes covered are given.

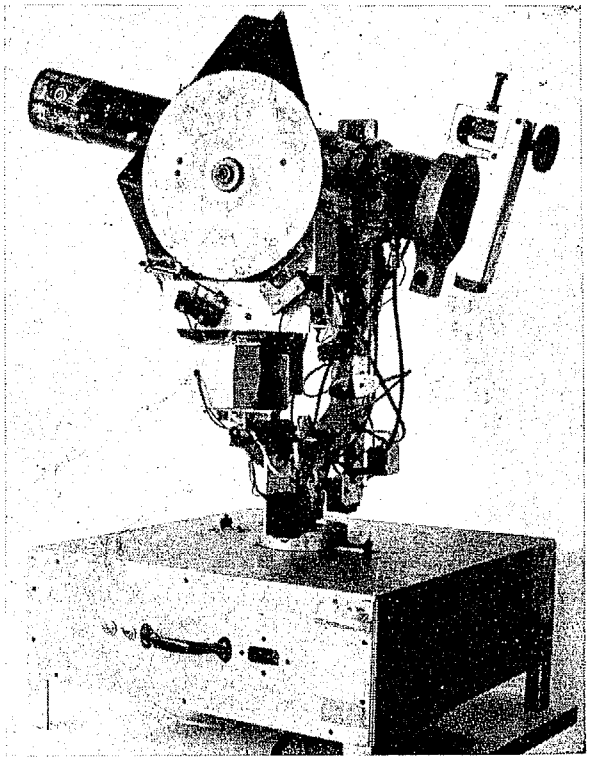

Fig. 1.6 Scanning Photometer

TABLE 1 - II

Distances covered along the earth's surface at different zenith angles by the scanning photometer.

Mt.Abu (24.6°N, 72.7°E)

Emission	6300 A		5577 A		Na and OH	
Assumed height of the layer	280 km		100 km		85 km	
Zenith angle (Z)	Distance covered in degrees of latitude	Kms.	Distance covered in degrees of latitude	Kms.	Distance covered in degrees of latitude	Kms.
0°	-	-	-	-	-	-
40°	2.0°	222	0.73°	81	0.7°	78
60°	4.0°	445	1.50°	167	1.4°	156
70°	5.8°	645	2.40°	267	2.2°	259
75°	7.4°	822	3.00°	333	2.9°	322

The transmission curves of the filters used on this photometer are given in Figure 1.4. (See page 17) The filters can be easily interchanged with other filters. On many nights the OH filters are used on this photometer and the sky is scanned. Sample records obtained with this photometer are given in Figures 1.7 and 1.8.

1.3 Observations schedule and data collection:

The Pole and Red photometers are operated on all clear moonless nights whenever more than 3 hours of observations could be taken. The scanning photometer is operated for six to eight nights around new moon and also on the nights of special interest. On Tables 1-III A and I-III B the data collected at Mt. Abu with the Pole photometer during 1964-1969 is given.

In Tables I-IV and 1-V the data collected with the Red photometer and the scanning photometer during 1966-69 is given. The results of all these observations are discussed in the following chapters.

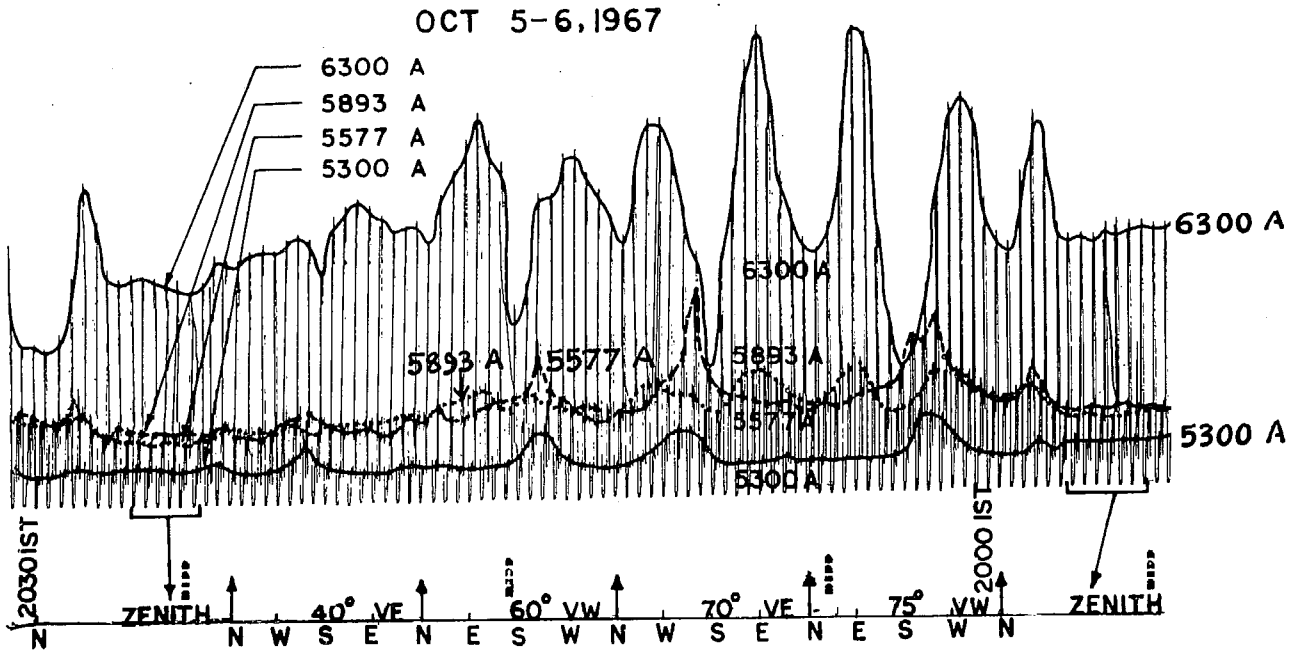

Fig. 1.7 A Sample record obtained with the Scanning Photometer with filters 6300 A, 5893 A, 5577 A and 5300 A

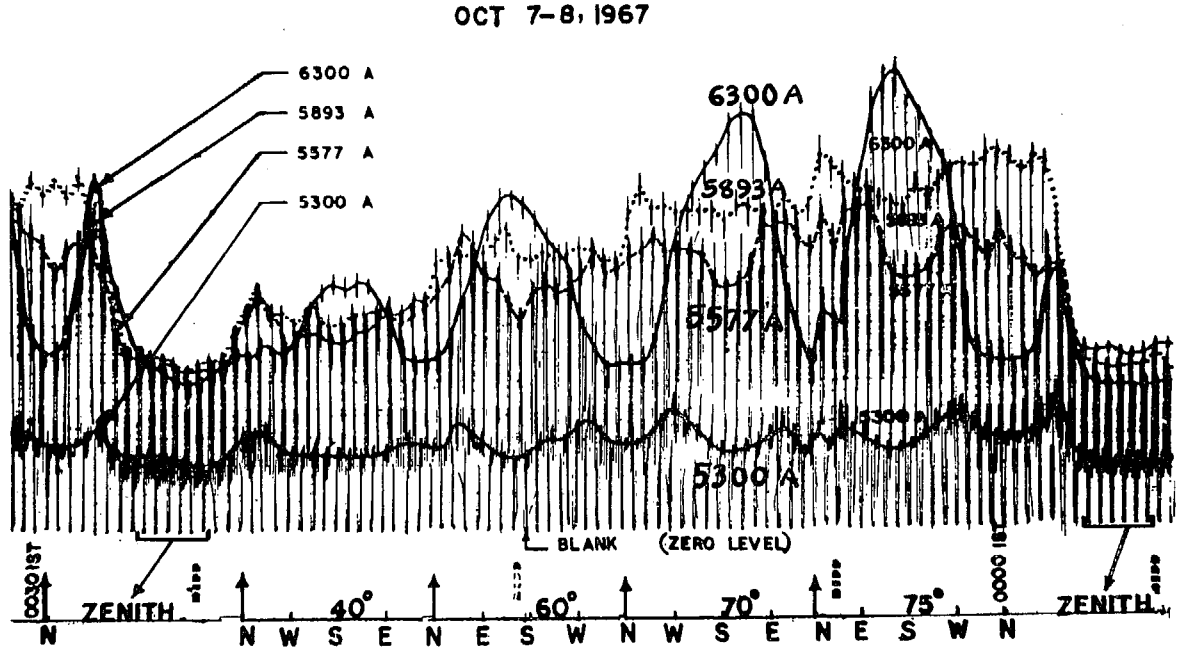

Fig. 1.7 B Sample record obtained with the Scanning Photometer with filters 6300 A, 5893 A, 5577 A and 5300 A

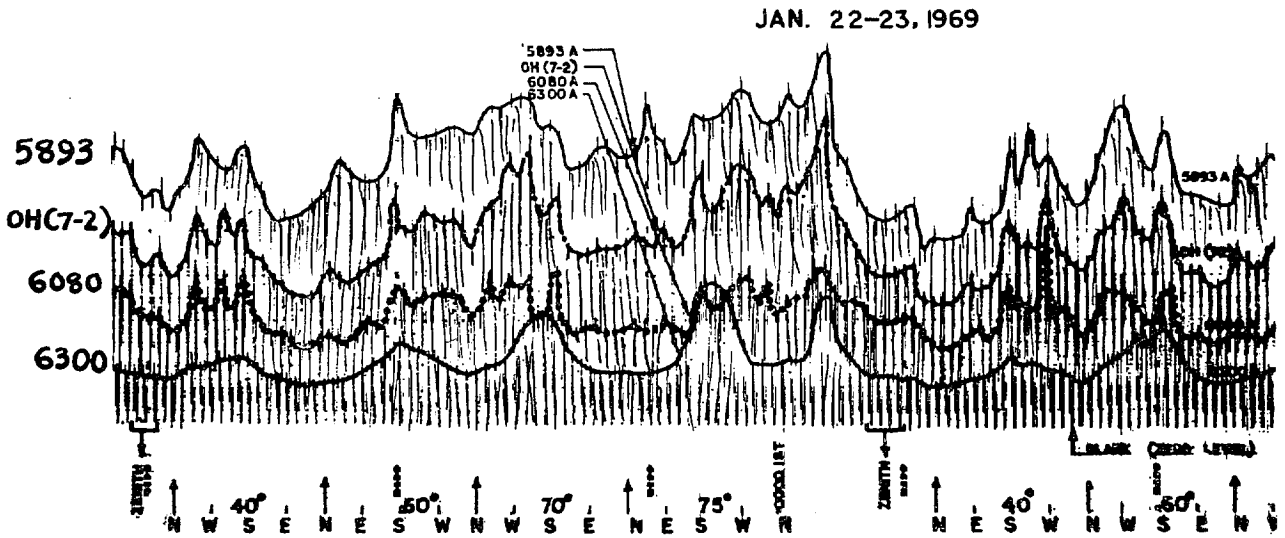

Fig. 1.8 Sample record obtained with the Scanning Photometer With filter OH (7–2), 6300 A, 6080 A and 5893 A

TABLE 1 - III A

Number of nights and number of hours of data collected at Mt. Abu with Pole photometer.

	1964-65			1965-66			1966-67		
	Lunation period	N.N.	N.H.	Lunation period	N.N.	N.H.	Lunation period	N.N.	N.H.
1	--	-	-	Sep 18 to Oct 7	17	96	-	-	-
2	--	-	-	Oct 17 to Nov 4	18	130	Oct 7 to Oct 26	19	126
3	Nov 24 to Dec 16	20	134	Nov 14 to Dec 5	21	123	Nov 4 to Nov 23	19	138
4	Dec 26 to Jan 13	16	102	Dec 15 to Jan 4	20	140	Dec 5 to Dec 23	18	139
5	Jan 24 to Feb 11	17	141	Jan 11 to Feb 1	22	132	Jan 2 to Jan 20	19	125
6	Feb 21 to Mar 10	17	101	Feb 10 to Mar 2	20	116	Feb 3 to Feb 20	18	79
7	Mar 24 to Apr 9	10	64	Mar 12 to Mar 31	19	120	Feb 28 to Mar 20	20	72
8	Apr 22 to May 9	12	61	Apr 9 to Apr 29	20	127	Apr 3 to Apr 17	13	82
9	May 27 to Jun 7	9	46	May 12 to May 28	15	95	Apr 30 to May 16	10	50
10	Jun 20 to Jun 29	8	28	Jun 8 to Jun 18	8	24	May 29 to Jun 12	4	19
		109	677		180	1103		140	830

N.N.: Number of nights on which data is collected.

N.H.: Number of hours of data collected.

TABLE 1 - III B

Number of nights and number of hours of data collected at Mt.Abu with Pole Photometer.

	1967 - 1968			1968 - 1969		
	Lunation period	N.N.	N.H.	Lunation period	N.N.	N.H.
1.	Oct 1 to Oct 15	8	40	Sep 17 to Oct 2	12	67
2.	Oct 23 to Nov 12	11	61	Oct 12 to Oct 31	18	116
3.	Nov.21 to Dec 12	14	80	Nov 10 to Nov 29	15	102
4.	Dec 21 to Jan 10	16	106	Dec 10 to Dec 29	18	127
5.	Jan 20 to Feb 9	9	77	Jan 9 to Jan 28	11	92
6.	Feb.18 to Mar 9	17	119	Feb 7 to Feb 18	10	68
7.	Mar 18 to Apr 7	15	105	Mar 7 to Mar 27	7	36
8.	Apr 17 to May 7	20	123	Apr 7 to Apr 25	12	61
9.	May 17 to Jun 5	17	83	May 5 to May 23	12	76
10.	Jun 14 to Jul 1	13	49	Jun 7 to Jun 15	9	41
		140	843		124	806

N.N: Number of nights on which data is collected
N.H: Number of hours of data collected.

TABLE 1 - IV

Number of nights and number of hours of data collected at Mt. Abu with Red Photometer.

1966 - 67				1967 - 68			1968 - 69		
	Lunation period	N.N.	N.H.	Lunation period	N.N.	N.H.	Lunation period	N.N.	N.H.
1.	...	-	-	Oct 1 to Oct 15	14	81	Sep 17 to Oct 2	14	78
2.	Oct 7 to Oct 26	19	126	Oct 25 to Nov.13	18	111	Oct 12 to Oct 31	18	112
3.	Nov 4 to Nov 23	19	138	Nov 21 to Dec 12	19	112	Nov 10 to Nov 29	17	98
4.	Dec 5 to Dec 23	18	139	Dec 22 to Jan 10	17	124	Dec 10 to Dec 29	18	120
5.	Jan 2 to Jan 19	17	130	Jan 20 to Feb 9	9	76	Jan 9 to Jan 28	13	108
6.	Feb 3 to Feb 20	18	122	Feb 18 to Mar 9	16	113	Feb 7 to Feb 28	17	84
7.	Feb 28 to Mar 29	20	111	Mar 20 to Apr 6	18	123	Mar 7 to Mar 27	18	110
8.	Apr 3 to Apr 17	14	101	Apr 17 to May 6	20	115	Apr 7 to Apr 26	12	61
9.	Apr 30 to May 16	15	100	May 17 to Jun 5	18	102	May 5 to May 23	12	66
10.	May 29 to Jun 12	14	46	Jun 14 to Jul 1	6	31	.....	-	-
		154	1013		155	988		139	837

N.N. Number of nights on which data is collected.

N.H. Number of hours of data collected.

TABLE 1 - V

Number of nights and number of hours of data collected with scanning photometer.

	1967-68				1968-69			
	Lunation period	N.N.	N.H.	N.S.	Lunation period	N.N.	N.H.	N.S.
1.	Oct 1 to Oct 15	8	44	88	-----	--	--	--
2.	Oct 25 to Nov 13	5	24	48	-----	--	--	--
3.	Nov 21 to Dec 12	10	66	132	Nov 10 to Nov 29	4	27	54
4.	Dec 21 to Jan 10	10	84	168	Dec 10 to Dec 29	6	58	115
5.	Jan 20 to Feb 9	8	56	112	Jan 9 to Jan 28	10	78	156
6.	Feb 18 to Mar 9	5	37	74	Feb 7 to Feb 28	6	45	90
7.	Mar 20 to Apr 6	5	30	60	Mar 7 to Mar 27	9	58	118
8.	Apr 17 to May 6	8	55	110	Apr 7 to Apr 26	12	78	156
9.	May 17 to Jun 5	5	27	54	May 5 to May 23	12	78	156
10.	----	--	--	--	Jun 9 to Jun 16	7	25	50

N.N. :- Number of nights the scanning photometer is operated in the lunation.

N.H. :- Number of hours of data collected.

N.S. :- Number of scanning sets of data (duration of each set is $\frac{1}{2}$ hour).

CHAPTER II

EXTINCTION COEFFICIENT (τ_λ) OF THE ATMOSPHERE

2.1 Introduction:

The airglow emissions from the upper atmosphere, the zodiacal light, and the light from stars are weakened by passing through the lower layers of the earth's atmosphere. The decrease in intensity is due partly to scattering and partly to absorption. The total attenuation is called 'EXTINCTION'.

The extinction has three components caused by

a) Rayleigh scattering by air molecules;

b) Scattering by aerosols (dust and haze - particles much larger than molecules);

c) Selective absorption by air molecules.

Component (a) follows λ^{-4} law. Variations due to seasonal changes in the total air mass and changes in the water vapour content are of small importance. Component (b) is subject to large variations in space and time. Component (c) includes absorption due to O_3, O_2, H_2O, CO_2 etc. In the visible region, the absorption due to the Chappuis bands of ozone is the most important.

In Table 2-I, the total atmospheric absorption coefficients are given for wavelengths in which we are immediately interested. These are the central wavelengths transmitted by the optical filters. The values of absorption were interpolated from ALLEN'S tables (1963a).

In airglow studies, since the airglow emitting layer is an extended source (the whole sphere radiates), the scattered light also contributes to the measured light even if the field of view of the instrument is small. Hence, for accurate determination of intensities, the observations must be corrected for the scattering of light into the field of view as well as for the attenuation due to the atmosphere between the observer and the emission layer. The method of correcting the observations is given in Chapter III. Here, the experimental determination of total extinction using point sources, is discussed.

The measurement of extinction coefficient is usually made with a point source and an optical instrument by which the intensity of the light of the point source can be measured. If the field of view of the instrument is small (say 3^{o}) the addition of scattered light to the transmitted light can be neglected.

TABLE 2-I

CONTINUOUS ATMOSPHERIC ABSORPTION
(Referred t sea-level)

λ in A →	5300	5350	5577	5750	5893	6080	6300	6860	7270
Molecular scattering (per atmosphere)	0.1120	0.1080	0.0910	0.0800	0.0720	0.0630	0.0540	0.0380	0.0310
Water vapour (per cm. precipitable water)	0.0023	0.0022	0.0020	0.0020	0.0020	0.0020	0.0020	0.0012	0.0010
Ozone (per 3 mm at S.T.P.)	0.0240	0.0260	0.0335	0.0385	0.0420	0.0430	0.0350	0.0105	0.0055
Dust condition (per atmosphere)	0.0685	0.0670	0.0640	0.0610	0.0595	0.0570	0.0550	0.0490	0.0450
TOTAL	0.207	0.203	0.191	0.182	0.176	0.165	0.146	0.099	0.083

For a point source of light, we have the well known formula

$$I' = I_o e^{-\tau M} \qquad (1)$$

where

I' is the intensity as observed from the earth's surface, I_o the intensity unaffected by extinction, that is, the intensity above the layers of the atmosphere which cause the extinction. τ is the optical depth (or) the extinction coefficient.

$e^{-\tau}$ is the coefficient of transmission and M is the number of airmasses traversed by the light with zenith airmass at sea-level as unit.

To a first approximation, M = Sec Z, Z being the zenith angle of observation. This is valid upto 70^o. When Z exceeds 70^o, due to the curvature of the earth, the actual oblique airmass is smaller than Sec Z. In Table 2-II the actual air-mass and Sec Z are tabulated for some zenith angles (ALLEN, 1963b). Also in the same table the effect of refraction on the true zenith distance and the observed zenith distance is tabulated. The effect of refraction is very small (about $\frac{1}{2}^o$ at 90^o zenith angle) and is unimportant in the present context.

TABLE 2 - II

Values obtained by M = Sec Z and Actual Airmass at various zenith angles.

Apparent zenith angle Z	True zenith angle	Sec Z	Air Mass
90°	90° 35'	∞	38.000
85°	85° 10'	11.470	10.400
80°	80° 5'	5.760	5.600
75°	75° 4'	3.860	3.820
70°	70° 3'	2.920	2.900
60°	60° 2'	2.000	1.995
50°	50° 1'	1.556	1.553
40°	40° 1'	1.305	1.304
30°	30° 1'	1.155	1.154
20°	20° 0'	1.064	1.064
10°	10° 0'	1.015	1.015
0°	0° 0'	1.000	1.000

Before describing the procedure for determining τ experimentally by using star brightness, the importance of determination of τ in the airglow measurements, is mentioned below.

As τ occurs in the exponent, its magnitude affects the intensities considerably. In reduction of all ground based observations of airglow, τ plays an important part. Its importance is particularly marked in the height determination of airglow layers, by Van Rhijn method. In this method, the heights of airglow emission layers are determined from the intensity at zenith, and at a high zenith angle. ROACH et al. (1958a) in one of their earlier papers have commented that if a constant extinction coefficient (0.164 at 5577 A) is used in the reduction of data of all the nights they analysed, the deduced heights varied from 51 km to 136 km, with 100 km as the mean value for 5577 A emission. They concluded that a more probable interpretation would be that the actual height was near 100 km and that the extinction coefficient varied from night to night (0.12 to 0.19 for 5577 A).

CHAMBERLAIN (1961b) comments that the Van Rhijn method is notorious for the wide variation in the calculated heights of emission. In Tables 2-III A, 2-III B, 2-III C, and 2-III D

TABLE 2 - III A

Height of night airglow 5577 A emission

From ground observations		By rockets	
Height kms.	Reference	Height kms.	Reference
260	Karimov (1947,1952)	92.5	Berg et al.(1956)
400-1000	Abadie et al.(1949)	96	Koomen et al.(1956)
110	Roach and Barbier(1950)	97	Heppner and Meredith (1958)
300	Davis (1951)	98	Tousey (1958)
215	Barbier et al.(1951,1954)	96	Cooper et al.(1960)
200	Roach and Pettit(1952)	98	Huruhata et al.(1962)
403	Huruhata (1953)	90	Tarasova (1963)
250	Dufay et al.(1953)	94.5	O'Brien et al.(1965)
180	Roach et al.(1953)	98	Huruhata et al.(1966)
100	Roach et al.(1954)	245	Gulledge et al.(1966)
62-104	Roach and Meinel (1955)	94.5	Greer and Best (1967)
80-100	St.Amand et al.(1955)		
195	Dufay and Tcheng (1955)		
270-300	Huruhata et al.(1955, 1956)		
90	Elsasser and Siedentopf (1956 a,b)		
100	Barbier and Glaume (1957)		
85	Manring and Pettit (1958 a,b)		
100	Roach et al.(1958 a,b)		
226	Chiplonkar and Kulkarni (1960)		
214	Chiplonkar et al.(1961)		
140	Dandekar (1961)		
145	Kulkarni (1965)		
152	Chiplonkar et al.(1966)		
170	Tillu (1966)		
170	Chiplonkar and Tillu (1970)		

TABLE 2 - III B

Height of night airglow 6300 A emission

From ground observations		By rockets	
Height kms.	Reference	Height kms.	Reference
400-100	Abadie et al.(1949)	>163	Heppner and Meredith (1958)
275	Roach and Pettit(1952)	>146	Tousey (1958)
260	Karimov (1952)	>130	Tarasova (1963)
170	Huruhata (1953)	270-280	Huruhata et al.(1966)
116-143	Roach and Meinel(1955)	245	Gulledge et al.(1966)
280	Dufay and Toheng(1955)	>205	Greer and Best (1967)

TABLE 2 - III C

Height of night airglow 5893 emission

From ground observations		By rockets	
Height kms.	Reference	Height kms.	Reference
150	Barbier (1944)	85	Koomen et al.(1957)
310	Roach and Barbier (1950)	95	Tousey (1958)
275	Roach and Pettit (1952)	89	Packer (1961)
125	Karimov (1952)	93.5	Huruhata et al.(1962)
356	Huruhata (1953)	82.5	Tarasova (1963)
108-129	Roach and Meinel (1955)	89	Greer and Best (1967)
200	Dufay and Tcheng (1955)		

TABLE 2 - III D

Height of night airglow OH emission

From ground observations		By rockets	
Height kms.	Reference	Height kms	Reference
70	Roach et al.(1950)	56-100	Heppner and Meredith (1958)
900	Pavlova et al.(1950)		
306-335	Huruhata (1953)	83	Packer (1961)
160-180	Berthier (1956)		

the heights determined by different observers for the different night airglow emissions are reproduced. From recent rocket experiments and from the theoretical knowledge of the relative importance of the various reactions giving these emissions, the heights of these emission layers are becoming clearer. Of all the uncertainties in the Van Rhijn method, the error due to using incorrect values of τ is perhaps one main reason for so much diversity in the heights determined from ground observations. Hence for precise determination of emission heights from ground based photometric observations, τ should be correctly determined. KULKARNI (1965) has determined the height of 5577 A emission using measured values of τ (WEINBERG, 1964) and the birefringent photometric observations of 5577 A.

As τ affects the individual observations, the pattern of the isophote lines is also dependent on the value of τ. To demonstrate the effect of τ on the isophote maps on the dome of the sky, with different assumed values of τ for 5300 A and 5577 A the isophotes are plotted in Figure 2.1 from the observations obtained from the scanning photometer at Mt. Abu on the night of Dec 3-4, 1967. In the case of 5577 A with low values of τ there is concentration of more intensity at the centre. With increasing τ the overall intensities increase; whereas the intensity

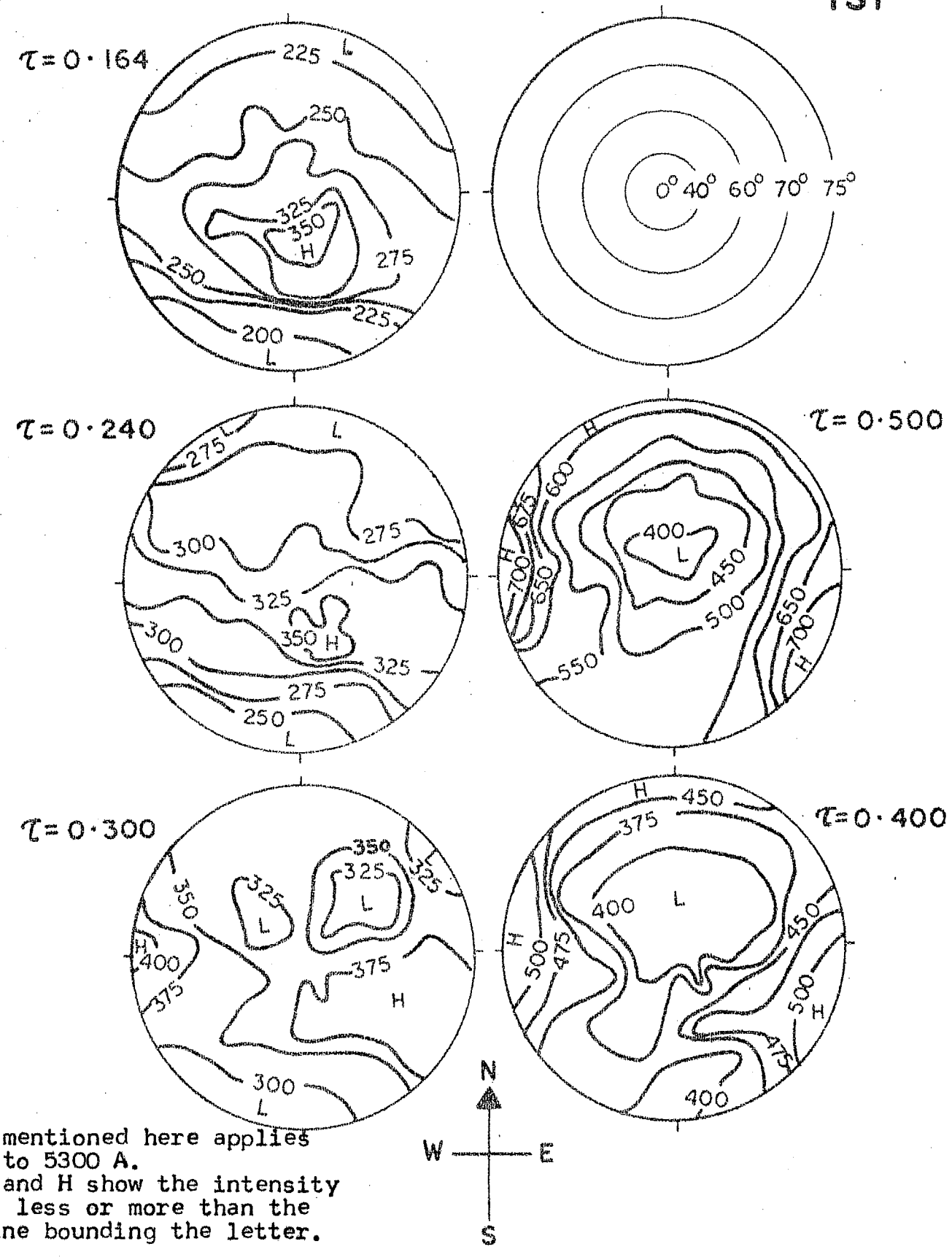

τ mentioned here applies to 5300 A.
L and H show the intensity is less or more than the line bounding the letter.

FIGURE 2.1 Isophote maps of λ 5577 A on December 3-4, 1967 with different values of τ .

in the centre is less and the periphery becomes more intense. Thus the nature of the isophote lines changes with the value of τ that is assumed.

Out of more than two dozen airglow observatories in the world, at very few places, τ is measured simultaneously with airglow observations and used for the reduction of airglow data. To the best of our knowledge only at three/four places, τ is measured and used in the reduction (ABADIE et al., 1945; ELSASSER and SIEDENTOPF, 1956a,b; HURUHATA et al., 1957; KULKARNI, 1965; BROWN, 1969). The extinction coefficients by broad band filters are determined at many places for Astronomical studies (JOHNSON and MORGAN, 1951; ARP, 1958; JOHNSON, 1963; DACHS et al., 1966; GUTTAMAN, 1968; IRVINE and PETERSON, 1970 etc.).

In general, the higher the altitude of the place the less will be the value of τ as the atmosphere will be free from the dust and haze to some extent. Also it may remain more or less constant in different seasons if contribution due to water vapour is very small. In general, for all stations and especially for observatories around 5000' altitude, including Mt. Abu, determination of τ on day to day basis is very important for airglow calculations.

Keeping this in view, and to have improved quality of reduced absolute intensity values, we started measuring the extinction coefficients daily since 1967. A photometer was constructed in September 1967 with one filter having peak transmission at 5360 A and half width 130 A. In 1968 September another photometer was constructed with provision for three filters having transmission peaks at λ 5360 A (half width = 55 A), λ 5750 A (half width = 34 A), λ 6080 A (half width = 48 A). The constructional details of both the photometers, are described below. Later the method of determining τ_λ from star brightness observations, is described and finally the observational results are given. These photometers are named as 'EXTINCTION PHOTOMETERS'.

2.2 Extinction Photometers - Description:

2.2.1 Extinction Photometer I:

This photometer was constructed in the month of September 1967 and used for observations from October 1967 to September 1968. Figure 2.2 gives the detector part of the photometer. A simple stand is made with iron plates and the photomultiplier assembly is fixed at the centre. It is possible to rotate the photometer in any desired direction manually. A shutter is used to shield the photometer and record the dark current.

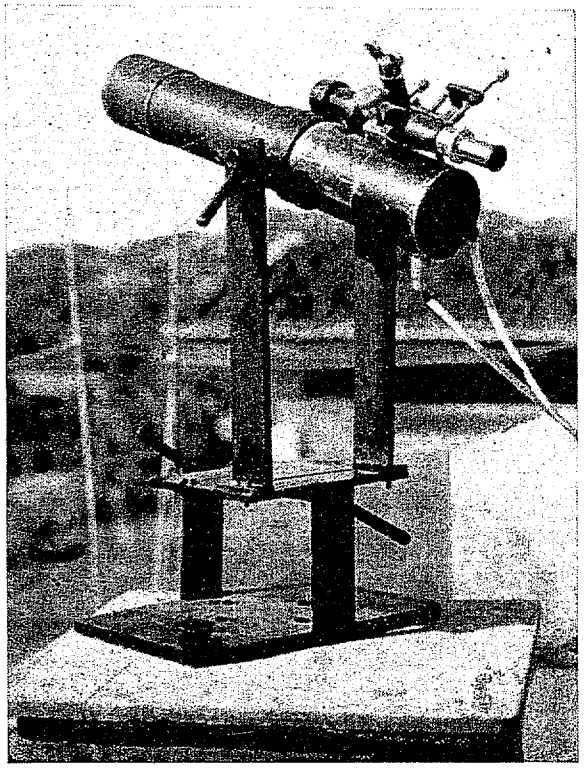

Fig. 2.2 Extinction Photometer I

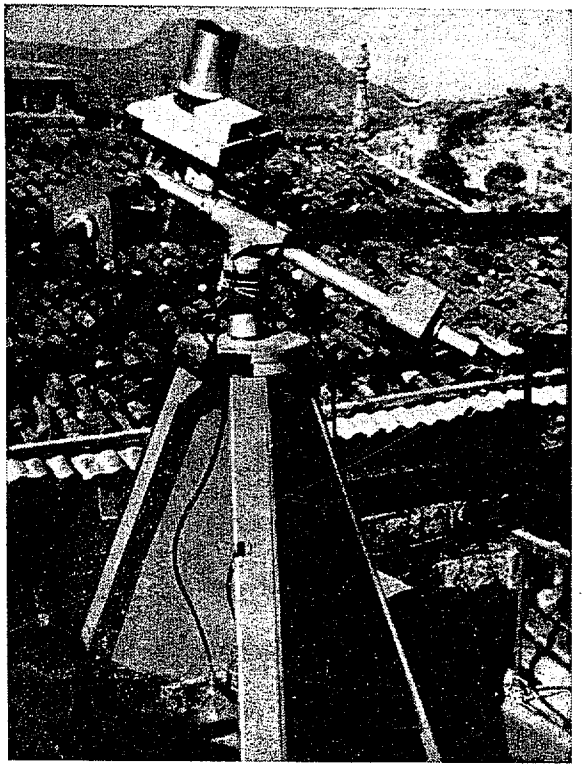

Fig. 2.5 Extinction Photometer II

Only one filter centered at 5360 A is used and is kept above the photomultiplier inside an aluminium tube which is coupled to the brass tube in which the photomultiplier is kept. The transmission curve of the filter is given in Figure 2.3 . An achromatic lens with diameter 6.5 cm and focal length 19.0 cm is fixed at the other end of the aluminium tube and its position is so adjusted that the photocathode of the photomultiplier is at near the focus of the lens. A circular aperture of 1 cm diameter is kept before the photomultiplier and this together with the focal length of the lens determine the angle of view of the photometer. The angle subtended by this photometer was $\sim 3^{o}$. An RCA 6217 (S-10 response) end-on photomultiplier is used.

A negative d.c. voltage of 1000 volts is applied to the photomultiplier from a well regulated power supply. The output of the photomultiplier is given to a tube d.c. amplifier the input resistance of which is $10^{9} \Omega$. The output of the amplifier is recorded on a 1 ma current meter of Evershed and Vignoles. The circuits of the power supply and the amplifier are given in Figure 2.6.

A 1" objective guiding telescope is fixed on the photometer to position a star on the photocathode of the multiplier. A sample record of the star deflections obtained with this photometer is given in Figure 2.7.

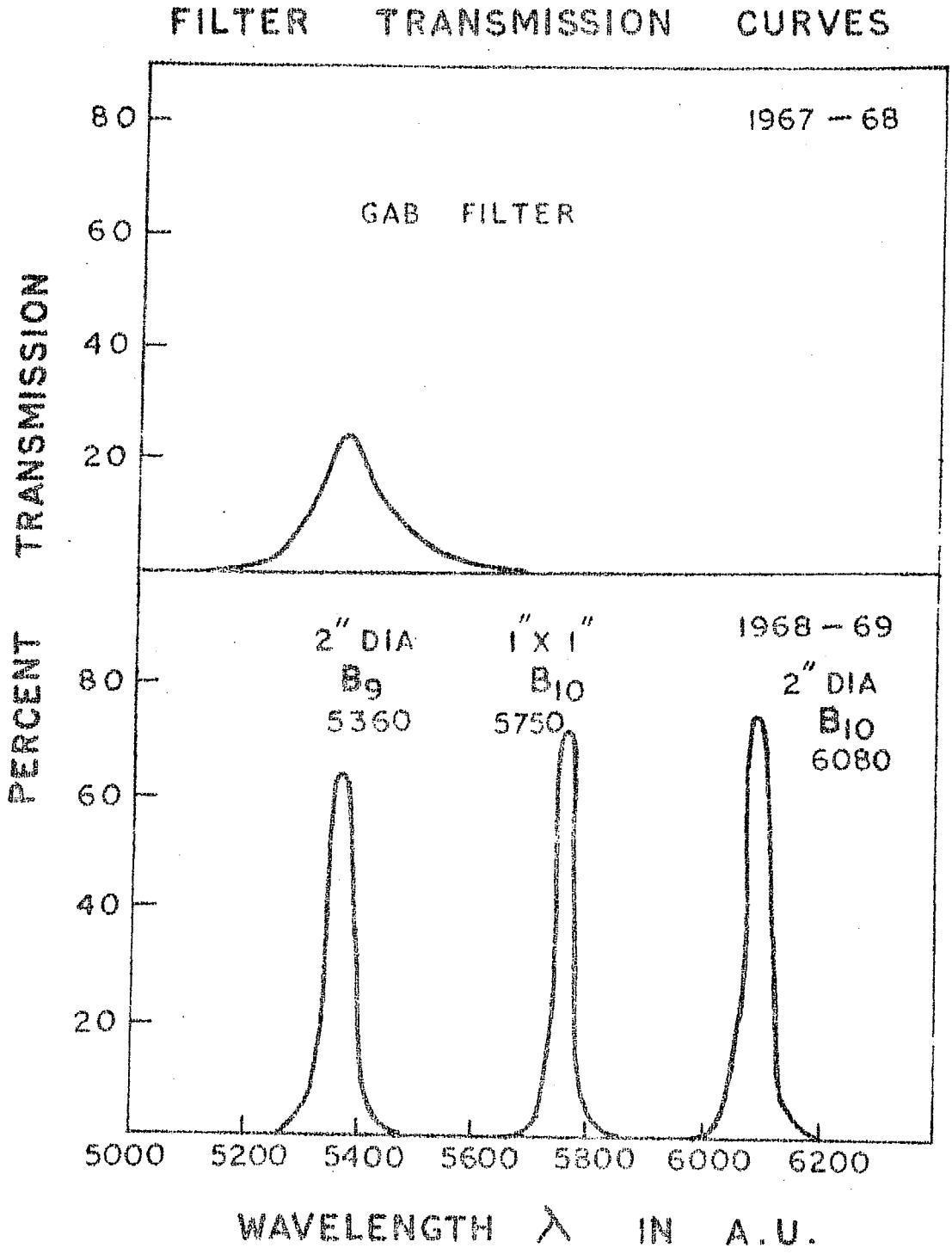

Fig. 2.3

Fig. 2.4

FIGURE 2.3 and 2.4 Transmission of the filters used in the Extinction Photometers.

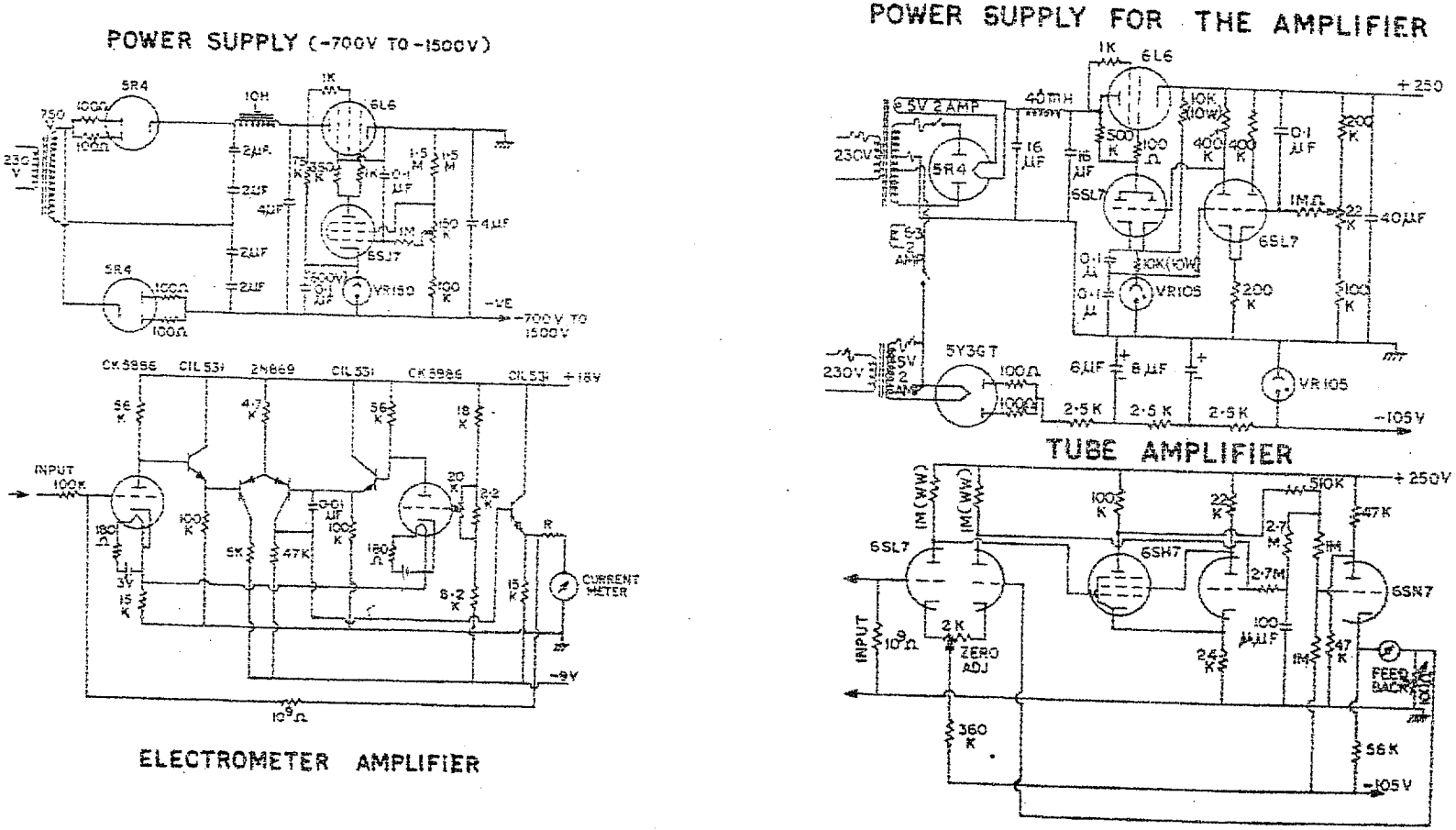

FIGURE 2.6 ELECTRONIC CIRCUITS OF THE POWER SUPPLIES AND THE AMPLIFIERS.

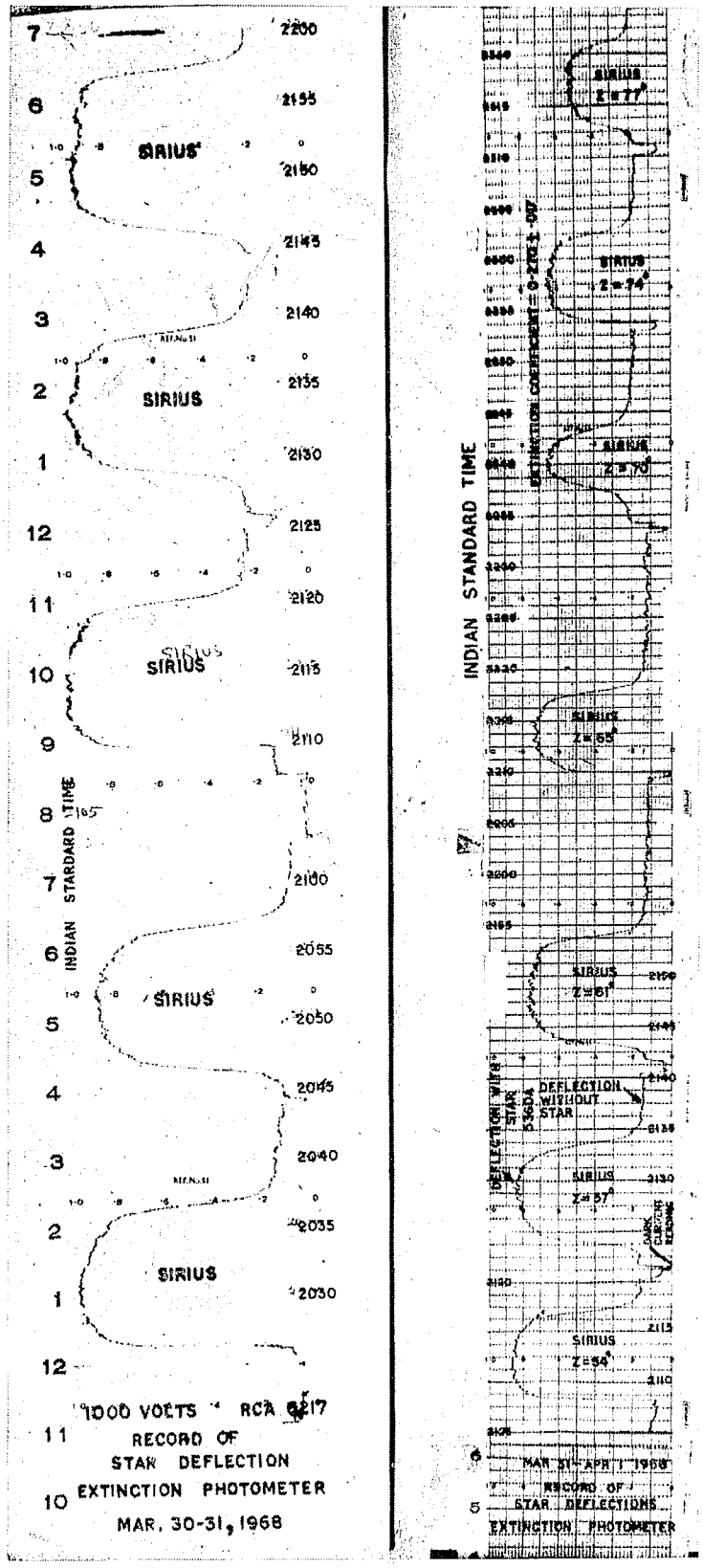

Fig. 2.7 Sample records obtained with the Extinction Photometer I

2.2.2 Extinction Photometer II:

This photometer was constructed in the month of September 1968 and used for observations from October 1968 to May 1969. Figure 2.5 gives a view of the complete photometer (See page 42)A polar mounting stand is made and the photometer is fixed on the stand. The advantage with this set-up is that it is easy to adjust for any star, and once a particular star is in the field of view it is easy to follow the star with the adjusting screws till the star sets.

A turret is made where the filters are mounted symmetrically and an opaque shutter is provided for recording the dark current of the photomultiplier. The turret box contains a geneva gear assembly which positions the filters on the photomultiplier. The turret is driven by a four sector geneva in such a way that each filter stays for 30 seconds on the photocathode so that one rotation of the turret is completed in 2 minutes. The turret is driven through gears by a Hurst motor (110 volts AC, 120 ounces torque, 60 CPS,, 1 RPM) mounted directly under the filter box.

Three Baird Atomic Inc. filters having peak wavelengths at 5360 A, 5750 A, 6080 A are used. The transmission curves of these filters are given in Figure 2.4(see page 44).

The optics and the sighting telescope are similar to the ones used as in Extinction Photometer I. The angle subtended by this photometer is also $\sim 3^{o}$.

An EMI 9592 B (S-10 response) photomultiplier is used. This photomultiplier has less dark current than RCA 6217 used in Extinction Photometer I. The output signal from the photomultiplier is given to an electrometer amplifier which is very stable and has very small or no drift. The input resistance of this amplifier is $10^{8}\ \Omega$. The circuit diagram of this amplifier is given in Figure 2.6. (see page 45).

A Kipp and Zonen micrograph recorder which can record currents from 0.1 μa to 5.0 μa full scale in various ranges on a scale of 100 divisions of chart breadth 21 cm is used. A sample record obtained with this photometer is given in Figure 2.8.

2.3 Method of observation and procedure of determining τ :

The procedure to be described applies to both the photometers. Each time the photometer is pointed to a star (non-variable type) and the deflection on the current meter is observed. After the star trails away from the photocathode of the photomultiplier the deflection without the star

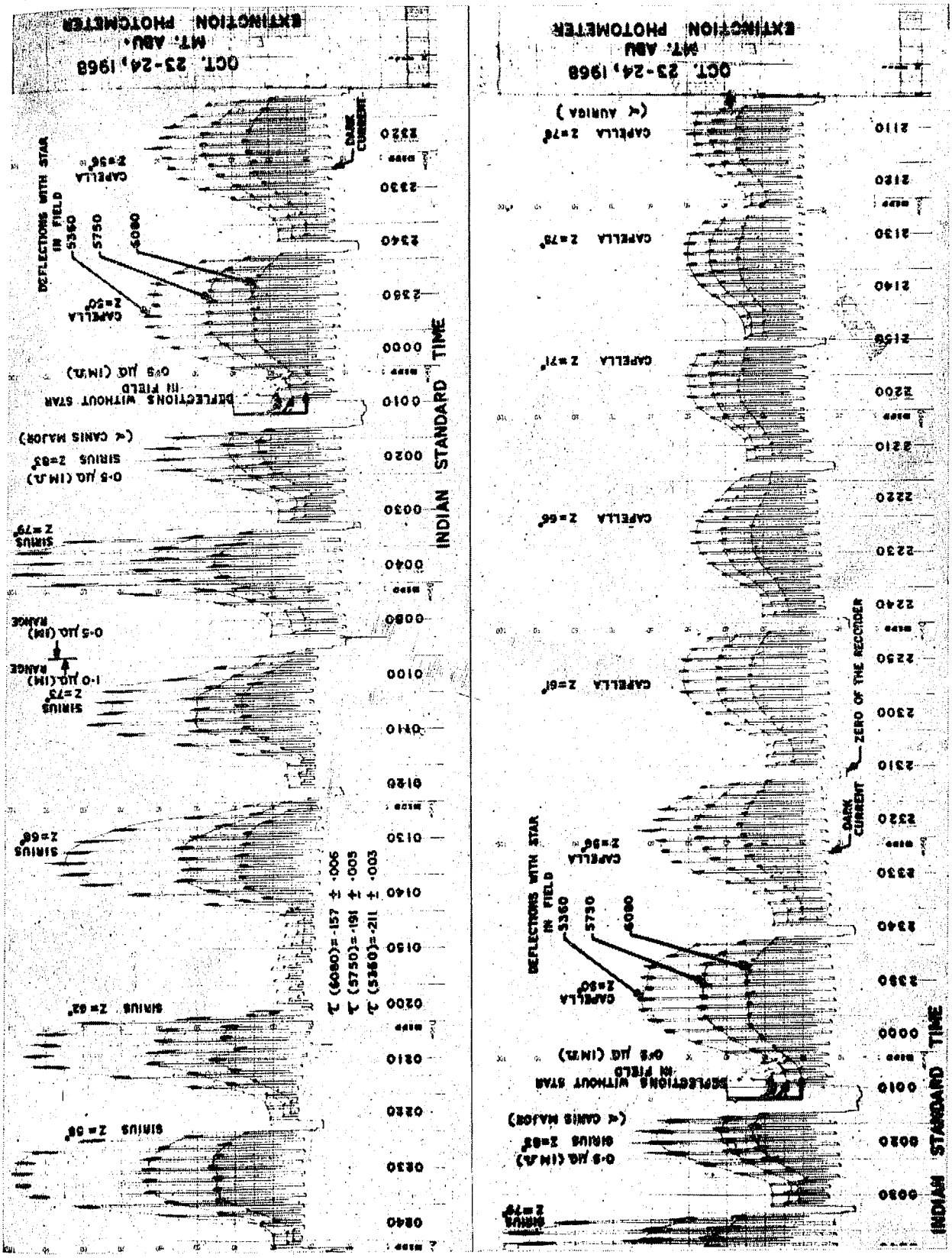

Fig. 2.8 Sample records obtained with the Extinction Photometer II

in the field is also observed. This is in general the airglow plus other continuum radiations in the field. The deflection without the star in the field is subtracted from that with the star which gives the deflection due to the star alone. This is a function of the star brightness and the position of the star in the sky. For each observation about 15 to 20 minutes are required to have the full trace of the star.

Three methods are feasible to determine the extinction coefficients.

1) If a good calibration source is available a single observation of any star can give the measurement of τ from relation (1) provided we know the absolute brightness of the star (I_o) and the zenith angle of observation. From the observed deflection, and the deflection with the calibration source we can determine observed brightness (I') at any time of observation. Then using relation (1) we can determine τ with a single observation. We have avoided this method purposely although we have calibrated radioactivated phosphorescent light sources, simply to avoid the errors in the absolute calibration.

2) If one bright star is observed at about 6 to 8 zenith angles say from 20° to 80°, so that we have its intensity measurements (I), the extinction coefficient τ can be determined by plotting a graph of $\log_{10} I$ vs. M the airmass traversed by the light ray. A straight

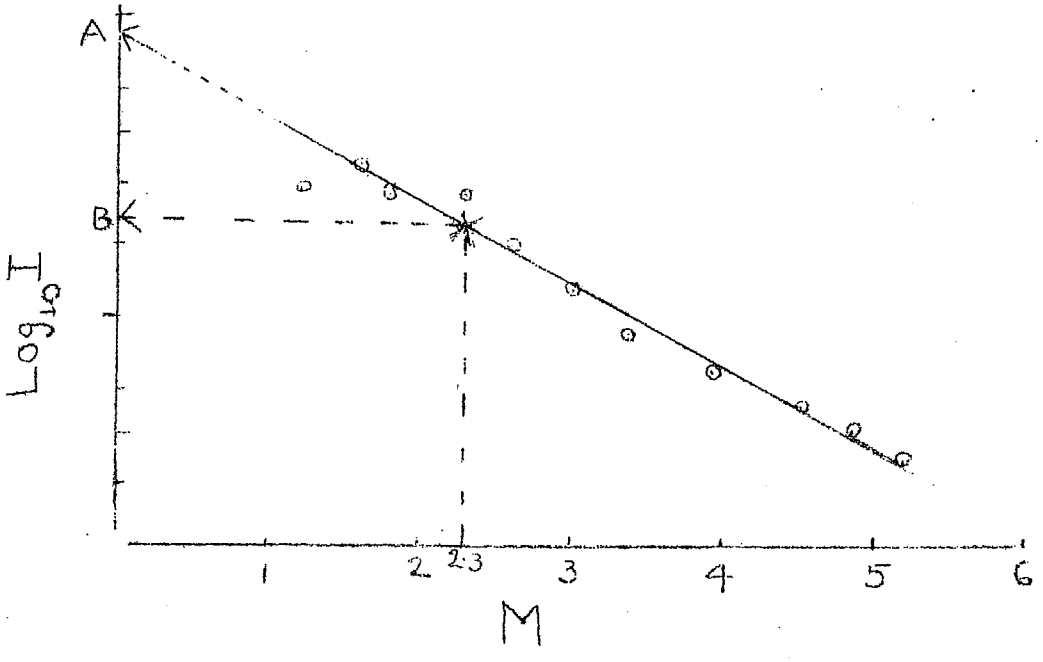

line should result. This line is extended to cut the ordinate at A. The ordinate value corresponding to M = 2.3 is read at point B. Then $(\log_{10} I_A - \log_{10} I_B)$ directly gives the extinction coefficient. Alternately if $\log_e I$ is plotted against M the value of the slope gives directly the extinction coefficient.

3) In a short interval of time, say half an hour or less, if six to eight different bright stars are observed (without complete trails) and their intensities are measured, a similar procedure described in the second method can be used for determining τ. But this method involves the normalisation of the intensities of the different stars to a single magnitude and single spectral type star. The necessary reduction factors to normalise different stars to a single magnitude and colour must be known.

2.4 Observations:

2.4.1 Procedure:

In the year 1967-68 both the second (one star tracking) and the third (observing many stars) methods for measurements at 5360 A were used. For reduction by the third method the normalisation factors at 5250 A kindly provided by Dr.HURUHATA of the Tokyo Astronomical Observatory, Japan were used. The normalisation factors for some of the bright stars are reproduced in Table 2-IV.

In the second method, since a single star is observed, normalisation is not needed. This is comparatively easy

TABLE 2 - IV

EXTINCTION STARS

Normalisation to 1st Magnitude G0 type 5250 A
(From Tokyo Astronomical Observatory)

Sr. No.	Name of the star	Spectrum type	Magnitude at 5250 A	Normalisation factor
1.	α Andromedae	B8p	2.04	2.61
2.	β Casiopeioe	F3	2.27	3.22
3.	α Persei	F5	1.80	2.09
4.	α Taurui	K5	0.90	0.912
5.	α Aurigae	G1	0.13	0.449
6.	β Orionis	B8	0.06	0.421
7.	γ Orionis	B2	1.61	1.75
8.	β Tauria	B8	1.61	1.75
9.	ε Orionis	B0	1.60	1.74
10.	κ Orionis	B0	2.00	2.51
11.	β Aurigae	A2	1.96	2.42
12.	β Canis Major	B8p	1.87	2.23
13.	γ Gemini	A1	1.90	2.29
14.	α Canis Major	A1	-1.50	0.100
15.	α Gemini	A1	1.40	1.45
16.	α Canis Minor	F5	0.33	0.540
17.	β Gemini	G9	1.15	1.15
18.	α Leonis	B8	1.23	1.24
19.	β Ursa Major	A1	2.30	3.31
20.	α Ursa Major	G7	1.86	2.26
21.	α Virgo	B1	0.94	0.946
22.	α Bootis	K0	0.06	0.421
23.	α Lyrae	A0	-0.02	0.391
24.	α Cygni	A2p	1.16	1.16
25.	α Piscis Austuni	A3	1.13	1.13
26.	α Pegasi	A0	2.45	3.80

and using this method mostly in the year 1968-69, the extinction coefficients at three wavelengths 5360 A, 5750 A and 6080 A are determined. It is necessary to have a number of observations from 80° to 40° zenith angle to have a best fit line. In about 4 to 5 hours, 8 to 10 observations at reasonably spaced zenith angles could be taken so that the Z spacing of the plotted points is uniform. However, there is disadvantage with this method that it gives an average extinction coefficient for the entire period of observations. This is a good compromise if the value of τ does not change during the period of observation.

The zenith angle of the star at any particular instant can be determined accurately from the time of observation, the star co-ordinates (right ascension and declination), the sidereal time of the day and the co-ordinates of the observing station.

The zenith angle of the star is determined from the relation

$$\text{Cos } Z = \text{Sin } \phi \text{ Sin } \Delta + \text{Cos } \phi \text{ Cos } \Delta \text{ Cos } H \qquad (2)$$

where

Z is the zenith angle of the star

H is hour angle of the star

Δ is the declination of the star

ϕ is the geographical latitude of the observing station

H = Sidereal time - right ascension

Airmass M is calculated from the Sec Z law if Z is less than 70°. For higher values of Z the airmass is taken from the interpolated values given in Table 2-II reproduced from ALLEN (1963b).

Instead of drawing a straight line manually between log I and M, a computer program was written which fits the line of regression and computes the value of τ together with probable error in it.

2.4.2 Observation schedule:

As the adjustment of the instrument to measure the star deflections is manual, the measurements are restricted to about 6 to 8 nights around new moon in each lunation and the extinction coefficients are determined. However, in summer months as the local atmospheric conditions change erratically on many more nights the extinction coefficients were determined. Table 2-V gives the number of nights on which τ was determined.

TABLE 2 - V

Number of nights on which τ_λ was experimentally determined.

1967-68 5360 A filter			1968-69 5360 A, 5750 A, 6080 A filters:		
Sr. No.	Lunation	No. of nights	Sr. No.	Lunation	No. of nights
1.	October 1967	3	1.	October 1968	11
2.	Dec 1967-Jan 1968	7	2.	November 1968	5
3.	Jan - Feb 1968	9	3.	December 1968	8
4.	Feb - Mar 1968	6	4.	January 1969	6
5.	Mar - Apr 1968	10	5.	March 1969	6
6.	Apr - May 1968	14	6.	April 1969	2
7.	May - Jun 1968	15	7.	May 1969	7
8.	September 1968	8			
	Total	72			45

2.5 Results and conclusions:

In Figure 2.9 the value of the extinction coefficients (τ) determined on all the nights are plotted date-wise. It shows that τ varies from night to night at Mt. Abu. There are some occasions when τ is abnormally high and some occasions when it is very low compared to the average values. Lower values of τ imply that dust and haze content is very small and the atmosphere is tending to "ideal" molecular atmosphere. The nights when τ is low can be sorted out for more reliable airglow calculations. In general the variation of τ from night to night is less in the months from October to January and is more and random in the near summer months. It is to be expected that due to dust storms in the nearby desert areas and other reasons, in summer at Mt. Abu, there is more aerosol content in the upper atmosphere than in the winter months. Also especially on clear nights following a few showers the values of τ are lower than the normal.

In Figure 2.10 the histograms of the τ values using 60 night's data in the year 1967-68 and 43 nights data in the year 1968-69 are plotted. In Figure 2.11 the 'percentage error histograms' showing the percentage errors in the determined extinction coefficients of the above nights are plotted. With the 5360 A filter the maximum number of

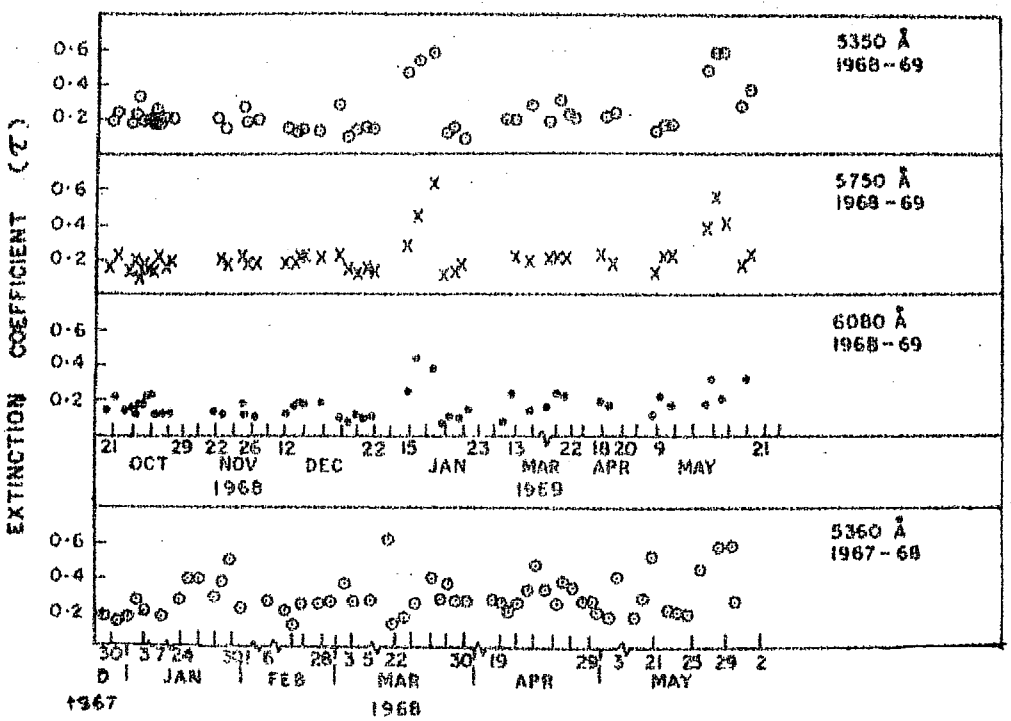

FIGURE 2.9 Variation of the extinction coefficients on different nights.

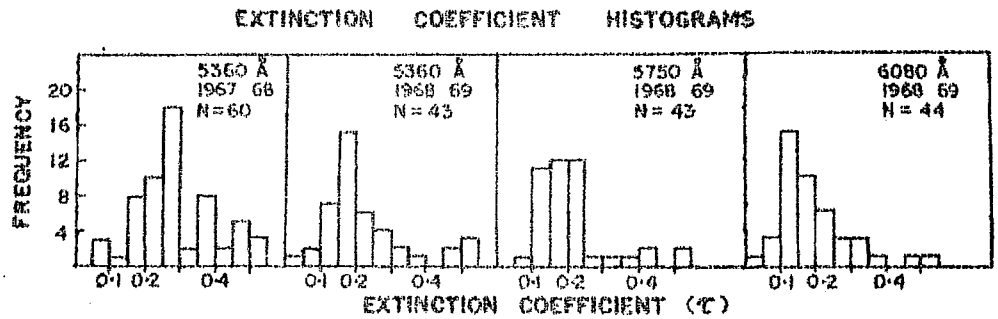

FIGURE 2.10 Histograms of the determined extinction coefficients.

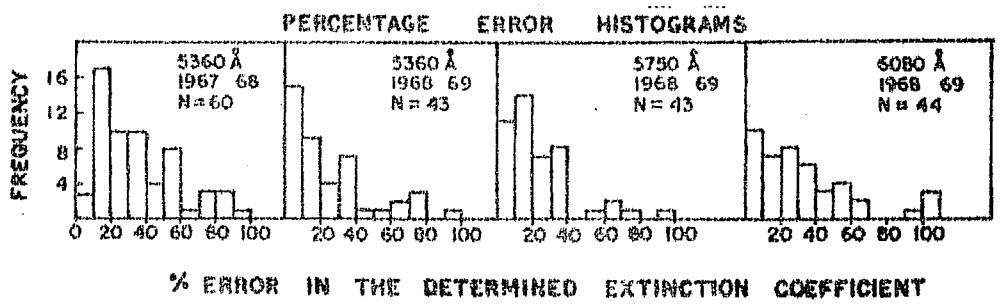

FIGURE 2.11 Histograms of the percentage errors in the determined extinction coefficients.

observations lie in the 10-20 % error region in 1967-68, while those in 1968-69 lie in 0-10 % error region. A major factor which might have contributed to less statistical errors in the determination of τ values in 1968-69 compared to 1967-68 could be attributed to the use of a better photomultiplier, and better filters and recording system. However, with the 5750 A and 6080 A filters the maximum number of observations are in the error ranges 10-20% and 20-30 % respectively. This is due to the fact that the deflections are small due to the smaller response of the photomultiplier at those wavelengths than that at 5360 A.

From the histograms of τ for the year 1967-68 the most frequent values of τ at 5360 A is 0.27 whereas in the year 1968-69 it is 0.18. This difference can be partly due to the fact that the filter used in 1967-68 was rather broad and with less peak transmission than that used in 1968-69. The most frequent value of τ at 5750 A is 0.17 whereas at 6080 A it is 0.15. In Figure 2.12 A the mean values of the extinction coefficients for the entire lunation are plotted lunation-wise. In Figure 2.12 B the average values of the entire data versus wavelength are plotted. It is seen that the extinction coefficient is less in Oct-Nov-Dec months and slowly and continuously increases in early summer months. But in Jan 1969 high extinction coefficients were observed because of other disturbed local conditions.

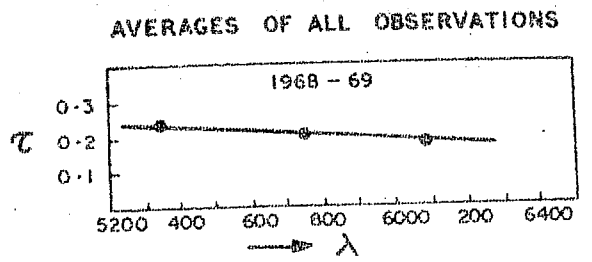

FIGURE 2.12 B - Averages of all the extinction coefficients

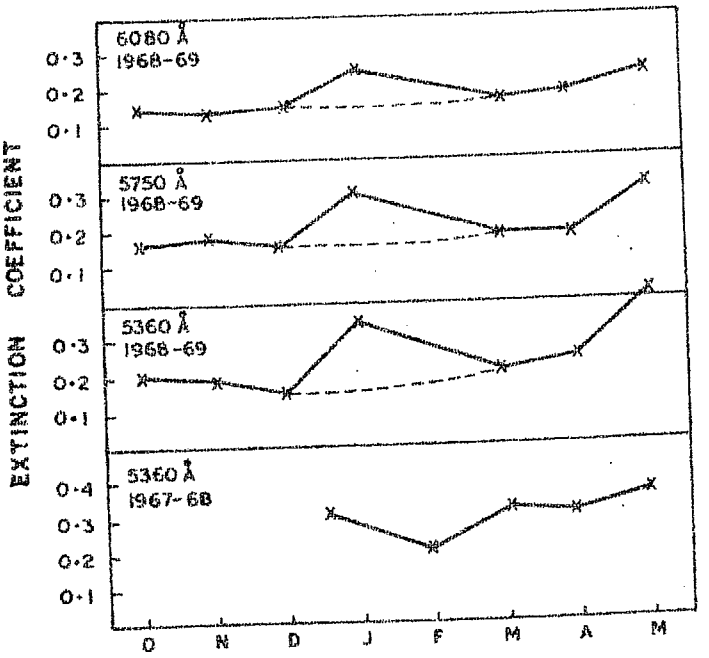

FIGURE 2.12 A - Variation of extinction coefficients with season.

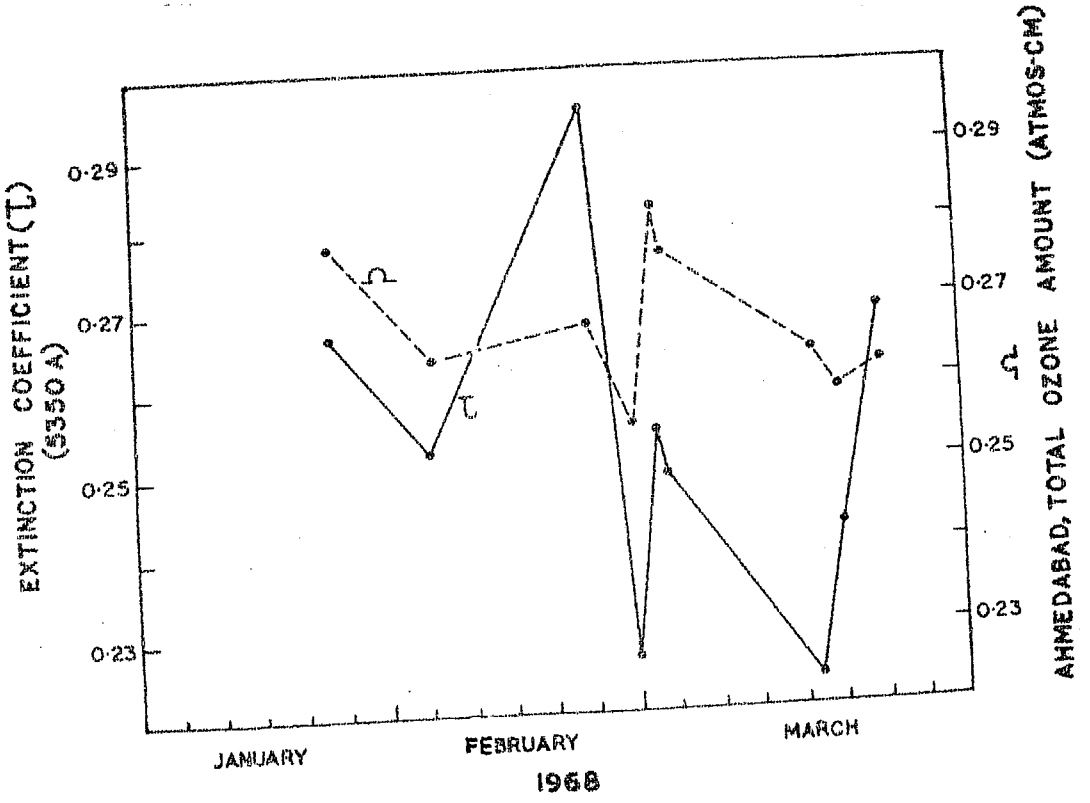

FIGURE 2.13 Comparison of the extinction coefficients and the ozone amounts.

The data of the daily ozone amounts determined by Dobson Spectrophotometer at Ahmedabad was looked into. Although the contribution due to ozone is small, whenever there is an increase in ozone amount the extinction coefficient determined is also more than normal. Very high values of extinction coefficients say greater than 0.3 at 5360 A always imply a major contribution due to aerosol. In Figure 2.13 the extinction coefficients of a few nights are plotted when they are less than 0.3 and the daily ozone amounts determined by Dobson Spectrophotometer at Ahmedabad. It is seen that the extinction coefficient increased with increase in ozone amount to some extent.

In Figure 2.14 the extinction coefficients versus wavelength are plotted on some nights to see how τ varies with wavelength.

i) On 70% of the occasions it was observed that τ decreased with increasing wavelength;

ii) On about 10% occasions τ increased with wavelength from 5360 A to 6080 A and

iii) On about 20% occasions τ was more at 5750 A than at 6080 A/5360 A and τ was less at 5750 A than at 6080 A/5360 A.

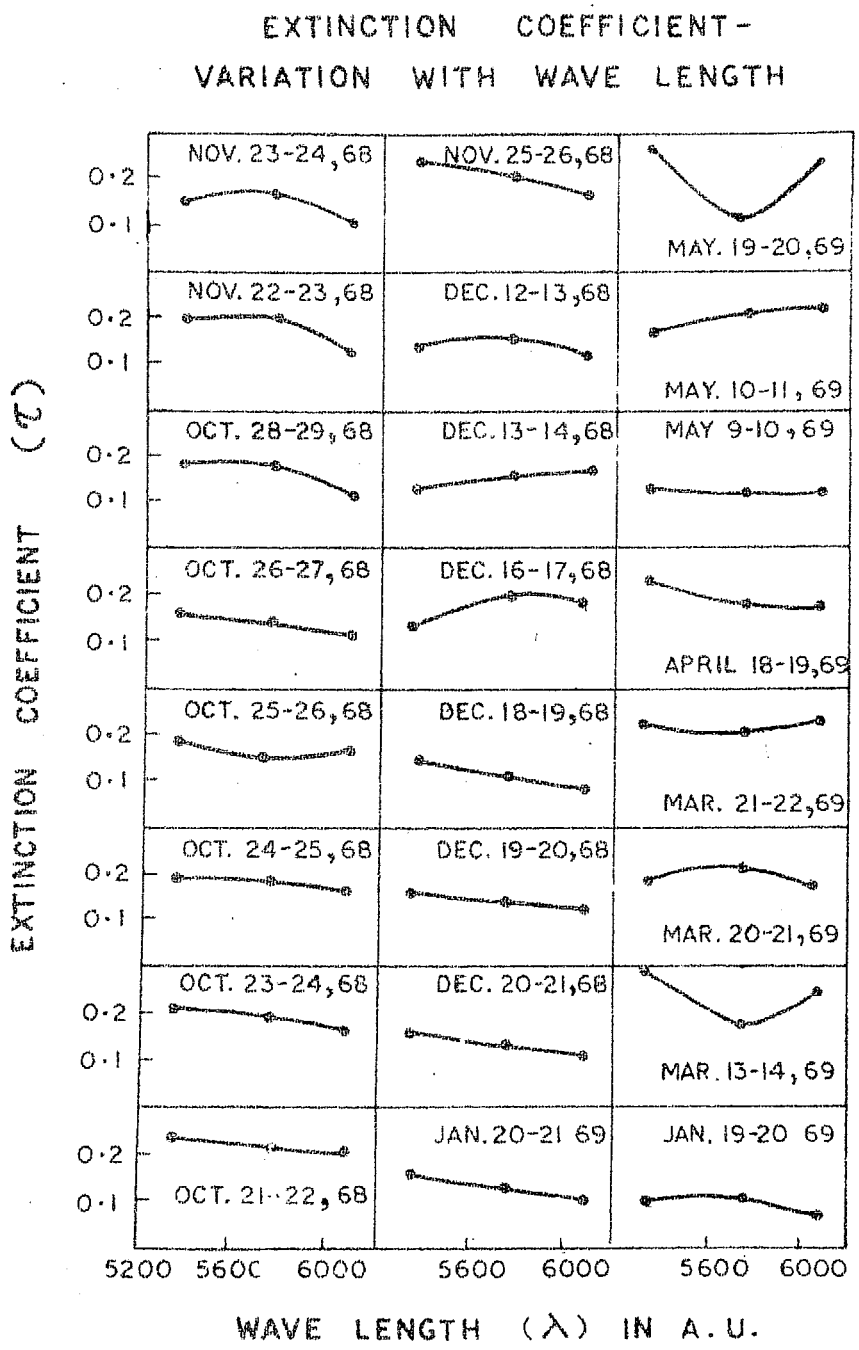

FIGURE 2.14 Variation of extinction coefficient with wavelength.

VAN DE HULST (1957) has summarised in his tretise on "light scattering by small particles" the work of VASSY and VASSY (1939) and DESSENS (1947 a,b) who distinguished the extinction from the particles of different sizes and the various occasions on which we can observe the variation of extinction coefficient with wavelength.

If 'a' is the radius of the particle -

i) Extinction roughly neutral; $a = \lambda_{max} > 0.8\mu$

ii) Extinction maximum at 5000 A; $a = \lambda_{max} = 0.5\mu$

iii) Extinction decreases gradually from 6000 A to 4000 A; $a = \lambda_{max} = 0.6\mu$

iv) Extinction maximum at 4000 A; $a = \lambda_{max} = 0.4\mu$

GOTZ (1944) concludes from the extinction measurements that the most common radii of particles are $a = 0.3\mu$ for light haze and $a = 0.4\mu$ for heavy haze.

From this it is clear that the nature of the variation of extinction with wavelength is critically dependent on the radii of the particles present. As 70% of the nights showed occasions when τ decreased with increasing wavelength it may be concluded that at Mt.Abu on most of

the occasions there are particles of sizes of radii 0.4 μ to 0.5 μ. However, on the rest of the occasions there are different τ variations, because of bigger sized particles of radii 0.6 μ or more.

The τ values are low on many nights in winter months at Mt.Abu. It may be concluded that on these nights the dust content is low and the atmosphere is approaching to the ideal 'molecular atmosphere'. These nights can be sorted out and can be used for a more rigorous study of determining heights and any other study, which demands greater accuracy in the reduced data.

It must be emphasised here that the primary object in the above study was the 'determination and use of extinction coefficients for airglow studies'; and not the interpretation of the variations in τ.

2.6 Actual use of τ in night airglow calculations:

At present, as there are no observations at all the wavelengths, the interpolated τ values at the wavelengths of the current interest from the smooth curve were obtained from three wavelengths for which there are observations and they were used for the reduction of

the night airglow data. The mean values of the extinction coefficients as determined from all the observations are used in the reduction of the en mass data from the various photometers. However, in reducing the scanning photometer data on nights of special interest, the extinction coefficients determined on those nights are used.

...

CHAPTER III

REDUCTION OF AIRGLOW DATA TO ABSOLUTE UNITS(RAYLEIGHS):

3. Introduction:

For an extended area source the brightness (I) of the emitted light is usually expressed as ergs cm^{-2} sec^{-1} $sterad^{-1}$. In airglow-aurora work the intensity of light emission is measured in rayleighs where a rayleigh is defined as 4π I, and I is measured in 10^6 quanta cm^{-2} sec^{-1} $sterad^{-1}$. (HUNTEN, ROACH and CHAMBERLAIN, 1956).

The photoelectric current that is recorded as a deflection on a current meter is a function of the intensity of light received by the photocathode in a certain range of wavelengths. The deflection is related to the spectral response of the photomultiplier S (λ)and the filter transmission T (λ).

A radioactive C^{14} phosphor source (Y-240) (half life of C^{14}= 5720 years) which emits β particles

$$C^{14} \longrightarrow N^{14} + \beta \quad (.16 \text{ MeV})$$

and produces light emission from the phosphor is used

for calibration. This source is calibrated in absolute units against a primary standard by Dr.M. Gadsden of ESSA, Boulder, (U.S.A.) at intervals.

3.1 Principle of the 'two colour method':

The 'two colour method' of ROACH and MEINEL (1955) is used for reducing the data to absolute units (Rayleighs). In this method, two filters are used, one centered at or near the emission wavelength and the second at wavelength where there is no line emission but is as near as possible to the emission wavelength. We shall call the first filter as the line filter (l-filter) and the second as the background filter (b-filter). From the response of the second filter, the contribution of the total background intensity transmitted by the line filter is determined and this is subtracted from the total response of the line filter to determine the intensity of the emission line. The photomultiplier response, transmission of the filter and the ratio of the background intensity at both line and background filters are all taken into consideration.

The same procedure is used in the case of the triplet lines of oxygen (OI), the double lines of Na, and the molecular bands of OH, taking into consideration the relative line intensities.

The observed deflections have to be corrected for atmospheric extinction and scattering. The method of correcting the observed intensity to "outside atmosphere" is described in section 3.5. In section 3.2 the theory of using the C^{14} source for calibration is given.

The procedure and the formula given by SMITH and ALEXANDAR (1963); KULKARNI and SANDERS (1964) are used for the reduction of the line intensities of airglow emissions.

3.2 Method of using C^{14} source for calibration:

The present measurements are concerned with the emission lines 5577 A/ 6300 A/ 5893 A and the near infrared OH bands, OH (7-2) (band origin at 6862 A) and OH (8-3) (band origin at 7273 A). The reduction procedure for the emission lines of atomic oxygen and sodium, is described in section 3.2.1, and the procedure for hydroxyl bands, is described in section 3.2.2.

The various symbols and the notation used (in this chapter) to describe the reduction procedure are listed below for the sake of clarity.

Notation used :

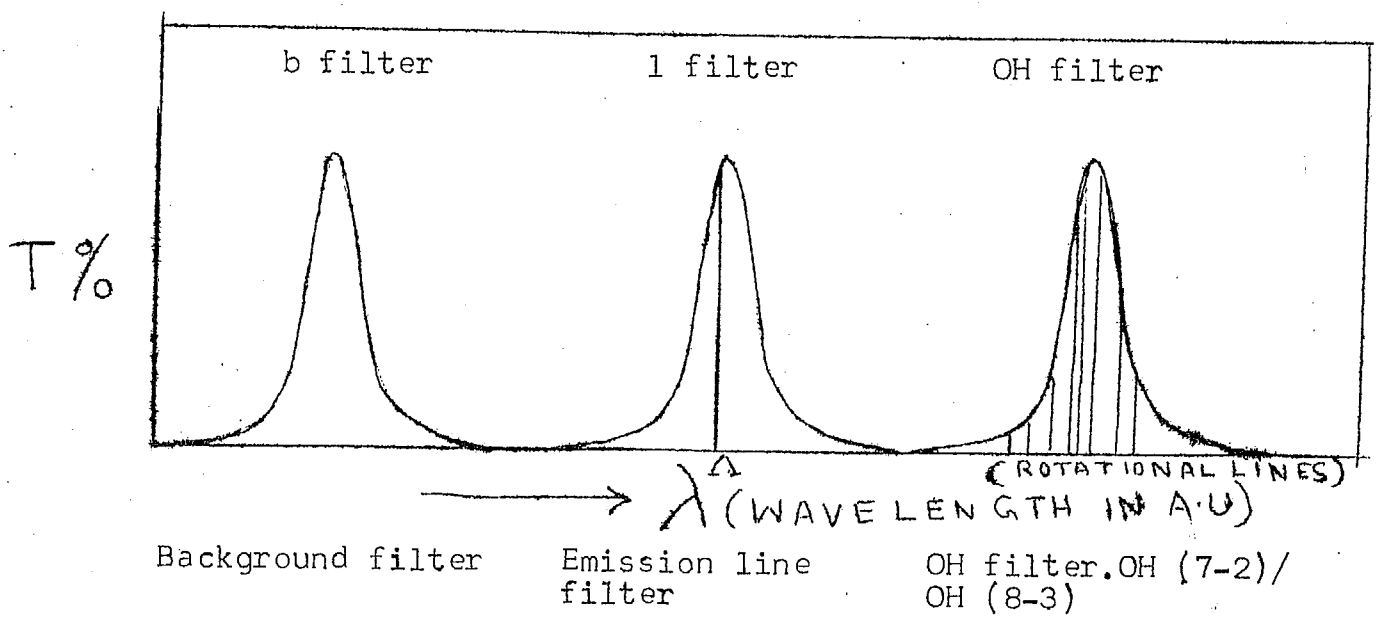

Λ is the wavelength of an emission line such as 6300 A/ 5893 A/ 5577 A.

S_λ is the spectral response of the photomultiplier at any wavelength λ .

S_Λ is the spectral response of the photomultiplier at Λ .

$S_{P_1(2)}$, $S_{P_1(3)}$..... $S_{P_2(2)}$, $S_{P_2(3)}$.....etc. are the spectral responses of the photomultiplier at the wavelengths of the rotational lines. $P_1(2)$, $P_1(3)$..... $P_2(2)$, $P_2(3)$ ....etc. of the OH band.

S_Q and S_R are the spectral responses of the photomultiplier at the mean wavelength of the Q and R branches of the OH band.

T_λ is percentage transmission of the filter at any wavelength λ .

T_Λ is percentage transmission at Λ .

$T_{P_1(2)}$, $T_{P_1(3)}$ .....$T_{P_2(2)}$, $T_{P_2(3)}$.....are the percentage transmissions of the filter at the wavelengths of $P_1(2)$, $P_1(3)$.....$P_2(2)$, $P_2(3)$...etc.

T_Q and T_R are the percentage transmissions of the filter at the mean wavelengths of Q and R branches of the OH band.

$\alpha_{P_1(2)}$, $\alpha_{P_1(3)}$..... $\alpha_{P_2(2)}$, $\alpha_{P_2(3)}$..... are the relative intensities of the rotational lines $P_1(2)$, $P_1(3)$....$P_2(2)$, $P_2(3)$.....etc.

α_Q and α_R are the relative intensities of Q and R branches of the OH band.

N_λ is the radiance of C^{14} source at any wavelength λ .

R_λ is the nightglow intensity of the emission line in rayleighs.

R_{OH} is the OH band intensity in rayleighs.

B' is the background intensity in rayleigh/A at the peak wavelength of the background filter b.

B is the background intensity is rayleighs/A at the peak wavelength of transmission of the line emission filter or OH filter.

K_l is the ratio of the background intensity at the peak wavelength of the emission line to the background intensity at the peak wavelength of transmission of the background filter.

K_{OH} is the ratio of the background intensity at the peak wavelength of the OH filter to the background intensity at the peak wavelength of the background filter.

d_b is the deflection on the current meter due to the night sky intensity through the background filter b.

dC_b is the deflection obtained on the current meter due to the C^{14} source through the background filter b.

d_1 is the deflection due to the night sky intensity through the emission line filter 1.

dC_1 is the deflection due to the C^{14} source with the emission line filter 1.

d_{OH} is the deflection due to the night sky with the OH filter.

dC_{OH} is deflection due to C^{14} source with the OH filter.

k is the geometrical constant of the photometer (i.e. energy per unit deflection on the current meter).

Correction to be applied to observed intensities:

I^f intensity (deflection) measured at the ground at any wavelength.

I intensity outside the atmosphere.

Sc Scattering term

Ex Extinction term

τ_1 Molecular scattering coefficient

τ_2 Total extinction coefficient.

M is the airmass at any zenith angle ($M = m_o \sec Z$)

m_o is the mass of the atmosphere overhead

Z is the zenith angle of observation

Chamberlain's procedure:

$I_{inc}(-\mu)$ Intensity above the ozone layer at any zenith angle Z.

$\mu = \cos Z$ Z is angle angle

I_o is zenith intensity outside the atmosphere.

$I_{trans}(\tau|-\mu)$ is the intensity of the scattered light due to molecular scattering.

$I^*(\tau | -\mu)$ is the scattered light due to ground albedo.

τ_o extinction coefficient due to ozone.

τ is extinction coefficient due to the scattering atmosphere.

3.2.1 Method for the emission line:

Let the corrected deflection for atmospheric scattering and absorption through the line filter when the photometer is pointed to the night sky be d_1. This deflection is due to the emission line intensity plus the background intensity passing through the filter due to the finite width of the filter.

Let the deflection due to the C^{14} source through line filter be dC_1. The response of the photometer in the above two cases can be written

$$S_\Lambda \, T_\Lambda \, R_\Lambda + \int_1 S_\lambda \, T_\lambda \, B \, d\lambda = k \, d_1 \ldots\ldots \quad (1)$$

where

k is the geometrical constant of the photometer. (energy per unit deflection).

T_Λ is the filter transmission at the line emission wavelength Λ

B is the total night sky background brightness in Rayleighs/A.

and

$$\int_1 S_\lambda \; N_\lambda \; T_\lambda \; d\lambda = k \; dC_1 \ldots\ldots\ldots\ldots \quad (2)$$

N_λ is the radiance of C^{14} source in rayleighs. (converted from ergs $sec^{-1}cm^{-2}sterad^{-1}A^{-1}$).

The integrals $\int_1 S_\lambda \; T_\lambda \; B \; d\lambda$ and $\int_1 S_\lambda \; N_\lambda \; T_\lambda \; d\lambda$ give the response of the photometer to the night sky continuum and the C^{14} source respectively through the line filter. The integral is to be taken over the range of wavelengths transmitted by the filter (ideally from 0 to ∞).

For moderately narrow filters ($\sim$ 50 A) B can be considered as constant in the small spectral region transmitted by the filter. From (1) and (2)

$$\frac{S_\Lambda \; T_\Lambda \; R_\Lambda + B \int_1 S_\lambda \; T_\lambda \; d\lambda}{\int_1 S_\lambda \; N_\lambda \; T_\lambda \; d\lambda} = \frac{d_1}{dC_1} = D_1$$

The ratio of deflections of sky to carbon^{14} source through the same filter is represented by D

$$S_\lambda T_\lambda R_\lambda + B \int_\ell S_\lambda T_\lambda d\lambda = D_1 \int_1 S_\lambda N_\lambda T_\lambda d\lambda \quad (3)$$

To evaluate B the background intensity in R/A, another filter where there are no airglow emission lines is used.

Let the deflection due to the sky with this background filter be d_b and that with the C^{14} source be dC_b.

The responses of the photometer are

$$\int_b S_\lambda T_\lambda B' d\lambda = k \, d_b \quad (4)$$

$$\int_b S_\lambda N_\lambda T_\lambda d\lambda = k \cdot dC_b \quad (5)$$

B' is the background intensity in Rayleighs per A. In the spectral region of this filter b. B' can be assumed to be constant in the spectral region of the filter, if the filter is not wide.

Therefore from (4) and (5)

$$\frac{B' \int_b S_\lambda \; T_\lambda \; d\lambda}{\int_b S_\lambda \; N_\lambda \; T_\lambda \; d\lambda} = \frac{d_b}{dC_b} = D_b$$

Therefore

$$B' = D_b \cdot \int_b S_\lambda \; T_\lambda \; N_\lambda \; d\lambda \Big/ \int_b S_\lambda \; T_\lambda \; d\lambda \quad \ldots\ldots (6)$$

when B' is known, B can be calculated provided the ratio of the background intensities at these two wavelengths is known. If the ratio of background intensity at peak wavelength of the 1 -filter to the background intensity at peak wavelength of b — filter is K_1 then

$$B = K_1 \; B'$$

Therefore

$$B = D_b \; K_1 \int_b S_\lambda \; N_\lambda \; T_\lambda \; d\lambda \Big/ \int_b S_\lambda \; T_\lambda \; d\lambda \quad \ldots\ldots (7)$$

substituting this value of B in equation (3) and rearranging the terms we get

$$R_\Lambda = \left[D_1 \cdot \frac{\int_1 S_\lambda \; N_\lambda \; T_\lambda \; d\lambda}{S_\Lambda \; T_\Lambda} - K_1 \cdot D_b \frac{\int_b S_\lambda \; N_\lambda \; T_\lambda \; d\lambda}{\int_b S_\lambda \; T_\lambda \; d\lambda} \cdot \frac{\int_1 S_\lambda \; T_\lambda \; d\lambda}{S_\Lambda \; T_\Lambda} \right] \quad (8)$$

3.2.2 Reduction of OH band intensity into Rayleighs:

Let the total absolute intensity of the OH band be R_{OH} rayleighs.

Let N_λ be the C^{14} source radiance and S_λ be the relative sensitivity of the photocathode at any wavelength λ. Let the deflection due to OH filter when the photometer is pointed to the night sky be d_{OH} and the deflection obtained with C^{14} source through the same filter be dC_{OH}.

Let the relative intensities of the rotational lines in the band in P, Q, R branches be

$\alpha_{P_1(2)}, \alpha_{P_1(3)}, \alpha_{P_1(4)} \cdots\cdots \alpha_{P_2(2)}, \alpha_{P_2(3)} \cdots\cdots$

$\cdots\cdots\cdots\cdots \alpha_Q$ and α_R.

In the case of Q and R branches the separation of the lines is very small and the relative integrated intensity of the branch is considered at its mean wavelength.

The α's are computed by CHAMBERLAIN (1961c) with a Boltzman distribution of levels for $T = 225^{\circ}K$ and the line strengths from the Honl-London formula (1925) as quoted

by HERZBERG (1950). These values are used in the reduction. Let the filter transmission at the rotational line wavelengths be

$T_{P_1}(2)$, $T_{P_1}(3)$, $T_{P_1}(4)$.....$T_{P_2}(2)$, $T_{P_2}(3)$, $T_{P_2}(4)$..... .....T_Q and T_R

and similarly the photocathode relative sensitivity S be

$S_{P_1}(2)$, $S_{P_1}(3)$, $S_{P_1}(4)$..... $S_{P_2}(2)$, $S_{P_2}(3)$, $S_{P_2}(4)$..... ..... S_Q and S_R

The conversion between Q_e in ergs cm^{-2} $sterad^{-1}$ sec^{-1} A^{-1} to Q_R in rayleighs at any wavelength λ is given by

$$Q_R = Q_e \times 6.3227 \times 10^9 \times \lambda$$

where λ is in A.

The response due to the rotational line intensities in all the branches is

$$R_{OH} \alpha_{P_1(2)} S_{P_1(2)} T_{P_1(2)} + R_{OH} \alpha_{P_1(3)} S_{P_1(3)} T_{P_1(3)} + \ldots$$
$$+ R_{OH} \alpha_{P_2(2)} S_{P_2(2)} T_{P_2(2)} + R_{OH} \alpha_{P_2(3)} S_{P_2(3)} T_{P_2(3)} + \ldots$$
$$+ R_{OH} \alpha_Q S_Q T_Q + R_{OH} \alpha_R S_R T_R$$

In the night sky there is background continuum due to starlight, zodiacal light and genuine airglow continuum (it is not known whether true airglow continuum is there in the infrared region). This will also contribute to the observed response through the OH filter. The deflection observed is a mixture of the deflection due to the total continuum, and the deflection due to the emission rotational lines.

If the continuum intensity is B R/Å in an OH band and under the assumption that B is same (as the bands under consideration are spread to about 200 Å only) the total continuum included in the OH filter is $B \int_{OH} S_\lambda \; T_\lambda \; d\lambda$.

Therefore the response of the photometer is

$$\sum_{\substack{P \\ P_1=2 \\ P_2=2}}^{8} (R_{OH} \; \alpha_P \; S_P \; T_P) + R_{OH} \; \alpha_Q \; S_Q \; T_Q + R_{OH} \; \alpha_R \; S_R \; T_R + B \int_{OH} S_\lambda \; T_\lambda \; d\lambda = k \; d_{OH} \qquad (9)$$

where k is the geometrical constant of the photometer. In the P branch the lines upto J = 8 only (J being the rotational quantum number) are considered as tabulated by CHAMBERLAIN (1961c). Lines with J $>$ 8 are very weak.

$$R_{OH}\left[\sum_{P}^{P_1=2}\left(\alpha_P S_P T_P\right) + \alpha_Q S_Q T_Q + \alpha_R S_R T_R\right] + B\int_{OH} S_\lambda T_\lambda \, d\lambda = k\, d_{OH} \qquad (10)$$

Let

$$A = \sum_{P}^{P_1=2}\left(\alpha_P S_P T_P\right) + \alpha_Q S_Q T_Q + \alpha_R S_R T_R$$

Therefore $R_{OH} \cdot A + B\int_{OH} S_\lambda T_\lambda \, d\lambda = k\, d_{OH}$ (11)

The response of C^{14} source with the OH filter is

$$\int_{OH} S_\lambda T_\lambda N_\lambda \, d\lambda = k\, dC_{OH} \qquad (12)$$

From (11) and (12)

$$R_{OH} = \frac{D_{OH}}{A}\cdot\int_{OH} S_\lambda N_\lambda T_\lambda \, d\lambda - \frac{B}{A}\int_{OH} S_\lambda T_\lambda \, d\lambda \qquad (13)$$

where D_{OH} is equal to d_{OH}/dC_{OH}

To evaluate B the background intensity in rayleighs per A, another filter, where there are no airglow emission lines is used. In the present case a filter having peak transmission at 6080 A, has been used.

Let the deflection due to this filter from sky be d_b and that due to C^{14} source be dC_b.

The response of the photometer with C^{14} source is

$$\int_b S_\lambda \, N_\lambda \, T_\lambda \, d\lambda = k \, dC_b \qquad (14)$$

If the total night sky continuum intensity is B' R/A in this spectral region and is assumed to be the same in the region transmitted by the background filter, we have

$$B' \int_b S_\lambda \, T_\lambda \, d\lambda = k \, d_b \ldots\ldots \qquad (15)$$

Therefore from (14) and (15)

$$B' = \frac{d_b}{dC_b} \cdot \frac{\int_b S_\lambda \, N_\lambda \, T_\lambda \, d\lambda}{\int_b S_\lambda \, T_\lambda \, d\lambda} \qquad (16)$$

$$B' = D_b \cdot \frac{\int_b S_\lambda \, N_\lambda \, T_\lambda \, d\lambda}{\int_b S_\lambda \, T_\lambda \, d\lambda} \qquad (17)$$

Thus when B' is known B can be calculated provided the ratio of background intensity at the two peak wavelengths of the filters is known. If this ratio is K_{OH}, then

$$B = K_{OH} B' \qquad (18)$$

Therefore the intensity of the OH band is given by

$$R_{OH} = \frac{D_{OH}}{A} \cdot \int_{OH} S_\lambda N_\lambda T_\lambda \, d\lambda - \frac{B}{A} \int_{OH} S_\lambda T_\lambda \, d\lambda \qquad (19)$$

Substituting for B, we get

$$R_{OH} = \left[\frac{D_{OH}}{A} \int_{OH} S_\lambda N_\lambda T_\lambda \, d\lambda - K_{OH} \frac{D_b}{A} \frac{\int_b S_\lambda N_\lambda T_\lambda \, d\lambda}{\int_b S_\lambda T_\lambda \, d\lambda} \cdot \int_{OH} S_\lambda T_\lambda \, d\lambda \right]$$

R_{OH} is in rayleighs.

3.3 Approximations and errors in the two colour method:

KULKARNI and SANDERS (1964) have assumed an average value for both S_λ and N_λ for the whole filter range when the range is $\sim$30 A. Also they assume that the background continuum intensity for adjacent spectral regions does not change appreciably within 200 A.

BLACKER and GADSDEN (1966) have pointed out the following objections to the procedure adopted by KULKARNI and SANDERS (1964).

a) Long term variation of the C^{14} source is not considered.

b) Transmission of filters in the infrared region is not considered (possibility of "secondary" transmission in interference type filters).

c) Approximation of one single value of S_λ and N_λ for the entire filter transmission range is not satisfactory. In short, $S_\lambda N_\lambda \int T_\lambda \, d\lambda$ is not a sufficiently good approximation for

$$\int S_\lambda N_\lambda T_\lambda \, d\lambda$$

Regarding (a) we are of the view that long term variation of C^{14} is yet to be established. It is dependent on the properties of the phosphor. We get our C^{14} source calibrated at intervals by Dr. M.Gadsden of ESSA and have used appropriate values of the radiances in the reduction.

The C^{14} source Y-240 is calibrated at temperatures 13^{o} and $20^{o}C$. There is slight difference in the radiances at these two temperatures. These are the normal night-time temperatures at Mt. Abu in the winter and summer respectively. At Mt. Abu, during night, there is only a change of a few degrees in temperature. Appropriate values of C^{14} radiances are used in the reduction of the data.

Regarding (b) one must admit that if there is a secondary transmission band in the filter and if the photometer is sensitive to it, this is of serious concern. All our filters have been calibrated with the help of a Beckman quartz spectrophotometer at the Ahmedabad Textile Industries' Research Association. And these calibrations are repeated occasionally. Modern interference filters are subjected to special treatments so that they do not have any secondary transmission bands. In some of the filters wherever it was necessary, additional filters have been used to cut all secondary transmission bands. Also we have used S_{10} and S_{20} type of photomultipliers. They do not have any sensitivity at $\lambda\lambda > 8000$ A.

Regarding (c), the response of the photomultiplier as supplied by the manufacturers, is considered.

In Tables 3-I A and 3-I B are given the data for all the filters which are used on the different photometers and S_λ, N_λ values at the peak transmission of the said filters.

In Tables 3-II A and 3-II B are presented the values of the responses of the photometer as

$$S_\lambda \, N_\lambda \, T_\lambda \text{ (at } \tfrac{1}{2} \text{ max. transmission)} \ldots\ldots \quad (21)$$

$$S_\lambda \, N_\lambda \int T_\lambda \, d\lambda \quad (22)$$

$$S_\lambda \int N_\lambda \, T_\lambda \, d\lambda \quad (23)$$

$$N_\lambda \int S_\lambda \, T_\lambda \, d\lambda \quad (24)$$

$$\int S_\lambda \, N_\lambda \, T_\lambda \, d\lambda \quad (25)$$

$d\lambda$ is taken in intervals of 5 A.U.

Tables 3-II A and 3-II B are self explanatory. Values of the responses obtained through equations (22), (23), (24) and (25) do not differ by more than 1 to 2% for all the narrow filters. In case of (i) broad filters and (ii) when the relative response of the photocathode is small, the values calculated from equations (22), (23), (24) and (25) differ by more than 5 to 10 per cent.

TABLE 3-I A

Giving the details of the various filters used on different photometers

	SCANNING PHOTOMETER					RED PHOTOMETER			
Photomultiplier	RCA 7265 (S-20 response)					EMI 9558 B (S-20 response)			
Filter No. / Peak of the filter	I 6306	II 5894	III 5750	IV 5586	V 5300	VI 6330	VII 6090	VIII 6880	IX 7270
Filter Type	B10	B10	B10	B10	B&L+ OGRI	B1	B10	Schott Red + 1025II	B&L + Deep Red MN04, 22
Size of the filter	1"x1"	1"x1"	1"x1"	1"x1"	2"x2"	2"x2"	2"x2"	2"x2"	2"x2"
Emission wavelength	6300	5893	--	5577	--	6300	--	OH(7-2)	OH(8-3)
T_{max} (max transmission %)	69	79	74	78	14	71	77	42	32
$\frac{1}{2}$ peak transmission band width in A.U. at $(\frac{1}{2} T_{max})$	47	41	34	38	130	105	48	120	100
S_λ relative response of the photomultiplier at the emission wavelength	41.3	53.1	57.4	62.8	70.5	40.4	47.4	23.2	12.75
N_λ radiance of C^{14} source (Y-240) at peak of the filter in units of 10^{-13} watts cm^{-2} sec^{-1} $sterad^{-1}$ A^{-1}.	5.133	15.60	17.97	19.37	15.81	4.710	10.36	1.412	0.9059

TABLE 3-I B

Giving the details of the various filters used on different photometers

	POLE PHOTOMETER				EXTINCTION PHOTOMETER			
Photomultiplier	EMI 6995 S (S-10 response)				EMI 9552 B (S-10 response)			RCA 6217 (S-10 response)
Filter No. / Peak of the filter	X 6340	XI 5880	XII 5580	XIII 5350	XIV 6080	XV 5750	XVI 5360	XVII 5360
Filter type	B&L + Plastic Red	B&L+ DRM No.1	GAB 550/8	Blazers B-20 531	B10	B10	B9	GAB 528/9
Size of the filter	2"x2"	2"x2"	2"x2"	2"x2"	2"dia.	1"x1"	2"dia.	2"x2"
Emission wavelength	6300	5893	5577	--	---	---	---	---
T_{max} (max transmission %)	40	43	24	27	79	74	64	24
$\frac{1}{2}$ peak transmission band width in A.U. at $(\frac{1}{2} T_{max})$	135	97	80	45	48	34	35	130
S_λ relative response of the photomultiplier at the emission wavelength	17.0	32.0	42.0	47.5	24.8	35.5	47.6	-
N_λ radiance of C^{14} source (Y-240) at peak of the filter in units of 10^{-13} watts cm^{-2} sec^{-1} $sterad^{-1}$ A^{-1}	4.57	15.91	19.37	18.38	10.36	17.97	18.84	18.84

TABLE 3-II A

Showing the response ofthe Photometers (in Arbitrary units)

Filter	SCANNING PHOTOMETER					RED PHOTOMETER			
	I 6300	II 5893	III 5750	IV 5577	V 5300	VI 6300	VII 6080	VIII OH(7-2)	IX OH(8-3)
$S_\lambda N_\lambda T_\lambda$ (at $\frac{1}{2} T_{max}$)	9.965	3.396	3.508	4.624	1.450	1.857	2.263	1.965	4.155
$S_\lambda N_\lambda \int T_\lambda \, d\lambda$	8.092	3.094	2.931	4.117	2.728	1.445	2.026	2.353	5.019
$S_\lambda \int N_\lambda T_\lambda \, d\lambda$	7.865	3.096	2.921	4.11.	2.649	1.439	2.019	2.403	4.973
$N_\lambda \int S_\lambda T_\lambda \, d\lambda$	8.009	3.094	2.932	4.116	2.733	1.442	2.023	2.382	4.950
$\int S_\lambda N_\lambda T_\lambda \, d\lambda$	7.839	3.099	2.935	4.101	2.622	1.443	2.019	2.413	5.004

TABLE 3-II B

Showing the response of the photometers (in Arbitrary units)

Filter	POLE PHOTOMETER				EXTINCTION PHOTOMETER		
	X 6300	XI 5893	XII 5577	XIII 5350	XIV 6080	XV 5750	XVI 5360
$S_\lambda N_\lambda T_\lambda$ (at $\frac{1}{2} T_{max}$)	10.489	4.938	6.508	3.929	1.246	2.169	4.932
$S_\lambda N_\lambda \int T_\lambda d\lambda$	5.773	3.359	2.672	1.431	1.091	1.808	3.384
$S_\lambda \int N_\lambda T_\lambda d\lambda$	5.647	3.261	2.600	1.437	1.062	1.800	3.393
$N_\lambda \int S_\lambda T_\lambda d\lambda$	5.528	3.324	2.738	1.435	1.069	1.802	3.371
$\int S_\lambda N_\lambda T_\lambda d\lambda$	5.656	3.281	2.536	1.438	1.044	1.795	3.377

It may be noted that results obtained by equation (21) and (25) may differ by 10% to 20% in the case of narrow filters and a little more in the case of broad filters.

Similar calculations are also done with another C^{14} radioactive source (O-315) which we got recently. The results are similar.

It may therefore be concluded that the only important step is to include T_λ inside the integral sign. That is the value of $\int T_\lambda \, d\lambda$ is to be obtained from the filter transmission curve. It matters little whether S_λ and N_λ are inside or outside the integral sign. However, since we had all the detailed calculations including S_λ and N_λ in the integral, we have used them in our reduction.

Perhaps the weakest point of the two colour method is the assumption K_1 or $K_{OH} = 1$ when the transmission of the background continuum filters used is not very near that of the emission line filter.

The following table shows details about the background filters that are used in different photometers.

Photometer	Emission wavelength filters	Background filter peak
Pole photometer	5577 Å, 5893 Å, 6300 Å	5350 Å
Red photometer	6300 Å, OH (7-2), OH (8-3)	6080 Å
Scanning photometer	5577 Å, 5893 Å, 6300 Å	5750 Å/5300 Å

When the background filter transmission is not very near those of the emission line filter, it is necessary to know the value of K_1 or K_{OH} to eliminate the background continuum intensity properly. The percentage error in determining the absolute intensities if K_1 is not exactly known, is largely dependent on the width of the filter and also on the emission line intensities. This error increases with wider filters and it will be greater in case of less intense lines such as the sodium lines in summer, or if incorrect values of K_1 are used in the reduction.

SHEFOV (1959) has given the total intensity of night sky (both airglow and astronomical components included), in R/Å for a few nights in the year 1957. Table 3-III shows the average values of continuum intensity from Shefov's curves (1959). There are variations in the intensity values of different nights.

TABLE 3 - III

The background intensity in R/A at a number of wavelengths on a few nights.

Date → / λ in A.U ↓	Background intensity in R/A				
	Oct.22-23, 1957	Apr.4-5, 1957	Nov.19-20, 1957	Mar.31-Apr.1, 1957	Mean
5300		3.0		2.4	2.7
5350		2.8		2.4	2.6
5570	2.0	2.4	3.9	2.3	2.6
5750	3.1	3.1	4.7	3.9	3.7
5890	2.8	3.3	4.3	4.2	3.7
6080	2.3	2.9	3.7	3.8	3.2
6330	1.6	2.4	2.8	2.9	2.4

The background continuum intensities (total) at three wavelengths 5360 A, 5750 A and 6080 A are measured with the help of the Extinction photometer II described in Chapter II. This photometer is directed towards zenith and the background intensity is continuously recorded. A sample record is given in Figure 3.1. The observations are only interrupted when star deflection are needed for determining the extinction coefficient.

Using equation (17) the background intensity can be determined at each of the three wavelengths separately. The K_1 values are determined from the extrapolated curve of (intensity vs. wavelength) obtained from the above measurements; and used them for the correct evaluation of airglow.

3.4 Contamination of OH in the intensities of emission lines:

It should be noted that OH (9-3) band at 6256 A ($\sim$110 R) is a source of contamination for measurements, when a coarse filter is used for isolating the 6300 A line. Also OH (8-2) band at 5886 A ($\sim$57 R) will contaminate the observations of sodium D lines at 5890 and 5896; especially in summer when OH and Na intensities are of

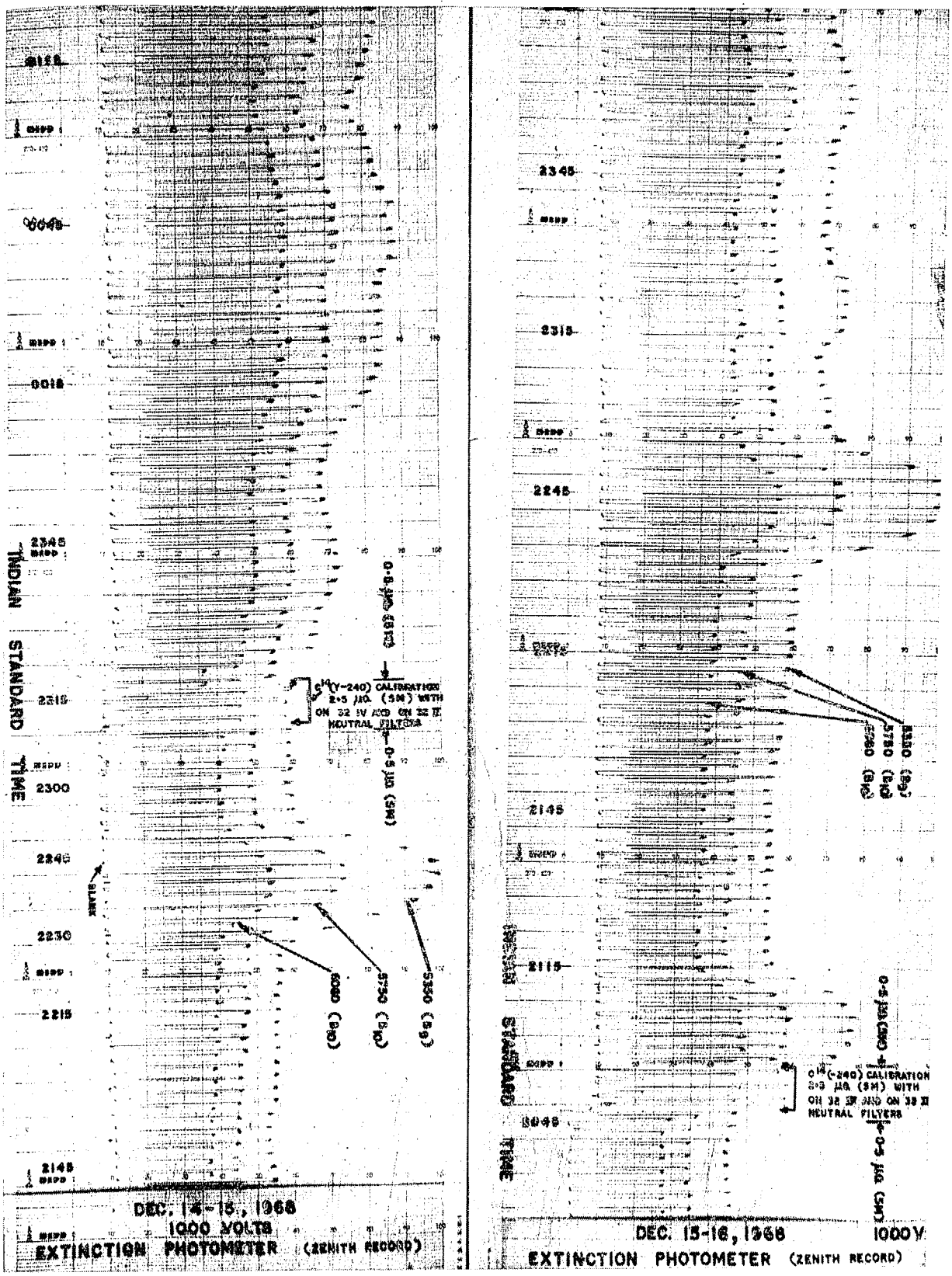

Fig. 3.1 Sample records obtained with the Extinction Photometer II pointing the photometer to zenith (with filters 6080 A, 5750 A and 5360 A)

the same order. The OH (7-1) band at 5562 is quite weak ($\sim$ 22 R) and a minor source of contamination in 5577 (OI) measurements.

Since there are measurements of absolute intensities of two OH bands OH (7-2) and OH (8-3) with the Red photometer, OH contamination could be corrected in 6300 A and 5893 A observations. Assuming that all OH bands covary at all times and knowing the ratio of intensities of OH (7-2) or OH (8-3) to OH (9-3) from the absolute intensities determined by CHAMBERLAIN and SMITH (1959) and KRASSOVSKY et al.(1962) and the percentage contribution of OH (9-3) in the 6300 filter, the contribution of OH (9-3) is calculated and subtracted from the observations. This assumption is quite satisfactory in the case OH (7-2) and OH (8-3) and is substantiated from our intensity measurements (These results are discussed in Chapter V). A similar method can be employed for 5893 observations.

As an example the nocturnal variation of one typical night for 6300 is given in Figure 3.2.

A more effective method of eliminating OH contamination in 6300/5893 observations is given below.

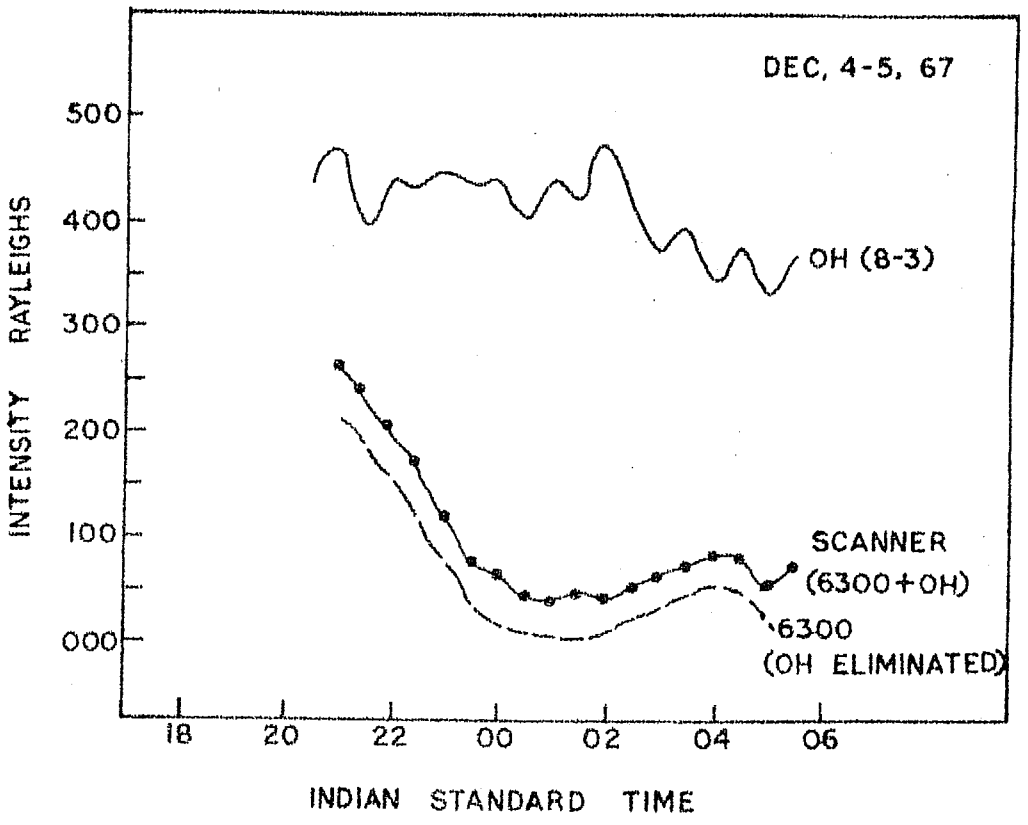

FIGURE 3.2 Example of the nocturnal variation of 6300 A after subtracting OH (9-3) contamination. OH (9-3) contamination is estimated from the intensity measurements of OH (8-3).

There are simultaneous 6300 A observations with 3 different filters on different photometers.

i) Pole photometer;

ii) Red photometer and

iii) Scanning photometer.

There are two 5893 filters on (i) and (iii). The 6300 percentage transmission of 6300 filters and the relative intensities of OH (9-3) rotational lines are given in Tables 3-IV and 3-V and in Figure 3.3.

The 6300 filters on (i) and (ii) contribute effectively the same amount of OH (9-3) to the 6300 observations (see last line of Table 3-V). With this added advantage our red photometer (ii) was turned towards the pole from January 1968 and the observations are compared with the recordings of pole photometer (i). After reduction of data with both photometers, identical values of 6300 A intensities, were obtained which showed that the method of eliminating the background contribution is quite satisfactory.

From the observations of (ii) and (iii) photometers we can effectively eliminate the OH contamination from

TABLE 3 - IV

The percentage transmissions of different filters for 6300-64 lines and OH (9-3) rotational lines.

Line	Wave-length	Relative intensity	Scanner Photometer B_{10}		Red Photometer B_1		Pole Photometer B&L	
			T %	αT_λ	T %	αT_λ	T %	αT_λ
(OI)	6300	3	62.5		52.5		38.0	
(OI)	6364	1	45.0		55.0		35.5	
$P_1(2)$	6287.6	0.0763	32.0	2.442	33.0	2.518	32.0	1.679
$P_1(3)$	6306.8	0.0922	68.5	6.316	59.0	5.440	32.0	2.950
$P_1(4)$	6329.2	0.0772	37.5	2.895	72.0	5.558	39.0	3.010
$P_1(5)$	6355.1	0.0497	8.0	0.397	62.5	3.106	38.0	1.889
$P_1(6)$	6384.4	0.0260	1.2	0.031	30.5	0.793	26.5	0.689
$P_1(7)$	6416.9	0.0117	0.1	0.001	9.5	0.111	8.5	0.099
$P_1(8)$	6458.5	0.0043	--	0	2.5	0.011	2.5	0.010
$P_2(2)$	6279.2	0.0279	19.0	0.530	26.5	0.739	19.5	0.544
$P_2(3)$	6298.7	0.0390	57.5	2.242	50.0	1.950	26.0	1.014
$P_2(4)$	6321.7	0.0357	60.0	2.142	68.5	2.445	38.0	1.357
$P_2(5)$	6348.2	0.0252	11.0	0.277	67.0	1.688	39.5	0.995
$P_2(6)$	6378.1	0.0143	1.5	0.021	38.5	0.551	29.0	0.415
$P_2(7)$	6411.6	0.0068	0.2	0.001	11.0	0.075	9.5	0.065
$P_2(8)$	6452.3	0.0027	--	--	2.5	0.007	2.6	0.007
Q	6264.0	0.2270	6.0	1.362	14.5	3.292	15.0	3.405
R	6240.0	0.2840	2.0	0.568	7.0	1.988	10.0	2.840
				19.225		30.272		20.968
Total OH (9-3) transmission percentage				19%		30%		21%

TABLE 3 - V

Effective Transmission percentages of different filters for OH(9-3) band.

	Transmission percentage of filters		
	Scanner B_{10}	Red B_1	Pole
6300	62.5	52.5	38.0
6364	5.0	56.5	35.5
Effective Transmission	48.0	53.5	37.5
OH (9-3) at effective	19.0	30.0	21.0
Effective Transmission	39.5%	56.0%	56.0%

Assumed absolute zenith intensity 6300 + 6364 = 200 R

Absolute zenith intensity OH (9-3) = 110 R

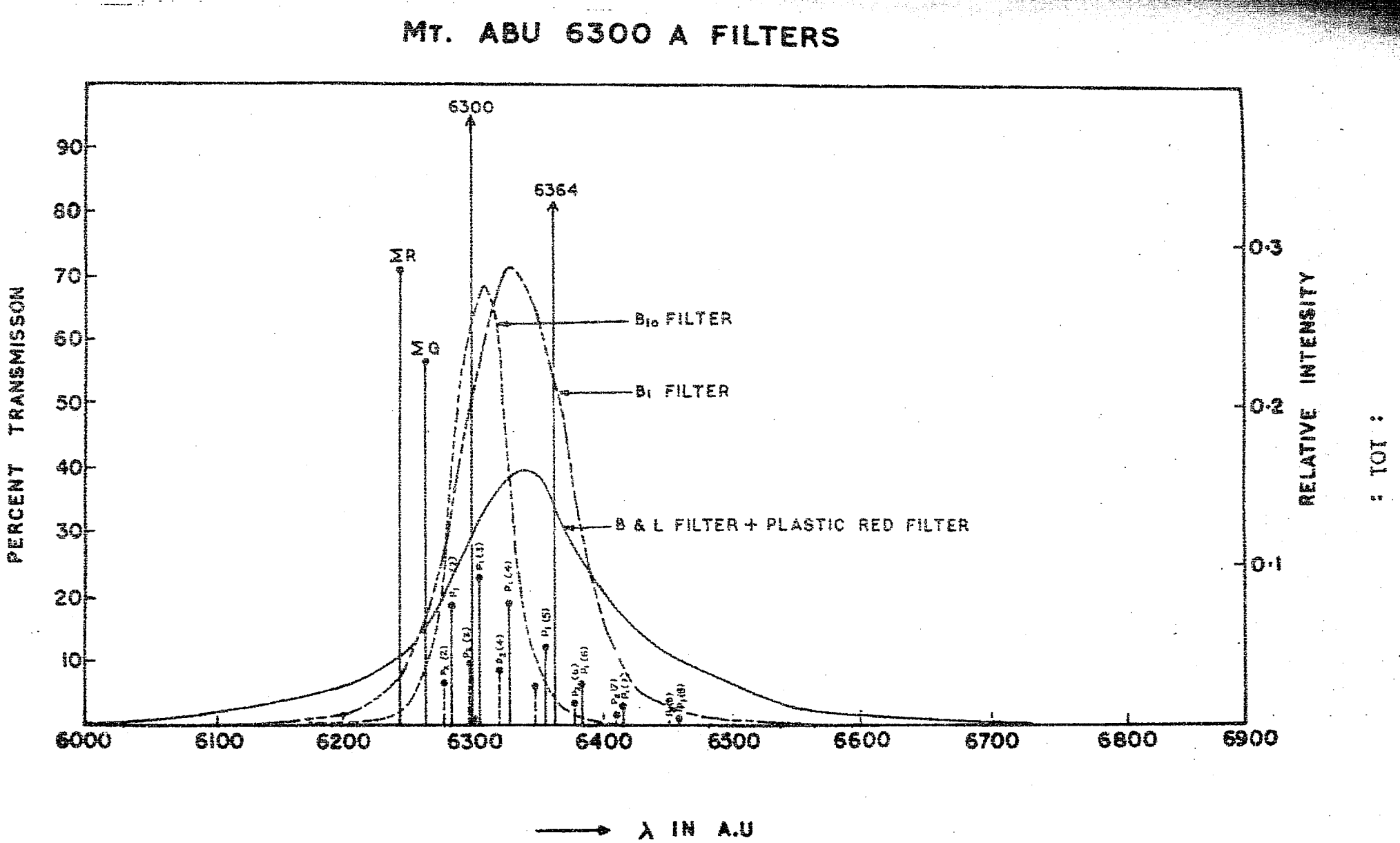

FIGURE 3.3 6300 A filters used on different photometers at Mt. Abu. The rotational structure of OH (9-3) band and their relative intensities are shown. The scale of relative intensity on the right hand side applies to only OH (9-3) band.

the 6300 observations and determine the absolute intensity of OH (9-3). The following is the procedure.

On photometer (ii) there is a B_1 filter and on photometer (iii) there is a B_{10} filter. Let T_{6300} and T_{OH} be the effective transmissions for 6300 A and OH (9-3) through B_1 filter and let T'_{6300} and T'_{OH} be the effective transmissions through B_{10} filter, and let R_{6300} and R_{OH} be the absolute intensities of 6300 and OH (9-3). Then we can write the following equations.

$$R_{6300}\, T_{6300} + R_{OH}\, T_{OH} = X \quad (B_1 \text{ filter}) \tag{26}$$

$$R_{6300}\, T'_{6300} + R_{OH}\, T'_{OH} = Y \quad (B_{10} \text{filter}) \tag{27}$$

X and Y can be determined from the observed deflections and from equation 8.

Solving the above two equations we get -

$$R_{6300} = \frac{X\, T'_{OH} - Y\, T_{OH}}{T_{6300}\, T'_{OH} - T'_{6300}\, T_{OH}} \tag{28}$$

$$R_{OH} = \frac{X\, T'_{6300} - Y\, T_{6300}}{T_{OH}\, T'_{6300} - T'_{OH}\, T_{6300}} \tag{29}$$

Similarly from observations with photometer (i) and (iii) we can determine the intensities of OH (8-2) and 5893 A. A sample curve for 6300 is given in Figure 3.4. For this method it is necessary to have two filters which cover the entire region of OH band and the emission line, with different transmission percentages so as to account properly for the OH contamination in 6300 A observations and in turn determine the OH band intensity. The background subtraction has to be properly accounted for. Thus this method is preferable to the method of using very narrow band filters and facing the inherent difficulties in their use.

Accurate determination of airglow intensities is very necessary for studying the long term variations of airglow intensities, quantitative study of solar terrestrial effects, Barbier's relation, and also to understand the relative importance of the various reactions giving these emissions.

3.5 Corrections to be applied to the observed deflections:

In what follows, the procedure of correcting the observed intensities is described. These relations are used with the observed deflections which are measures of the intensities.

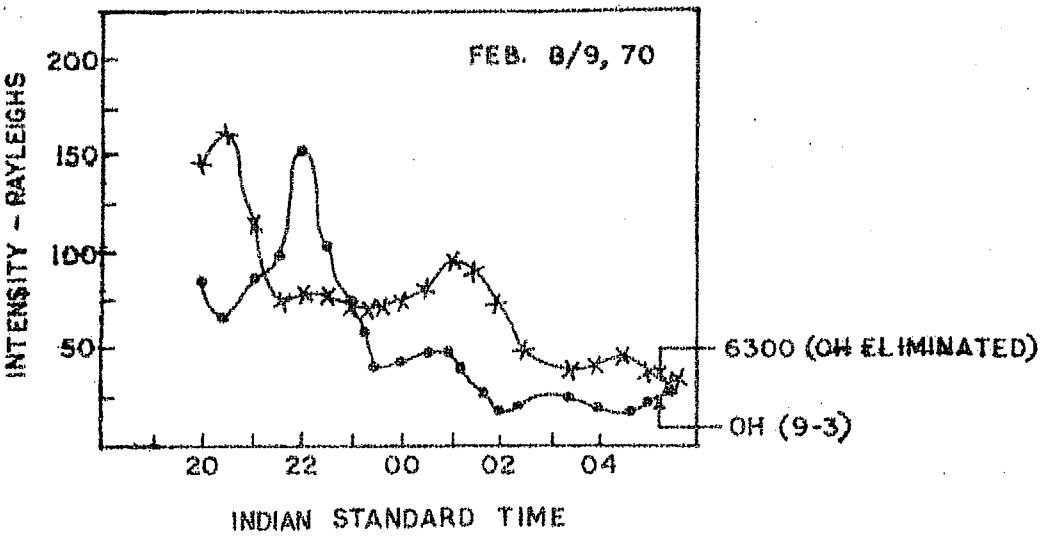

FIGURE 3.4 Example of the nocturnal variation of OH (9-3) and 6300 A. The OH (9-3) contamination in 6300 A observation is eliminated from the responses of 6300 A filters used on different photometers.

Two types of correction have to be applied to the observed intensities, because the emitted light from an extended layer has to travel through the atmosphere below it to reach the photometer. So the observations have to be converted to the values just below the emitting layer or "in the absence of lower atmosphere". After this conversion, the observations are referred to as the "observations outside the atmosphere".

3.5.1 Atmospheric correction:

Because the airglow layer is considered to be a uniformly diffused light source and the photometer has a finite field, some intensity is added due to scattering which must be subtracted and some intensity is subtracted due to attenuation by molecular and aerosol scattering, and absorption by water vapour, ozone etc. in atmosphere; this must be added.

The usual practice (IQSY manual 1963) has been the following. If I' is the observed intensity at any wavelength from a ground-based photometer, then the intensity I outside the atmosphere is obtained by

$$I = (I' - Sc)\, Ex \qquad (30)$$

where Sc is the scattering term

Ex is the extinction term.

3.5.2 Scattering correction:

As a first approximation the scattering is proportional to $(1 - e^{-\tau_1 M})$ where τ_1 is the molecular scattering coefficient and $M = m_o$. Sec Z where m_o is the mass of the atmosphere vertically overhead, at the observing station and Z is the zenith angle.

In Table 3-VI the relative airmass for different zenith angles for Mt. Abu is given. In Table 3-VII the wavelength dependent molecular scattering coefficients as compiled by ALLEN (1963a) are given.

3.5.3 Extinction correction:

After correcting the intensity for scattering as described above, it is corrected for extinction by multiplying by a factor $e^{\tau_2 M}$ where τ_2 is the total extinction coefficient which is again wavelength dependent and is contributed by scattering, due to dust, haze, water vapour, and ozone etc.

TABLE 3 - VI

Relative Air-mass at different Zenith angles.

Zenith angle	75°	70°	60°	40°	0°
Air Mass Mt. Abu	3.29	2.49	1.72	1.12	0.86

Air Mass is taken as unity for see-level zenith
Air Mass at Mt. Abu zenith = 0.86.

TABLE 3 - VII

The molecular extinction coefficient (τ_1) and assumed total extinction coefficients (τ_2) at different wavelengths.

Wavelength in A	τ_1 molecular extinction coefficient	τ_2 Total extinction coefficient(assumed)
5300	0.1120	0.248
5350	0.1080	0.240
5577	0.0910	0.225
5750	0.0800	0.215
5893	0.0720	0.206
6080	0.0630	0.195
6300	0.0540	0.180
6860	0.0380	0.150
7270	0.0310	0.120

In Table 3-VII the values of τ_2 which are estimated from our experience are given. These values are used for the en masse data reduction of observations with the fixed photometers (Pole and Red). In the reduction of the scanning photometer data, the extinction coefficients determined on the individual nights are used. The extinction coefficients measured on the various nights in the years 1967-69 are tabulated and discussed in Chapter II.

Alternately, instead of assuming the scattering to be proportional to $(1 - e^{-\tau_1 M})$ ASHBURN (1954) has calculated the scattering values in terms of the incident zenith intensity for different zenith angles, using Chandrasekhar's radiative transfer equations. To use Ashburn's tables one must know m_o the airmass at the zenith of the observing station, h the height of the emitting layer, λ the wavelength of emission and 'a' the albedo of the ground. Albedo correction is small, and for ordinary ground (no snow) $a = 0.25$ is a fair value. Ashburn's tables have been widely used since 1954 for scattering corrections.

To use Ashburn's tables for different zenith angles other than the zenith one must have observations at zenith along with those at the other angles.

Under these circumstances, method given in Chamberlain's text book (1961d) to covert the observations to "outside the atmosphere" values can be used. In the scanning photometer data there are zenith observations, along with observations at various zenith angles. Hence for reducing scanning photometer data the method given in Chamberlain's text book, has been used. The method is briefly given below.

The intensity above the ozone layer is written

$$I_{inc}(-\mu) = I_o \qquad (31)$$

where I_o is the zenith intensity outside the scattering atmosphere, if the emission originates in an optically thin, plane parallel layer, $\mu = \cos Z$ where Z is the zenith angle of the observation. Then the intensity incident on the scattering atmosphere is

$$I(0|-\mu) = I_{inc}(-\mu)\, e^{-\tau_o/\mu} \qquad (32)$$

where τ_o is the optical thickness of ozone. The observed intensity at the ground is then

$$I(\tau|-\mu) = I_{inc}(-\mu)\, e^{-(\tau+\tau_o)/\mu} + I_{trans}(\tau|-\mu) + I^*(\tau|-\mu) \qquad (33)$$

$I_{trans}(\tau|-\mu)$ is the intensity of the scattered light due to molecular scattering.

$I^*(\tau|-\mu)$ is the scattered light due to ground albedo.

ASHBURN (1954) has given the values of I_{trans} and I^* in units of zenith intensity entering the atmosphere $I(0|-1)$, for several values of zenith distances of observations (i.e. μ) for a range of τ between 0.01 to 1.00 for h = 100 km, 200 km, 300 km and ∞. The values needed for intermediate τ and Z can be interpolated from those values.

The relation to be used between the observed and outside-atmosphere intensity is

$$I(\tau|-\mu) = I_{inc}(-\mu)\, e^{-(\tau+\tau_o)/\mu} + I_{inc}(-1)\, e^{-\tau_o} \times \left[\frac{I_{trans}(\tau|-\mu)}{I(0|-1)} + \frac{I^*(\tau|-\mu)}{I(0|-1)}\right] \quad (34)$$

where τ applies to the scattering atmosphere only and τ_o to the ozone layer.

According to this equation the values obtained from Ashburn's tables should be multiplied by $I_{inc}(-1)e^{-\tau_o}$ to give the total scattering component of the intensity.

$\mu = 1$ in the above equation gives zenith intensity.

$$I_{inc}(-1) = I_o = I(\tau|-1)\left[e^{-(\tau+\tau_o)} + e^{-\tau_o} \times \left\{\frac{I_{trans}(\tau|-1)}{I(0|-1)} + \frac{I^*(\tau|-1)}{I(0|-1)}\right\}\right]^{-1} \quad \text{——(35)}$$

Determining this zenith intensity, the intensity at an angle can be determined from equation (34). Substituting equation (35) in (34) and rearranging the terms we get -

$$I_{inc}(-\mu) = \left[I(\tau|-\mu) - I_{inc}(-1)e^{-\tau_o} \times \left\{\frac{I_{trans}(\tau|-\mu)}{I(0|-1)} + \frac{I^*(\tau|-\mu)}{I(0|-1)}\right\}\right] e^{(\tau+\tau_o)/\mu} \quad \text{——(36)}$$

where

$$I_{inc}(-1) = I(\tau|-1)\left[e^{-(\tau+\tau_o)} + e^{\tau_o} \times \left\{\frac{I_{trans}(\tau|-1)}{I(0|-1)} + \frac{I^*(\tau|-1)}{I(0|-1)}\right\}\right]^{-1}$$

The values of ozone amount at Ahmedabad are available for all days in the year, as measured with a Dobson Spectrophotometer. These values are used for determining τ_o values at the wavelengths of our interest. The method given by Chamberlain is used for reducing the scanning photometer data obtained in the years 1967-69.

.....

CHAPTER IV

5577 A AND 5890-96 A EMISSIONS IN NIGHT AIRGLOW

4. Introduction:

At Mt. Abu, observations of 5577 A (OI) green line and 5890-96 A NaI D lines were taken earlier by DANDEKAR (1961) during 1957-60 and later by PAI (1968) during 1964-67; and the results were discussed by them. The observations have been continued by the present author on all clear moonless nights since 1967. For obtaining additional information, all-sky scanning photometer observations have been taken on many nights since October 1967. The results of all these observations are discussed in this chapter.

A brief summary of 5577 A emission and 5890-96 A emission in night airglow is given in sections 4.1.1 and 4.1.2 respectively and the excitation mechanisms of these emissions are discussed.

The observational results of 5577 A and 5890-96 A, their statistical distribution, nocturnal and seasonal variations, spatial variations, and the correlation between

them are discussed in sections 4.2.1 through 4.2.5. In section 4.2.6, the effect of solar flares and magnetic storms on these emissions is studied.

4.1 Brief Review of the Earlier Work:

4.1.1 Atomic oxygen (OI) 5577 A emission:

5577 A (OI) line of atomic oxygen is the most prominent upper atmospheric emission in the visible part of the airglow spectrum. SLIPHER, (1919) at the Lowell Observatory discovered the green line 5577 A in the spectrum of the night sky. This was confirmed by RAYLEIGH (1922) in England. An evaluation of the several experimental measurements of wavelengths (BABCOCK, 1923; CABANNES and DUFAY, 1956; etc.) gave a wavelength 5577.345 $\pm$ .002 Å. The line was produced by McLENNAN and SHRUM, (1924) in the laboratory.

McLENNAN McLEOD and IRETON (1928) and RAYLEIGH. (1929) reported a maximum in the intensity of 5577 A near midnight from mid-latitude observations. Since then, people in many countries including India, have studied this emission and its nocturnal variations. ANGREJI (1961) from Srinagar data and DANDEKAR, (1961) and PAL (1968) from Mt.Abu data drew attention to a seasonal variation in the

time of occurrence of the midnight maximum. SILVERMAN (1964) and later BRETON and SILVERMAN (1970) concluded from the IGY data of 22 stations that the diurnal variation was not the same everywhere but shows marked variations. Even at the same station, the diurnal variation can be markedly different in different seasons. Statistically significant regular nocturnal variations are not found at higher latitudes.

Lord Rayleigh using colour filters studied the seasonal variation of 5577 A emission from 1923 to 1927, and found that it had a minimum brightness in December and two maxima in March and in October. Later, many people with improved techniques of observation and narrow band filters have studied the seasonal variation(RAYLEIGH and SPENCER JONES, 1935; DANDEKAR et al., 1961; DANDEKAR, 1961; CHRISTOPHE GLAUME, 1965; ANGREJI, 1967; PAL, 1968) and substantiated the earlier finding by RAYLEIGH (1928).

The variation of 5577 A (OI) emission intensity with sunspot cycle was first pointed out by RAYLEIGH and JONES (1935). Subsequent published studies have provided information on this variation (RAYLEIGH and JONES, 1935; DUFAY and TCHENG, 1946; DUNCAN, 1960; NAKAMURA, 1961; HERNANDEZ and SILVERMAN, 1964; ROSENBERG and ZIMMERMAN, 1967; ANGREJI, 1967). SILVERMAN (1968) has reviewed

the literature on the day-to-day variation of 5577 and the effect of magnetic disturbances and solar activity. BARBIER (1959) found an increase in the mean annual intensity of 5577 A corresponding to an increase in sunspot number from 1953 to 1958 at Haute Provence. ROACH (1955) on the other hand reported no correlation between mean annual green line intensity at Cactus Peak (36°04' N, 117°48' W) California and sunspot number in 1949-53. More recently, HERNANDEZ and SILVERMAN (1964) using data obtained at Sacromento Peak (32°43' N, 105°45' W) New Mexico during the 1953-62 period found a correspondence between mean annual green line intensity and Zurich sunspot number. CHRISTOPHE-GLAUME, (1965) considering the data covering a solar cycle beginning in July 1953, also found that the mean annual and monthly intensities of the green line showed a positive correlation with the Wolf numbers averaged for the corresponding periods. DANDEKAR, (1961) did not find a relation between 5577 A emission and sunspot number on a day-to-day basis from Mt.Abu data during IGY.

The influence of solar flares of class 2+ or 3 on the variation of 5577 A was examined by DANDEKAR (1961) and subsequently by DANDEKAR and SILVERMAN, (1964). From these studies it was concluded that a substantial increase in 5577 A intensity occurred on nights following solar flares.

RAYLEIGH and SPENCER JONES (1935) found from the Capetown observations that the intensity of 5577 A emission was greater on magnetically disturbed days. DUFAY and TCHENG MAO-LIN (1947) found negative correlation, while MANRING and PETTIT (a, b,) (1958) found no correlation between the two phenomena. SANDFORD (1964) reported an increase in 5577 A emission with increase in magnetic activity. An increase in the green line intensity following sudden commencement storms has been noted by CHRISTOPHE-GLAUME, (1965); WEILL and CHRISTOPHE-GLAUME (1965) and SILVERMAN and BELLEW (1965). CHRISTOPHE-GLAUME (1965) noted that magnetic storms having sudden commencement were followed by an 8% increase in intensity 45 minutes later at Haute Provence, and by 10% increase at Tamanrasset(Sahara) one hour later. WEILL and CHRISTOPHE-GLAUME (1965) noted that about two hours after the sudden commencement the intensity of 5577 A (OI) increased again and correlated with Δ H during the main phase.

The study by SILVERMAN and BELLEW (1965) at Sacromento Peak, New Mexico confirms the existence of an increase following sudden commencement of a magnetic storm. The delay time of the intensity is of the order of one hour following sudden commencement, similar to that observed at Haute Provence and Tamanrasset. However, SILVERMAN and BELLEW (1965) found from the Sacromento Peak data that the effects begin some hours prior to the onset of sudden commencement.

The idea that there are zones of maximum intensity and that there are cells of diameter ~ 2500 kms has been examined by ROACH et al. (1958b) and BARBIER and CHRISTOPHE-GLAUME (1959). It was found that at Fritz Peak (39.9°N) and Haute Provence (43.9°N) the southern sky was brighter, while at Sacromento Peak (32.7°N) and Cactus Peak (36°N) the northern sky was brighter. The seasonal variation of the zone of maximum intensity was studied at Fritz Peak by ROACH (1959).

Rocket measurements in the middle latitudes have shown that the height of emission of 5577 A is near 100 km. A second layer of 5577 A emission which in low latitudes makes a substantial contribution to the intensity of 5577 A has been shown to be present at F layer heights (KULKARNI, 1965; GULLEDGE et al., 1966).

The most important contribution to the theory of 5577 A night airglow was made by CHAPMAN (1931). He hypothesised that the most likely excitation mechanism was the recombination of two oxygen atoms in the presence of a third oxygen atom with the energy of recombination appearing in the electronic excitation of the third atom. He placed the height of emission at 100 km. A more recent version of this theory is given by BARTH (1964). He has argued that the energy of recombination first appears as electronic energy in the oxygen molecule that is formed in the recombination.

$$O + O + M \longrightarrow O_2^* + M$$

where O_2^* is an excited oxygen molecule in a level higher than 4.16 eV. The electronic energy is transferred to the oxygen atom in a subsequent collision as

$$O_2^* + O \longrightarrow O_2 + O^*$$

A consequence of this mechanism is that above the maximum at 97 km the intensity of the 5577 A emission is proportional to the product of the square of atomic oxygen concentration times the neutral particle concentration.

$$I_{5577} = [O]^2 . [M]$$

Below this level where collisional deactivation of the excited intermediate molecule is important the intensity is proportional to the cube of the atomic oxygen concentration.

$$I_{5577} \sim [O]^3$$ (BARTH, 1967)

Further calculations on the relative importance of the above mechanisms were done by TOHMATSU and NAGATA (1963) and LAGOS (1968). Thus there is a great deal of information

about the morphology of 5577 A emission in the night airglow. However, the causes of the variations observed in 5577 A are not yet firmly established.

4.1.2 Sodium 5890-96 A emissions in the night airglow:

The resonance doublet 5890-96 of Na I was discovered by SLIPHER (1929) in the night airglow spectrum and identified conclusively by CABANNES et al.(1938) and BERNARD (1938a. b.c) Excellent reviews are given by CHAMBERLAIN (1961a); DONAHUE (1967) and GADSDEN (1967). Sodium D lines do not show a regular pattern of nocturnal variation. DUFAY and TCHENG (1946) reported a slow increase of intensity during the night. The sodium D lines show almost at all latitudes pronounced seasonal variation with a maximum in winter and a minimum in summer (DUFAY and TCHENG, 1946; PETTIT et al.,1954; MANRING and PETTIT, 1957; FISHKOVA, 1962; BARBIER, 1963; STEIGER, 1967; PAL, 1968). ROACH and PETTIT (1951) have shown that in the northern hemisphere the sodium intensity shows a minimum in summer and a maximum 3 to 5 times stronger in winter and this variation is six months out of phase with the annual variation in the southern hemisphere.

PACKER (1961) reported the data of two rocket flights measuring Na intensity with little contamination

from OH glow and duly corrected for background. He showed that Na D lines were observed from 70 to 107 km with peak at 84 km. CHAPMAN (1939) proposed that the reaction

$$Na\ O + O \longrightarrow Na^* + O_2$$

produces the night airglow Na emission. The essence of this suggestion is that this excitation, like that of the 5577 line, originates in atomic oxygen recombination. Inspite of changes in details, this reaction still seems acceptable. BATES and NICOLET (1950) in an analysis of the sodium problem doubted the exothermicity of the above reaction and suggested that

$$Na\ O_2 + H \longrightarrow Na\ H + O_2$$

$$Na\ H + O \longrightarrow Na^* + OH$$

as an alternative to the Chapman reaction. KRASSOVSKY (1958) and POTTER and DEL DUCA (1960) have postulated excitation by vibrationally excited O_2.

$$O_2^*\ (V \geqslant 16) + Na \longrightarrow O_2 + Na^*$$

This suggestion has been criticized by BALLIF and VENKATESWARAN (1962, 1963) who argue that the covariability of Na and OH nightglow follows from a combination of the Na O and Na H

processes but not from the O_2^* process. Further DALGARNO (1963) has indicated that there is reason to doubt that O_2^* can survive vibrational deactivation long enough to give excited Na^* to produce the nightglow emission at the observed rate.

BALLIF and VENKATESWARAN (1962) have indicated that the covariability of OH and Na glows in the night sky might follow as a consequence of the nocturnal variations of O_3 at their common levels of origin. The production of O_3 at the mesospheric levels depends on atomic oxygen. Thus in this chain of reactions, ultimately Na emission is dependent on concentration of atomic oxygen. Since 5577 A also depends on the atomic oxygen concentration we have considered the two emissions together and their possible interrelation in the following sections of this chapter.

4.2 Observational results:

4.2.1 Statistical distributions:

In Figure 4.1 a, the intensities of 5577 A at Mt.Abu during 1964-68 are plotted as a histogram by grouping the intensities in interval of 25 R, using all the half hourly data. The intensities around 50 R - 200 R are more frequent.

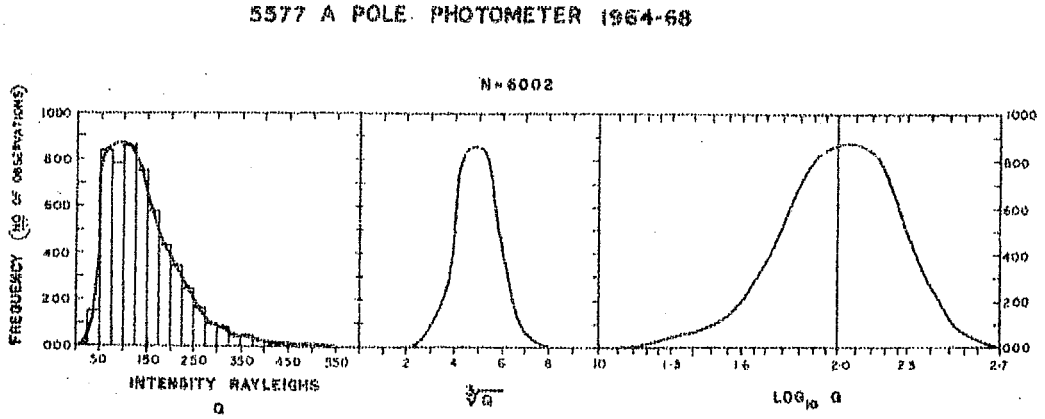

FIGURE 4.1 a Histogram of the intensities of 5577 A (Q) during 1964-68 grouped in intervals of 25 R.

FIGURES 4.1 b and c show the distributions with $\sqrt[3]{Q}$ and $\log_{10} Q$ respectively.

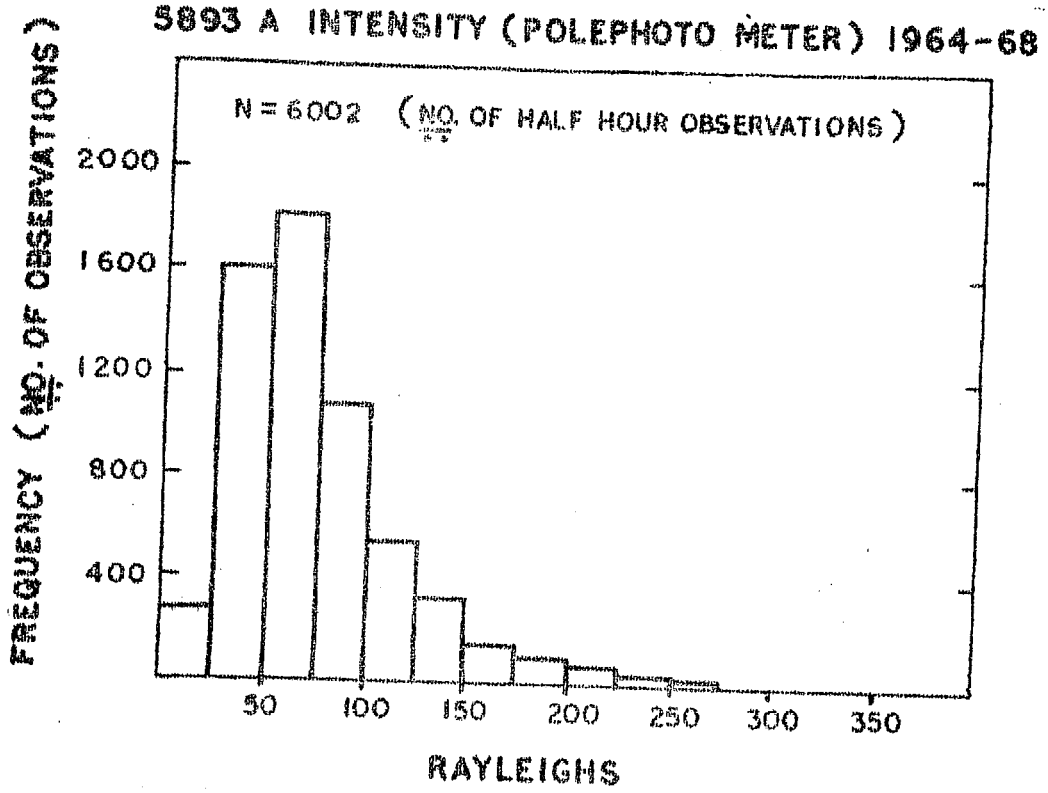

FIGURE 4.2 Histogram of the intensities of 5893 A during 1964-68 grouped in intervals of 25 R.

A positive skewness is shown in the intensity distribution as pointed out earlier by ROACH (1963a). The positive skewness is expected as on the low intensity side there is a definite boundary at zero intensity, whereas on the right side any intensity is possible. The skewness in the distribution may be empirically removed by using a cube root of the intensity or logarithm of the intensity as shown in Figure 4.1.b and Figure 4.1.c. The fact that the use of the cube root leads to an essentially 'normal' distribution is in support of the Chapman triple collision mechanism as the source of the excitation (BARBIER, 1960; ROACH, 1963a).

The histogram of 5893 A shows more frequent intensities around 25 R - 100 R (see Figure 4.2).

4.2.2 Nocturnal variation:

Figure 4.3 shows a few examples of nocturnal intensity variations of 5577 A emission in the year 1967-68. It shows three types of variation showing intensity maximum around midnight (22-02); after midnight (02-06), and before midnight (19-22). Considering all the nights data during 1964-68, it is noted out of 352 nights 200 nights (57%) showed a maximum around midnight, 63 nights (18%) showed

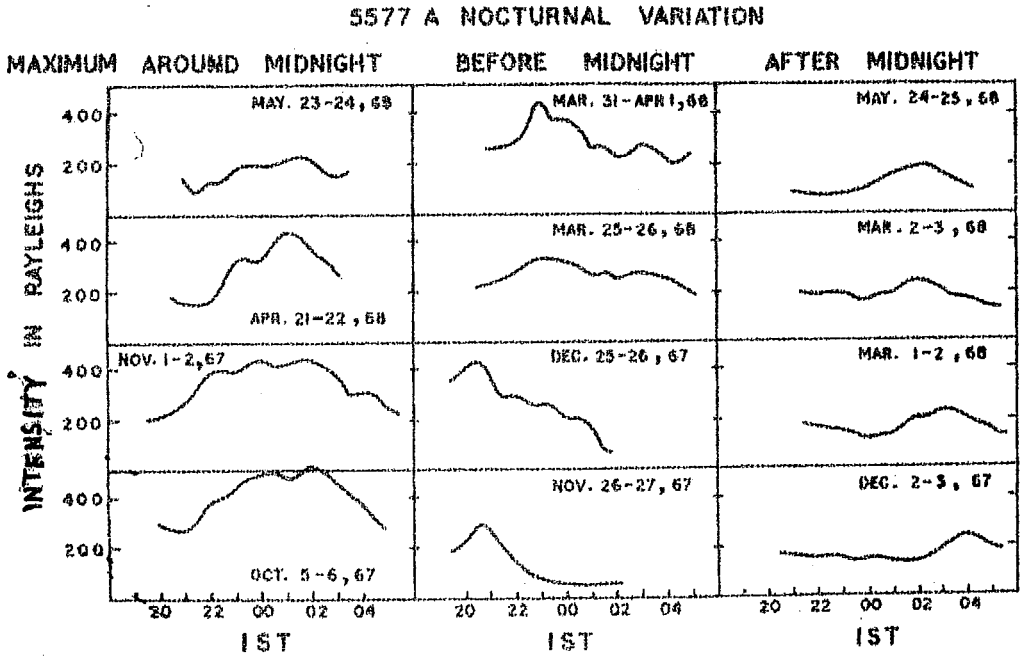

FIGURE 4.3 Nocturnal variation of 5577 A showing the types of variation on a few nights.

a maximum before midnight and 89 (25%) nights showed a maximum after midnight. The time of occurrence of the midnight maximum is different in different months. Analysing data of all the nights, it is noted that the midnight maximum is quite prominent in Equinoctial months, the time of occurrence being around midnight. In winter months, on many nights the maximum occurred before midnight. Thus on the average 5577 A shows a maximum intensity in the night, the time of maximum intensity being different in different months.

The nocturnal and seasonal variations of the intensities of 5577 A in the pole-ward direction from Nov. 1964 to May 1968 are shown in Figure 4.4. in a composite isophote map. Half-hourly average intensity values in each lunation were plotted lunation-wise and isophote lines plotted. The two maxima (cross hatched) of 5577 A one in October and another in April are seen in all the years; the October intensities being more than those in April. The large nocturnal variation with a broad maximum around midnight in April and October may be noted. The range of intensity variation during the night in November, December, January and February, in all the years was small while there were much larger intensity variations in the months of April-May, September-October.

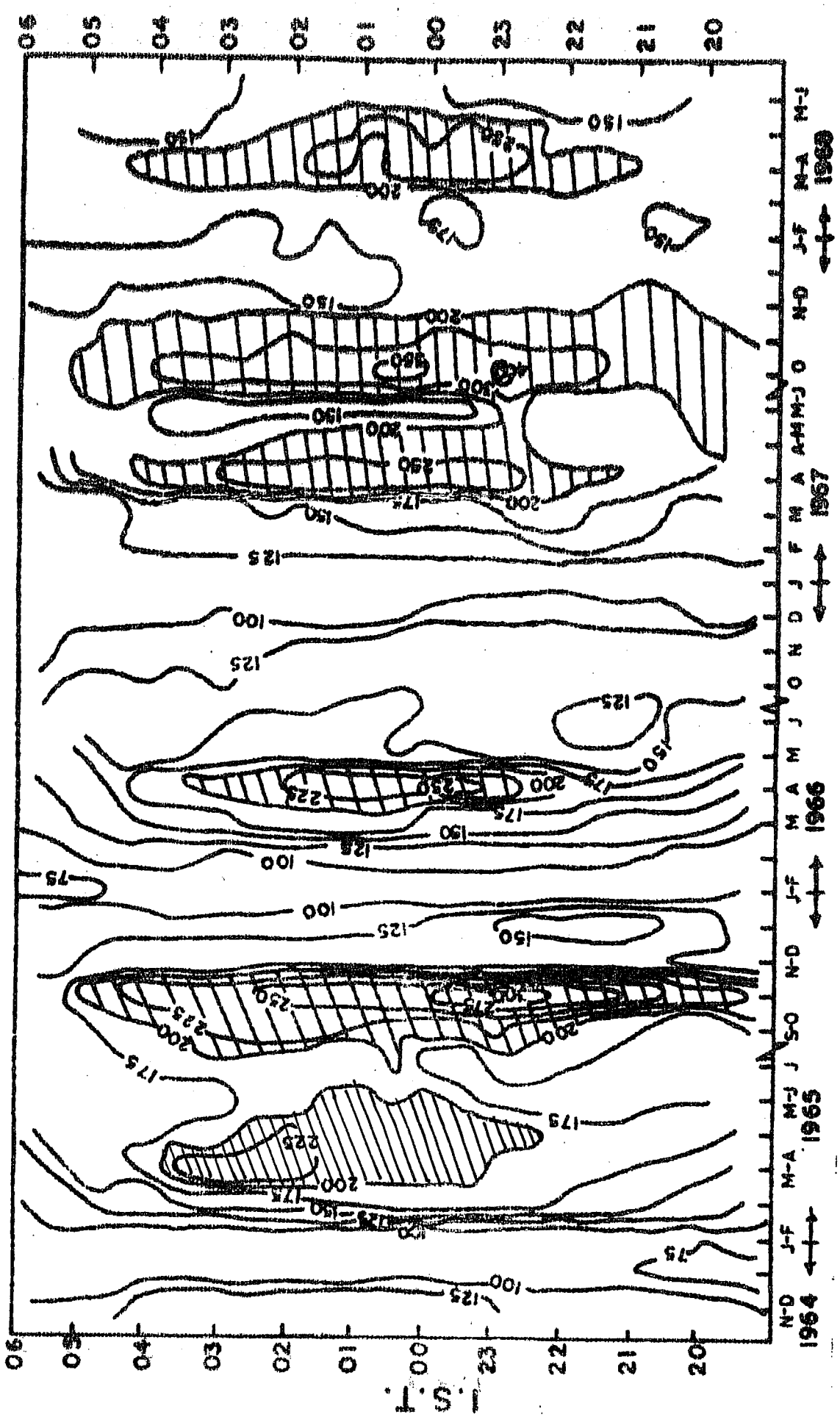

FIGURE 4.4 Isopleth map of 5577 Å (1964–1968)

The data of 5577 A from the scanning photometer were reduced by the procedure described in Chapter III. The slant intensities of all the zenith angles were converted to local zenith intensities using appropriate Van Rhijn factors. The data of the meridonal scanning of a few individual nights are presented in Figure 4.5. The data of one night in each lunation is presented. (In general, nights belonging to the same lunation showed the same general trends of variation). The maximum around midnight on October 5-6, 1967 and April 27-28, 1968 were clearly seen at all the latitudes covered by the scanning photometer. In November, December, January and February months, a maximum before midnight is noted in latitudes south of Mt. Abu. The isophote maps of a few nights (one in each of the months - October, December, Jan., are shown in Figure 4.6) which show the general behaviour of 5577 A at Mt. Abu and near latitudes.

Thus it can be concluded that 5577 A at Mt.Abu (24.6°N) shows a prominent maximum around midnight in April and October.

The nocturnal variation of sodium D lines (given in Figure 4.7 of a few nights in 1967-68) does not show any statistically obvious regular feature like 5577 A but shows

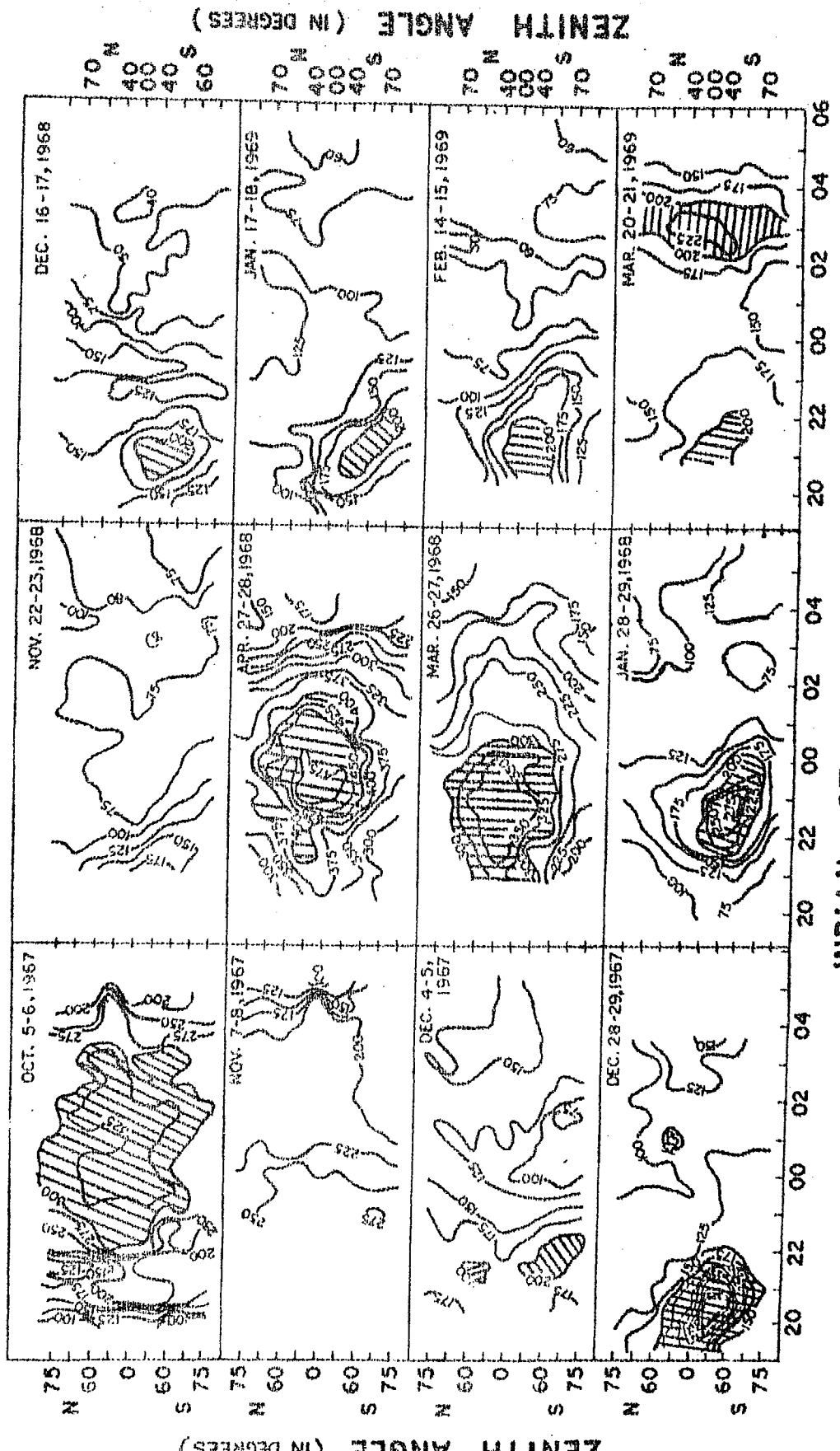

FIGURE 4.5 Meridonal scanning (75°, 70°, 60°, 40°, 0° zenith angles) of 5577 A.intensity. plotted as isophotes.

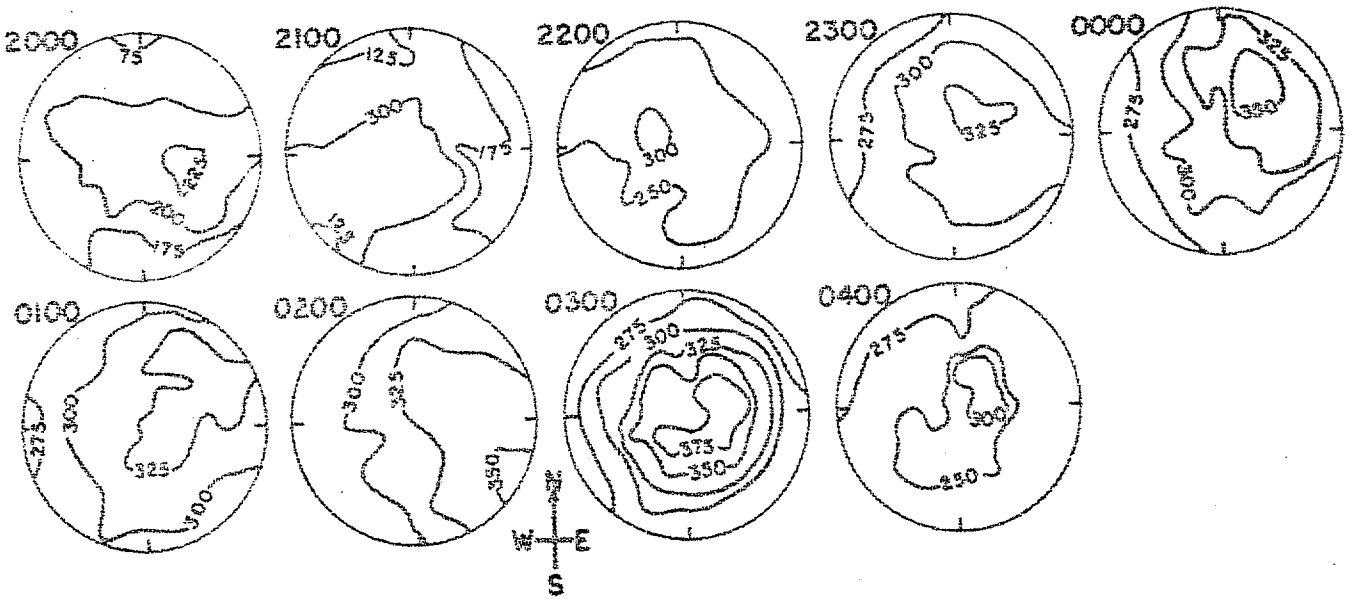

FIGURE 4.6 A Isophote maps of 5577 A on October 5-6, 1967.

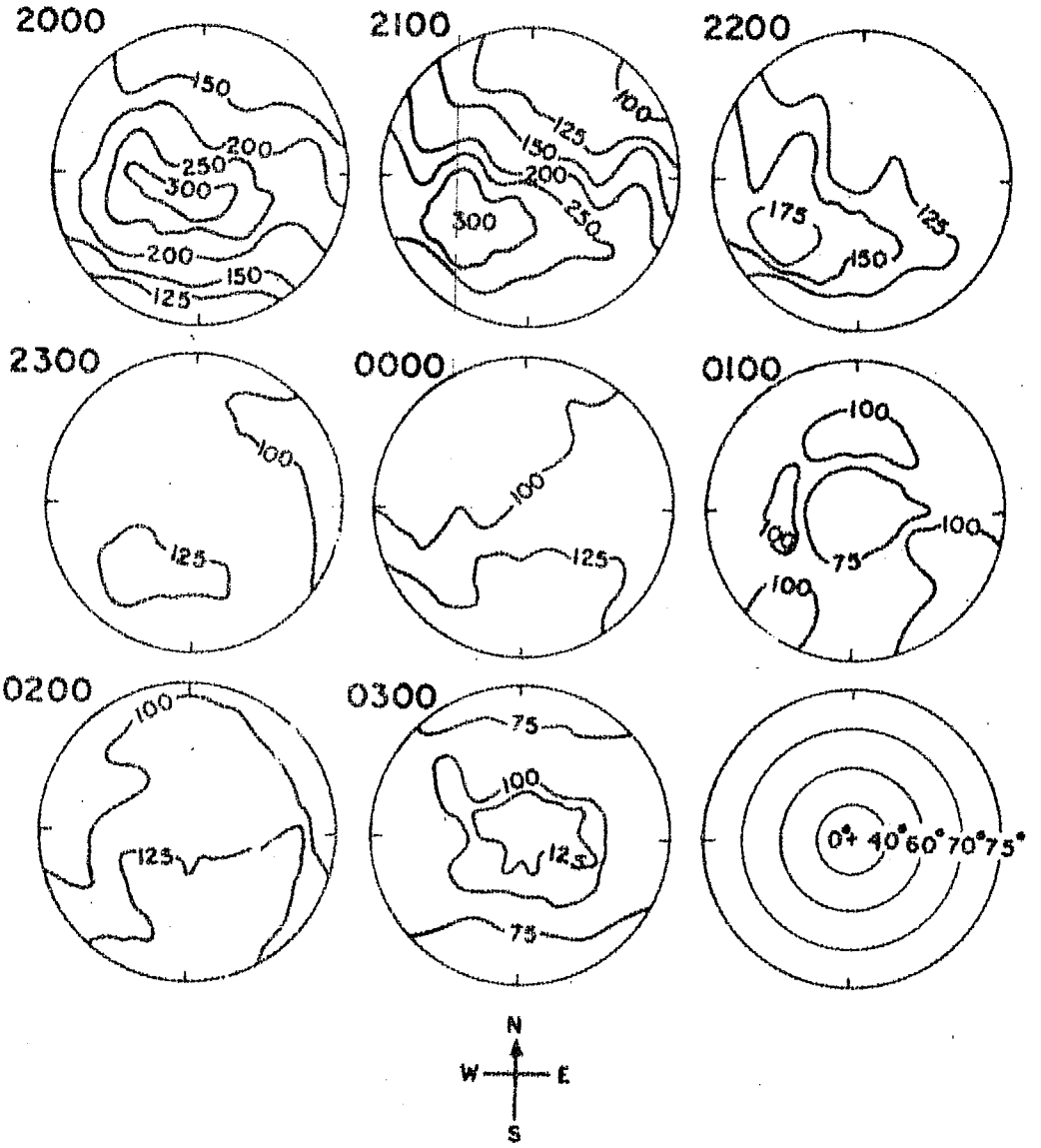

FIGURE 4.6 B - Isophote maps of 5577 A on December, 28-29, 1967.

MT. ABU 5577 A ISOPHOTE MAPS · INTENSITY IN RAYLEIGHS.
DEC. 29-30, '67

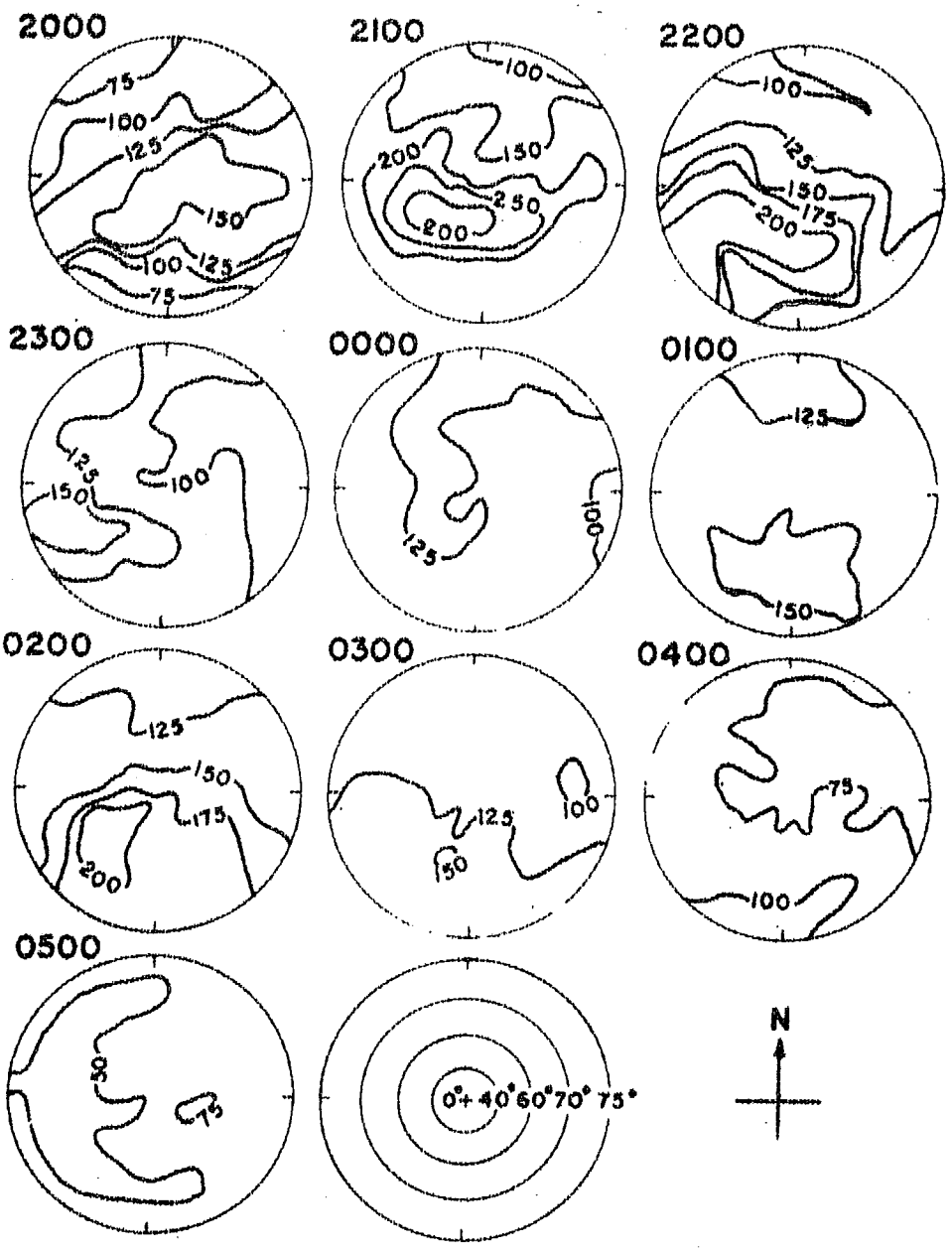

FIGURE 4.6 C - Isophote maps of 5577 A on December 29-30, 1967.

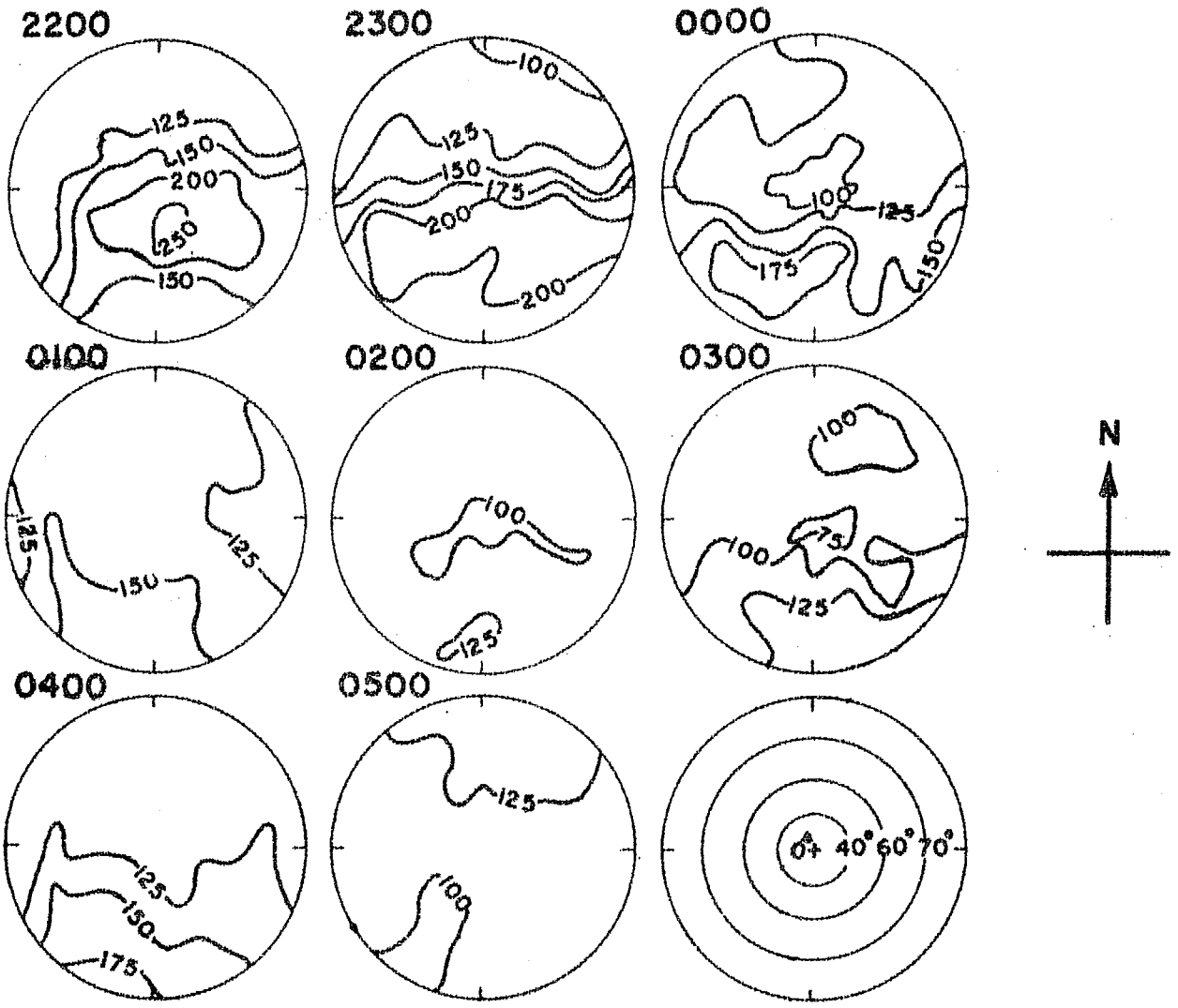

FIGURE 4.6 D - Isophote maps of 5577 A on January 29-30, 1968

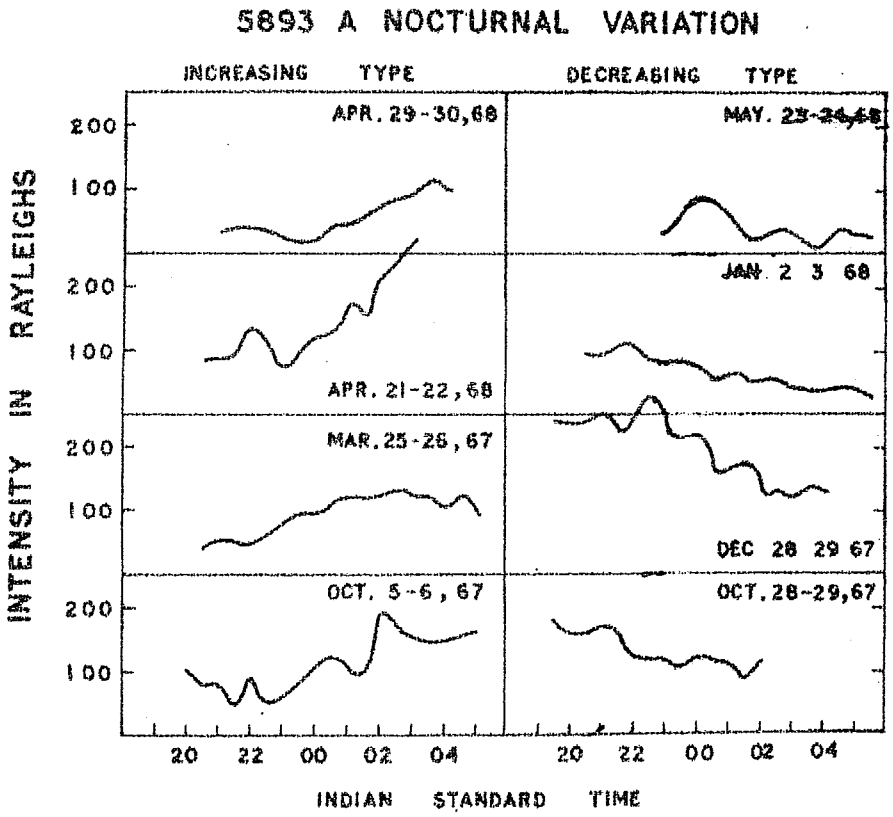

FIGURE 4.7 Nocturnal variation of 5893 A showing the two types of variation on a few nights.

a continuous increase or decrease in intensity. There is not much intensity variation during a night in the Na emission like 5577 A. It may be noted that at Mt. Abu, the intensity of 5893 A in more than 50% cases gradually increases throughout the night. Such type of continuous rise in intensity (see Figure 4.7) has been observed and reported by many people (DUFAY and TCHENG, 1946; ROACH, 1955; BARBIER, 1961. STEIGER, 1967). In other cases, the intensity of 5893 A slowly decreases or is more or less constant throughout the night. On many nights, intensity fluctuations are observed. Observations at Poona (CHIPLONKAR and AGASHE, 1961), Barbier's observations(1954)[a,b] at Haute Provence and Tamanrasset, and observations at Haleakala (STEIGER, 1967) show similar fluctuations in nocturnal variation of sodium intensity.

From the isopleth map given in Figure 4.8 for 5893 A (for 1964-68 data) it may be noted that in November, December and May, June months, the sodium intensity remains more or less the same in the course of a night. In October, March & April 5893 A intensity shows an increase towards morning. The meridonal scanning data of a few nights (one night in each lunation) are given in Figure 4.9. On October 5-6, 1967; November 3-4, 1967; April 27-28, 1968 5893 A intensity showed a continuous increase in the intensity. In December, January months

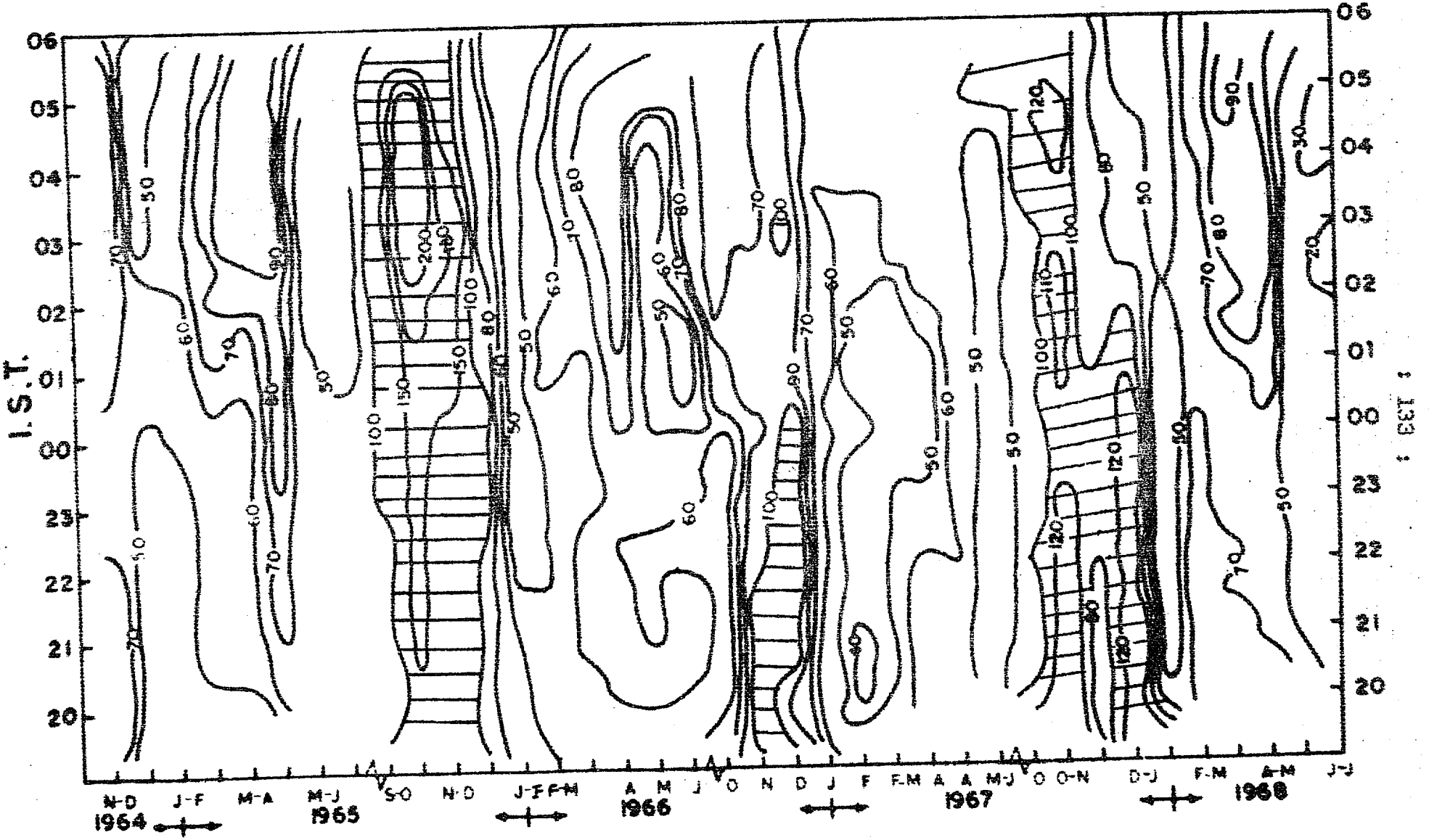

FIGURE 4.8 Isopleth map of 5893 A (1964-1968)

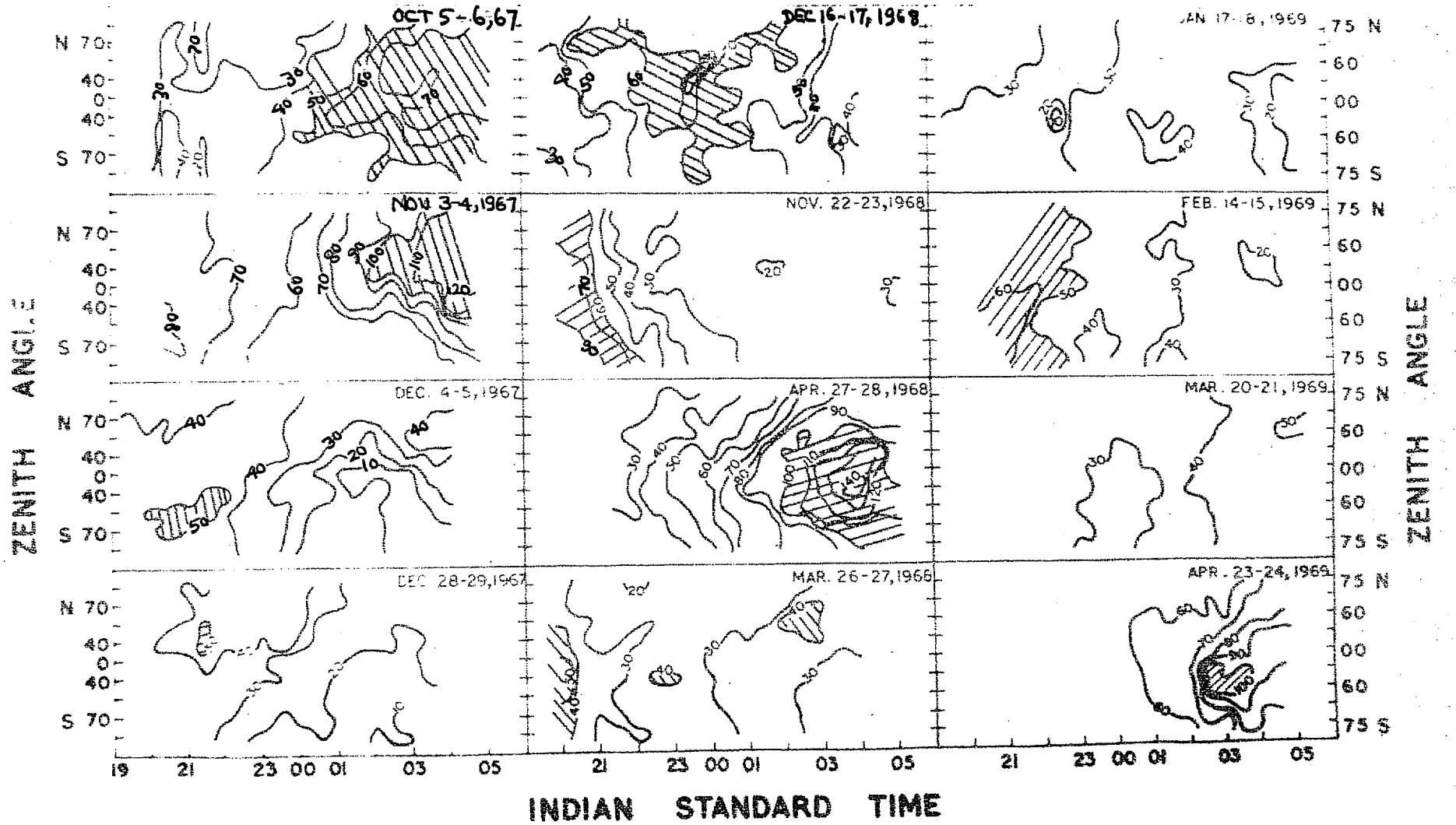

FIGURE 4.9 Meridonal Scanning (75°,70°,60°,40°,0° zenith angles) of 5893 A intensity plotted as isophotes.

there is not much variation during the night. The isolines are more or less vertical showing that the behaviour is in general similar at all the latitudes covered by the scanning photometer.

The isophote maps of a few nights when the intensity continuously increased and of a few nights when the intensity continuously decreased are shown in Figure 4.10 and Figure 4.11 respectively. Two nights are shown for each of the above types. It is noted that in the case of continuous increase type, (Figure 4.10) the regions became active within half an hour on both the nights October 5-6, 1967 and April 27-28, 1968. A cell formation near zenith can be noted. This cell developed in the successive isophote maps. Thus a continuous development of new cells with increased intensity occurred on both these nights. On December 18-19, 1968 the intensity increased from 2030 IST to 2130 IST and afterwards the intensity continuously decreased with some superposed fluctuations. Thus the development of cells in the case of continuously increasing type of variation and the irregular behaviour superposed cause a fluctuating pattern of sodium line intensity. This type of fluctuating behaviour has been noted on many nights at Mt. Abu.

MT. ABU 5893 A ISOPHOTE MAPS. INTENSITY IN RAYLEIGHS.
OCT. 5-6, 1967

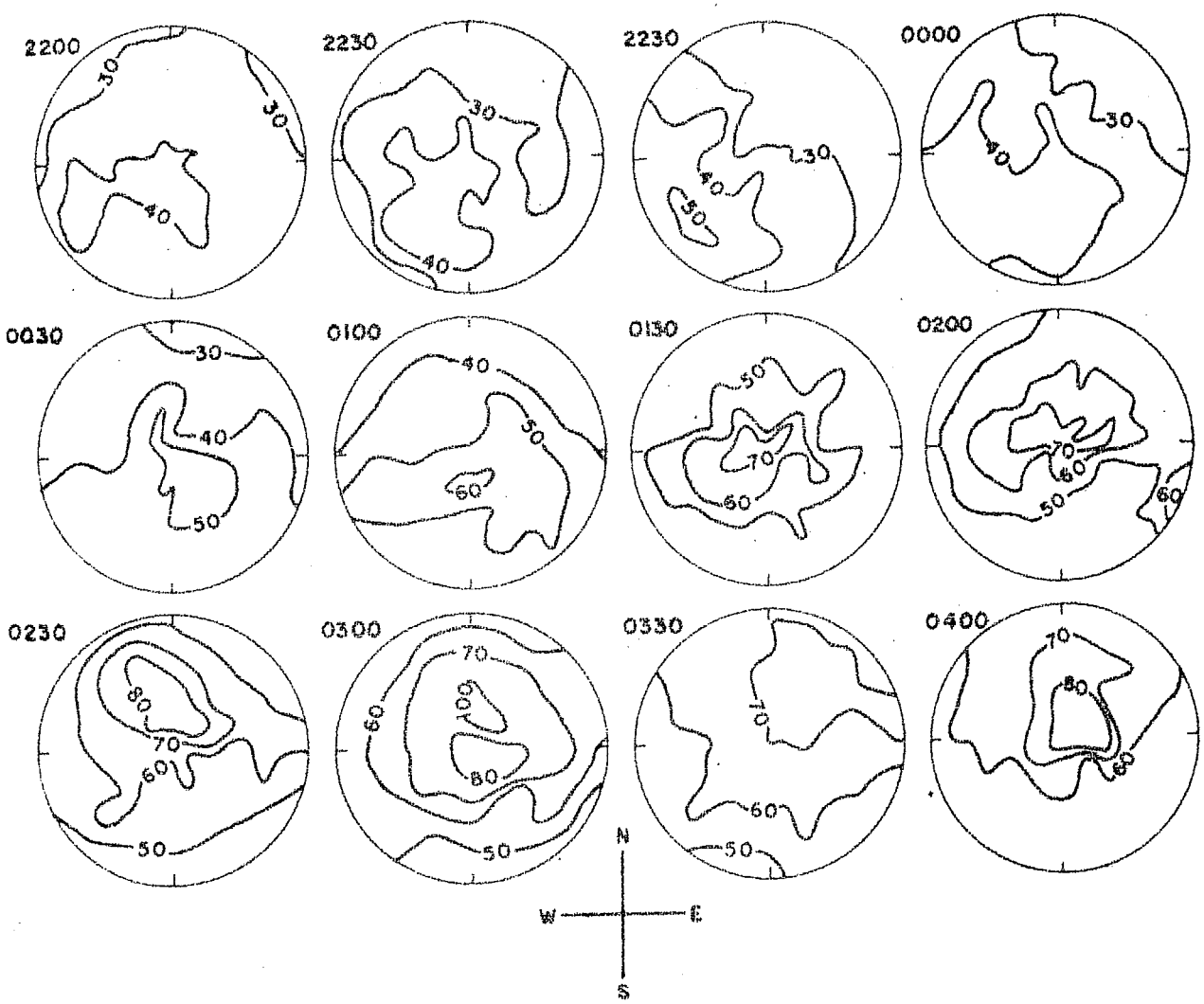

FIGURE 4.10 A - Isophote maps of 5893 A showing continuous increase in intensity up to 0300 hours IST on October 5-6, 1967.

MT. ABU 5893 A ISOPHOTE MAPS INTENSITY IN RAYLEIGHS
APR. 27 - 28, 1968

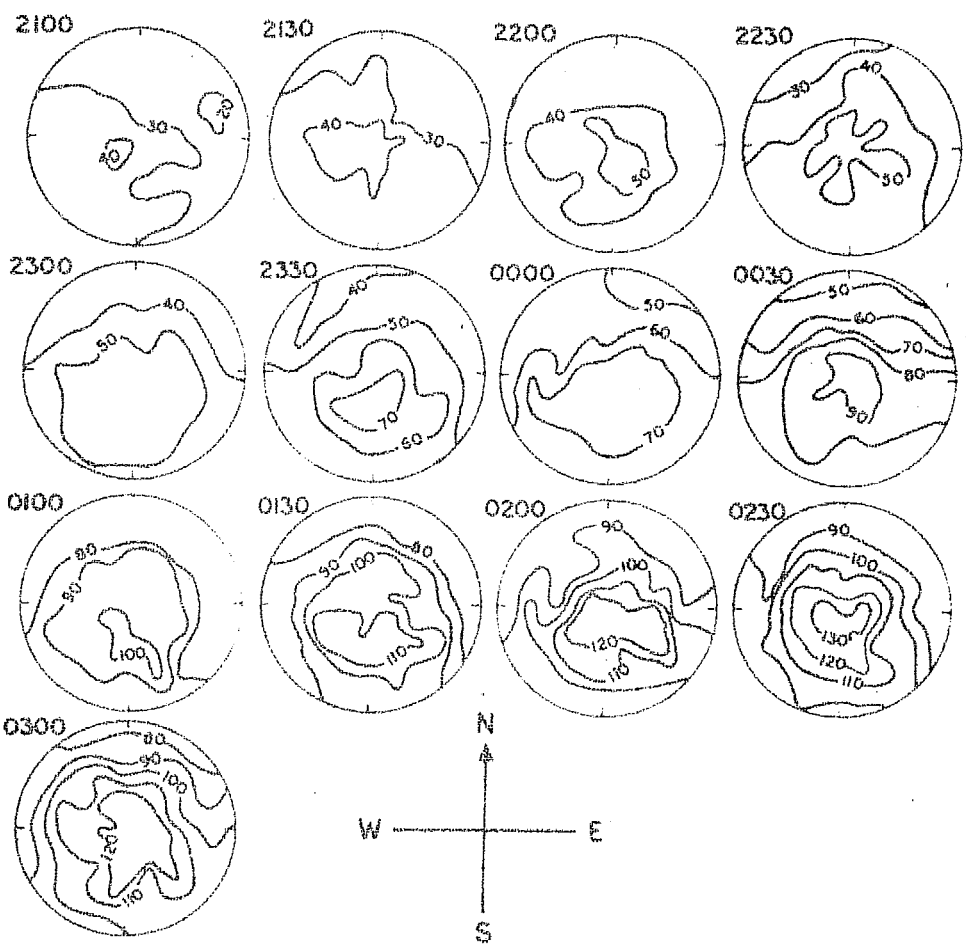

FIGURE 4.10 B Isophote maps of 5893 A showing continuous increase in intensity with time on April 27-28, 1968.

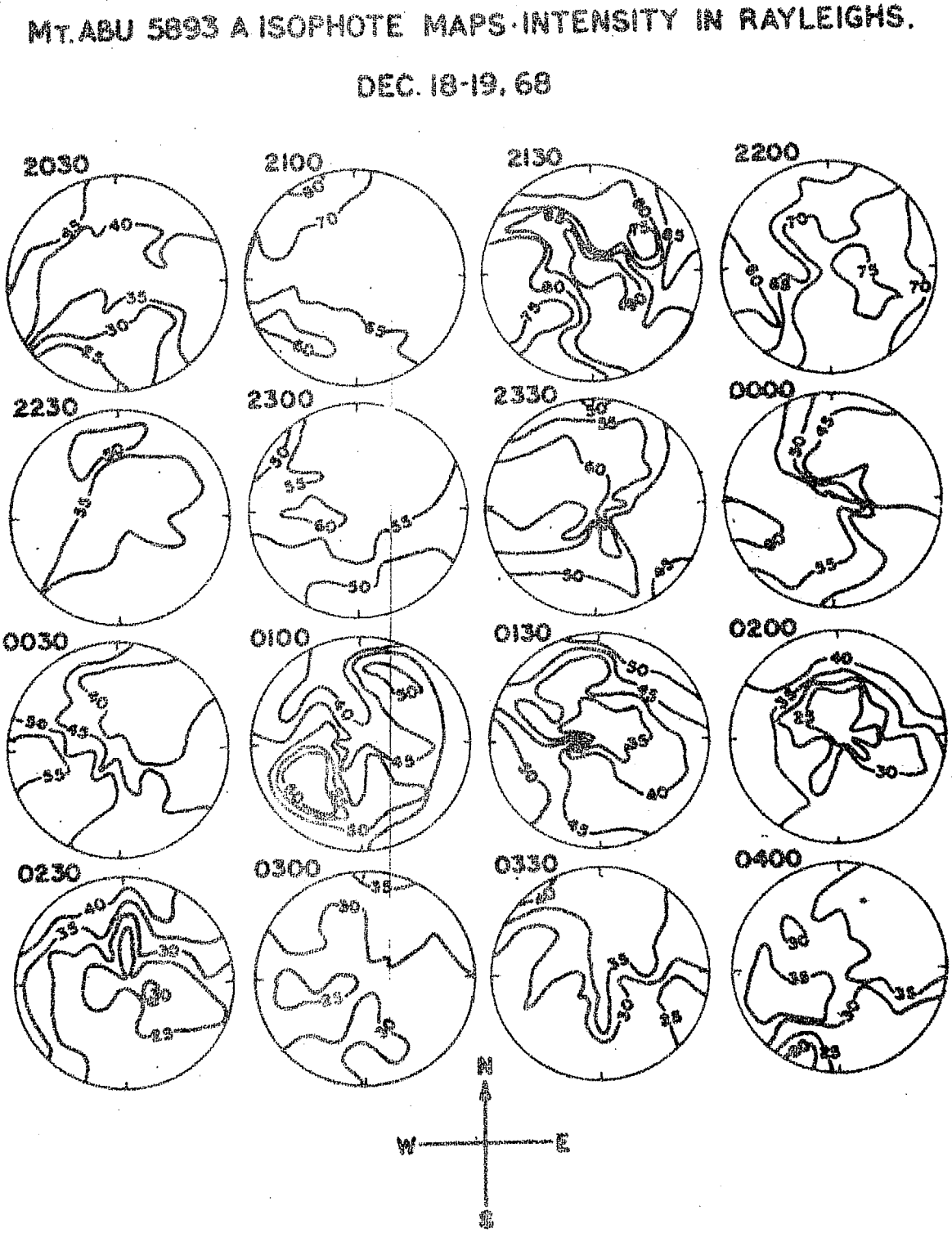

FIGURE 4.11 A - Isophote maps of 5893 A on December 18-19, 1967.

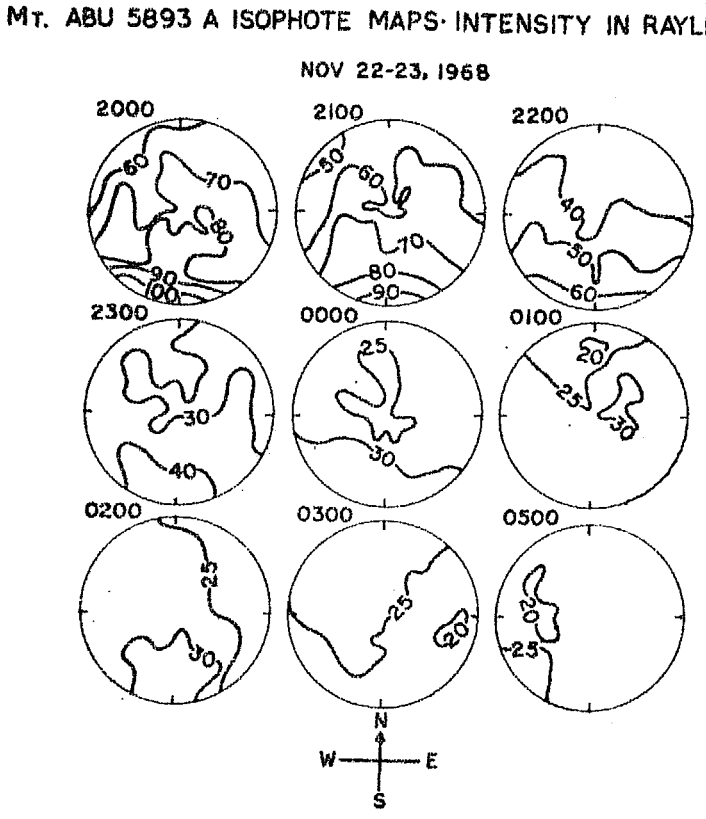

FIGURE 4.11 B Isophote maps of 5893 A showing decrease of intensity with time on November 22-23, 1968.

BALLIF and VENKATESWARAN (1962) have suggested that the sodium emission in the night airglow is governed by ozone concentration at the height of Na emission. BATES and NICOLET (1950) and WALLACE (1962) have given theoretical estimates of $n(O_3)$ by taking pure oxygen, and oxygen-hydrogen atmosphere at the appropriate heights. They have shown that after sunset the ozone concentration increases towards morning which increases the sodium emission (BALLIF and VENKATESWARAN, 1962).

Observations of Na intensity show that though on many nights, the intensity rises continuously, there are other nights on which it continuously decreases or remains steady during the night. If BALLIF and VENKATESWARAN (1962) hypothesis is assumed this leads to the conclusion that ozone has similar variations during these nights at the height of sodium emission.

4.2.3 Seasonal variation:

To study the seasonal variation, the half hourly intensities were averaged for each complete lunation round the new moon. The data from 1964-68 are presented in Figure 4.12 for 5577 A and 5893 A.

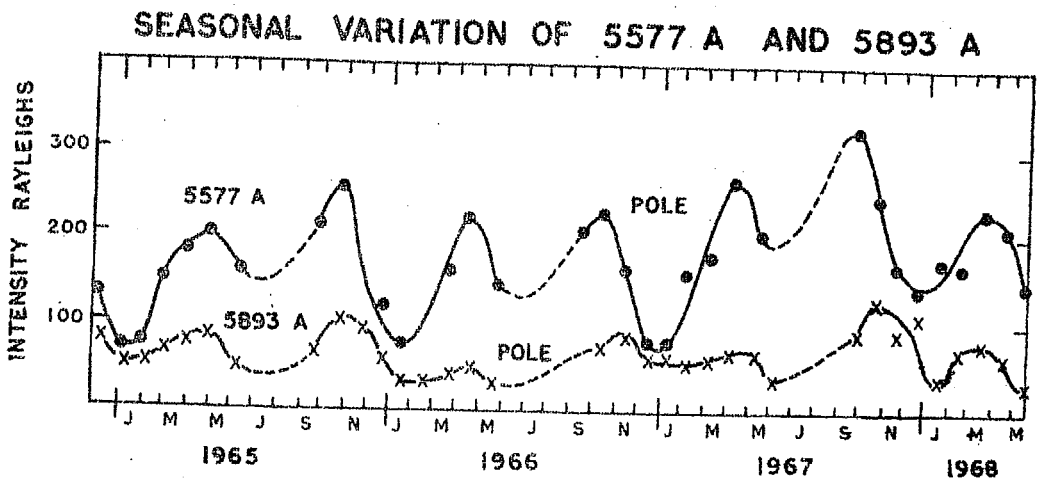

FIGURE 4.12 Seasonal variation of 5577 A and 5893 A (1964-1968).

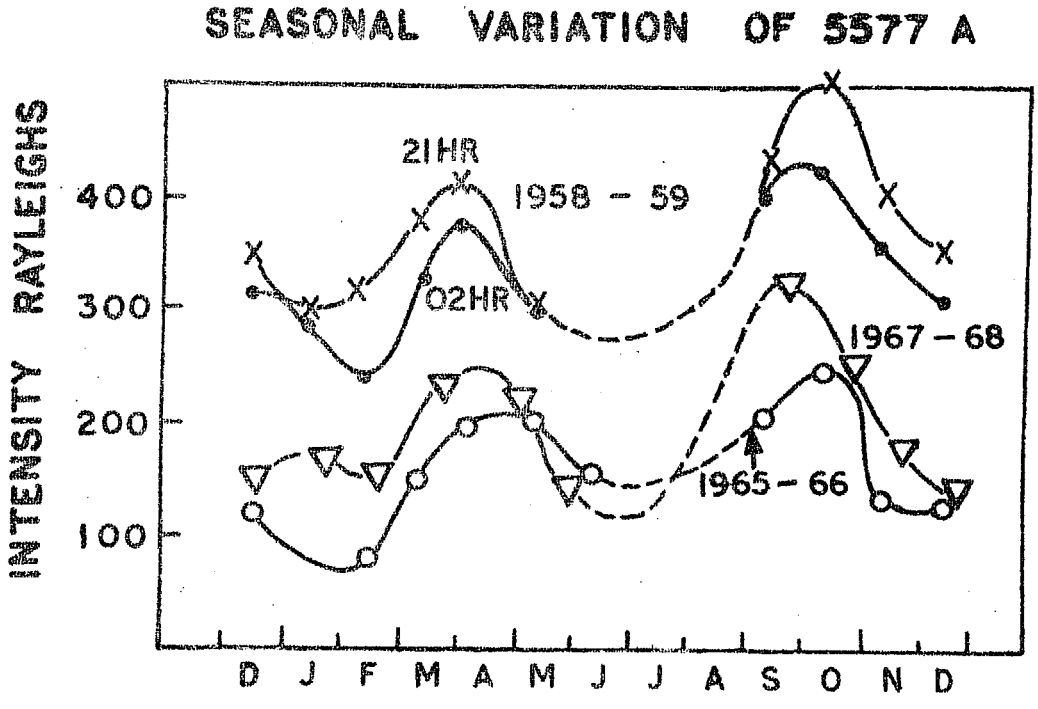

FIGURE 4.13 Seasonal variation of 5577 A in 1967-68 compared with 1965-66 and 1958-59.

Both 5577 A and 5893 A showed a minimum intensity in January in each of the years. A maximum is noted in April and a second maximum in October. The October maximum was stronger than the April maximum for both 5577 A and 5893 A emissions. Thus there is a broad similarity between the seasonal variations of 5577 A and 5893 A, but there seems to be a small delay in the occurrence of the maximum of 5893 A with respect to the 5577 A maximum. A similar conclusion was reached by DAVIES and McCORMAC, (1967).

The seasonal variation of 5577 A in 1967-68 is compared with those in 1965-66 (IQSY) and 1958-59 (IGY) (DANDEKAR, 1961)(Figure 4.13). The months of maximum intensity (October and April) and minimum intensity (in January) are noted in each of the years. In 1958-59, intensities were greater than in 1967-68 and the latter were slightly higher than in 1965-66. Thus year-to-year seasonal variation runs nearly parallel to solar activity.

It may be noted from the lunation average curves presented in Figure 4.14 that 5577 A intensities from November to March in 1967-68 were higher than the corresponding months in 1964-65. In April, May, June 5577 A intensities were smaller in 1967-68 (than those in 1964-65). In the case of 5893 A (Figure 4.15) there seems to be no solar cycle variation in contrast to 5577 A.

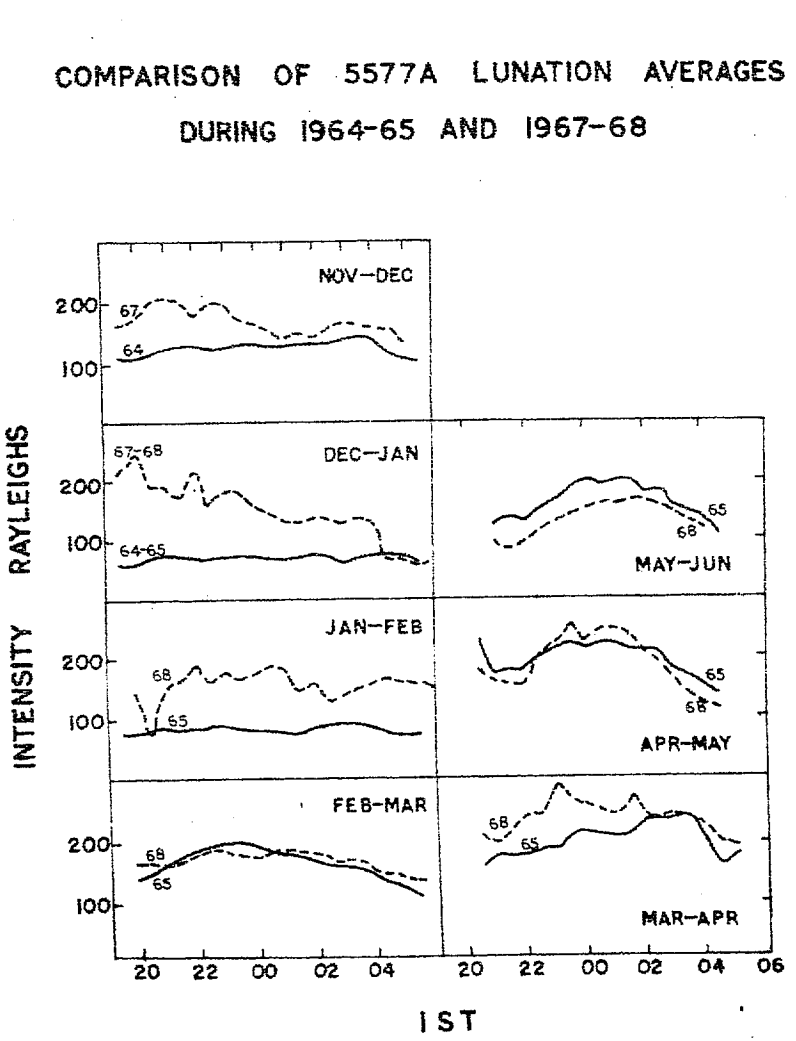

FIGURE 4.14 Average nocturnal variation of intensities of 5577 A in different lunations in 1967-68 and 1964-65.

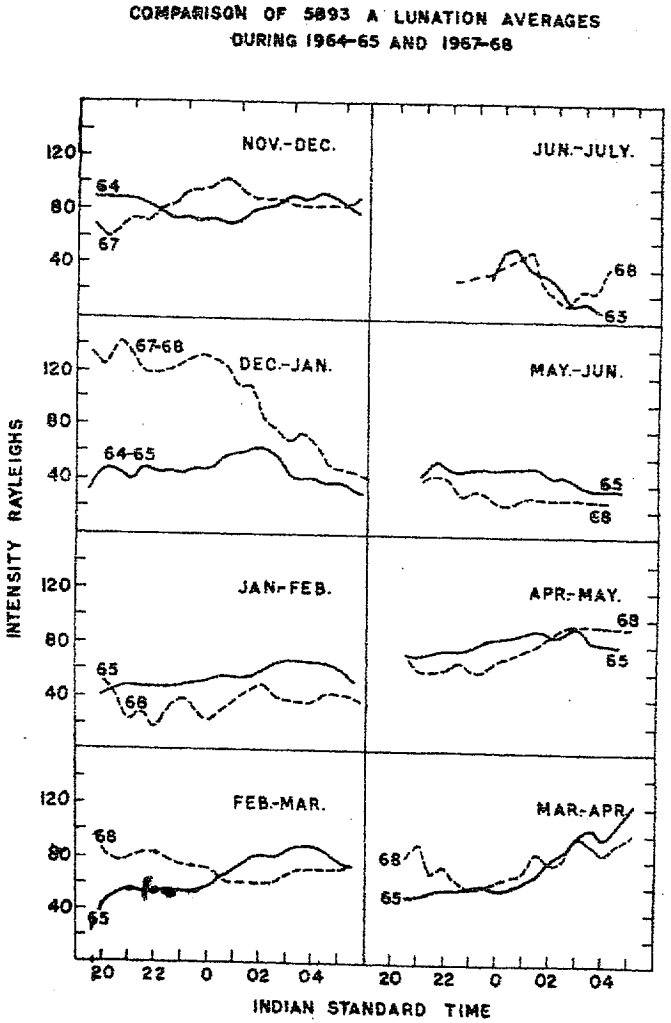

FIGURE 4.15 Average nocturnal variation of intensities of 5893 A in different lunations in 1967-68 and 1964-65.

4.2.4 Spatial Variations:

A simple technique of some usefulness is to compare the intensity at some zenith angle south to that at north. The greater the zenith angle the greater the latitude difference in comparison (STEIGER, 1967). 75^{o} zenith angle is chosen as the optimum angle in scanning the sky of Mt. Abu in consideration of the possibility of the various uncertainties at large zenith angles (extinction, definite field of views of the photometer etc. (ROACH, et al 1958.a. CHAMBERLAIN ;1961 d)

The average nocturnal variations of the intensity ratios of 75^{o} zenith angle south and north at Mt. Abu for 5577 A and 5893 A emission are shown in Figures 4.16 and Figure 4.17. The average values of the lunation are also plotted.

In the case of 5577 A, a maximum intensity ratio of 75S/75N is seen in January and a minimum in April. In the case of 5893 A a maximum is seen in February/March. Thus there seems to be an intensity maximum in south of Mt.Abu in the month of January and slightly later in the case of 5893 A. The average trends of the ratios in the course of a night can be seen in the Figures 4.16 and 4.17.

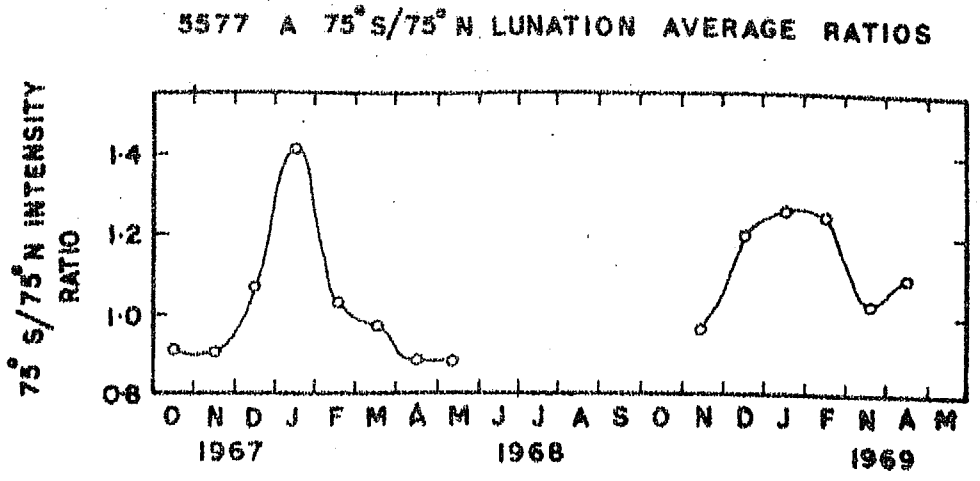

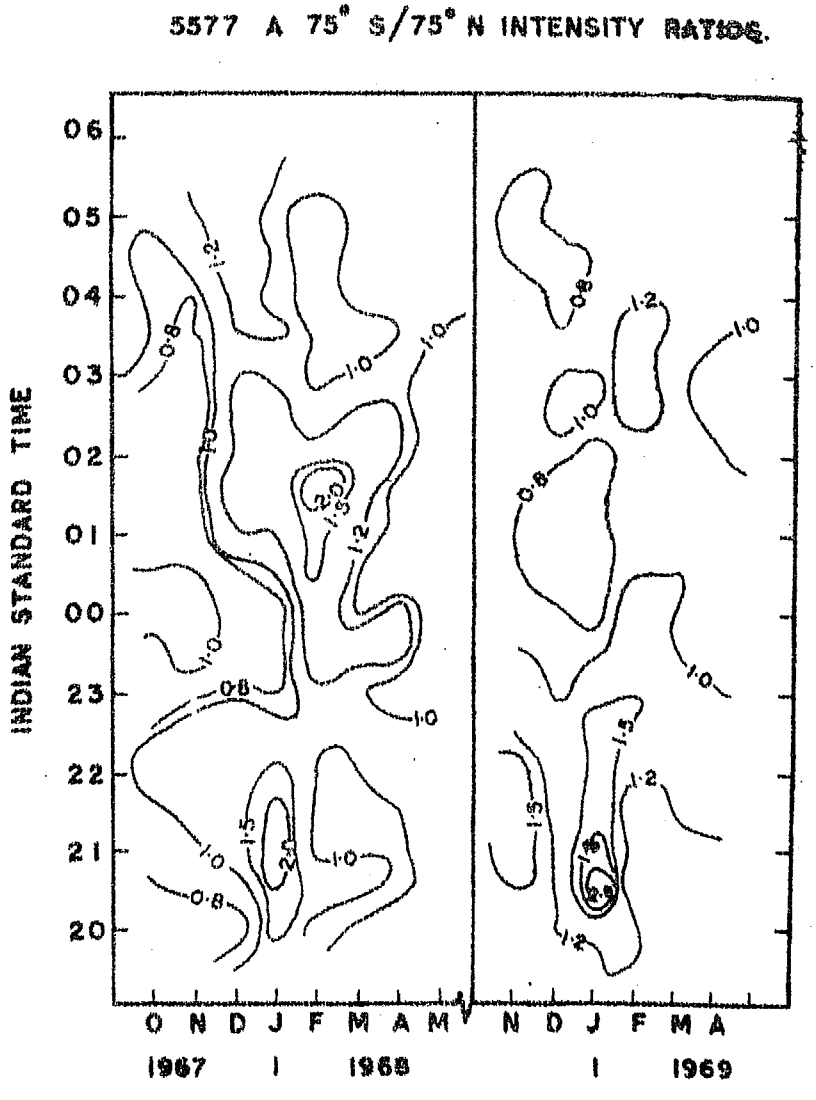

FIGURE 4.16 5577 Å intensity ratios of 75°S to 75°N zenith angles.

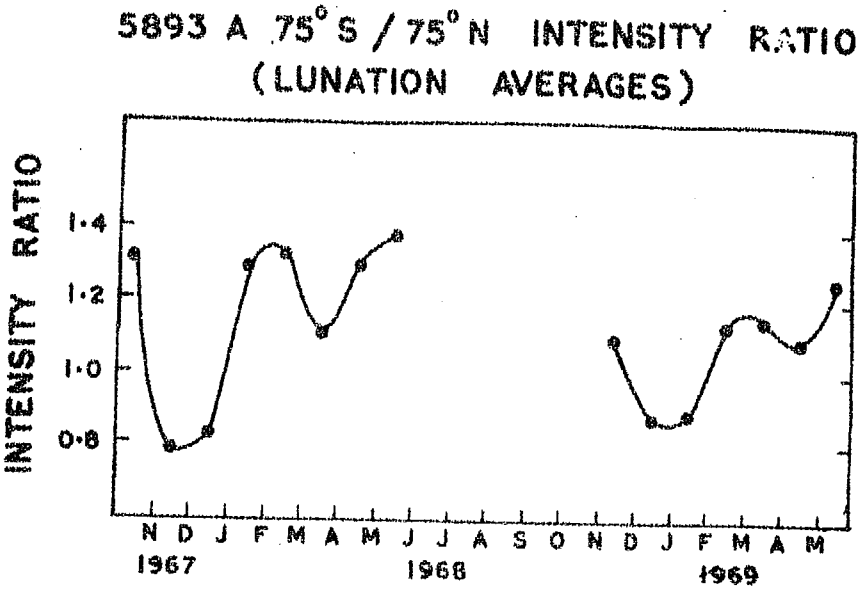

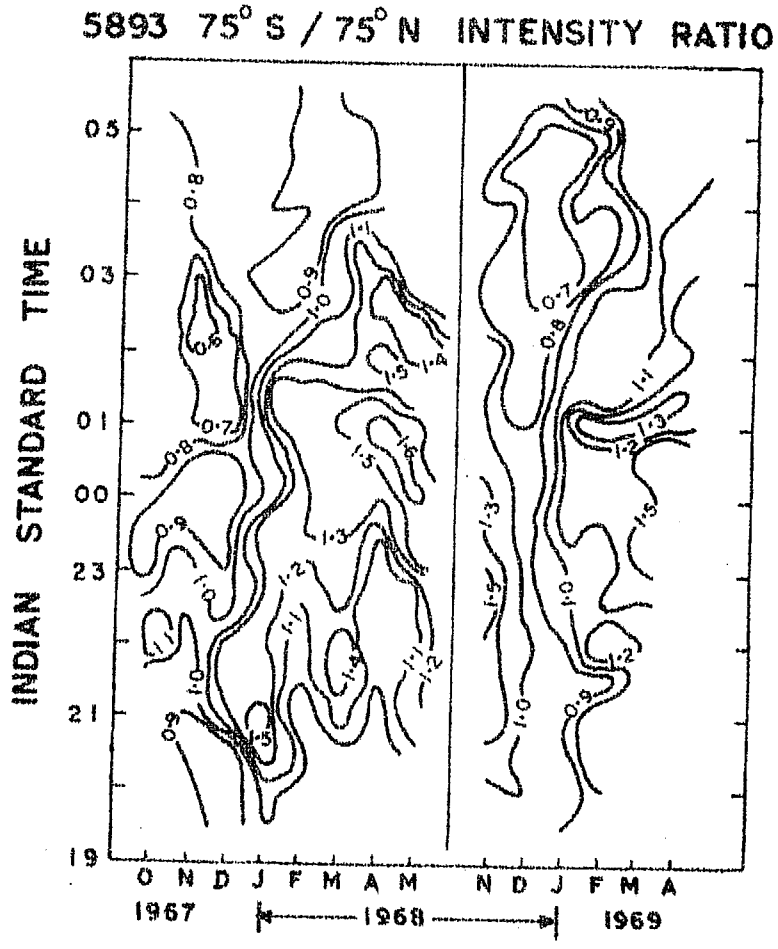

FIGURE 4.17 5893 A intensity ratios of 75°S to 75°N zenith angles.

4.2.5 Correlation of 5577 A and 5893 A:

Numerous investigations have sought correlations for the intensities of the atomic lines 6300 A, 5893 A and 5577 A. In particular the observations with an eight colour photometer by BARBIER (1954, 1956) have been valuable in establishing three covariance groups. The emissions within each group are well correlated with one another. These groups are -

a) The green line including λ 5577 A (OI), O_2 Herzberg bands, the blue bands, the green continuum and the O_2 atmospheric bands.

b) The sodium group including 5893 A and OH.

c) The red line λ 6300 A (OI).

BARBIER (1956) finds that whereas the two groups(a) and (b) tend to vary independently, they may also appear to become coupled and vary in a parallel way for several hours.

As the heights of emission of 5893 A ($\sim$ 85 km) and 5577 A ($\sim$ 100 km) are near and as the concentration

of atomic oxygen is mainly responsible for the emission (as discussed in section 4.1), here it is proposed to see the interrelation between the emissions for Mt.Abu data. Correlation coefficients of all the individual nights were determined (one correlation coefficient for each night considering all half hour observations when data was available for more than 5 hours) and a histogram is prepared (Figure 4.18) for the 1964-68 data. It showed a wide spread in the correlation having values both positive and negative. This shows that there is no obvious relation between these emissions 5577 A and 5893 A, as noted earlier by KULKARNI and STEIGER (1967).

A close inspection of the data showed that on some individual nights an increase is seen in both these emission, the 5893 A lagging behind the 5577 A (see Figure 4.19). This may be interpreted as following, As the atomic oxygen comes down from slightly higher heights ($>$ 100 kms) the increase in 5577 A starts earlier to 5893 A. In the next chapter it will be shown that 5577 A and OH also showed increase on some occasions with a time lag, OH lagging behind 5577 A. A qualitative explanation may be suggested. From the delay time in the maxima of 5577 A and 5893 A it appears that if a common agency, (in this case atomic oxygen) vertically descends such

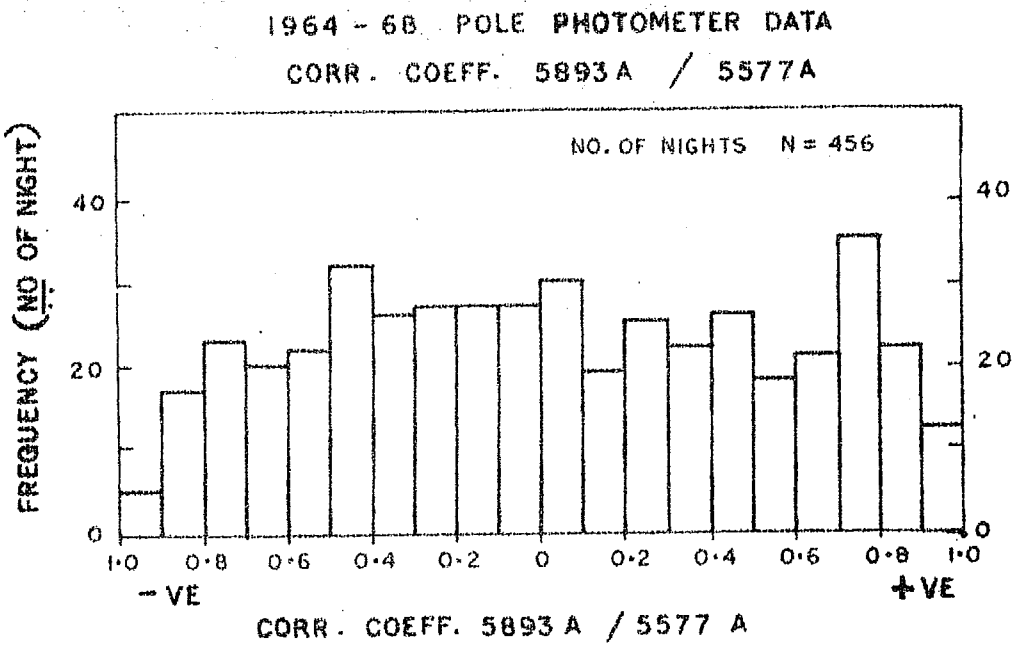

FIGURE 4.18 Histogram of the correlation coefficients of 5893 A and 5577 A.

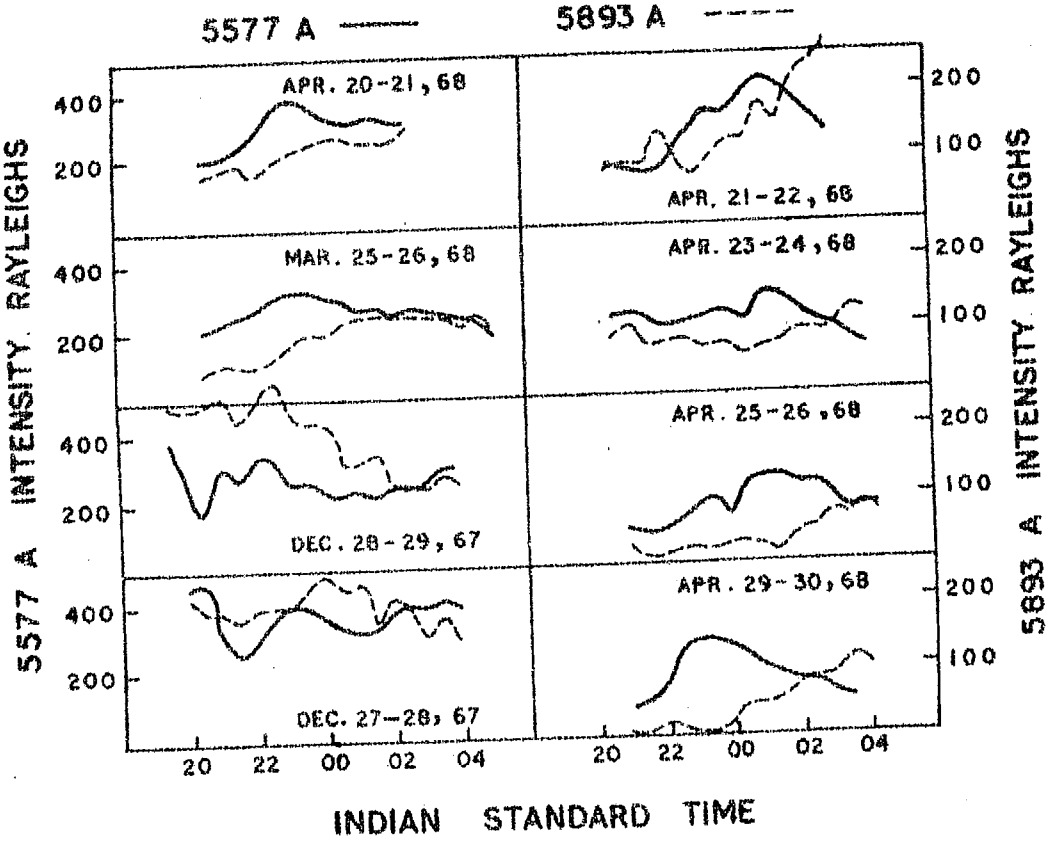

FIGURE 4.19 Examples of a few nights showing maxima in 5577 A and 5893 A with time differences.

maxima could be explained. However, it is noted the increase starts slightly earlier in case of sodium compared to that of OH; both lagging behind 5577 A. It is shown in section 4.2.4 that the seasonal variation of 5577 A and 5893 A show a broad similar behaviour. It is shown in the next chapter V that 5577 A and OH show a somewhat opposite behaviour in their seasonal variation. This shows that the height of 5893 A is slightly above the OH emission height and thus it is nearer to 5577 A and their seasonal variations (of OH and 5577/5893) relate to the seasonal variation of the amount of atomic oxygen at these heights.

4.2.6 Effect of solar flares and magnetic storms:

Day to day variation of the night airglow intensity of 5577 A at Mt. Abu and the relative sunspot numbers (R_Z) were compared for the data of 1964-68. The correlation is not conspicuous as noted from the scattered plot presented in Figure 4.20. A study of 3 hourly average intensities of 5577 A and K_p index values is also made. In this case also no obvious relation is observed.

An examination of the data of all nights during 1964-68 and other geomagnetic data of solar flares and magnetic storms (data taken from the Indian Journal of

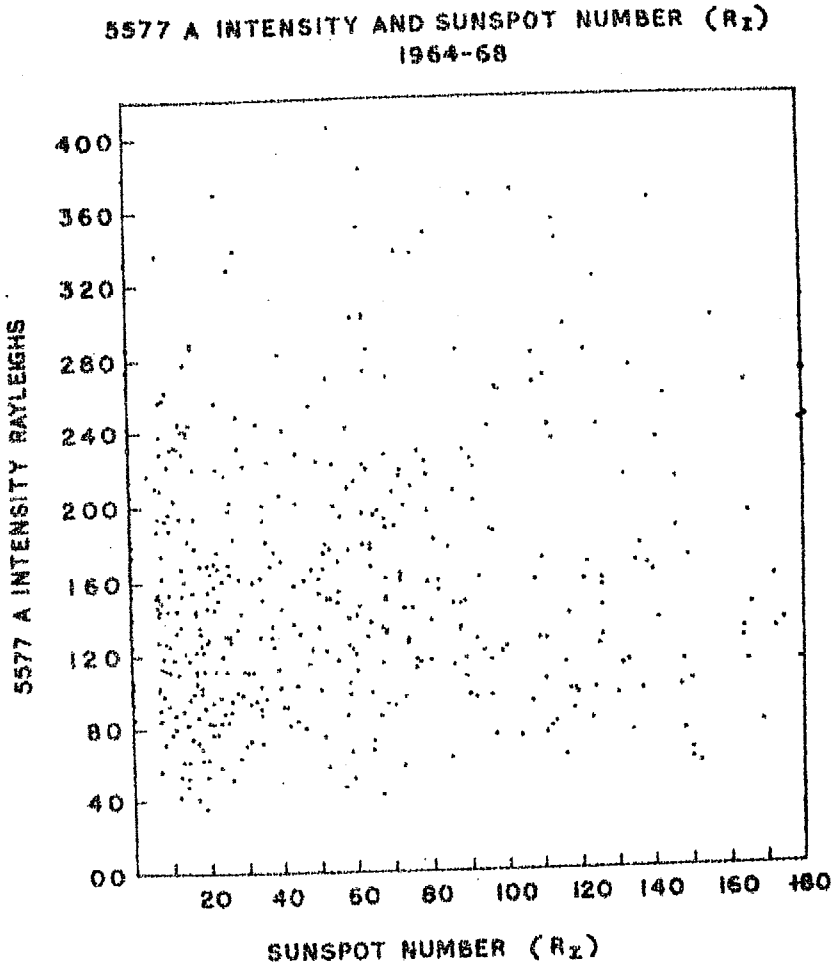

FIGURE 4.20 5577 A intensity and the sunspot number(R_z)

Meteorology) was made. It is noted that there is an enhancement of 5577 A intensity following an intense solar flare of importance 2+ or more. A few cases are shown in Figure 4.21 where the intensities of 5577 A on the following and preceeding nights of the flare day are plotted. A notable increase is observed on the following night of the flare day, as observed earlier by DANDEKAR (1961); DANDEKAR and SILVERMAN (1964).

An increase in intensity of 5577 A is also observed following magnetic storms. Storms during 1964-68 were analysed wherein simultaneous airglow data were also available. The particulars of some storms are tabulated in Table 4-I. Few examples of increase in 5577 A intensity following the magnetic storms are presented in Figure 4.22. Increase in 5577 A following sudden commencement is noted earlier by CHRISTOPHE-GLAUME (1965); WEILL and CHRISTOPHE-GLAUME (1965) and SILVERMAN and BELLEW (1965).

It is noted that, airglow emissions of 6300 A and 5893 A are not appreciably enhance after solar flares and magnetic storms at Mt. Abu.

.....

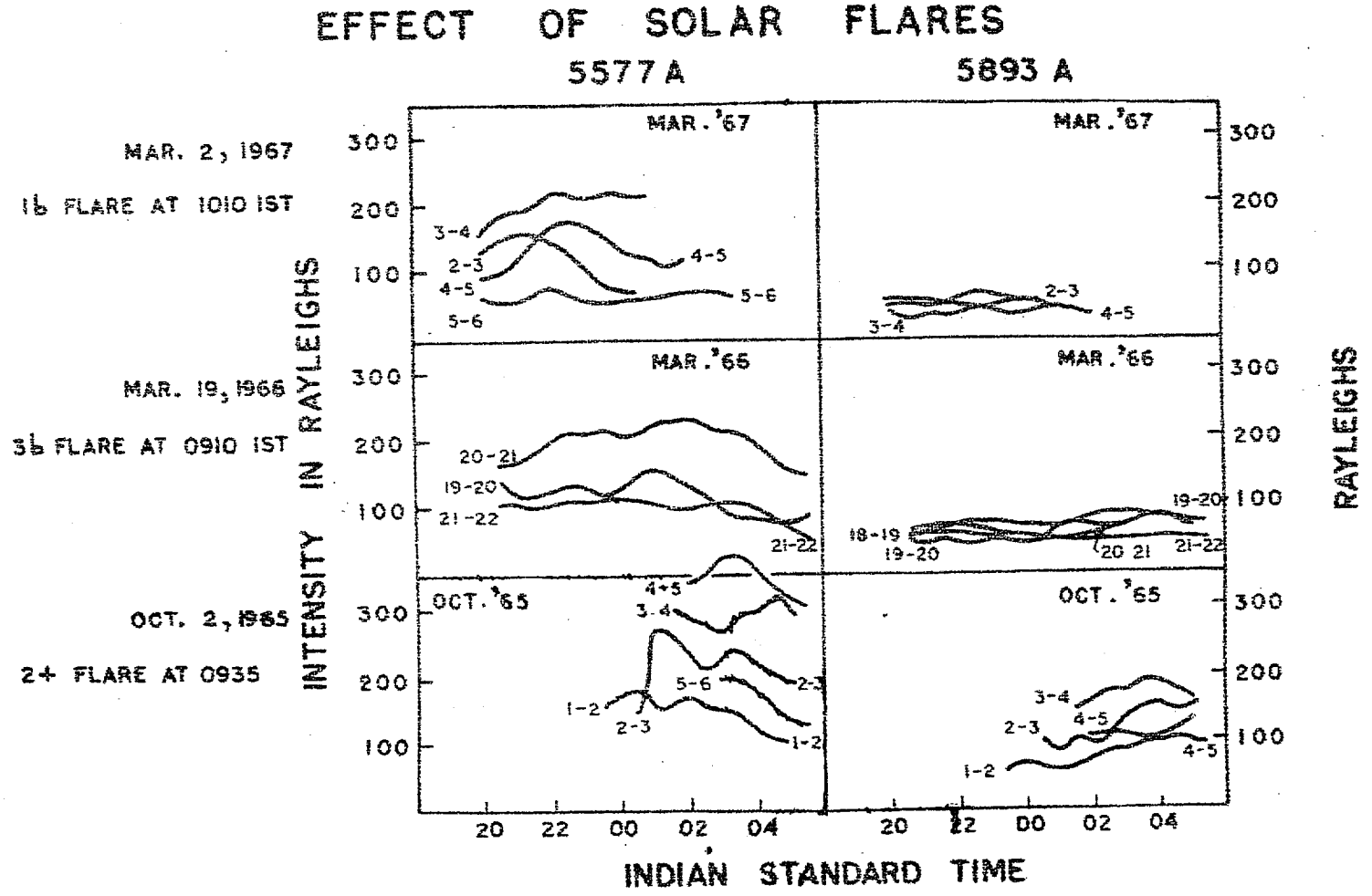

FIGURE 4. 21 Effect of solar flares on the intensities of 5577 A and 5893 A.

TABLE 4-I

Year date and month	Storm beginning Hrs. Min. (IST)		Time ending Day. Hrs. (IST)		Sudden commencement Amplitude Type	D′	H γ	Z γ	C figure degree of activity	Maximum activity greenvich day	Range D′	H γ	Z γ
1965													
Feb. 6	19	43	09	06	S.C.	1	22	13	m	7	5	195	30
Mar. 3	09	32	05	00	-	-	-	-	m	3	4	163	48
Oct.22	06	55	24	02	S.C.	1	11	8	m	23	4	174	44
Dec.15	16	52	03	00	-	-	-	-	m	1	3	90	28
Dec.18	11	53	19	16	S.C.	1	21	11	m	18	2	116	23
1966													
Mar.13	06	30	15	08	-	-	-	-	m	14	5	220	54
Mar.23	13	20	24	08	-	-	-	-	ms	23	6	265	55
Oct.15	15	22	17	09	S.C	1	27	10	ms	16	7	275	56
1967													
Jan. 7	13	28	10	00	S.C.	1	20	6	ms	8	8	300	78
Feb. 7	22	04	09	06	S.C.	1	20	16	m	8	6	202	42
Apr. 4	08	34	02	18	S.C.	1	65	25	m	1	3	215	41
May. 2	00	37	04	19	S.C.	1	30	17	ms	3	9	344	88
Oct.28	08	00	30	14	-	-	-	-	ms	30	4	280	62
Dec.30	04	00	2	05	-	-	-	-	m	31	6	225	70

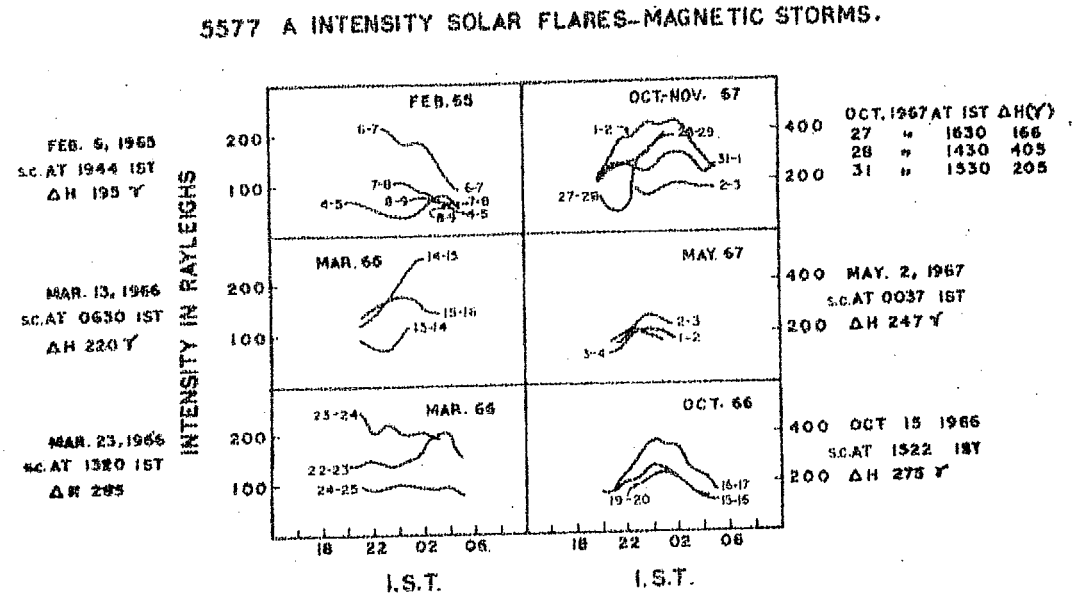

FIGURE 4.22 Effect of magnetic storms on 5577 A intensity.

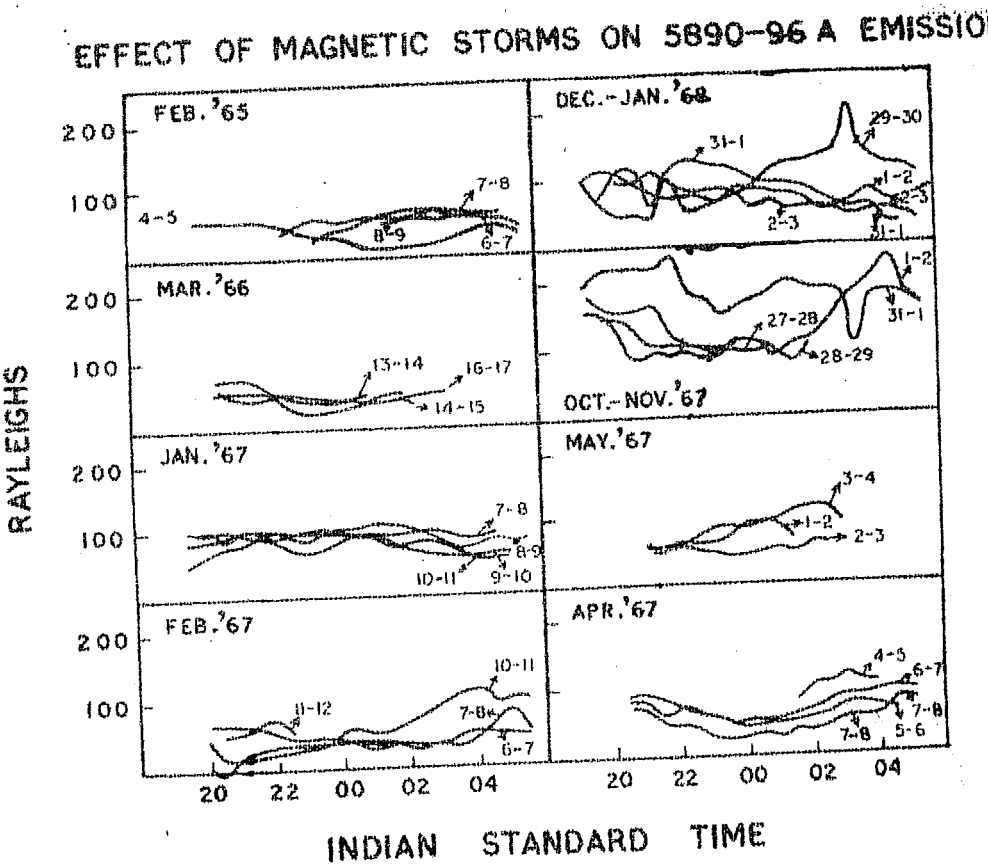

FIGURE 4.23 Effect of magnetic storms on 5893 A emission.

CHAPTER V

STUDIES OF OH BANDS IN NIGHT AIRGLOW

5. Introduction

A brief review of the present state of knowledge about the emission of OH bands in the night airglow, is given in section 5.1 and a few points are discussed in somewhat greater detail. In section 5.2 the observational results obtained at Mt. Abu of the intensities of OH (7-2) and OH (8-3) bands in night airglow during 1966-69 are summarised. In section 5.3, the interrelation between OH emission and other night airglow emissions 6300 A, 5893 A and 5577 A and the relation between the nocturnal variations of OH and 5577 A when vertical movements take place are discussed. Lastly, in section 5.4, an interesting new feature in OH nightglow emission is reported. It is observed that the time of maximum intensity of OH emission shifts with sidereal time, and approximately coincides with the transit times of celestial X-ray sources, when their zenith angle is a minimum. It is suggested that the increased ionisation in the mesosphere caused by these X-ray sources increases the amount of ozone and/or H atoms, which by mutual interaction are responsible for the formation of excited OH.

5.1 Brief Review of OH work:

As early as 1933, low resolution spectra of the night sky in the red and infrared obtained by SLIPHER (1933) demonstrated the presence of bright emissions in this region. With subsequent improvement in instrumentation and spectral resolution, observations were made by a number of workers (ELVEY,1943; STEBBINS, WHITFORD and SWINGS, 1944; 1945; RODIONOV and PAVLOVA, 1949; KRON, 1950; KRASSOVSKY, 1949). MEINEL (1950a) resolved the rotational structure of the bands between 7000-9000 A with a fast grating spectrograph and suggested that hydroxyl (OH) molecule may be the source of emission. More detailed work by MEINEL (1950b) and HERZBERG (1951) proved that the airglow features in the infrared upto about 5 μ, with the exception of an O_2 band at 8645 A, were rotation-vibration bands of hydroxyl (OH) radical.

The hydroxyl nightglow is quantally more than 1000 times richer than all other known nightglow emissions. ROACH (1963a) remarked that if the hydroxyl emissions were concentrated in the visible region of the spectrum, the night sky would glow like mid-twilight, the Milky Way would be invisible, and only the brightest stars would stand out against the competing background.

The Meinel system of hydroxyl bands is composed of rotation-vibration bands whose ground-state is $^2\Pi_{3/2}$. Each band has P, Q, R branches, the R branch being on the short wavelength side. The ground-state is designated as $^2\Pi_{3/2}$ and gives rise to the socalled P_1, Q_1, R_1 lines. Because of spin doubling, the electronic states are split into $^2\Pi_{1/2}$ and $^2\Pi_{3/2}$, the frequencies of $^2\Pi_{1/2}$ lines being approximately 140 cm^{-1} higher than $^2\Pi_{3/2}$. Its P_2, Q_2, R_2 lines are weaker than those in the lower, more populated state and consequently there is a difference in the intensities of the P_1 and P_2 lines in the band. There is also a Λ type doubling (which arises due to interaction of L, the azimuthal angular momentum vector with nuclear rotation) which has been observed in high resolution laboratory spectra, but not in airglow so far.

The intensities increase rapidly towards the longer wavelengths. Bands at the shortest wavelengths (about 5000 Å) are very faint and difficult to detect. From 6700 - 8000 Å the increased brightness makes them more easy to observe. BLACKWELL et al.(1960) working at Mount Chacaltaya in the Andes at wavelengths shorter than 6700 Å, and KVIFTE (1959 a,b) at $\lambda\lambda$ 5100-7300 Å made accurate determinations of the wavelengths of the rotational lines.

A review of the work done on OH bands in North America, W.Europe and USSR has been made by CHAMBERLAIN (1961f) and also by WALLACE (1967).

Work in USSR with image convertors has yielded excellent results from 5100 A to 1.2 μ and these are summarised in the "Atlas of the airglow spectrum 3000-12400 A, by KRASSOVSKY et al.(1962a). For ready reference Table 5-I is reproduced (KRASSOVSKY et al.,1962a) of CH band system giving band origins in A.U. and intensities in rayleighs.

The last OH band which has been detected from the ground is at 2.16 μ (NOXON et al., 1959; MOROZ, 1960). From a balloon with an interferometer, GUSH and BUIJS (1964) have observed bands in the 1.4 to 2.3 μ region. Concurrently, a number of important laboratory studies of the spectrum have made available precise wavelengths and intensities of the bands BENEDICT et al., 1953; GARVIN et al.,1960). The observed airglow band intensities are in reasonable agreement with the calculated intensities based on rotation-vibration transition probabilities using only the linear terms in the dipole moment expansion (SHKLOVSKY, 1950; HEAPS and HERZBERG, 1952; CHAMBERLAIN and SMITH, 1959; SHEFOV, 1961a; WALLACE, 1962; KRASSOVSKY et al., 1962b; LYTLE and HAMPSON, 1964). It allows an estimated 5000 kR for the emission

TABLE 5-I

Rotation-vibration bands of OH molecule

Average absolute intensities of OH Bands (after Krassovsky et al.)

V' \ V''	0	1	2	3	4	5	6	7	8	9
1	1030000 28006.7									
2	58000 14335.9	1040000 29369.2								
3	3900 9788.0	92000 15046.6	800000 30853.9							
4	300 7521.5	8000 10273.3	93000 15823.7	520000 32482.9						
5	35 6168.6	930 7911.0	12000 10827.7	90000 16681.9	360000 34293.6					
6	4 5273.3	120 6496.5	1700 8341.7	14000 11432.8	77000 17642.2	240000 36333.9				
7	0.6 4640.3	20 5561.8	280 6861.2	2500 8823.3	15000 12114.0	63000 18730	160000 38658			
8	0.1 4172.6	3 4903.3	60 5885.8	460 7273.3	3000 9371.8	14000 12896	48000 19992	97000 41403		
9	0.03 3816.3	0.9 4418.4	14 5201.0	140 6255.6	890 7746.3	3900 10108	16000 13813	47000 21493	82000 44695	
10	0.0001 3539.4	0.003 4051.3	0.04 4699.5	0.4 5544.1	3 6684.8	16 8302	65 10763	200 14916	450 23315	700 48734

THE TOP LINE SHOWS THE BAND INTENSITIES IN RAYLEIGHS AND THE LOWER LINES THE WAVELENGTH OF THE ORIGINS OF THE BANDS IN A.U.

of the whole system and vibrational temperatures 8500°K to 13000°K (CHAMBERLAIN and SMITH, 1959; SHEFOV, 1961 a,b; YARIN, 1962). Since these high vibrational temperatures indicate an yield of about 4 quanta per excitation, the excitation rate neglecting deactivation comes to about 10^{12} quanta/(cm^2(column)sec.) (WALLACE, 1967). No bands with $V > 10$ have been detected in OH airglow so far.

The resolved rotational structure of the bands makes it possible to determine the rotational temperatures. McPHERSON and VALLANCE JONES (1960) have noted that if the Einstein coefficient $A = 10^2$/sec, collisions would occur fast enough below 90 km to ensure thermal equilibrium distribution in the rotational levels. As the rocket observations of PACKER (1961) and TARASOVA (1963) indicate, the peak of the OH emission layer is between 80 and 90 km and the rotational temperatures would be not far from the gas temperatures. While an Einstein coefficient of 10^2/sec is generally accepted, there have been no measurements of the coefficien .

A large number of determinations of rotational temperatures have been made by many authors using different types of equipment. MEINEL (1950b); CABANNES et al. (1950); DUFAY et al.(1951); CHAMBERLAIN et al.(1953); KVIFTE (1960); McPHERSON et al.(1960) used spectrographs, GUSH et al.(1953); DUFAY et al.(1955); WALLACE (1960) used photometers, and SHEFOV (1969); KRASSOVSKY (1963) used image convertors.

All these measurements indicated temperatures of 200 - 250°K at 45°N and 220 - 300°K at 75°N. Direct measurements in the atmosphere over Churchill (59°N) indicate summer temperatures of around 180°K in the 80-90 km region; and winter temperatures of 240 - 290°K in the same altitude region (SPENCER et al., 1964). Seasonal variations of the rotational temperatures have been studied by KVIFTE (1959a,b) in Norway, WALLACE (1960, 1962) in U.S.A., KRASSOVSKY et al. (1962b) at Yakustak and FISHKOVA and MARKOVA (1962) at Abastumani. The ranges in temperatures are from 200° to 325°K at 62°N and from 200°K to 320°K at 42°N. The northern observations show maximum intensity and maximum temperature in January/February.

SHEFOV (1961a) has noted that the temperatures derived from V' = 9 to 6 are generally equal and those from V' = 5 to 3 are progressively lower. KRASSOVSKY (1963) comments that very high rotational temperatures do not reflect the gas temperatures. Much work has been done in establishing relations between intensity and rotational temperatures, seasonal variations, latitude variations of temperature and their interpretation. However, there have not been any low latitude measurements of OH rotational temperatures so far.

The work on intensity measurements of the OH bands is summarised in the following sections, and later, the results of the measurements at Mt. Abu of the two OH bands OH (7-2) and OH (8-3) are discussed.

A number of measurements have been made in the infrared OH spectral region. However, many of the measurements have been made with wide band filters which include the O_2 band at 8645 A in addition to some of the OH bands. It is difficult to interpret these results without knowing the relative intensities of the bands.

ELVEY (1943) recorded three types of night-sky OH variations from his photometer observations towards the polestar.

a) A steady fall in intensity from evening to morning;
b) A minimum at about midnight;
c) Enhanced emission with irregular variations.

HURUHATA (1950) observed a moving pattern in the form of a bright wave travelling mostly from north to south. He used a scanning photometer. BERTHIER'S (1956)results showed a decrease in intensity from evening to midnight followed by a steady value and then a sharp fall before dawn.

Midnight minimum type is the most prominent in Berthier's results. ARMSTRONG (1956) has classified the intensity variations into four types.

a) An over-all fall in intensity from evening to morning.
b) An almost constant intensity throughout the night.
c) An intensity rise in the morning hours.
d) A maximum of intensity near midnight.

He comments that these types are not considered to have any physical significance. Except the fourth type, all the others are similar to Elvey's types.

NAKAMURA (1961) studied the nocturnal variation in greater detail and classified the curves into six types.

Type A has a midnight minimum
Type B is similar to A but intensity decreases again in the early morning hours.
Type C decreases monotonically throughout the night.
Type D is almost constant intensity throughout the night.
Type E has a continuous increase in intensity.
Type F has maximum intensity near about midnight.

Thus Nakamura has added two more types. However, he concludes that types A and B are more common than the rest. At Poona (India), CHIPLONKAR and TILLU (1967) noted from a study of OH (7-3) and OH (9-4) from 3 months of observations (January to March 1964) that the nocturnal variation was of type C above, except on one night when a midnight maximum was observed. Also they note a maximum at 2100-2130 IST and after this the intensity continuously and rapidly decreased towards dawn. The maximum to minimum ratio is generally greater than 10.

BARBIER(1959) and FISHKOVA (1962) report a seasonal variation in OH with a maximum in winter and a minimum in summer similar to that of Na D lines. Berthier's extensive work (1956) showed very little variation in the monthly means. The observations of HARRISON and VALLANCE JONES (1957) with an infrared sensitive spectrometer did not also show any systematic seasonal variation, but the night-to-night fluctuations covered a range of a factor of two. Very recently, SHEFOV (1969) has discussed the average seasonal variations of intensity and rotational temperatures of the hydroxyl emissions at different latitudes from the observational data obtained over many years at Zvenigorod and other stations. He concludes that the seasonal variation of the OH emission is of a complicated nature. In the data

of different stations, two maxima during the year are observed, but their relative intensities and the seasons in which they occur differ. At present there are practically no data on the latitudinal variation of the rotational temperatures and intensities other than those from USSR. So it is not possible to draw any conclusion about the latitudinal and longitudinal variations and of long-term variations in OH emission. SHEFOV (1969) showed that periodic variations in the intensity and rotational temperatures appear after the commencement of a geomagnetic storm and lasts upto 30 days.

BARBIER (1954 a,b) with an eight-colour photometer established three covariance groups of the airglow radiations. Na D lines and OH were grouped together in 'sodium-group'. The correlation of Na and OH was found independently by BERTHIER (1954a). Earlier, BARBIER (1954a) included 6300 A also in this group, but the contamination from OH (9-3) band through the 6300 A filter had been inadequately corrected.

These are some of the results that have been obtained about the OH night glow. However, there are no systematic studies so far to establish nocturnal and seasonal variation, or long term variations, or latitudinal variations other than the work in USSR. There are no low latitude studies in this direction except the study for three months at Poona by CHIPLONKAR and TILLU (1967).

5.1.1 Mechanism of Excitation of OH bands:

Soon after the identification of the OH bands the ozone mechanism was suggested independently by BATES and NICOLET (1950) and by HERZBERG (1951). The primary reaction is

$$H + O_3 \longrightarrow OH^* + O_2 \qquad (+3.32 \text{ ev})$$

The excitation energy of V = 9 in the $^2\Pi$ ground-state of OH is 3.23 ev, whereas for V = 10 the energy is 3.49 ev.

KRASSOVSKY (1955) pointed out that OH with $V > 10$ could react with O_2, de-activating the excited OH molecules before they could radiate. He considers another mechanism which can give OH bands with $V > 10$ also as

$$O_2^* + H \longrightarrow OH^* + O$$

BALLIF and VENKATESWARAN (1963) and WALLACE (1962) examined these reactions and advanced arguments to show that the nighttime variation of the emission intensities stimulated by these two reactions would be characteristically different. Solving the necessary continuity equations with reasonable assumptions and using the known rate coefficients, BALLIF and VENKATESWARAN (1963) arrived at the conclusion that the

OH glow from any single level in the earth's atmosphere will simply reproduce the temporal variations of O_3 at that level. It is necessary to remember that the O_3 variations which are reflected in the net OH intensity whether recorded at the ground or observed from a satellite will be a weighted sum of the variation at the separate levels; the weighing for each level will be different at different times of the night.

Let $n(O)\ (h_3, t_o)$

$n(O_3)(h_3, t_o)$

and $n(H)\ (h_3, t_o)$

be the initial number of oxygen, ozone and hydrogen atoms at time $t = t_o$ at height $h_3 \sim 85$ km. Then BALLIF and VENKATESWARAN found that t_m, the time when $n\left(O_3\right)(h_3)$ reaches its maximum depends on the ratio

$$\frac{n(O)(h_3, t_o)}{n\ (H)\ \ (h_3,t_o)\ n\ (O_3)\ \ (h_3,t_o)}$$

If the values of this ratio are 2×10^{-3}, 2×10^{-4} and 2×10^{-5}, the corresponding values of t_m are 12 hours, 3 hours, and 10 minutes. Obviously the time variation of OH due to this reaction would fall under three different types.

a) an increase throughout the night;

b) a post-twilight increase followed by a decrease;

and c) a decrease throughout most of the night.

Similar calculations for the Krassovsky mechanism made by BALLIF and VENKATESWARAN (1963) showed that this reaction contributes a more or less steady component to the total OH excitation rate. If in the atmosphere, n (H) is constant at height h_3, quantal emission of OH will exhibit variation of O_3(BALLIF and VENKATESWARAN, 1963). They suggest that the relative importance of these reactions can therefore be judged by a systematic observational study of the intensity variation of OH.

According to HESSTVEDT'S (1968a)theoretical calculations, the Krassovsky mechanism yields only 1% of the total observed intensity. ELVEY (1943); HURUHATA (1950); RODIONOV and PAVLOVA (1949); ARMSTRONG (1956); BERTHIER (1956); and NAKAMURA (1961) have all noted that variability in the type of night-time variation is a characteristic feature of OH emission. However, systematic observations are very few and hence a quantitative study of the reactions and their relative importance is yet difficult to make.

BALLIF and VENKATESWARAN (1962) have discussed the covariation of Na and OH emissions by considering the respective

reactions. They conclude that the covariation is mainly due to the fact that their heights of emission are almost the same and that in each of these emissions the nocturnal variation of ozone is reflected.

Recently HESSTVEDT (1968a) has made elaborate calculations of the effect of vertical eddy transport on the atmospheric composition in the mesosphere and lower thermosphere. He gets a theoretical value of OH^* emission to be 2300 kR with maximum at 88 km and concludes that the incorporation of vertical eddy transport into the model atmosphere, represents an improvement in the earlier photochemical models. Introduction of horizontal transport in the model is not likely to cause any significant changes in the results. On the other hand, vertical mean motion will considerably influence the results. In section 5.3.3, it is shown that how some of the observational results can be of help in understanding the vertical mass motions.

Thus by studying the many features of OH nightglow, it is expected that transport processes, and chemical reactions taking place at the OH emission altitudes will get clearer.

5.2 Observational results:

5.2.1 Methods of observation:

The airglow observations at Mt. Abu reported and discussed in this chapter were obtained with the photometers described in chapter I. The intensities of the two OH bands OH (7-2) and OH (8-3) have been systematically recorded from Nov.1966 onwards. The Red photometer was pointed towards the zenith from November 1966 to January 1968 and later, it was directed towards the polestar ($24.6^{o}N$)*. Assuming the height of OH emission layer to be around 85 km, the pole-ward observations correspond to local zenith observations at a distance of $\sim$ 220 km north of Mt.Abu, that is, at $26.5^{o}N$ geographic latitude.

---

* The Red photometer also contains a 6300 A filter in addition to the two OH filters OH (7-2) and OH (8-3). The reason for changing the direction of observation from zenith to pole after January 1968 was to make an inter-comparison of the results of 6300 A intensity obtained with the Red photometer and with the 6300 A Pole photometer (both pointing to pole-star). With the two 6300 A filters and background filters at 6080 A and 5350 A, and a common calibrating source, a comparison of the reduced intensities was made and it showed more or less the same values of 6300 A intensities within the limits of experimental error. It was thus tested that the values of K_1 (the ratio of background intensity at the emission wavelength to the background intensity at the neighbouring continuum filter wavelength in the two-colour method of reducing airglow observations) is justified. The extrapolated value of K_{OH} from Shefov's curve was used for reducing OH data.

5.2.2 Data collection and reduction to absolute units:

The intensities of the two OH bands OH (7-2) and OH (8-3) were recorded from November 1966 to May 1969 on all clear moon-less nights. In Table I-IV are given the number of nights and hours on which data were acquired at Mt. Abu for OH bands with the Red photometer during the above mentioned period. Following the method described in Chapter III, the intensities were determined in rayleighs from the observed chart deflections. Also the pole-ward observations were converted to local zenith intensities using the appropriate Van Rhijn factors assuming the height of OH emission to be 85 km.

5.2.3 Covariation between OH (7-2) and OH (8-3):

The nocturnal variations of the intensities of these two bands on a few individual nights are shown in Figure 5.1. It may be observed that both OH (7-2) and OH (8-3) bands show strikingly similar time variations. The correlation coefficients obtained by considering all half-hourly intensity values are given in Table 5-II for the three years of data. On many individual nights (about 60%) the correlation coefficients are greater than +0.90. The histogram of the correlation between OH (7-2)and OH (8-3) from the three years' data is

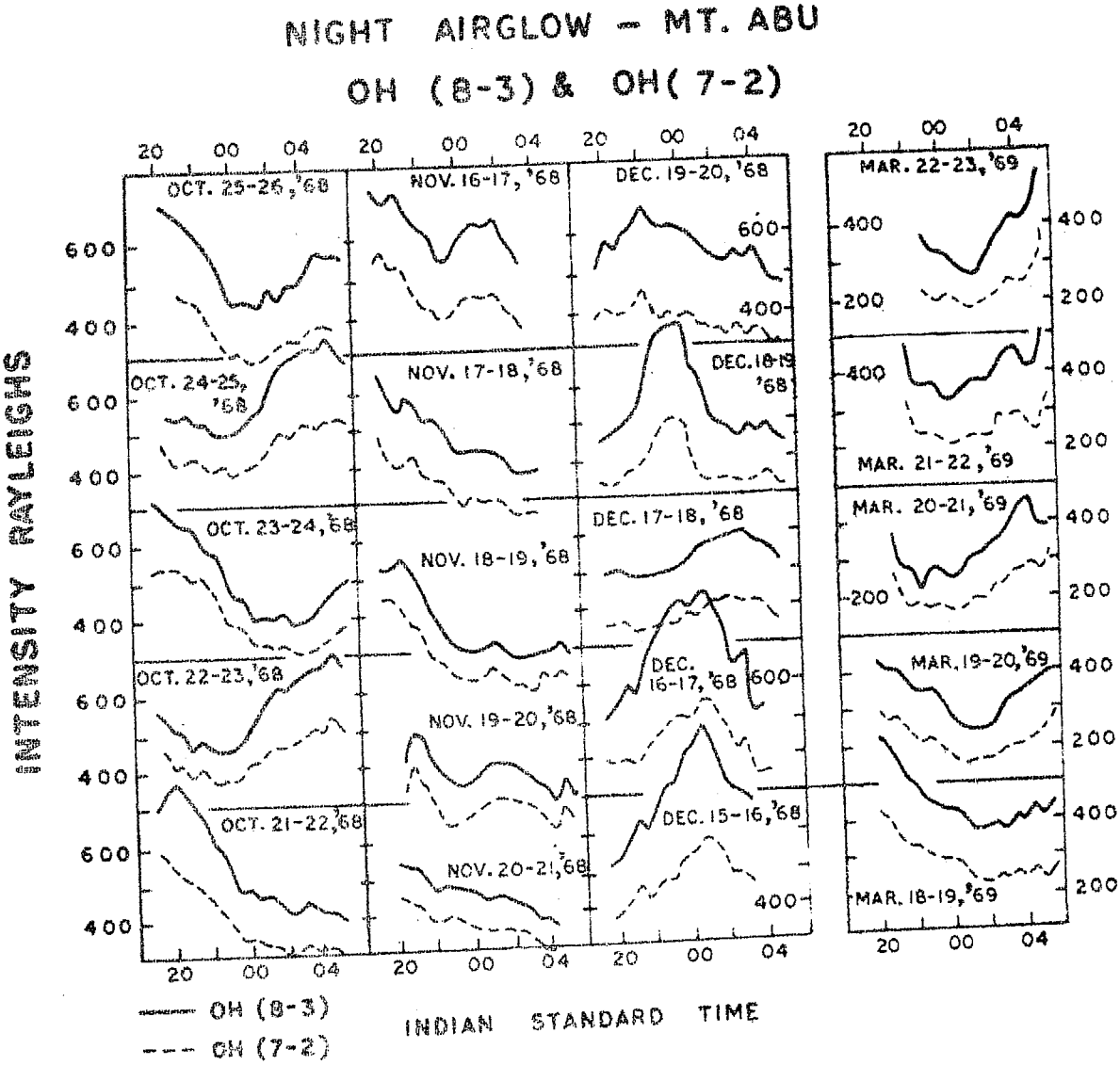

FIGURE 5.1 Nocturnal variation of OH (8-3) and OH (7-2) on a few nights.

TABLE 5-II

Correlation coefficients in OH (7-2) and OH (8-3) band intensities:

Period	Number of half hour observations	Correlation coefficient OH (7-2)/ OH (8-3) (intensities)
November 1966-June 1967	1663	+ 0.88
October 1967-July 1968	1736	+ 0.94
September 1968-May 1969	1739	+ 0.93

given in Figure 5.2 which shows very high positive correlation between the intensities of the bands OH (7-2) and OH (8-3).

In Figure 5.3 A, histograms of the intensity values of OH (7-2) and OH (8-3) are plotted considering all the half hour values during 1966-1969. It is noted the intensity of OH (8-3) has most frequent values between 300-500 rayleighs and OH (7-2) has between 200-400 rayleighs giving the average ratios of these bands between 1.2 to 1.3 (Figure 5.3 B).

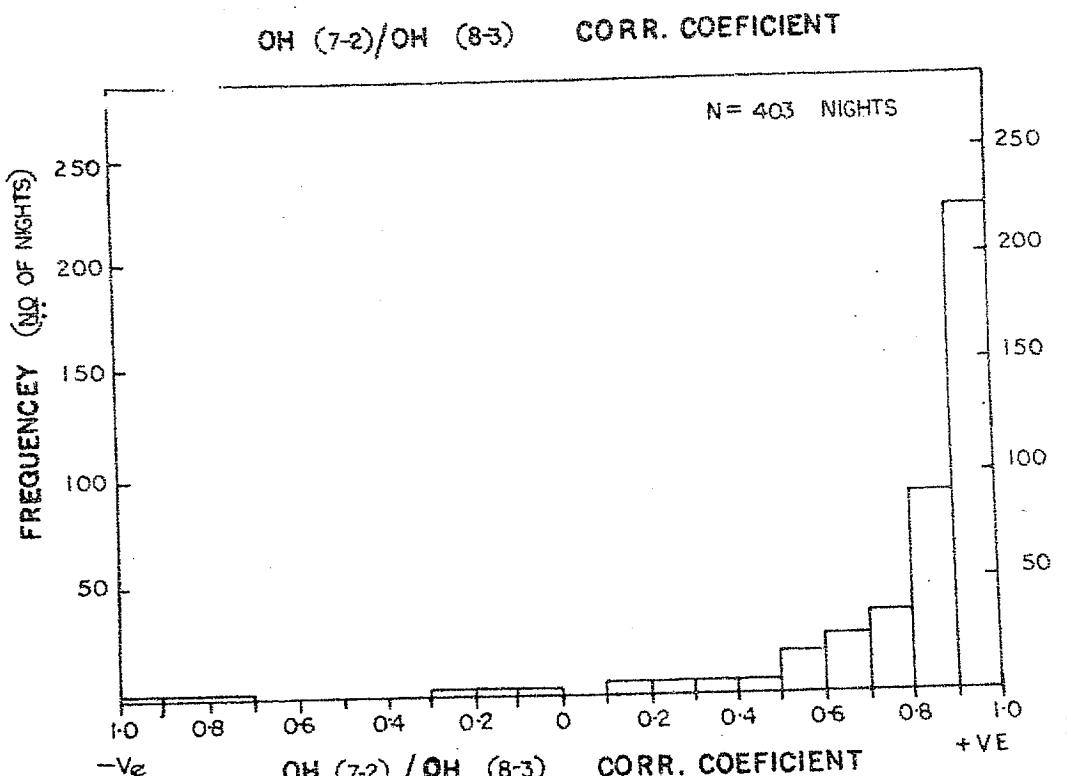

FIGURE 5.2 Histogram of the correlation coefficients between OH (8-3) and OH (7-2).

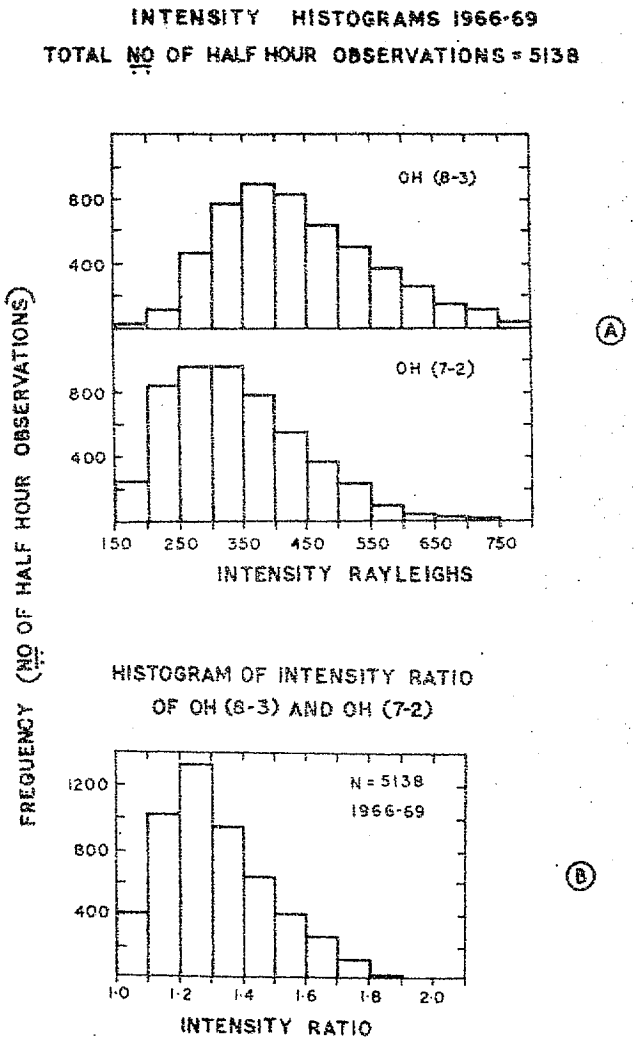

FIGURE 5.3 A - Histograms of the intensities of OH(8-3) and OH(7-2)

FIGURE 5.3 B - Histograms of the intensity ratios of OH(8-3) and OH(7-2).

In Figure 5.4 are shown the ratio of the average nocturnal variation of OH (8-3) and OH (7-2) for all the lunations from November 1966 to May 1969. There are considerable variations in these ratios. On most of the nights it is observed that the ratio increased for a few hours and then decreased. Some examples are shown in Figure 5.5. There are considerable fluctuations in these ratios during the course of the night which can be due to the temperature fluctuations at the height of OH emission.

5.2.4 Nocturnal variation of OH emission:

The night time variation of OH emission has been recorded on clear moon-less hours of all possible nights in each lunation covering a period of about 20 days around new moon. On Table 1-III the number of nights and hours on which data were acquired at Mt. Abu during November 1966 to May 1969 is given.

The OH intensity exhibits different types of night time variation. Although in a particular lunation, many nights show similar variation, on some successive nights the variation becomes different. All the data recorded at Mt.Abu during 1966-69 were grouped according to the six different types defined by NAKAMURA (1961) and a histogram

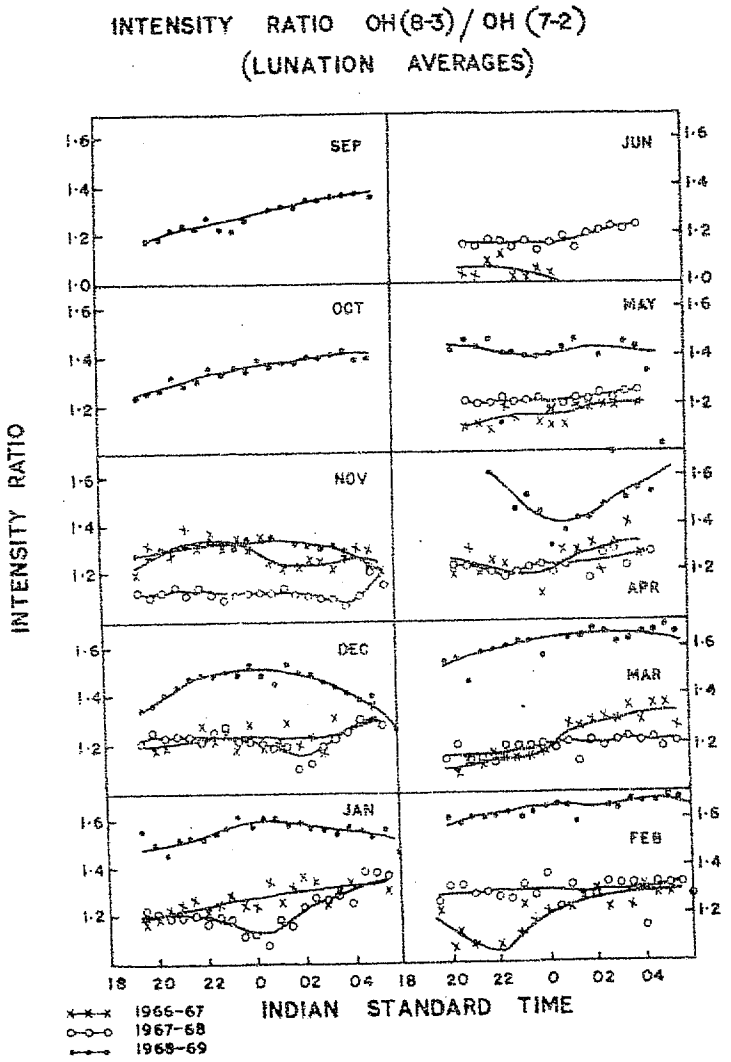

FIGURE 5.4 Average nocturnal variation of the intensity ratios of OH (8-3) to OH (7-2).

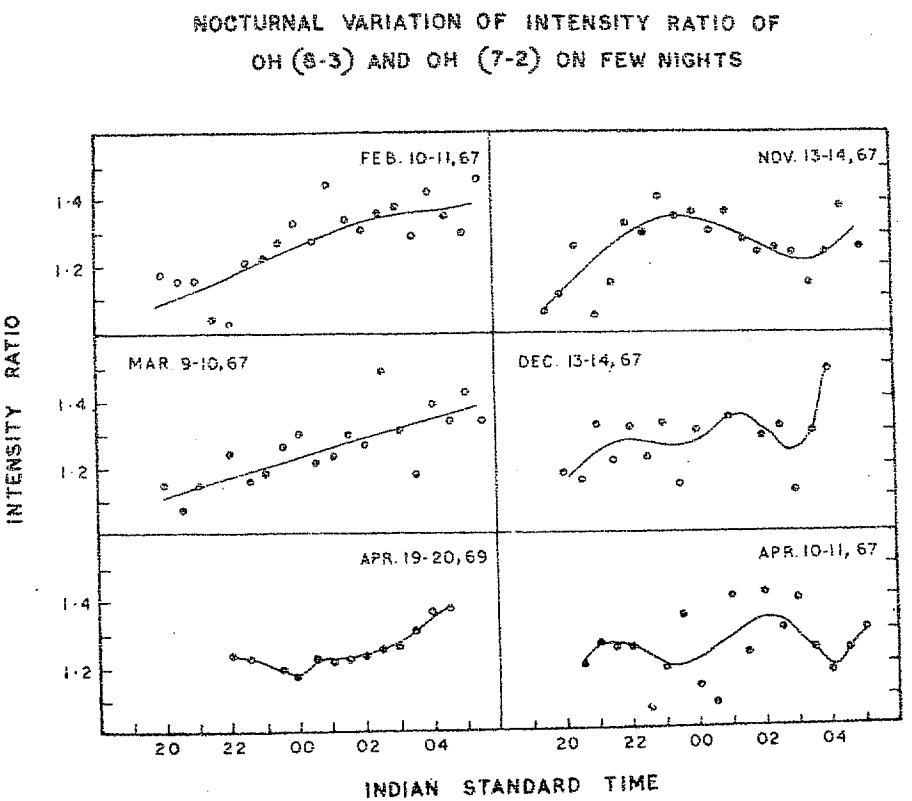

FIGURE 5.5 Nocturnal variation of the ratio of OH (8-3) to OH (7-2) on a few nights.

was prepared showing the frequencies of occurrence of the different types (Figure 5.6). Similar histograms were prepared for different months and different years and seasons. In plotting these histograms only the nights in which observations were available for more than 5 to 6 hours and on which the types of variation could be clearly assessed were considered.

The D and E types of Nakamura are less frequent at Mt.Abu than the other types. Type B is the most frequent. According to BALLIF and VENKATESWARAN (1963), A, B, C and F types imply that Bates and Nicolet hydrogen-ozone mechanism is the main reaction involved in the nocturnal variation of OH. Thus it appears that ozone-hydrogen reaction is the main reaction responsible for the nocturnal variation of OH at Mt. Abu.

The average variation obtained from the data of all nights in a lunation presents a general picture of the nocturnal variation in that particular lunation. The average curves of all the lunations from November 1966 to April 1969 are given in Figure 5.7. The similarity of different monthly curves over the three years of data can be seen from this figure.

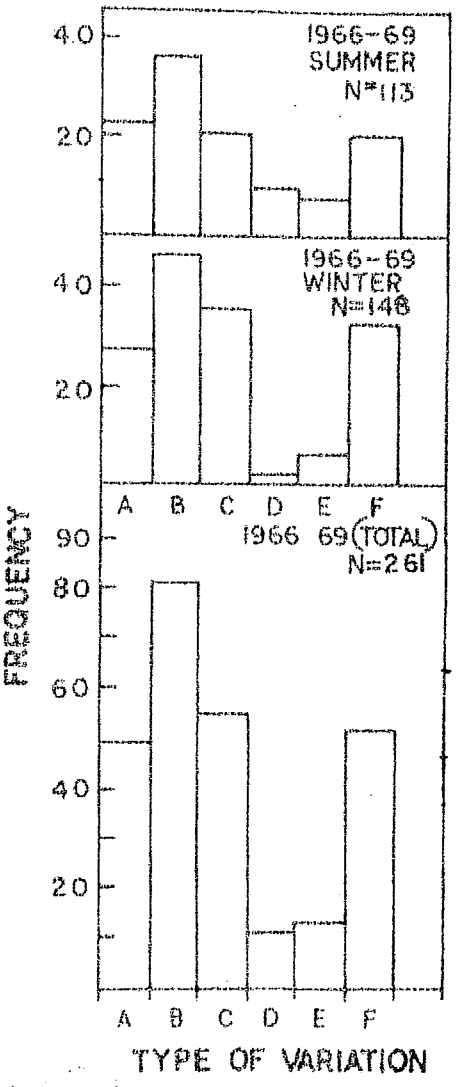

FIGURE 5.6 Histogram of the different types of variation observed in OH night airglow.

Type A has a midnight minimum.
Type B is similar to A but intensity decreases again in the early morning hours.
Type C decreases monotonically throughout the night.
Type D is almost of constant intensity throughout the night.
Type E has a continuous increase in intensity.
Type F has maximum intensity near about midnight.

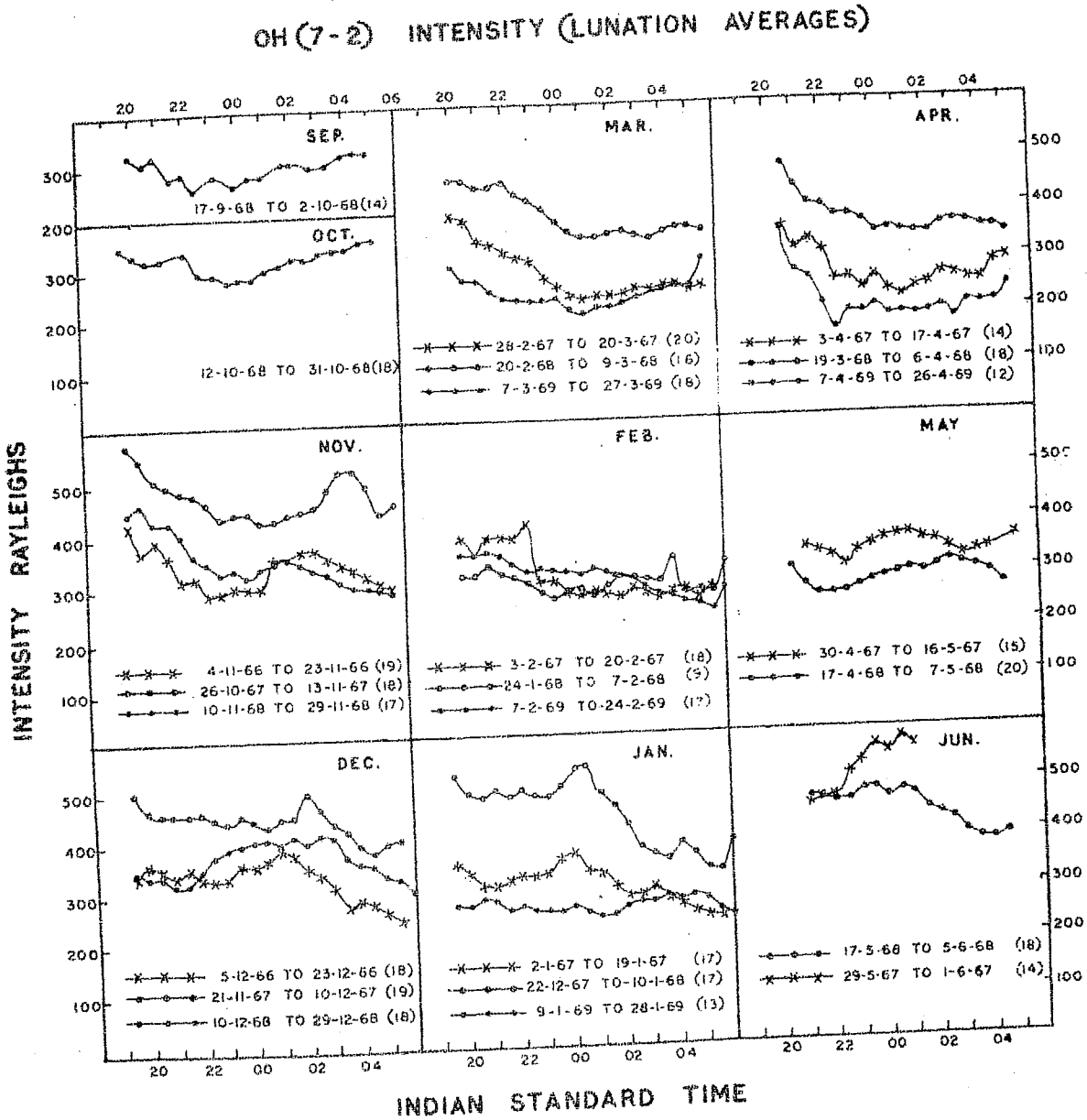

FIGURE 5.7 Average nocturnal variation of OH (7-2) observed in different lunations during 1966-1969.

It is seen that in the month of September and October, there is an increase in intensity in the second half of the night. In November a peak appears in the later part of the night. This peak shifts by about 2 hours from month to month and vanishes by March. In March, April the intensity is a maximum in the beginning of the night and decreases afterwards. Just before dawn it again increases slightly. In May, the intensity increases after 2200 IST. The trends of variation are more or less the same in the same months in each of the three years. However, it has to be remembered that the direction of observation after January 1968 was changed from zenith to pole. Some of the lunations fall in two months and hence there is a slight shift in the position of the peaks, owing to superimposition of two slightly differing types. Thus it can be concluded that in general, OH intensity decreases till the middle of the night and this is followed by a slight increase towards dawn. Also on many occasions, in the beginning of the night there is an increase which lasts for about an hour and then the decrease starts. Although types A, B and C are the more common types after removing the superposed peak, it is very difficult to predict the day to day variation. In Figure 5.8 some groups of successive nights are presented when OH nocturnal variations were markedly different.

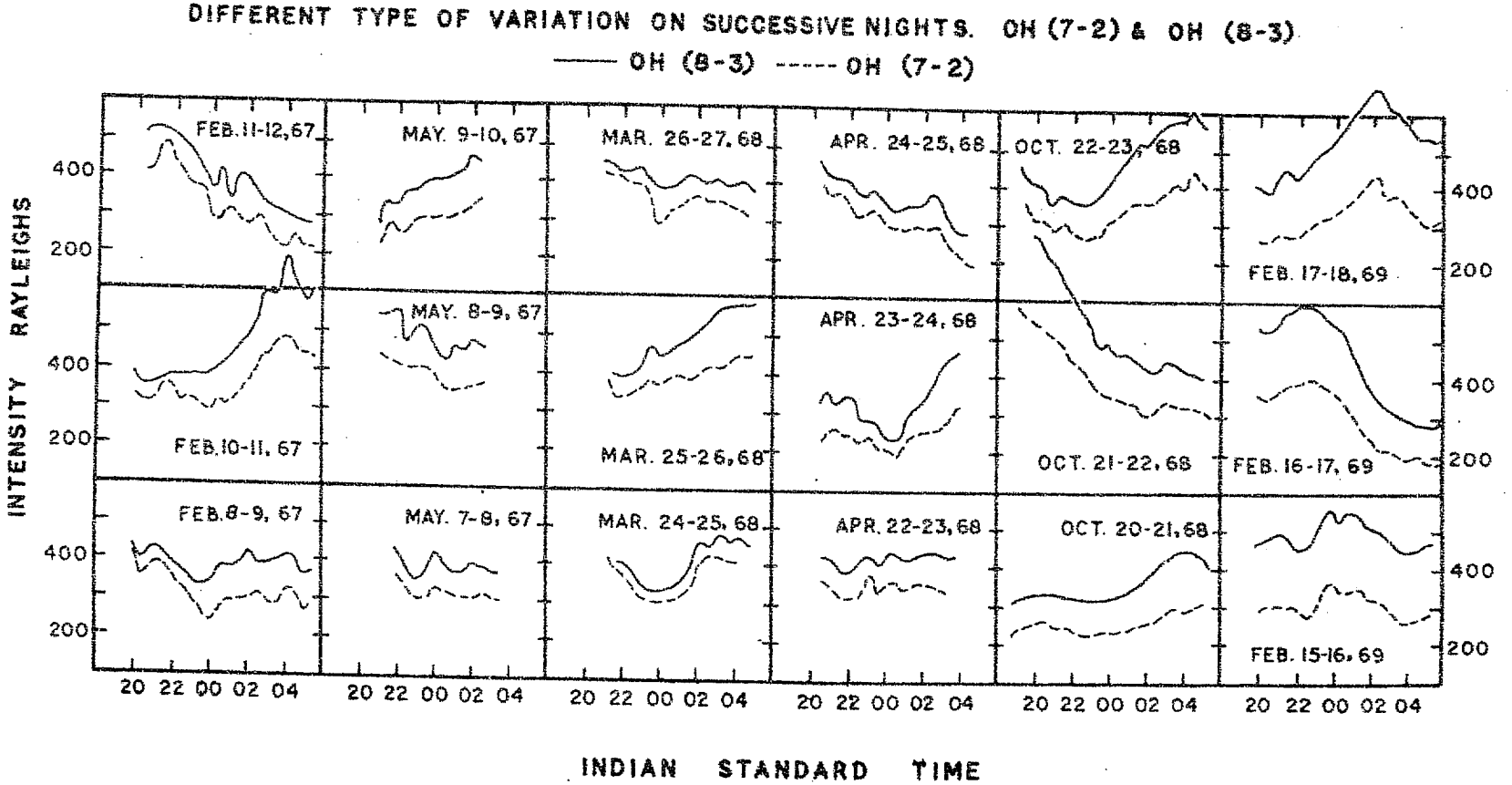

FIGURE 5.8 Some groups of successive nights showing markedly different types of nocturnal variations in OH intensity.

5.2.5 Possible cause of different types:

It is noted that these different types of variation on some successive nights are not the direct consequence of magnetic storms/solar flares etc. (It is noted that on nights following magnetic storms, the OH intensity increased but the type of variation remained the same. In Figure 5.9 the data on a few nights are plotted following and preceeding the magnetic storms in which the increase in OH intensity following the commencement of the magnetic storm is seen). It is probable that the initial value of oxygen atoms which determines the ozone density in the beginning of the night is responsible for the type of variation observed (BALLIF and VENKATESWARAN, 1963).

5.2.6 Fluctuations in the nocturnal variation:

A close examination of OH intensity curves on a day to day basis shows that the intensity can have "fluctuations" on many occasions. The same is the case with sodium emission also. These fluctuations' are superposed on the general trend of the variation, whether the intensity falls, or rises. In the average curves, these fluctuations are smoothed out. The genuineness of these fluctuations is confirmed as it is found that simultaneous 6300 A/5577 A

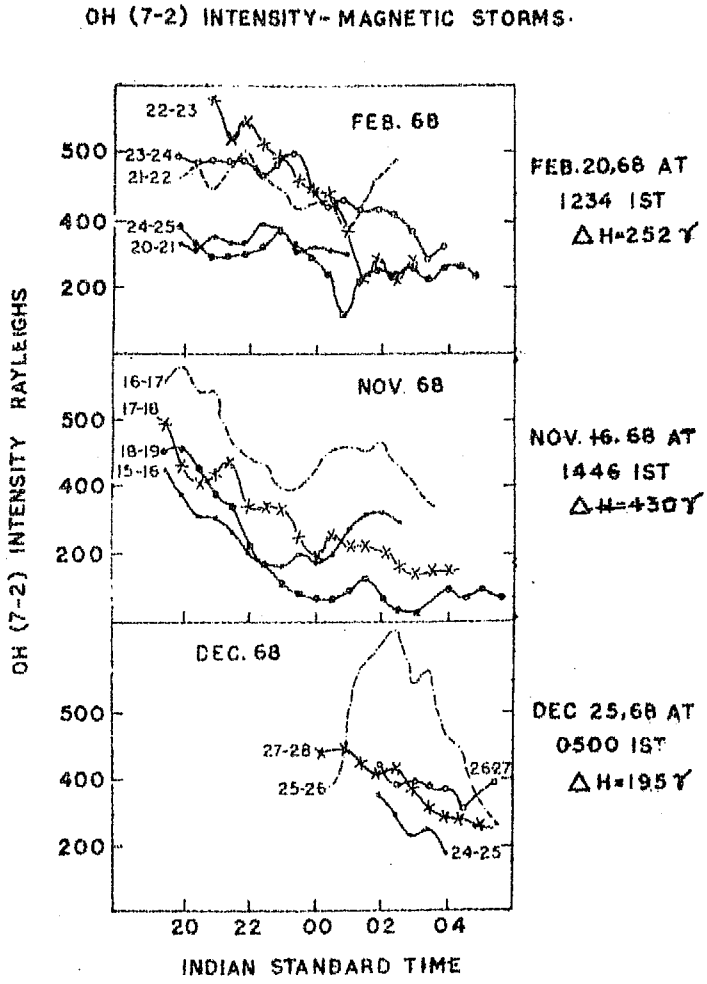

FIGURE 5.9 OH (7-2) intensity on nights following and preceeding magnetic storms.

observations reduced with common calibration do not show such fluctuations. These fluctuations may reflect the temperature fluctuations at the height of OH/Na emissions.

5.2.7 Seasonal variation:

To study the seasonal variation of OH emission, half-hourly intensities were averaged for each complete lunation. Half-hourly data of each lunation centred round each new moon were used for the averaging. The lunation averages from November 1966 to May 1969 are plotted in Figure 5.10. Observations were not possible in the months June to September due to cloudly skies. The continuous curve of Figure 5.10 with maximum and minimum values marked in it gives a picture of the seasonal variation of OH emission.

The following conclusions can be drawn regarding the seasonal variation of OH emission at Mt. Abu.

1) The minimum intensity is observed in April. This was repeated in each of the years 1967, 1968 and 1969.
2) The intensity apparently increases in May/June. This was observed in 1967 and 1968.

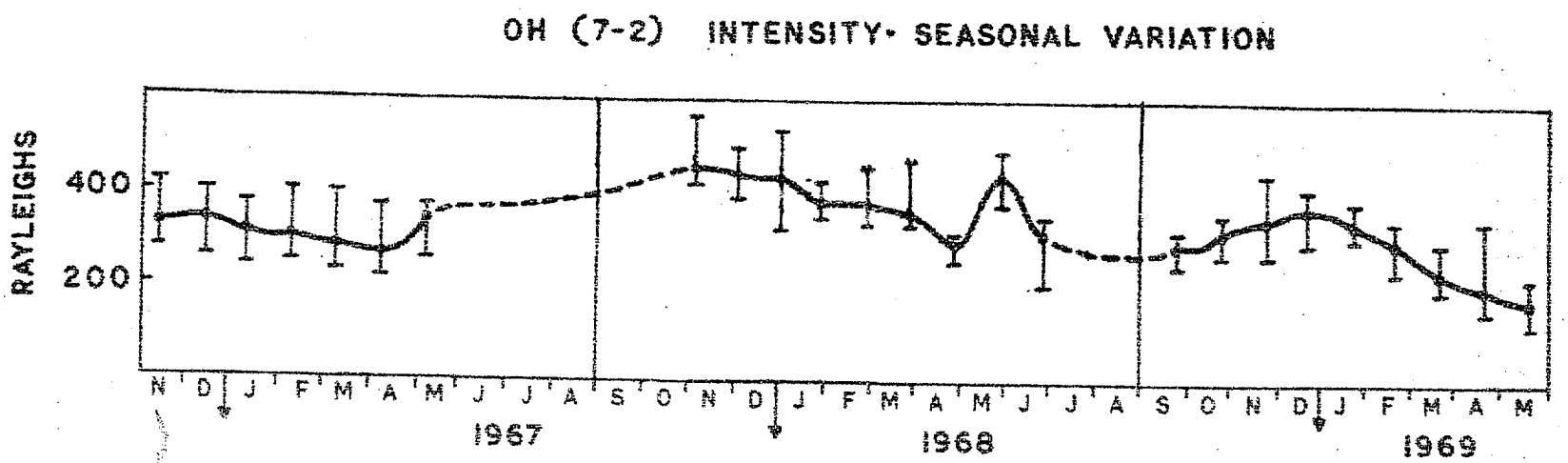

FIGURE 5.10 Seasonal variation of OH (7-2) (Lunation averages)

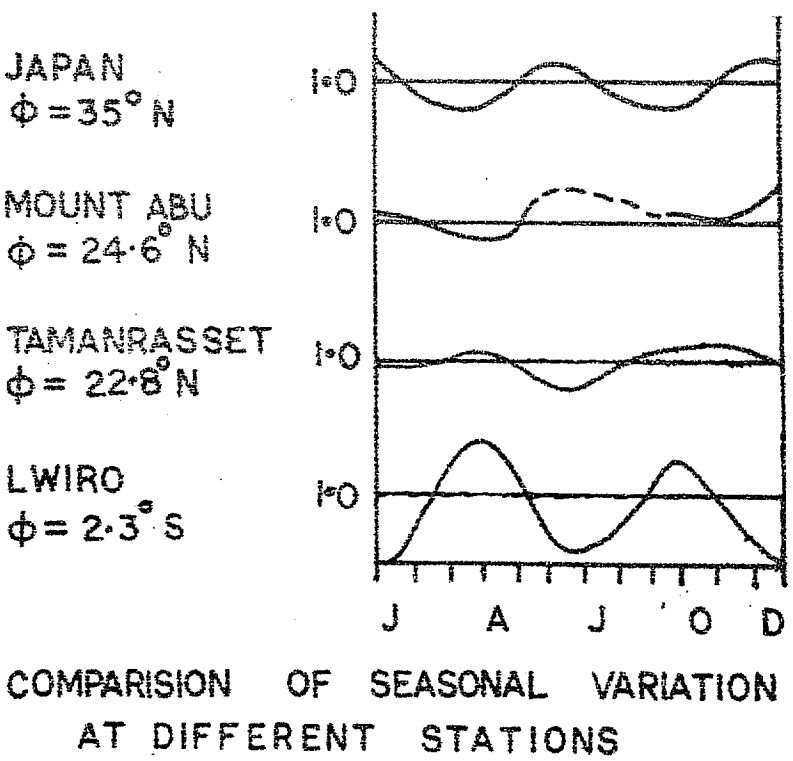

FIGURE 5.11 Comparison of the seasonal variation at different latitudes.

3) The first maximum of intensity appears in November/December in each of the years of observation.

Figure 5.11 shows a plot of the curve of seasonal variation of OH airglow intensity at Mt. Abu in 1967-68 and the seasonal curves at different latitudes as given by SHEFOV (1969). The seasonal variations of hydroxyl emission intensity are of a complicated nature. From the data of the different stations, two maxima are observed in a year and their relative intensities and seasons of appearance differ. The second maximum of intensity could not be confirmed at Mt. Abu due to lack of data in the monsoon months.

There is apparently a reversal of phase in the seasonal variations at stations north of 24^{o}N and at station south of 24^{o}N (geographic).

5.3 Interrelation between OH and other night airglow emissions:

5.3.1 Correlation between OH and 5893 A (Na) emissions:

Figure 5.12 shows a comparison of OH (8-3) and Na (5893 A) emissions on a few nights. There is a good general parallelism on most of the occasions; but there are

FIGURE 5.12 NOCTURNAL VARIATION OF OH (8-3) AND N_a (5893) AIRGLOW AT MT ABU ON SELECTED DAYS

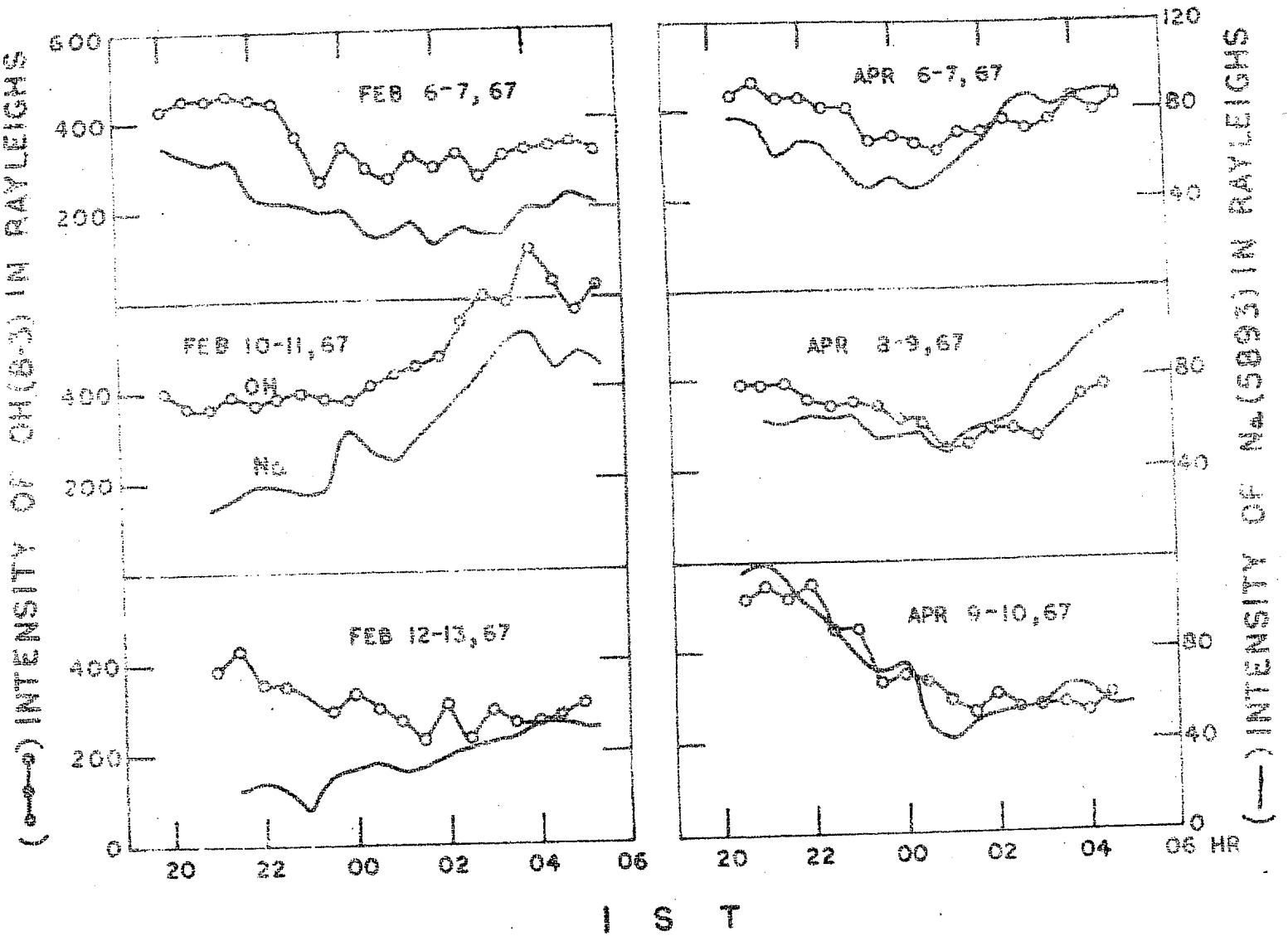

significant differences on some nights as for example on February 12-13, 1967. When the averages of observations on all nights are considered, the similarity between the intensities of OH and Na is less close. The OH intensities have a tendency to decrease at a faster rate in the first half of the night than the sodium line intensities (See Figure 5.13).

A correlation study was made between OH (7-2) and 5893 A for the two years 1966-67, 1967-68. Nights when observations were available for more than 5 hours are considered for correlation studies. From the half hourly observations a correlation coefficient is found for each of the individual nights. A histogram grouping of the correlation coefficients is made for the nights in intervals of 0.1.

From the histogram of the correlation coefficients in the case of OH (7-2) and 5893 A shown in Figure 5.14 it is seen that there is a high positive correlation ($\sim$0.6) between OH and 5893 A as noted earlier by BERTHIER (1954) and BARBIER (1955). However, there are occasions when the correlation is spread between -0.1 to +0.6. An explanation of the positive correlation between OH and sodium emissions was given by BALLIF and VENKATESWARAN (1962). They showed the interlinkage of the excitation mechanisms involved.

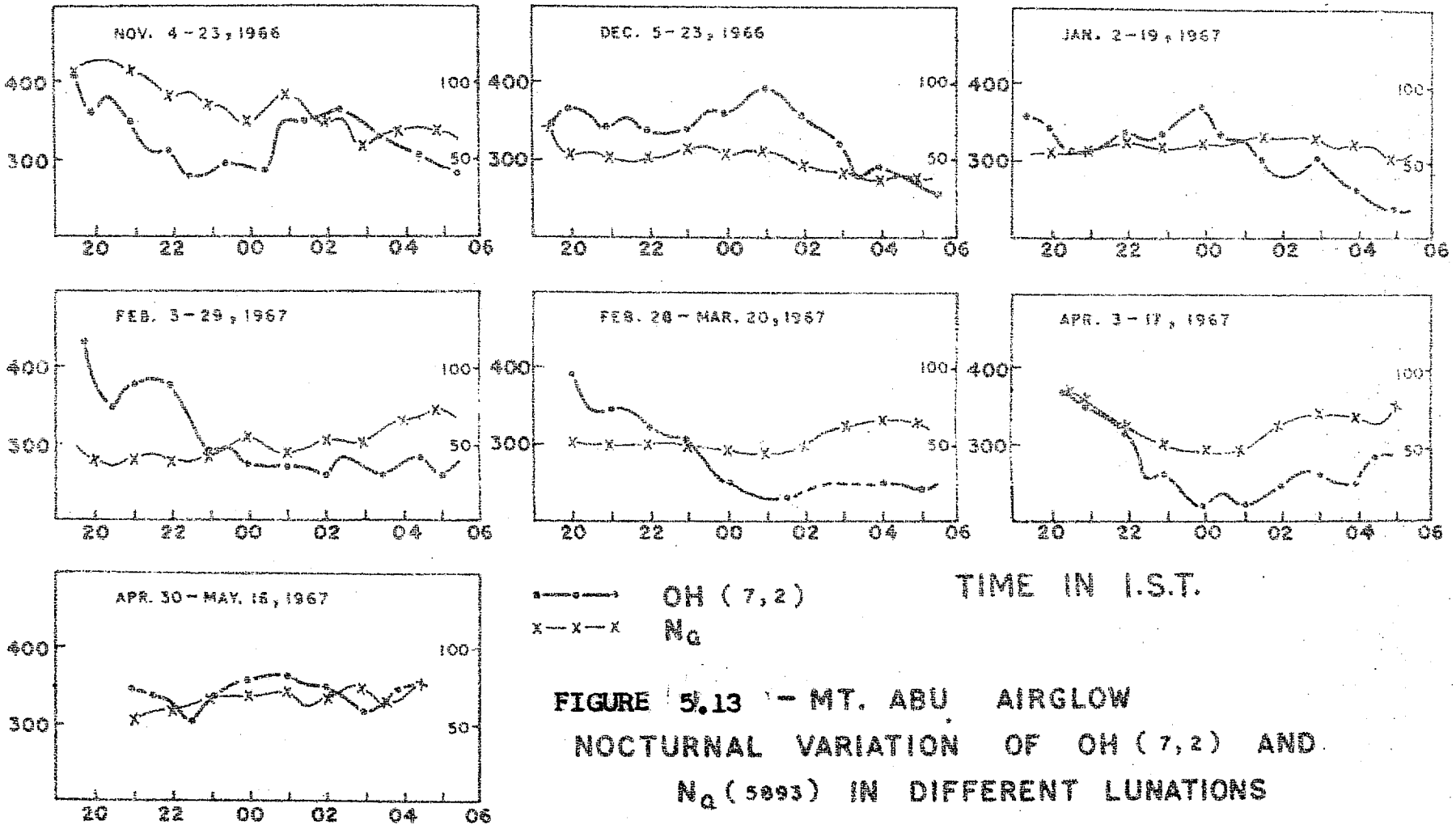

FIGURE 5.13 - MT. ABU AIRGLOW NOCTURNAL VARIATION OF OH (7, 2) AND N_a (5893) IN DIFFERENT LUNATIONS

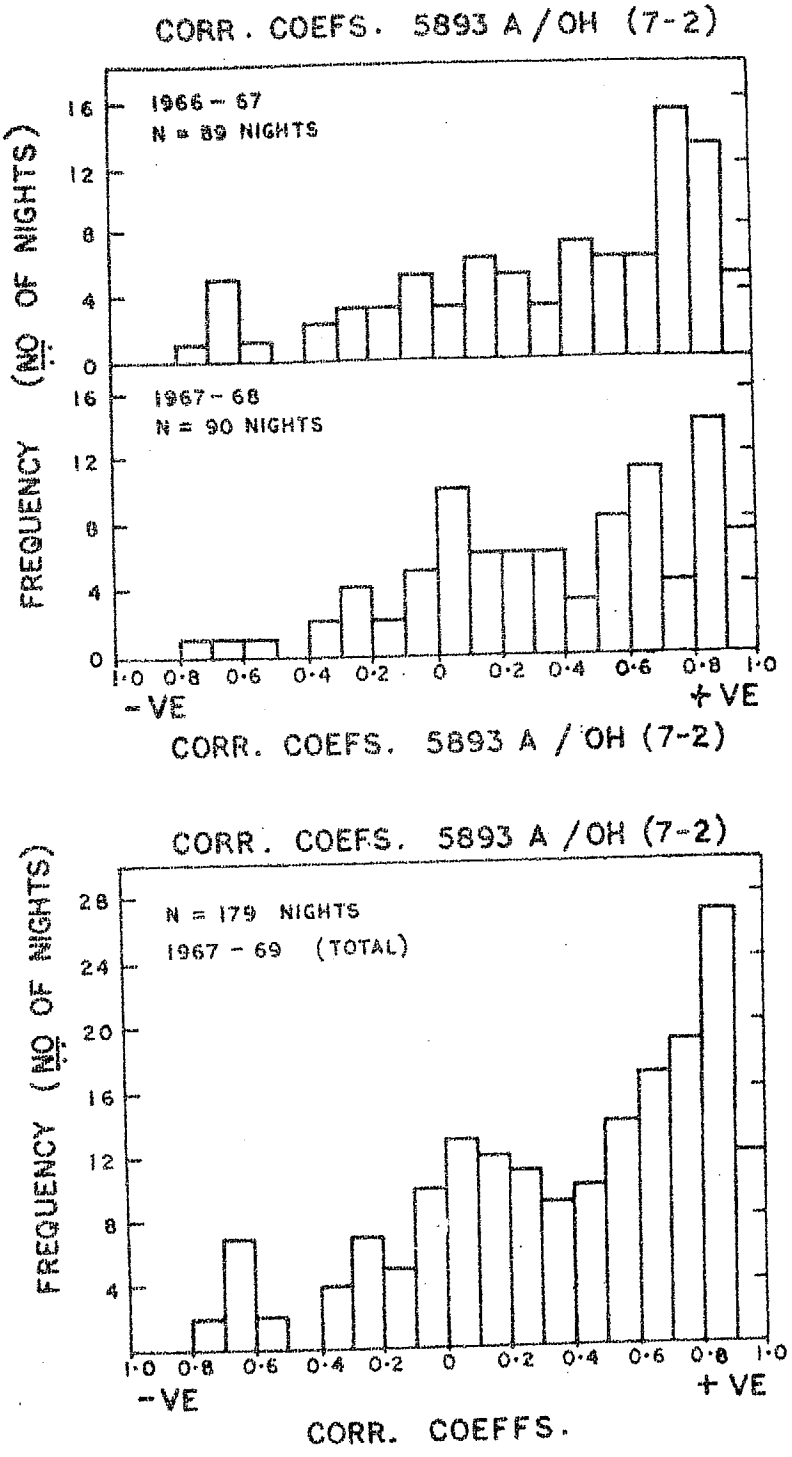

FIGURE 5.14 Histograms of the correlation coefficients between 5893 A and OH (7-2).

BATES and NICOLET (1950); and HERZBERG (1951) attributed the OH excitation to the two body reaction

$$O_3 + H \longrightarrow OH^* + O_2 \qquad (1)$$

where OH^* indicates the state of excitation.

At a given time 't' the rate of production of such excited OH molecules is given by

$$\in (OH^*, t) = \sum_{V'=1}^{V''} \in (OH^*, t)_V = k_1 \, n(H,t) \, n(O_3,t) \qquad (2)$$

$n(H)$ and $n(O_3)$ are the concentrations (particles cm^{-3}) of hydrogen and ozone; k_1 is the specific reaction rate of the reaction (1).

Assuming n (H) to be constant throughout the night, the alternate form of equation (2) is

$$\in (OH^*, t) = K \; n(O_3, t) \qquad 2(a)$$

where $K = k_1 \, n(H, t_o)$.

From 2(a) it is obvious that the OH glow from any single level in the earth's atmosphere will simply reproduce the temporal variations of O_3 at that level. However, it is necessary to remember that the integrated O_3 variations which are recorded either at ground or from a satellite will be a weighted sum of the intensities at the separate levels the weighings for each level being different at different times of the night.

A significant result shown by rocket photometry (PACKER, 1961) is that the OH and Na glows have nearly the same height of emission. This means that the chemical reactions involving Na and its compounds take place in the same reaction zone as that of OH emission. According to CHAPMAN (1939) the primary excitation mechanism for sodium was

$$Na\ O + O \longrightarrow Na^* + O_2 \qquad (3)$$

BATES and NICOLET (1950) doubted the exothermicity of the above reaction and advocated as an alternative.

$$Na\ H + O \longrightarrow Na^* + OH \qquad (4)$$

The sodium atoms formed by the reactions can undergo oxidation in the following ways.

$$Na + O_3 \longrightarrow Na\,O + O_2 \qquad (5)$$

$$Na + O_2 + Z \longrightarrow Na\,O_2 + Z \qquad (6)$$

$$Na + O + Z \longrightarrow Na\,O + Z \qquad (7)$$

$$Na\,O_2 + O \longrightarrow Na\,O + O_2 \qquad (8)$$

$$Na\,O_2 + H \longrightarrow Na\,H + OH \qquad (9)$$

The instantaneous volume emission rate is given as

$$\epsilon(Na^*,t) = n\,(Na,t)\left[k_5\, n(O_3,t) + \left\{k_6\, n(O_2)\, n(Z) + k_7\, n(O,t_o)\, n(Z)\right\}\right] \qquad (10)$$

which shows that sodium excitation rate has both a steady state component given by the curly brackets and a temporal component governed by $n(O_3,t)$. Only (O_2) can be treated as constant. (O) can be variable.

Hence the observed covariability of the OH and Na glows in the night sky might follow as a consequence of the fact that they primarily reflect in their intensities the nocturnal variation of O_3 at their common levels of origin. The different types of O_3 variations that can occur when K changes, may in fact be responsible for the different types of nocturnal variation of OH glow.

The OH emission is a maximum at 85 km, but there is a range of heights over which the emission extends. Even a slight difference in the level, of emission of OH and Na can show a change in the type of variation of the emissions, and lack of correlation.

5.3.2 Comparison of OH and 5577 A emissions:

A comparative study of the seasonal variation of OH and 5577 A (OI) was made. The 5577 A data were taken from the pole photometer and converted to local zenith intensities. The OH intensities were obtained from the Red photometer pointing to zenith during November 1966-January 1968. In Figure 5.15 the seasonal variation of OH (8-3), OH (7-2) and 5577 A are shown for one complete year. It can be seen that while there is a maximum in 5577 A in April, a minimum is observed in OH emission and when there is a maximum in OH (Nov/Dec), a minimum is observed in 5577 A (OI). The concentration of atomic oxygen has a seasonal variation at both OH and 5577 A heights, being greater above 100 km in April and less in December. It is probable that atomic oxygen descends to lower heights in the winter months and thus the formation of O_3 and the intensities of OH are greater in those months and thus behaviour of OH and 5577 A variation is opposite. Also, since the heights of 5893 A emission is nearer to that of 5577 A, the seasonal variation of 5893 A

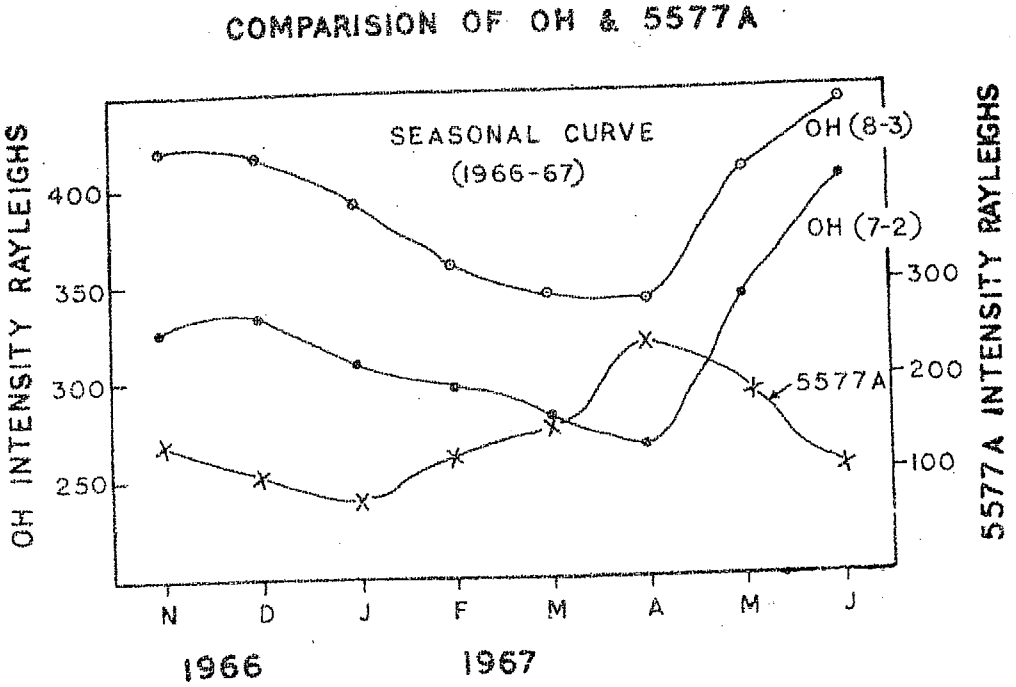

FIGURE 5.15 Seasonal variation of OH (8-3), OH (7-2) and 5577 Å.

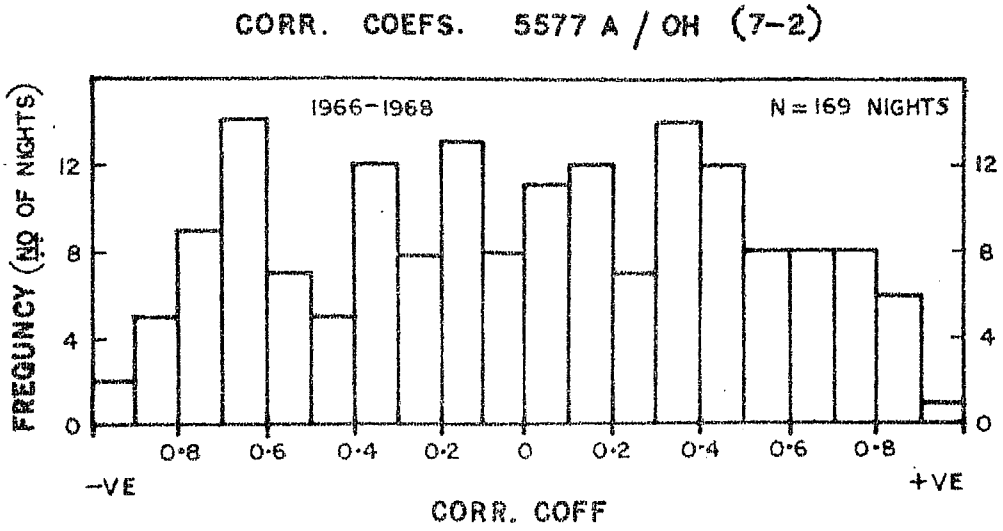

FIGURE 5.16 Histogram of the correlation coefficients between 5577 Å and OH (7-2).

and 5577 A are broadly similar. A model was developed by TOHMATSU (1958) and TOHMATSU and NAGATA (1963) for the explanation of mid-latitude maximum of 5577 A and its seasonal variation by invoking meteorological transport of oxygen allotropes by large scale circulation in the upper atmosphere.

5.3.3 Relation between 5577 A and OH due to vertical eddy transport:

From the correlation histogram of all the individual nights given in Figure 5.16 for 5577 A and OH (7-2), it is seen that there is no obvious relation between these emissions in their nocturnal variation.

Recently HESSTVEDT (1968a, 1968b) has made calculations of the various chemical reactions in the lower ionosphere including vertical eddy transport. He mentions that in the case of 5577 A and OH, horizontal gradients in the number density of atomic oxygen are likely to be less significant than the vertical gradients. With an upward vertical mean motion of air, both green line and OH would decrease, while descending motion will result in increased intensities. His calculations predict a sharp maximum at 88 km for OH emission (see Figure 5.17). The measurement of the half

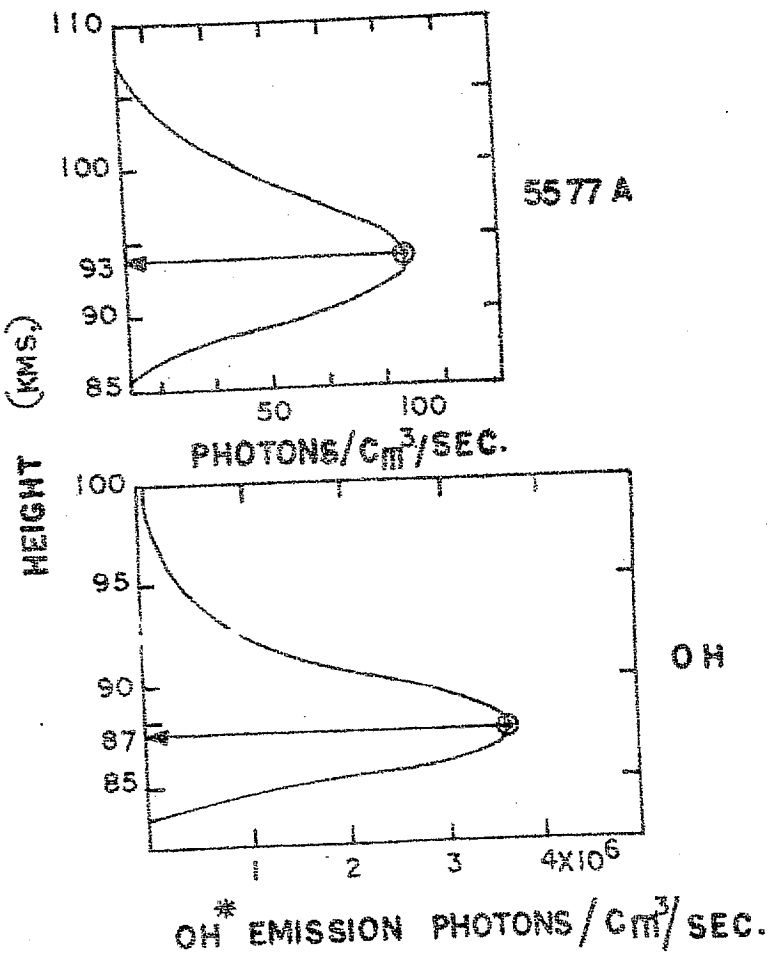

FIGURE 5.17 Heights of emission of OH and 5577 A (taken from Hesstvedt 1968b).

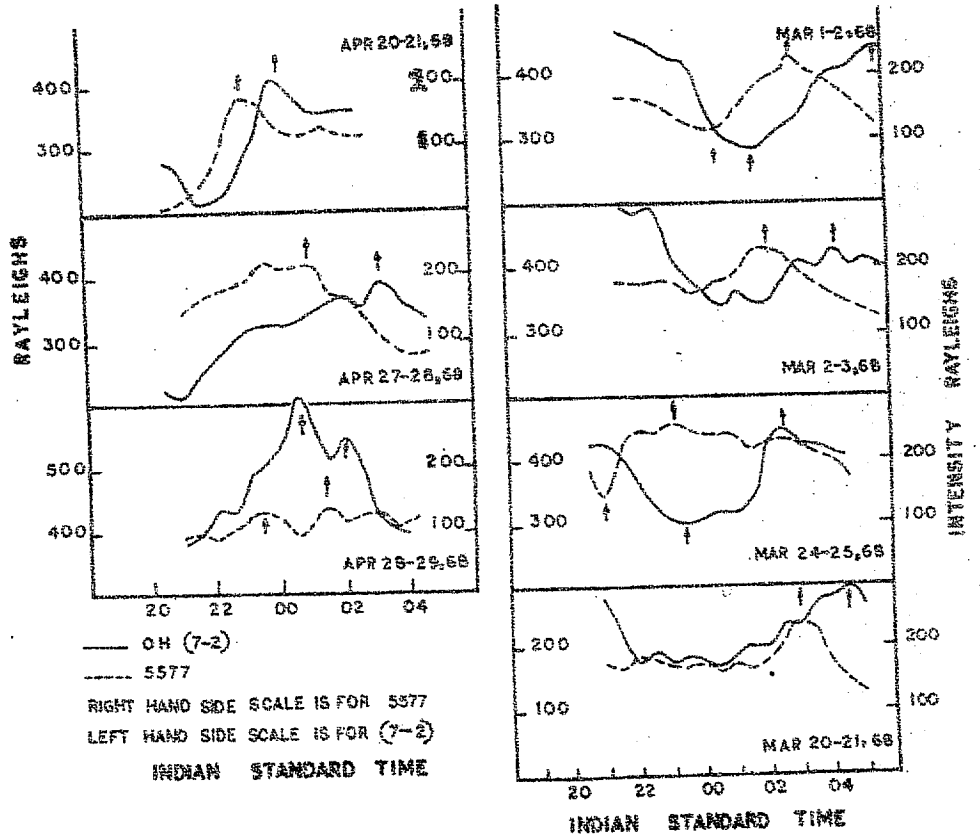

BEHAVIOUR OF 5577A AND OH ON FEW NIGHTS

FIGURE 5.18 Few nights showing maxima in OH and 5577 A, the OH maxima lagging behind 5577 A.

thickness of the emitting layers of 5577 (OI) and OH show an approximate value of 10 km. centered around 95 km for the green line and 85 km to 90 km for OH emission.

In the following Hesstvedt's suggestion is compared with our observational results. The data of all the nights for 5577 A, 5893 A and OH emissions were scanned. In the case of 5577 A, and OH on a few occasions (as shown in Figure 5.18) a decreasing tendency in both these emissions for a few hours after sunset was observed and then the intensities started increasing. A time difference in the times of their maxima was noted, the OH maximum lagging behind the maximum of 5577 A. This may be interpreted as follows. From the time delay in the maxima of 5577 A and OH, it appears that the descent of a common agency, (in this case atomic oxygen) might have been responsible for the increases of 5577 A and OH.

5.3.4 Correlation between OH and 6300 A emissions:

In general, 6300 A emission at Mt. Abu shows post-twilight decay followed by a steady value and then an increase on approaching dawn, and this variation is similar to type B variation of OH. Hence a high +ve correlation may be expected between OH and 6300 A emissions as type B

variation of OH is the most frequent. But one has to consider whether this positive correlation has any physical significance or whether it is merely due to a contamination of OH (9-3) intensity with that of 6300 A.

KRASSOVSKY (1963) comments "OH emission is closely correlated with the nocturnal variation of Na and H α". A tendency for a similar relationship is also seen in the case of 6300 A (OI) emission when its intensity is low and there are no magnetic disturbances or aurorae. He concludes that on the average, it is possible to note a certain tendency for similarity in the general progress of OH, O_2, Na and 6300 A (OI) night airglow variations and even those of 5577 A (OI) and the continuum. He gives a possible explanation of the correlation between 6300 A and OH emissions, namely that these two emissions are connected with intense upward penetration of molecular oxygen which reacts with N^+. This reaction is exothermic with an yield of 6.45 ev. Red oxygen emission may thus occur. At the same time more intense atmospheric circulation may also lead to intensification of hydroxyl emission. Together with this, he explains the red arcs also.

For a correlation study of 6300 A and OH emissions, 6300 A observations were taken with the same 'red photometer' as OH, and the correlation coefficient was determined

considering all the half hourly observations in a night. A histogram is plotted in Figure 5.19 for all the correlation coefficients determined for the nights during 1966-69. The correlation coefficients are grouped into 20 groups from -1.0 to +1.0 at intervals of 0.1.

It is seen from this histogram that the frequencies of nights of the correlation coefficients from -0.1 to +1.0 are more or less equally distributed. This is the consequence of observing the different types of variation and also the peak observed which moved with sidereal time in the OH night-glow and a more or less regular type of variation in 6300 A emission. It can be concluded that there is no relation between 6300 A and OH emissions at Mt. Abu as far as their excitation mechanisms and the dynamical processes are concerned; the main reason being, the heights of the two emissions are very different (85 km and 300 km) and it is difficult to see how the effects in these region could be similar.

The high positive correlation obtained on some nights is only due to the nature of the variation of the two emissions which are more or less similar on some nights and not merely due to the contamination of OH (9-3) band in 6300 A as reported by some earlier workers (BARBIER, 1958; CHAMBERLAIN, 1961f).

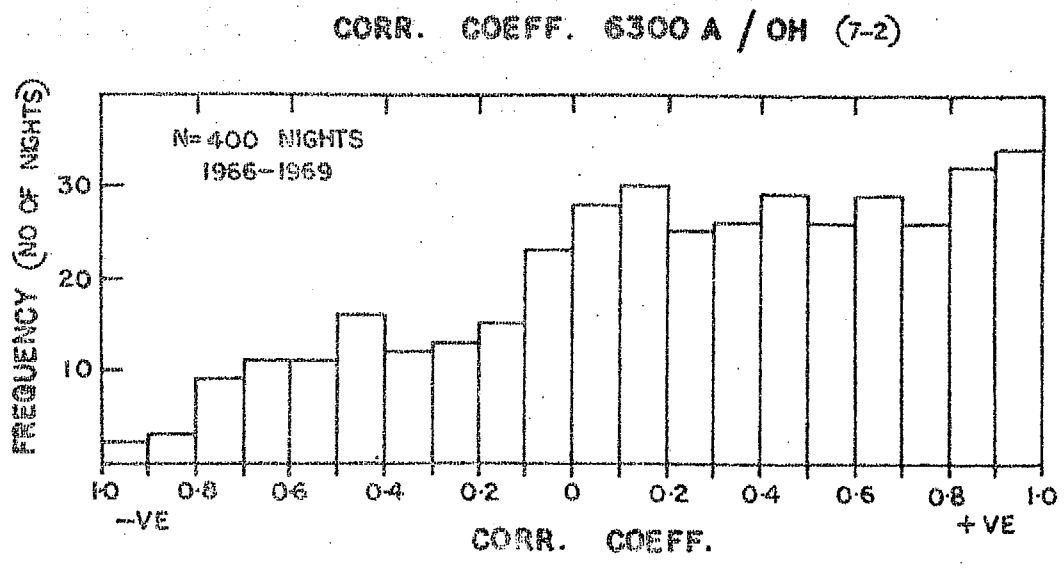

FIGURE 5.19 Histogram of the correlation coefficients between 6300 Å and OH (7-2).

M+ Abu

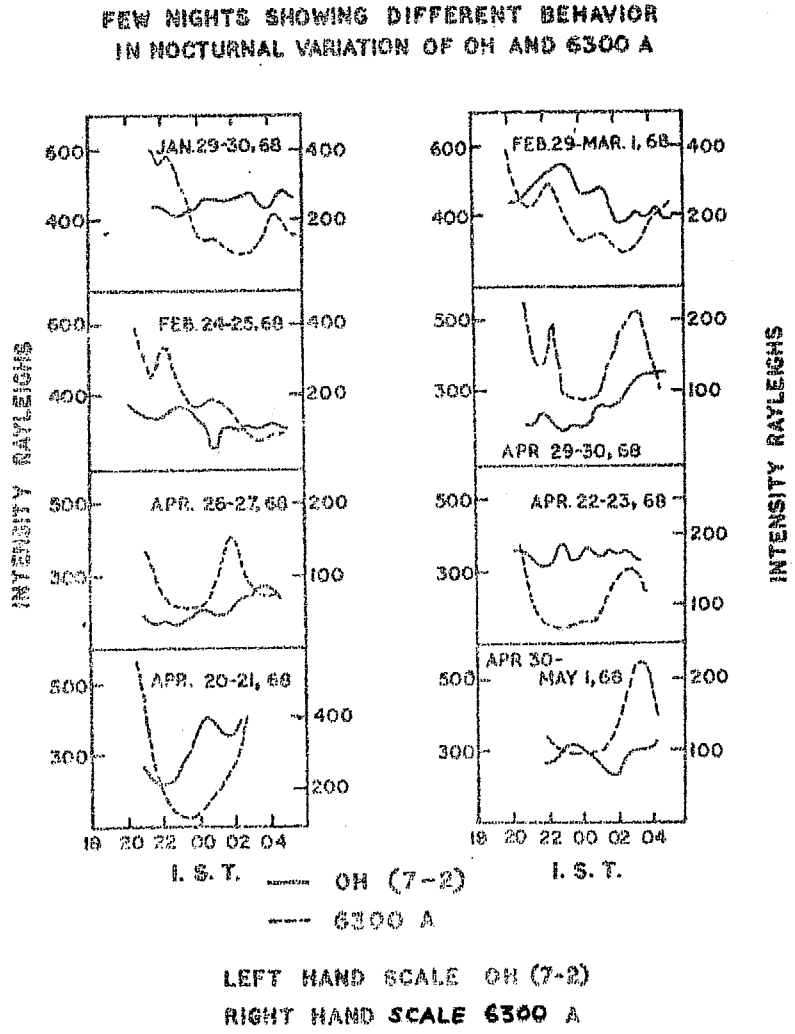

FIGURE 5.20 A few nights showing different behaviour in the nocturnal variation of OH and 6300 A.

Figure 5.20 shows the nocturnal variation of OH (7-2) and 6300 A on some typical nights when OH and 6300 A variations were different, which show that there is no relation between these two emissions.

5.4 Effect of celestial X-ray sources on OH night airglow intensity:

In this section an interesting finding is reported that celestial X-ray sources affect the atmosphere in the meso-pause region causing an increase in OH emission.

Recently, ANANTHAKRISHNAN and RAMANATHAN (1969) reported that there is an effect of X-rays from celestial X-ray sources Sco X-1, Tau X-1 and Cyg X-1 on the night time field strength of 164 KHz. radio waves transmitted from Tashkent and received at Ahmedabad over a distance of 2100 km. Later in a detailed paper, ANANTHAKRISHNAN et al. (1970) presented the calculations of ion production and the resulting electron densities from 75 to 90 km due to the X-ray sources.

In the average nocturnal variation curves of OH (7-2) in different lunations presented in Figure 5.21, a pronounced maximum is noted between 01 and 03 hours I.S.T. in Nov 1966 This maximum shifts to the earlier part of the night by about 2 hours

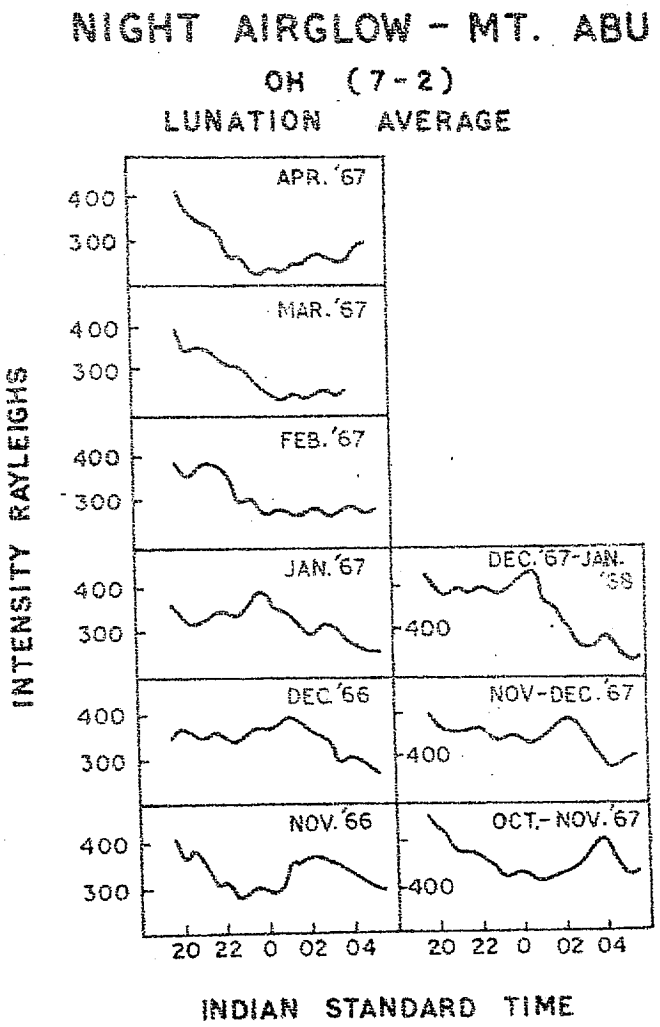

FIGURE 5.21 Average nocturnal variation of OH (7-2) in different lunations.

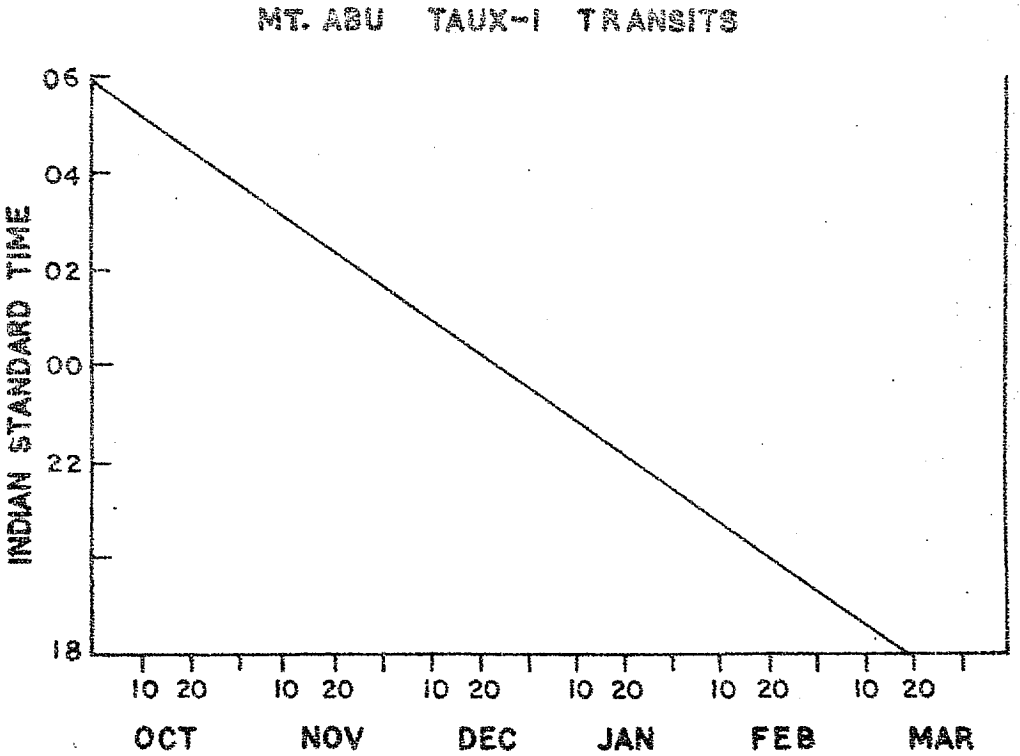

FIGURE 5.22 The times of transit of Taurus X-1 for Mt.Abu during October-March.

each month from November to March and merges with the twilight maximum in April 1967. The same is repeated in the next year. As the dark halves of the lunations in 1967-68 fall in two months, there is a small time difference between October-November 1967 maximum and November 1966 maximum. The times of occurrence of maximum intensity of OH glow nearly coincide with the minimum zenith angle (i.e. transit times) of the celestial X-ray source Taurus X-1 ($\alpha = 5^h31^m$, $\delta = +21^\circ59'$). The times of transit of Taurus X-1 for Mt.Abu (24.6°N, 72.7°E) from November to March are shown in Figure 5.22.

In Figure 5.23 the OH intensities of all the individual nights in each lunation from November 1966 to October-November 1967 are plotted in composite graphs. Almost all the nights showed an increase in OH intensity near the time of transit of Taurus X-1. The amount of increase in intensity varies somewhat from night to night, but in general the time of maximum agrees well with the transit time of Taurus X-1.

The months April, May and June are favourable to see the effect of Scorpius X-1 ($\alpha = 16^h17^m$; $\delta = -15^\circ53'$) and Cygnus X-1 ($\alpha = 19^h57^m$, $\delta = +34.5^\circ$) on the OH intensities, although to some extent the latter two months are effected by haze and cloud. The average nocturnal

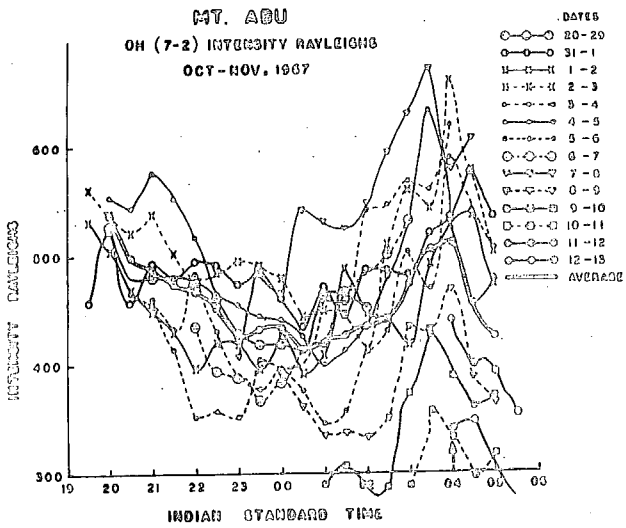

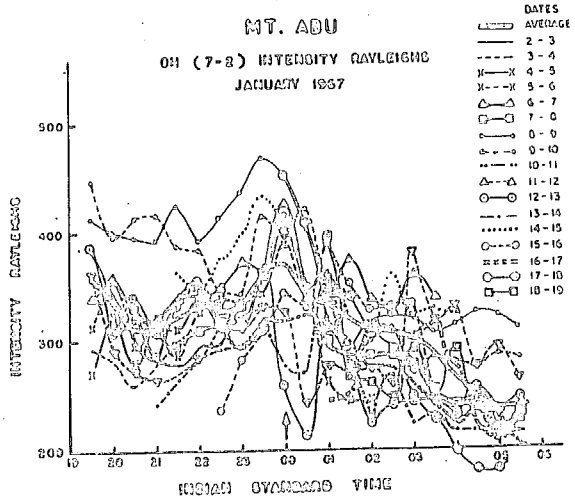

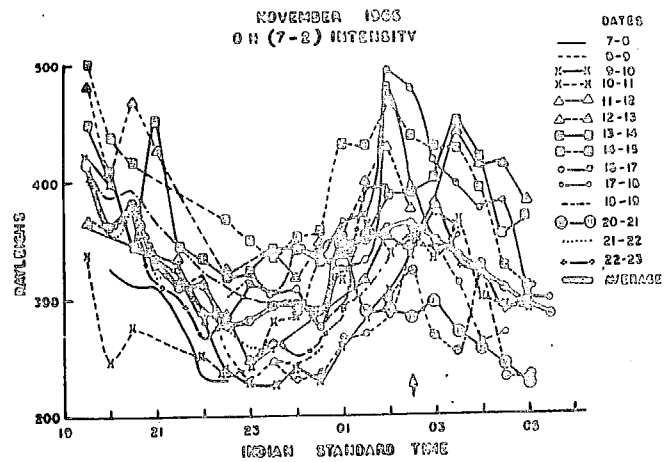

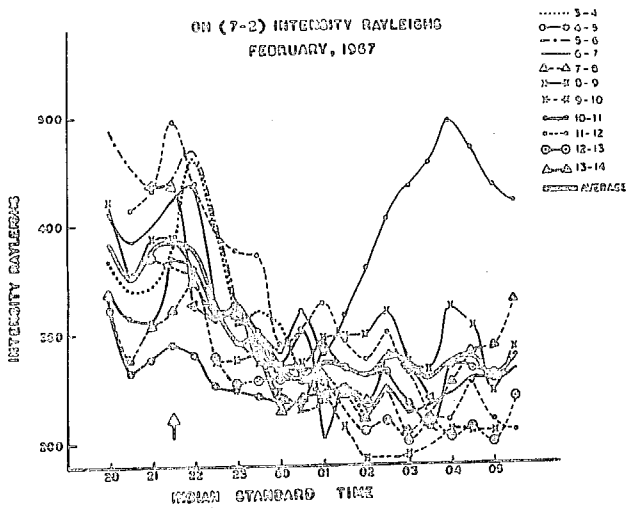

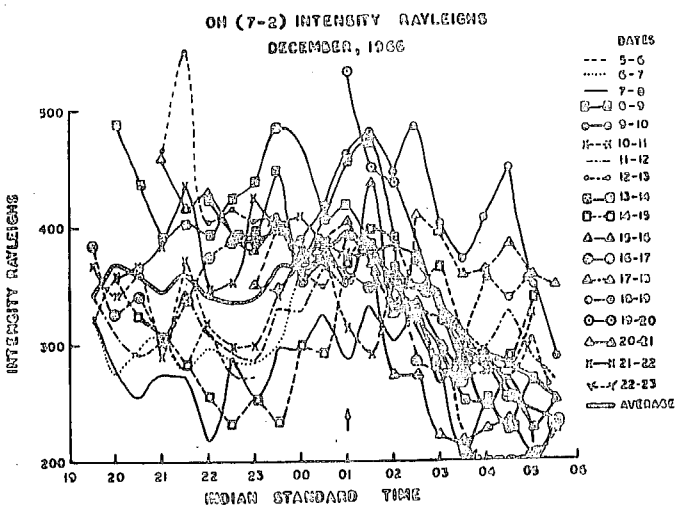

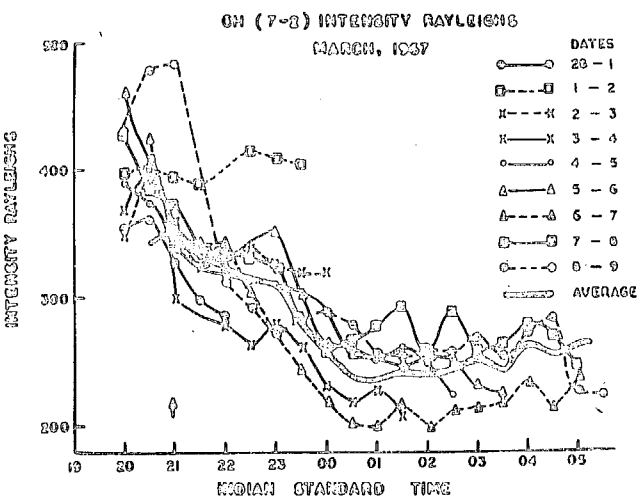

FIGURE 5.23 Mass plots of all individual nights in each of the lunations from November 1966 to October-November 1967.

variation curves of lunations in March, April and May 1967; and May-June, June-July March-April, April-May, 1968 are presented in Figure 5.24. A small maximum is noted in April 1967 which becomes a broad maximum in May 1967 with a shift in the time of maximum. The same is repeated more clearly in 1968. The transit times of Scorpius X-1 and Cygnus X-1 for Mt.Abu are also plotted in Figure 5.25.

5.4.1 Nocturnal variation of OH (7-2): Isophote maps:

On a number of occasions, the scanning photoelectric photometer has been operated with OH (7-2) filter. After appropriate reduction as described in Chapter III all-sky isophote maps have been drawn. The isophote maps of two nights are shown in Figure 5.26 and 5.27, which show the effect of the X-ray sources. In each isophote map, it is seen that the region of maximum intensity is around the position of the X-ray source. The maximum intensity moves with the movement of the X-ray source. If the zenith angle of the source is more than 60° (denoted by the inner circle) the effect is less clearly seen owing to variable scattering and extinction of light.

The increase in intensity of OH radiation which shifts with sidereal time may also be due to the transit of the Milky Way. Simultaneous measurements of 6300 A

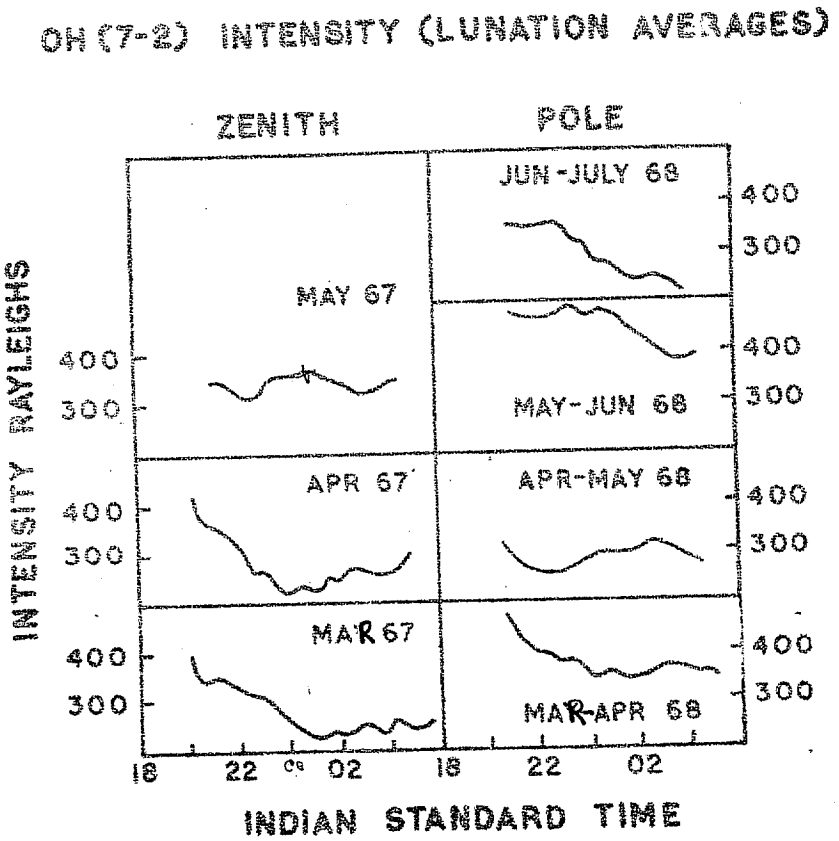

FIGURE 5.24 Average nocturnal variation of OH(7-2) in March to July lunations.

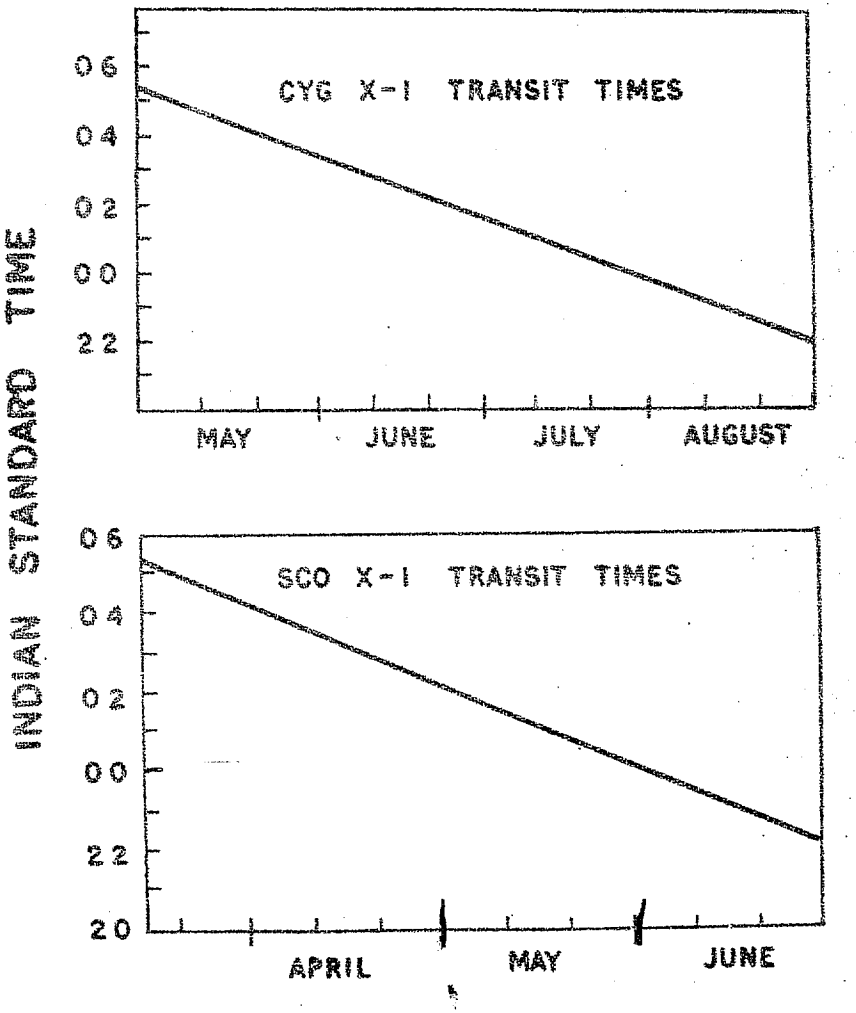

FIGURE 5.25 The times of transit of Sco X-1 and Cyg X-1 for Mt.Abu.

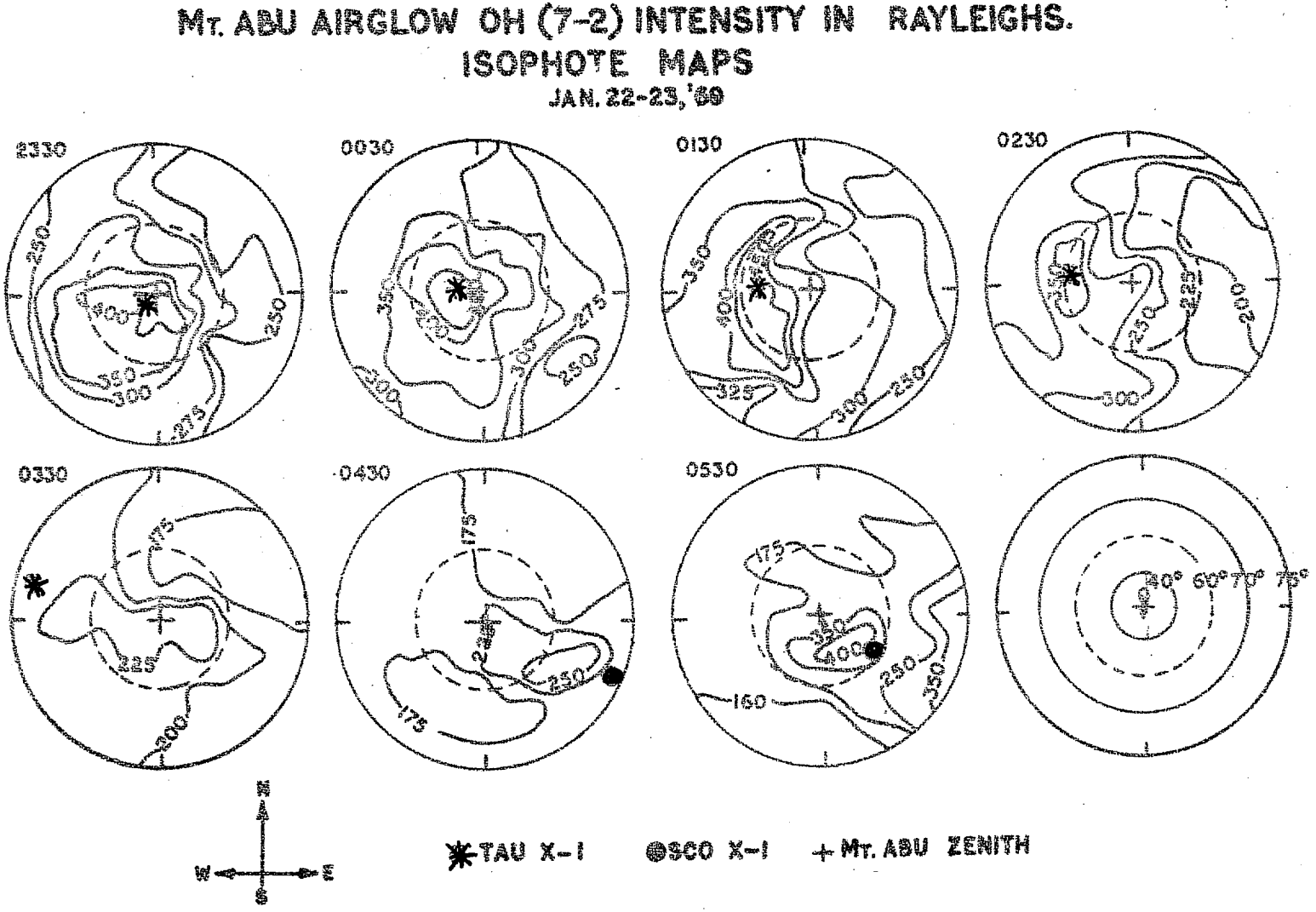

FIGURE 5.26 Isophote maps of OH (7-2) on January 22-23, 1969 showing the effect of celestial X-ray sources.

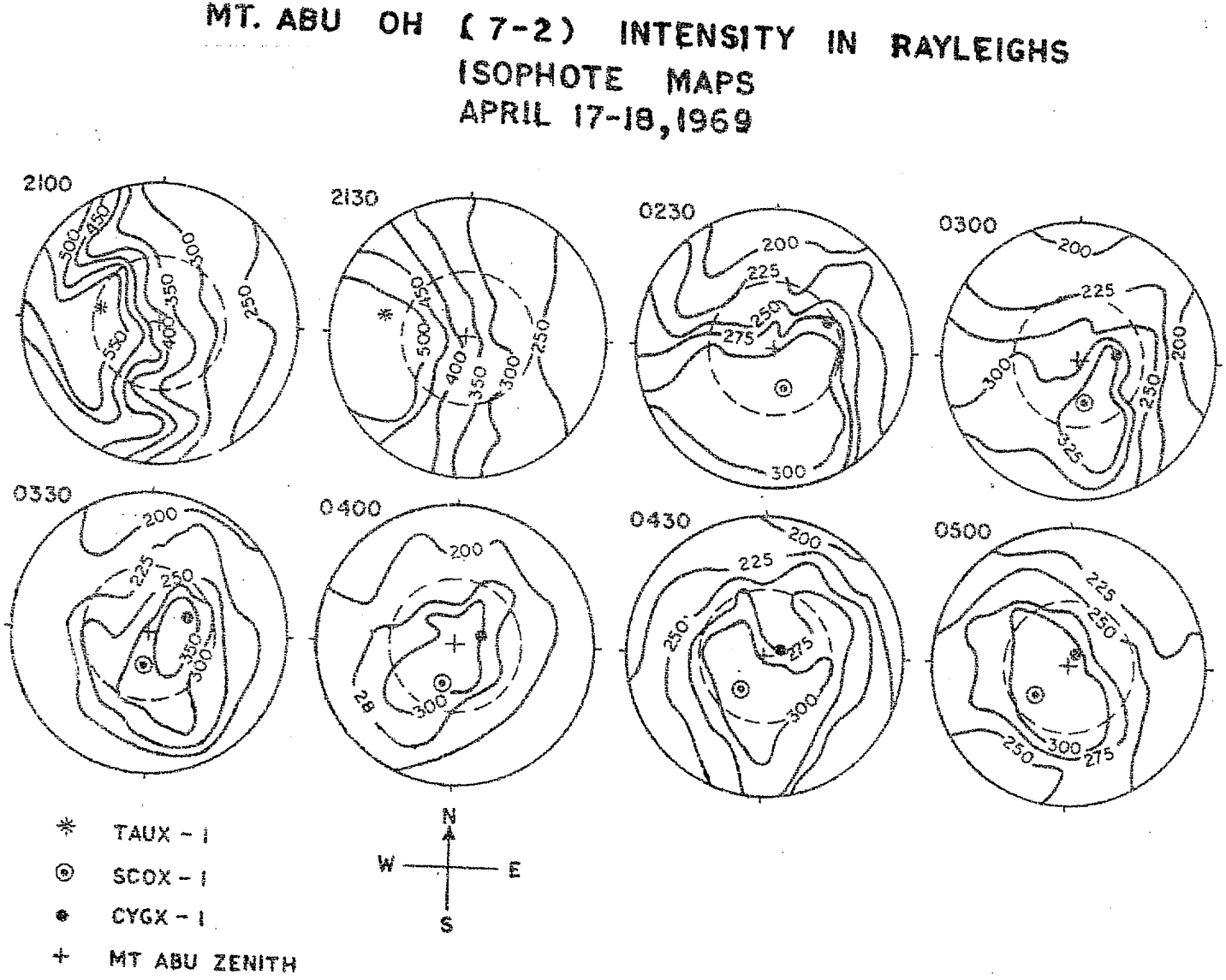

FIGURE 5.27 Isophote maps of OH (7-2) on April 17-18, 1969 showing the effect of celestial X-ray sources.

intensities with the same photometer, reduced to absolute intensities with similar calibration and reduction procedure as those used for OH (7-2) emission, do not show any increase which shifts with sidereal time. This confirms that the increase in the case of OH is not due to the transit of the Milky Way. The lunation average curves of OH (7-2), OH (8-3) and 6300 A of four lunations are plotted in Figure 5.28 where it is seen that OH (7-2), and OH (8-3) show a clear peak which is not seen in 6300 A. After January 1968, we changed the direction of observation from zenith to pole and due to higher zenith angle and Sec Z effect the magnitude of the increase in intensity is reduced.

The increase in OH intensity which is observed when X-ray star transits take place can be accounted for by an increase in ozone or hydrogen or both near the level of maximum intensity due to the increased ionization due to the X-ray source in the mesosphere. A detailed discussion of the possible chemical reactions and the mechanism of increase in OH intensity due to X-ray sources will be published elsewhere.

.....

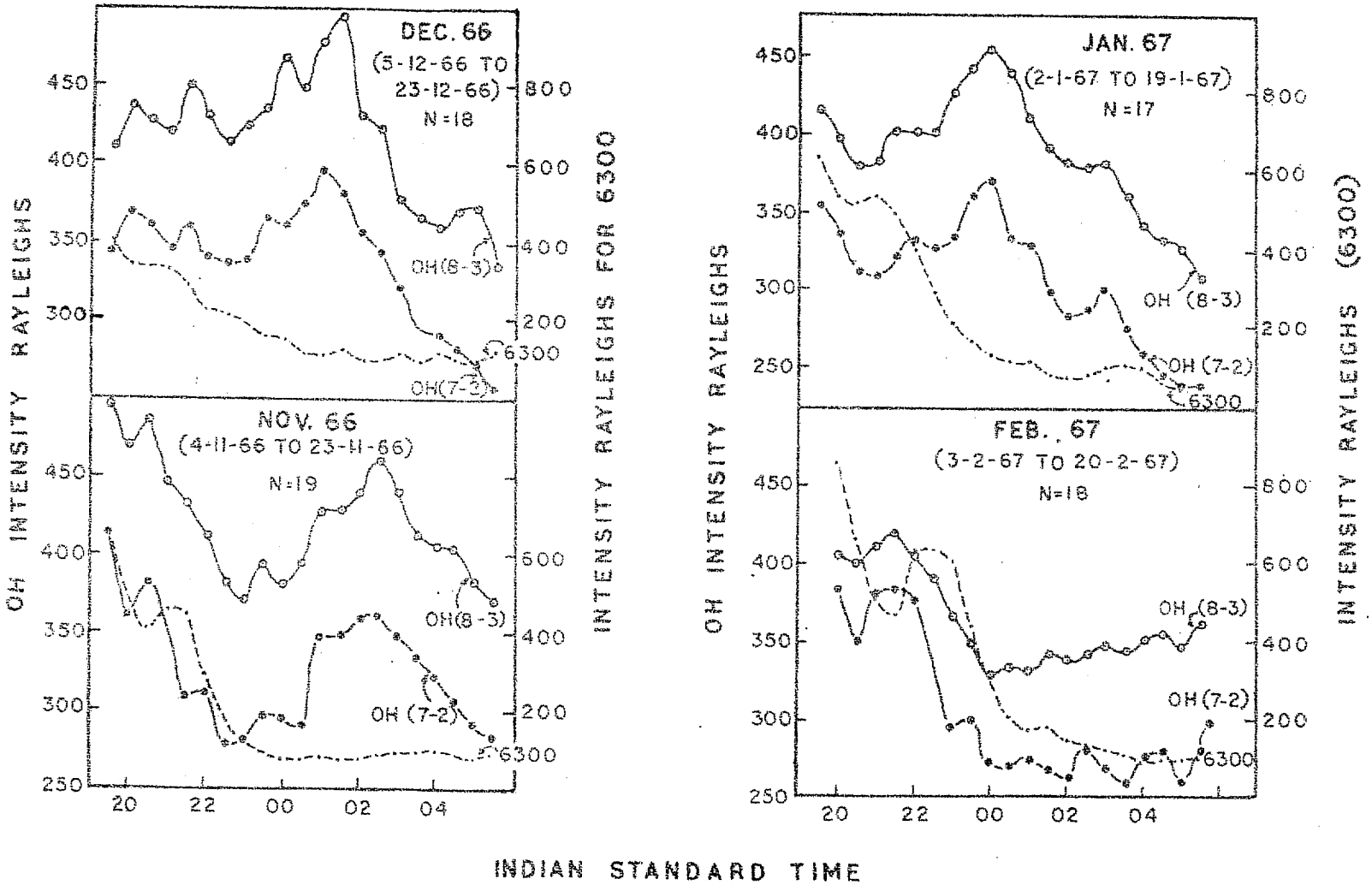

FIGURE 5.28 Comparison of the average nocturnal variations of OH and 6300 A.

CHAPTER VI

F-REGION NIGHTGLOW EMISSIONS OF ATOMIC OXYGEN

6. Introduction:

Among the night airglow emissions, 6300 A of atomic oxygen is particularly interesting due to its connection with the dynamical behaviour of the ionosphere and its close relation with the ionospheric parameters. In this chapter the results obtained from 6300 A measurements with the three photometers described in chapter I are discussed.

In section 6.1, a brief review of the present state of knowledge of 6300 A emission and its behaviour in low latitudes is described and the problems which require further study are outlined.

In section 6.2 the nocturnal variations, the pre-dawn and post-twilight decay effects and seasonal variations observed at Mt. Abu are discussed using the data acquired at Mt. Abu in 1964-69. From the ionospheric data of Ahmedabad and Delhi, using Barbier's relation, calculations are made for the quantal emissions of 6300 A and they are compared with the observed intensity of 6300 A. The behaviour of 6300 A during spread F conditions is investigated.

In section 6.3 the airglow enhancements in 6300 A observed at certain times of the night are discussed at length and a possible explanation of these enhancements is given with calculations of night time vertical drifts during those hours. The behaviour of the ionosphere in low latitudes during the times of these enhancements is considered.

In section 6.4 the relation of the electron density at different heights and 6300 A variations is considered and a method is given for relating the probable height of maximum emission of 6300 A from the electron content in the F-region and 6300 A ground observations.

In section 6.5 isophote maps of 6300 A emission on a number of nights obtained with the scanning photometer are considered and a classification of aligned and structured maps is made and the frequency of occurrence of these maps is given. The similarity between the movement of isolines and the crests of F-region peak electron density is pointed out (KING, 1968). Considering the data of many nights in different months, the decay phase of equatorial anomaly is studied.

In section 6.6, it is shown that on occasions when a good positive correlation is obtained between 6300 A and 5577 A Barbier's relation fits reasonably well even in

the case of 5577 A. The constant term in that relation is interpreted to be the contribution to 5577 A emission from the 100 km layer. Towards the end of this section an attempt is made to use the detailed expressions of PETERSON et al. (1966) for calculating the ^1D and ^1S terms from the electron density profiles obtained from Ahmedabad ionospheric data.

6.1 Brief review of earlier work:

6.1.1 Introduction

The F-region atomic oxygen nightglow consists of only two emissions in the visible region, a triplet at 6300 - 6364 - 6392 A $O(^1D)$ and 5577 A $O(^1S)$. The relevant part of the energy level diagram of atomic oxygen taken from PETERSON et al.(1966) is shown in Figure 6.1. Of the triplet lines of $O(^1D)$, 6392 A is very weak, and 6300 A is the brightest. The intensity ratio of 6300 to 6364 is 3:1 (CHAMBERLAIN, 1961g)and the ratio of 6300 A to the 5577 in the F-region is 3:1 (GULLEDGE et al.,1966, 1968).

BATES (1946) suggested that the oxygen atoms in the ionospheric F region are excited by dissociative recombination. This suggestion has been developed by several scientists (NICOLET, 1954; CHAMBERLAIN, 1958; LAGOS et al., 1963; PETERSON et al., 1966). The agreement between the

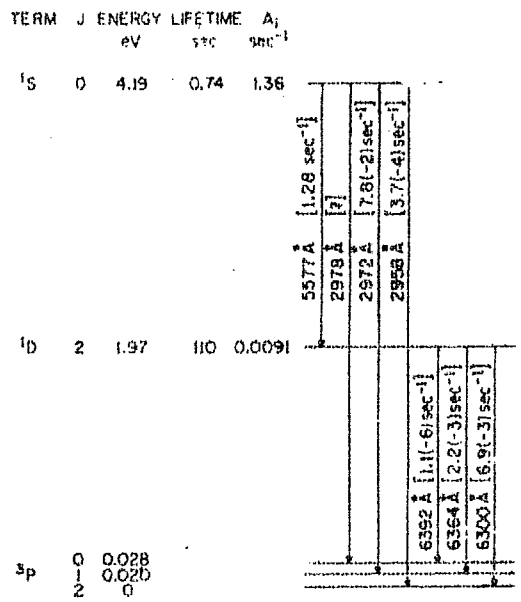

The low-energy portion of the atomic oxygen energy level diagram. The designation, total angular momentum quantum number, energy above ground level, and Einstein transition coefficient are indicated for each level. The wavelength (in A) and the Einstein coefficient A_i (in sec^{-1}) are also indicated for each transition. For the A_i, the exponent of 10 is in parentheses; thus, 7.8(—2) means 7.8×10^{-2}.

FIGURE 6.1 Energy level diagram of atomic oxygen.

observed intensity of 6300 A and the intensity computed from ionospheric parameters was shown by St.AMAND (1955) and BARBIER (1957)[a,b,c]. Later, the relation has been studied by many people. Using the electron density profiles, the close relation between the observed and computed 6300 A was shown by NAGATA and OGAWA (1964), PETERSON and STEIGER (1966) and VAN ZANDT (1969). Since the discovery of its connection with ionospheric parameters, the 6300 A and its dynamical behaviour in low latitudes has been studied by many people (PAL and KULKARNI, 1968; VAN ZANDT and PETERSON, 1968).

Review articles have been written from time to time by outstanding workers (BARBIER, 1961; CHAMBERLAIN, 1961a; ROACH, 1963a; 1963b; BARBIER, 1965; ROACH, 1968. VAN ZANDT, 1969). However, quantitative relationship between 6300 A and ionospheric parameters has been established, the correlation between the observed and computed intensities though good is not perfect. It is difficult to say whether the discrepancies are due to the approximations that have been made in the theory, or due to inaccuracies in the atmospheric and atomic data that have been used in the calculations, or to observational inaccuracies, or to contributions to emission from some other processes (PETERSON et al., 1966). It is the aim of the study of 6300 A to give

a quantitative basis to the relationship between the ionospheric recombination rates and the intensity of the 6300 A airglow radiation in the night sky. Work in this direction by different workers (PETERSON and STEIGER, 1966; BROWN and STEIGER, 1967; PETERSON and VAN ZANDT, 1969) is in progress.

6.1.2 Phenomena connected with 6300 A emission:

A) Barbier's Relation:

S.K. MITRA (1945) suggested that there was a relation between the optical and ionospheric properties of the high atmosphere. Later St.AMAND (1955) found evidence that the intensity of 6300 A emissine line was related to ionospheric F layer parameters. BARBIER (1957, 1959) made observations at Haute Provence (France) and empirically found the following relationship between the ionospheric parameters and the 6300 A quantal emission Q_{6300} as

$$Q_{6300} = A + B\,(f_oF_2)^2 \quad \exp\left\{-\frac{h'F-200}{H}\right\}$$

where

Q_{6300} is the quantal emission of 6300 A,

f_oF_2 and h'F are the critical frequency and virtual height of the F layer

H is the scale height of molecular oxygen

and A and B are constants.

Later, PETERSON (1968) derived the above relation from more detailed considerations.

BARBIER studied the above relationship and discovered and explained new phenomena of 6300 A airglow and related them to the physics of the ionosphere. The various phenomena observed in 6300 A are post twilight decay, predawn enhancement in nocturnal variation, western sheet, intertropical red arcs etc. In the following we shall very briefly describe these phenomena.

B) Nocturnal variation:

ELVEY and FARNSWORTH (1942) studied the nocturnal variation of 6300 A at the McDonald observatory in Texas. They detected a post twilight decay of 6300 A followed by a predawn enhancement. DUFAY and TCHENG (1946) also observed these features and termed them as 'post twilight'

and 'predawn' effects. These were later confirmed by other workers. Now post-twilight decay, steady values around midnight, and predawn enhancement can be considered to be the general nocturnal variation in midlatitude stations. But in low latitude stations this 'classical curve' is frequently disturbed by one or more rapid increase in intensity extending over a period of about two hours. The abrupt increases characteristic of the tropics have been observed by ROACH (1955), DELESEMME and DELESEMME (1960), SILVERMAN and CASAVERDE (1961), SILVERMAN (1962), BARBIER, ROACH and STEIGER (1962), SAITO (1962), DAVIS and SMITH (1964), BARBIER (1964), CARMAN et al. (1964), ROACH et al. (1964), PAL and KULKARNI (1968), PAL (1968), and BROWN (1969).

i) Post twilight decay:

CHAMBERLAIN (1958) gave a theoretical explanation of the post twilight decay of the red lines. Of the three processes, resonance scattering of sunlight at 6300 Å, dissociation of O_2 in the Schumann - Runge continuum, and the dissociative recombination of O_2^+, he found that the last one was the predominent contributor to the gradual decay in the early evening,

ii) Western sheet:

BARBIER (1957a,b,c) found that the intensity in the evening to the east of Haute Provence at 75° zenith distance was equal to that at the West 80 minutes later and the height of emission of 6300 A was 300 km. This phenomena was named as 'Western sheet'. He announced another low latitude phenomenon observed at Tamanrasset in Algeria. Here the intensity during some hours increases by a factor of 10 and later decreases in about two hours. BARBIER (1958) showed that these bursts had no relation to magnetic activity and occurred more frequently in winter than in summer (BARBIER, 1959).

iii) Intertropical Arcs:

BARBIER and GLAUME (1960) observed from Tamanrasset observations an East-West oriented arc which was present in both 5577 A and 6300 A. This arc appeared in the north and moved to south and was not perpendicular to the geographic meridian. The deduced height for this arc was 210 km. BARBIER, WEILL and GLAUME (1961) announced the existance of an intertropical arcs system (ie., a pair of zones of increased intensity in the red lines centered near $\pm$ 15° magnetic latitudes and about 10° width.).

They found that as the night progressed the arcs closed towards the equator. The northern arc was stronger in November and the southern arc was stronger in March. Their behaviour is perhaps dependent on longitude.

BARBIER (1964) from simultaneous observations from three stations determined the heights of 6300 Å to be 235 to 280 km. BARBIER and GLAUME (1962) used hourly values of h'F and f_oF_2 from many ionospheric stations around the world and studied the morphology of the intertropical arcs. They found that these arcs were not homogeneous bands but contained a lot of fine structure. This phenomenon was also observed at Haleakala(BARBIER, ROACH and STEIGER, 1962). The existance of the intertropical arc has been verified by CHIPLONKAR and AGASHE (1961) at Poona in India. NAKAMURA (1961) using observations from the research ship 'SOYA' also found the intertropical arcs and showed its close relationship to ionospheric morphology. The existance of intertropical arc is yet to be established at other latitudes.

Another discovery by BARBIER (1965) concerns observations of the red line at Haute Provence. It is common in winter nights near 2200 UT when the 6300 Å airglow shows a brightening to the south and frequently this brightening is very large and increases rapidly for a short time.

iv) Predawn enhancement:

BARBIER (1961) discovered a travelling ionospheric disturbance in which the intensity of the red lines did not obey the usual relation. Towards the morning, out of north, comes brightening which propagates and spreads over the entire sky.

The intensity gradually increases and finally merges into dawn. This phenomenon, the predawn enhancement, or sub-polar sheet has been attributed by COLE (1965) to the effect of photoelectrons from the sunlit atmosphere of the conjugate hemisphere. The predawn enhancement has been observed at both Haute Provence and Tamanrasset, but not at Haleakala, possibly because of the displacement of the magnetic equator. Many people have tried to test Cole's hypothesis from actual observations (CARLSON and WEILL, 1967; CARLSON, 1968; BROWN, 1969; PAL and KULKARNI, 1968; COGGER and SHEPPARD, 1969; SMITH 1969; NICHOL, 1970). Theoretical calculations have also been made by different people (DUBOIN et al., 1968; FONTHEIN et al., 1968).

C) Seasonal variation:

The seasonal variation of 6300 A has been studied by different people (BARBIER, 1965; OKUDA, 1965; STEIGER, 1967; PAL, 1968), but its character remains indecisive because

of the large variations in the daily post-twilight decay. The occurrence of a minimum in the red line intensity around midnight shows very little seasonal variation (BARBIER,1965).

D) Longterm variation:

STEIGER (1967) has described the seasonal, solar-cycle and spatial variations of 6300 Å at Haleakala. The 6300 Å in 1961-62 went through a very strong autumn maximum with a maximum immediately after twilight. In 1964-65,this evening maximum in autumn shifted to summer. The magnetic control in the variation of 6300 Å has been discussed by STEIGER from Haleakala observations. CARMAN, KILFOYLE and GIBSON-WILDE (1964) have reported the appearance of a patchy structure in 6300 Å at Townsville (Australia).

E) Studies at equatorial stations:

DELESEMME and DELESEMME (1960) made zenith airglow observations at Lwiro, Belgian Congo, four degrees south of magnetic equator and found that what Barbier had described as 'intensity bursts' and concluded that dissociative recombination of O_2^+ could explain these bursts, a general property of the tropical ionosphere.

SILVERMAN and CASAVERDE (1961) presented the observations of 6300 A at the equator at Huancayo. They noted that 6300 A passes a maximum at some time between 2200 and 0200 hours local time. WEILL (1967) reviewed the observation at the magnetic equator. VANZANDT (1969) also reported an increase of 6300 A intensity around midnight from observations made at Jicamarca observatory, Peru, and he attributed that the height changes of F-layer caused an increase or decrease in intensity of 6300 A.

F) Airglow enhancements and their explanation:

The occurrence of the tropical enhancements is statistically similar to the occurrence of the Appleton anomaly (KING, 1968). From a careful considerations of the effects of electromagnetic drift and from observations made at Jicamarca observatory, Peru, VANZANDT and PETERSON (1968) concluded that the enhancements are caused by downward equator-ward and/drift. The occurrence of tropical enhancements decreases with decreasing sunspot number (WEILL, 1967; SMITH and STEIGER, 1968). They occur most often during September, October, November in the northern hemisphere (BARBIER, 1961) and six months later in the southern hemisphere (DELESEME and DELESEME, 1960, BARBIER, 1963).

G) Correlation with 5577:

Early work of CHIPLONKAR and KULKARNI (1958) at Poona showed a high correlation between 5577 A and 6300 A intensities. ANGREJI (1969) showed that at low latitudes Barbier's formula is equally adequate in case of 5577 A also, considering the observations at Haleakala, Huancayo, Tamanrasset, Lwiro, Poona and 'SOYA'. CHIPLONKAR and TILLU (1970) also determined the F layer component from the Poona observation of 1964 by correlation analysis of 6300 A and 5577 A.

H) Effect of Magnetic storms:

The tropical F region nightglow is perturbed by large magnetic storms (BARBIER, 1961; WEILL and CHRISTOPHE-GLAUME, 1967; WEILL et al.,1968). All these are associated with F_2 layer disturbances and electromagnetic drifts (VANZANDT, 1969).

6.1.3 Earlier work at Mt.Abu:

DANDEKAR (1961) showed that the intensity of 6300 A at Mt.Abu decreases rapidly in the first part of the night which is prominent in autumn and less so in summer, that the intensity of 6300 A depends on f_0F_2, and a decrease of

h_pF_2 and increase of h'F. PAL and KULKARNI (1968) have observed as a regular feature a hump-like increase of 6300 A which is separate from the predawn enhancement and they have interpreted this as being due to vertical downward drift of the layer of maximum electron density.

6.1.4 Problems for further study of 6300 A in low latitudes:

Because the nightglow can be observed with good directional and temporal resolution over a large area (radius $\sim$1000 km) from a single station, it provides a very convenient method of studying the complex structure and variations of the F_2 layer. There are not many such observations with fast scanning other than those from Haleakala (Hawaii).

Detailed further study of the tropical nightglow enhancements are useful for studying the physics of the excitation processes. As the low latitude enhancements are much lighter than those in midlatitudes and as they are less contaminated by particle bombardment effects, the study of these enhancements can provide critical tests for theoretical models when the vertical motions of the ionosphere are related to the variations in the rate of change of intensity (VAN ZANDT, 1969). Thus further detailed study of 6300 A will provide information on electron loss processes and movements of ionisation.

Change in atmospheric composition have been invoked to explain the anomalous seasonal behaviour of the F_2 region and the changes associated with magnetic storms. It would appear that observations of the twilight effect in 6300 A emission could indicate whether such atmospheric changes do occur (THOMAS, 1968). Thus it will be sufficient to say that for some of these reasons given above, night-glow observations of 6300 A will be very useful in understanding some of the atmospheric processes of F region (VAN ZANDT, 1969).

An attempt has been made by CHIPLONKAR and TILLU (1967) to subtract CH contamination in 6300 A observations with available OH (7-3) and OH (9-4) bands intensity measurements. SMITH (1969) has also accounted for the OH contamination for Haleakala observation from OH (8-3) measurements. It is very necessary to account properly for this OH contamination if we wish to study the quantitative relationship between 6300 A and ionospheric and geomagnetic phenomenon. In the study of Barbier's relation, PETERSON and VANZANDT (1969) comment that if very narrow filter observations are made, as they have done, there may not be the 'A' term in Barbier's relation and the total 6300 A emission can be determined from the dissociative recombination reactions. Further observations at other low latitude

stations with very narrow filters or observations with OH contamination properly accounted for, will decide this point at other latitudes. We have made an attempt to account for the OH contamination from the methods outlined in Chapter III; on nights of special interest.

6.1.5 Scope of the present work:

Pole photometer observations of 6300 A, correspond to the zenith of geographic latitude 29°N. Red photometer which was operated from November 1966 to January 1968 at zenith gave observations at a geographic latitude of 24.6°N. The measurements of 6300 A (OI) line in the nightglow made with the scanning photometer at Mt.Abu are made use of to understand the dynamical state of the night time F layer (geographic latitudes 17°-32°N). If we assume that the effective height of 6300 A emission is 280 km then the outer circile with 75° zenith angle has a radius of ~960 km and includes a region 14° geographic latitude (7°N and 7°S of Mt.Abu ie. 32°N to 18°N geographic latitudes). The geomagnetic co-ordinates covered by the scanner are 20°N dip to 48°N dip. The geomagnetic parallels are inclined about 1°W to the geographic parallels. As Mt. Abu is near the sub-tropical peak of F layer equatorial anomaly, nightglow observations from Mt. Abu (34°N dip) with the scanning

photometer are most useful in studying the spatial structure of F layer as well as the changes during the decay phase of the Appleton anomaly. Regular ionospheric observations are made at Ahmedabad (geographic latitude 23°N) and Delhi (geographic latitude 29°N). 6300 Å observations made with the pole photometer at Mt. Abu are compared with ionospheric data of Delhi. Mt. Abu airglow zenith observations and observations at 40°S zenith angle from the scanning photometer, and ionospheric observations of Ahmedabad are compared and calculations are made of 6300 Å intensity from N(h) profile obtained from Ahmedabad ionosonde data. These results together with other results are discussed in section 6.2 through 6.6.

6.2 Behaviour of 6300 Å at Mt. Abu:

6.2.1 Introduction:

In Tables 1-III, 1-IV, 1-V, the 6300 Å data collected (from the three photometers described in Chapter I) are shown.

6300 A observations at Mt. Abu show significant temporal changes. Some examples of different nocturnal variations of intensity of 6300 A are given in Figure 6.2. (In Figure 6.2 A the post-twilight decay and the predawn enhancement are clearly seen. Figure 6.2 B is an example when an enhancement is superposed on the post-twilight decay. In Figure 6.2 C an enhancement superposed on the predawn enhancement is seen. Figure 6.2 D shows many enhancements superposed on the normal variation of 6300 A. For each of these types two examples are given). All these examples are dealt within this chapter.

The intensity variation of red lines during a night under normal and disturbed conditions and in different months present many interesting features. In Figure 6.3, the nocturnal average values at half hours in all the lunations are plotted as isophotes. These data were obtained with the pole photometer looking towards the pole star (65°zenith angle, ie, 30°N). The period covered is 1964-1969. The following conclusions can be drawn.

6.2. Post-twilight decay:

A post-twilight decay is observed in all the lunations in both low and high active periods. Starting from the beginning of the night the intensity decays roughly

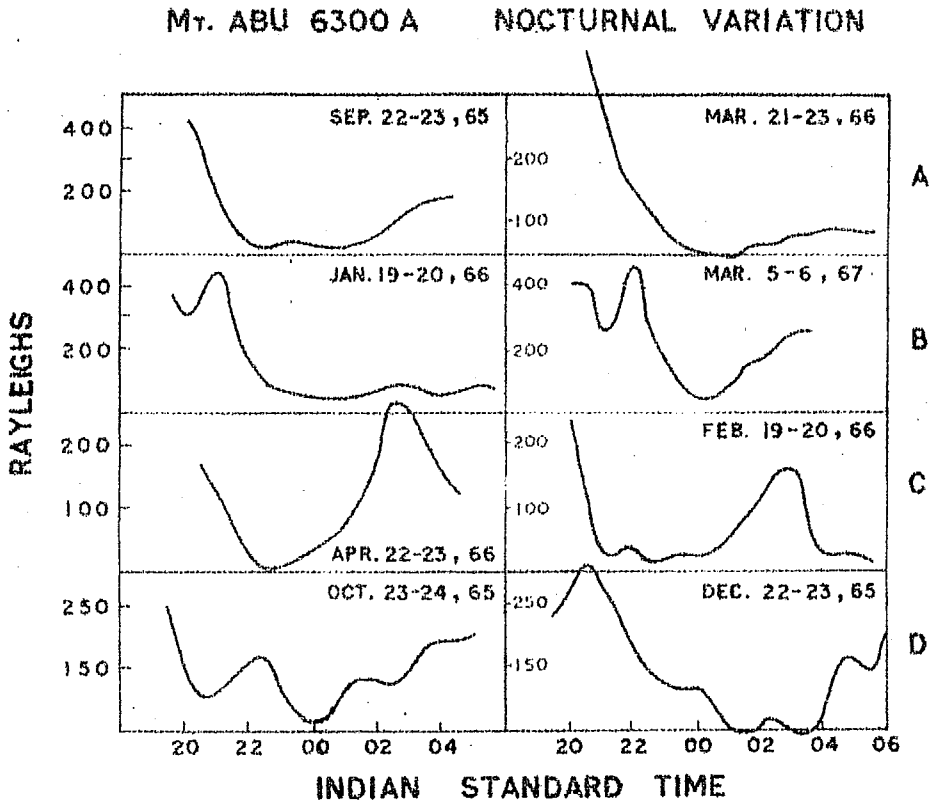

FIGURE 6.2 Examples of nocturnal variation of 6300 A at Mt. Abu.

FIGURE 6.2 A Post twilight decay and predawn enhancement are seen.

FIGURE 6.2 B Enhancement superposed on post twilight decay is seen (Pre-midnight enhancement).

FIGURE 6.2 C Enhancement superposed on predawn enhancement (Post-midnight enhancement).

FIGURE 6.2 D Shows many enhancements superposed on the general trend of the nocturnal variation of 6300 A.

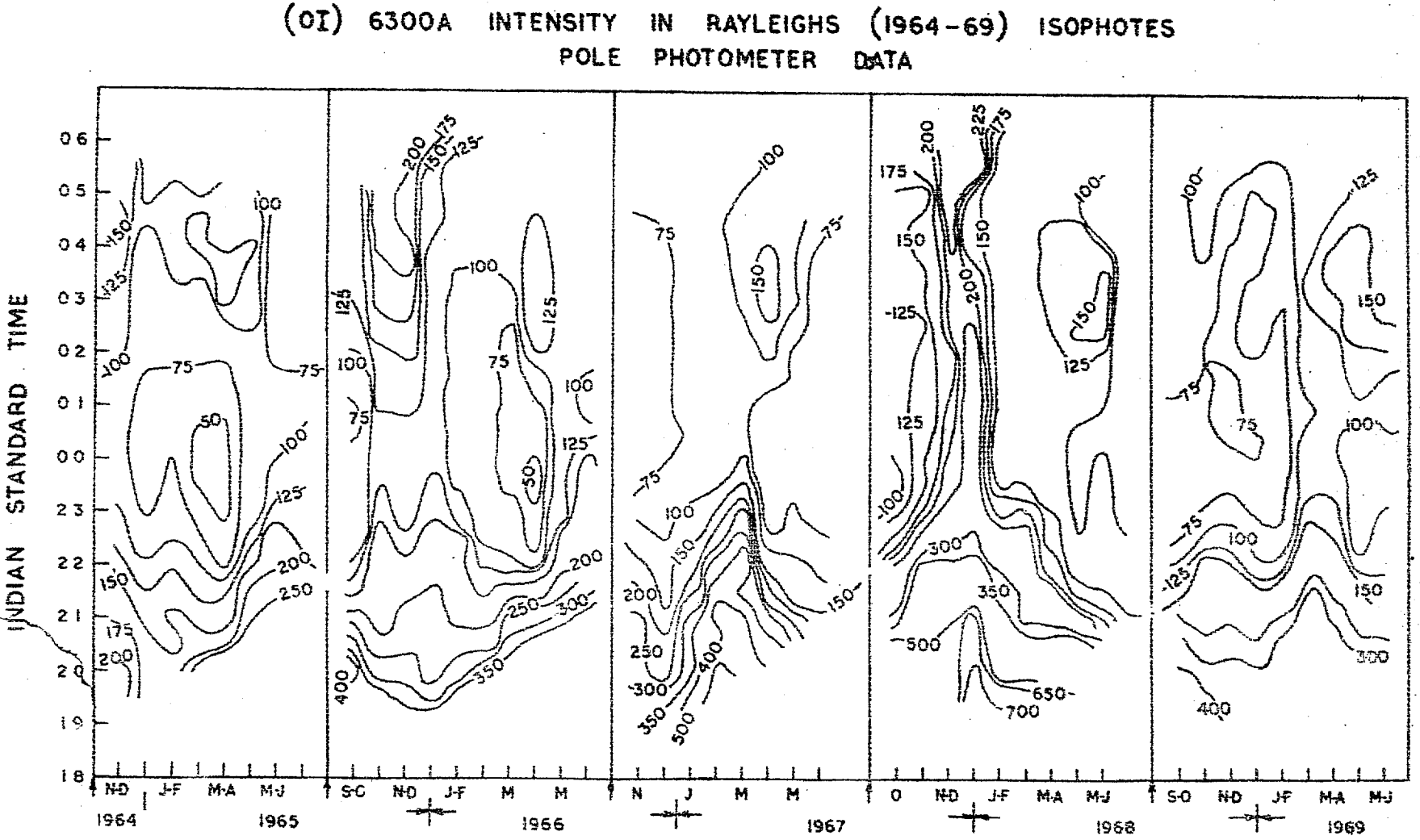

FIGURE 6.3 Isopleth map of 6300 A (nocturnal average values at all half hours in all lunations plotted as isophotes).

exponentially and proportional to e^{-Tt} where t is the time and T is a constant on any given night (CHAMBERLAIN, 1958). T is not necessarily the same from night to night. Figure 6.4 is the histogram of T values on all the individual nights (340 nights) in the years 1964-1969. T was determined by fitting a least square line to the logarithm of the first 12 readings of the intensity during the night provided the first value was within one hour of the end of astronomical twilight. There is difficulty in fitting this line on many nights in winter, when an enhancement is superposed on the post-twilight decay. In section 6.3 this enhancement is dealt with in detail. But here it is smoothed out for determining the T values. From the histogram it will be seen that T values are most frequent between 8.0 to 12.0 x $10^{-5} sec^{-1}$.

6.2.3 Intensity around midnight:

Around midnight the 6300 A emission attains its minimum value and this minimum value is different in low and high active periods, being more in the high active period. Normal intensity is 50-100 R. It has been more or less accepted that the duration for which the minimum intensity remains more or less steady is much larger in middle latitudes than in the tropics. However, NICHOL (1970)

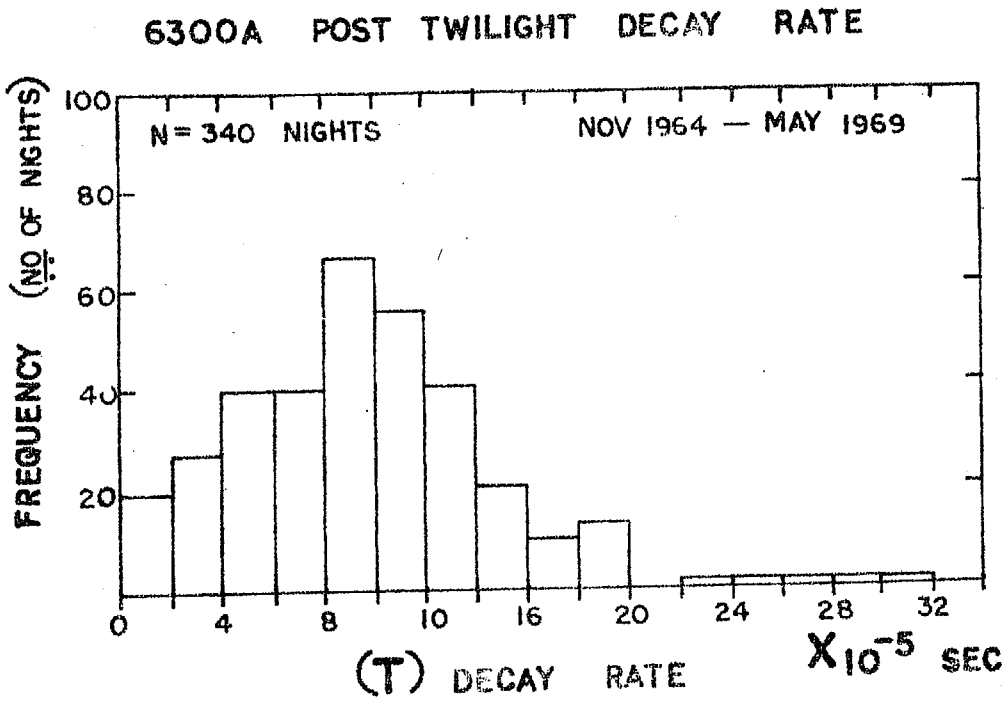

FIGURE 6.4 Histogram of T values (Rate of post twilight decay) on all the nights during 1964-69.

from observations from Hobart (geomagnetic latitude 54°S) noted that there is a wide spread in the commencement time of predawn enhancement but that it is always after 0100 LMT.

6.2.4 Predawn enhancement: Cole's hypothesis.

The predawn enhancement is seen in all the months in both low and high active periods, and this enhancement starts just after midnight on many summer nights and much later in winter nights.

This predawn enhancement of 6300 Å airglow emission was observed by BARBIER (1959) from Haute Provence data and later observed and reported at many low latitude stations.

In 1965, COLE suggested that even before dawn in winter, normal O atoms could be excited to $O(^1D)$ state by collision with energetic electrons which are produced by the photoelectric action of sunlight in the conjugate summer hemisphere and transported to the dark hemisphere along the magnetic lines of force.

Cole suggested that

$$Q_{6300} = A\ N_e\ n(O) \text{ per unit volume}$$

where N_e is the electron density, n(O) is the concentration of atomic oxygen, and A is a temperature dependent coefficient for excitation of atomic oxygen to ^1D state. COLE showed that for 100 R emission of 6300 A from 300 km layer the electron temperature T_e has to be about 2100°K when the normal temperature of atomic oxygen is 900°K. These hot electrons would be cooled by collisions with atoms in the atmosphere, while the latter would get excited. The 6300 A enhancements which were examined by COLE were most marked in winter and the hypothesis is certainly possible for a station like Haute Provence for which the conjugate point sunrise at 300 km is earlier by about 3½ hours in winter months. CARLSON (1967) has shown that at Arecibo (18.4°N) 6300 A starts increasing from the time of conjugate point layer sunrise at 300 km; this time is about 45 minutes before the beginning of local twilight. The predawn on-set of 6300 A enhancement has thus been found to occur at the same time as the conjugate point layer sunrise at 300 km in this case.

To examine whether this is true for Mt.Abu-Delhi the data of all (1964-69) the nights for Mt.Abu were examined. The time intervals by which the beginning of morning twilight at the magnetically conjugate point would be earlier (positive sign) at 300 km height than that at

$29^{o}N$ on January 20, 1965 and on April 6, 1965 would be $+0^{h}\ 58^{m}$ and $-0^{h}\ 10^{m}$ respectively. If the conjugate point photoelectron hypothesis is the explanation for the predawn enhancement of 6300 A at Mt. Abu, the enhancement should start only an hour before the beginning of the morning twilight at Mt.Abu-Delhi in January.

Figure 6.5 is a plot of 6300 A intensity on a few successive nights in the months of December and January. The conjugate point layer sunrise and Mt.Abu layer sunrise timings are marked. On all these graphs an increase in 6300 A intensity is observed according to Cole's hypothesis. It is noted that 5577 A does not show any such increase, which shows that the energy of the incident photoelectrons are capable of exciting the oxygen atoms to $O(^{1}D)$ state only, but not to $O(^{1}S)$. It can be concluded that in winter months there is some contribution to 6300 A from the photoelectrons reaching Mt.Abu from its conjugate point. This particular increase is observed on successive nights almost at the same time. This is expected as the sunrise time does not change appreciably on successive days. It may be mentioned that in plotting the intensities of 6300 A to test Cole's hypothesis, 5 minute values obtained from pole photometer data were used.

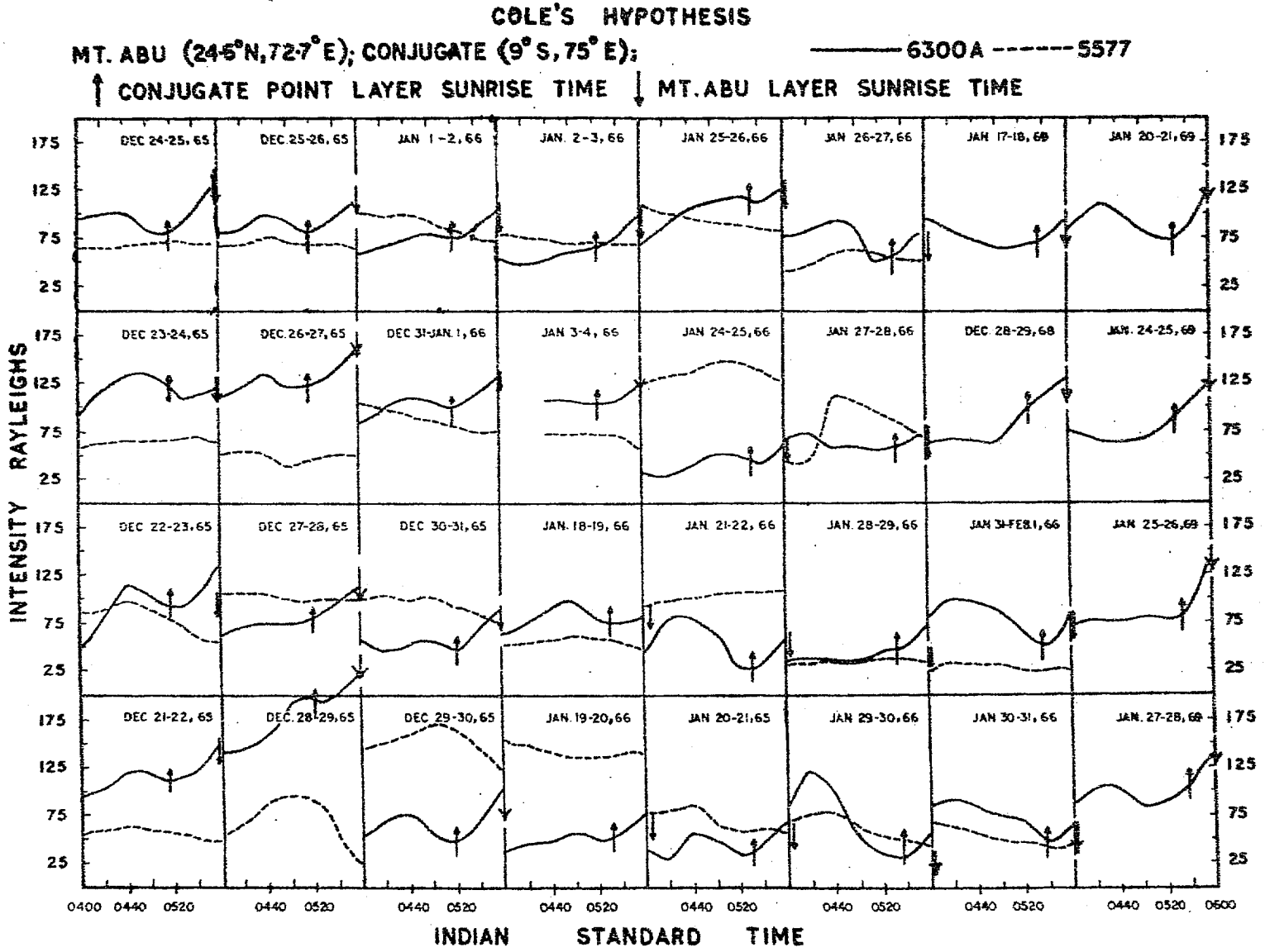

FIGURE 6.5 Intensity of 6300 A on a few successive nights in December, January months during 0400-0600 IST showing an increase in intensity according to Cole's hypothesis.

Figure 6.6 shows the isophote maps (intensities in rayleighs) on 3 successive nights in the month of December, 1968 obtained from the scanning photometer, at hour 0500 and 0530 IST. L and H show that the intensity is less or more than the isophote line bounding the letter. In the map of 0530 IST an increase in intensity is seen as compared to the map of 0500 IST in each of the nights in the directions from North to South through East (the layer sunrise time on these nights was 0600 IST). This increase in intensity the 'Subpolar sheet' could be due to the photoelectrons coming from their respective conjugate points.

But as the observed predawn enhancement at Mt.Abu actually starts much earlier (Figure 6.3) and is observed even more pronouncedly in summer months, Cole's hypothesis obviously cannot be the agency responsible for such enhancements. PAL and KULKARNI (1968) proposed that whenever there are vertical movements in the F region, there would be changes in I_{6300}. Actually, I_{6300} and the vertical drifts show good anticovariation.

6.2.5 Comparison of the intensity of 6300 A in low and high active periods:

The average nocturnal intensities in the year 1967-68 were higher than those in the low active year 1964-65. This shows that solar activity has a major role

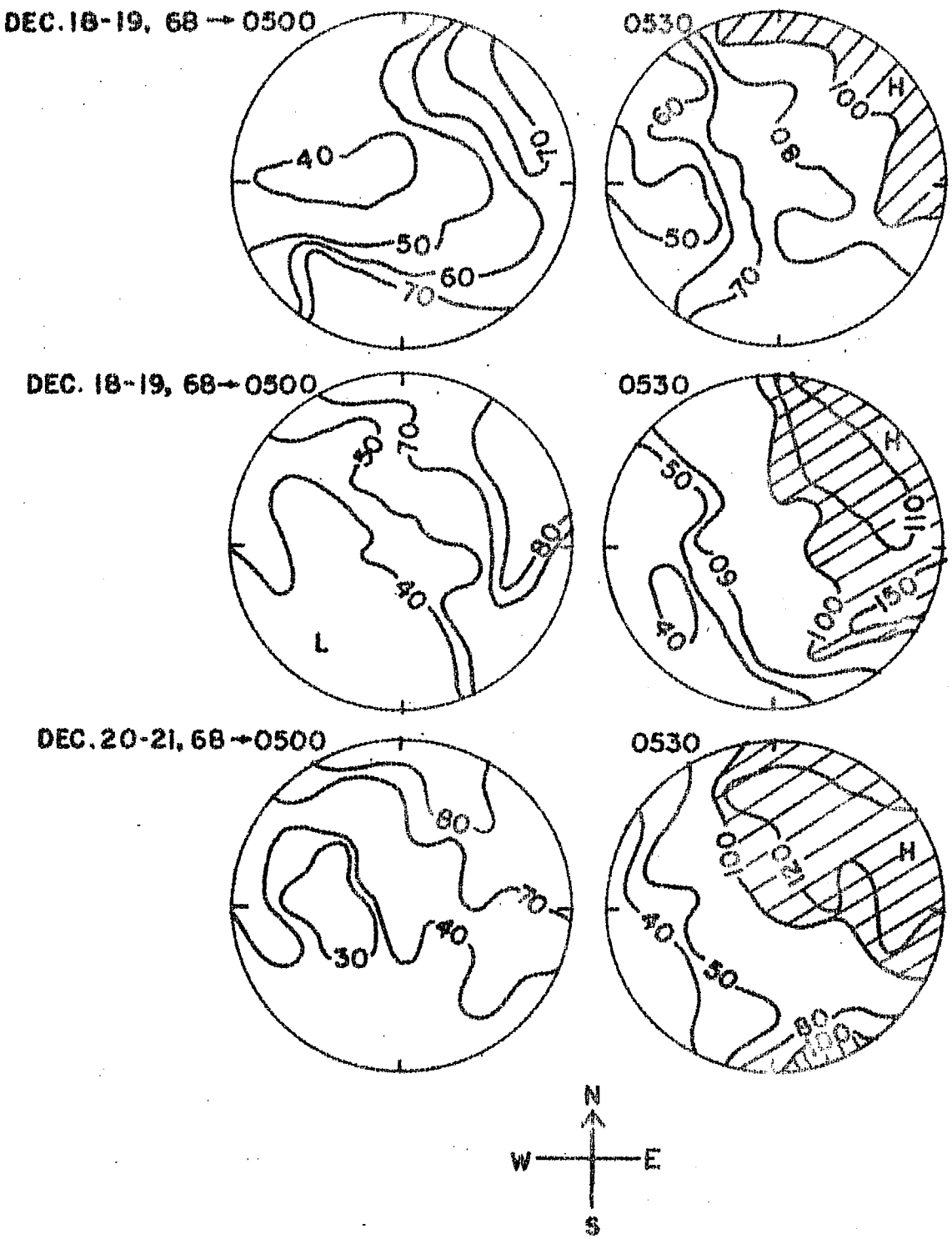

FIGURE 6.6 Isophote maps at 0500 IST and 0530 IST on a few nights showing increase in intensity according to Cole's hypothesis.

to play in the intensity of 6300 Å and its variations. Figure 6.7 is a plot of lunation-average intensities of 6300 Å in 1964-65 and 1967-68. In November-December, December-January, January-February, February-March, March-April lunations, the intensities in 1967-68 (high active year) were greater than in the year 1964-65 (low active year). However, the intensities in the summer months are more or less equal in 1965 and 1968.

As the range of intensity within a night is quite considerable, it is very difficult to draw any conclusion regarding the seasonal variation. From 1964 to 1968 there was, however, continuous increase in the level of the red line intensity running somewhat parallel to 10.7 cm wavelength solar flux. In 1968-69 there was decrease in 10.7 cm wavelength solar flux. In Figure 6.8 are plotted lunation-average values of 6300 Å (one average value for the entire lunation is marked by a point) and monthly average values of solar flux S (dotted line). It may be noted that the intensity of red line runs somewhat parallel to the curve of solar flux, the values in 1968-69 being smaller than those in 1967-68.

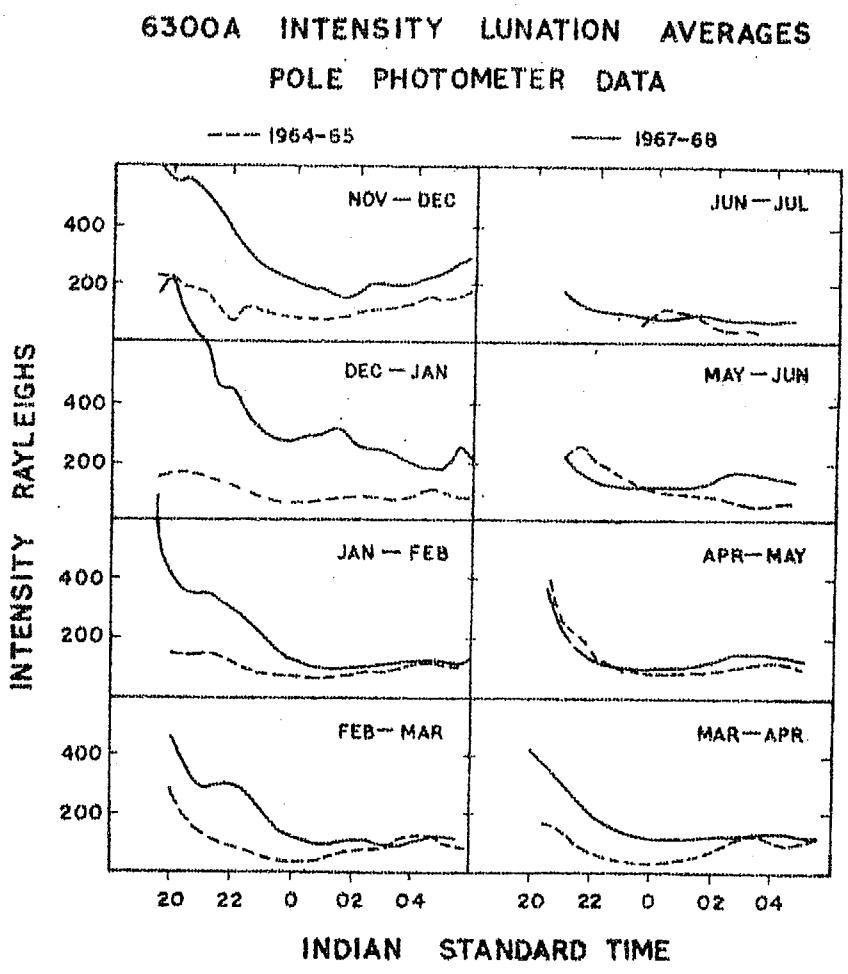

FIGURE 6.7 Average nocturnal variation of the intensities of 6300 Å in different lunations in 1964-1965 and 1967-1968.

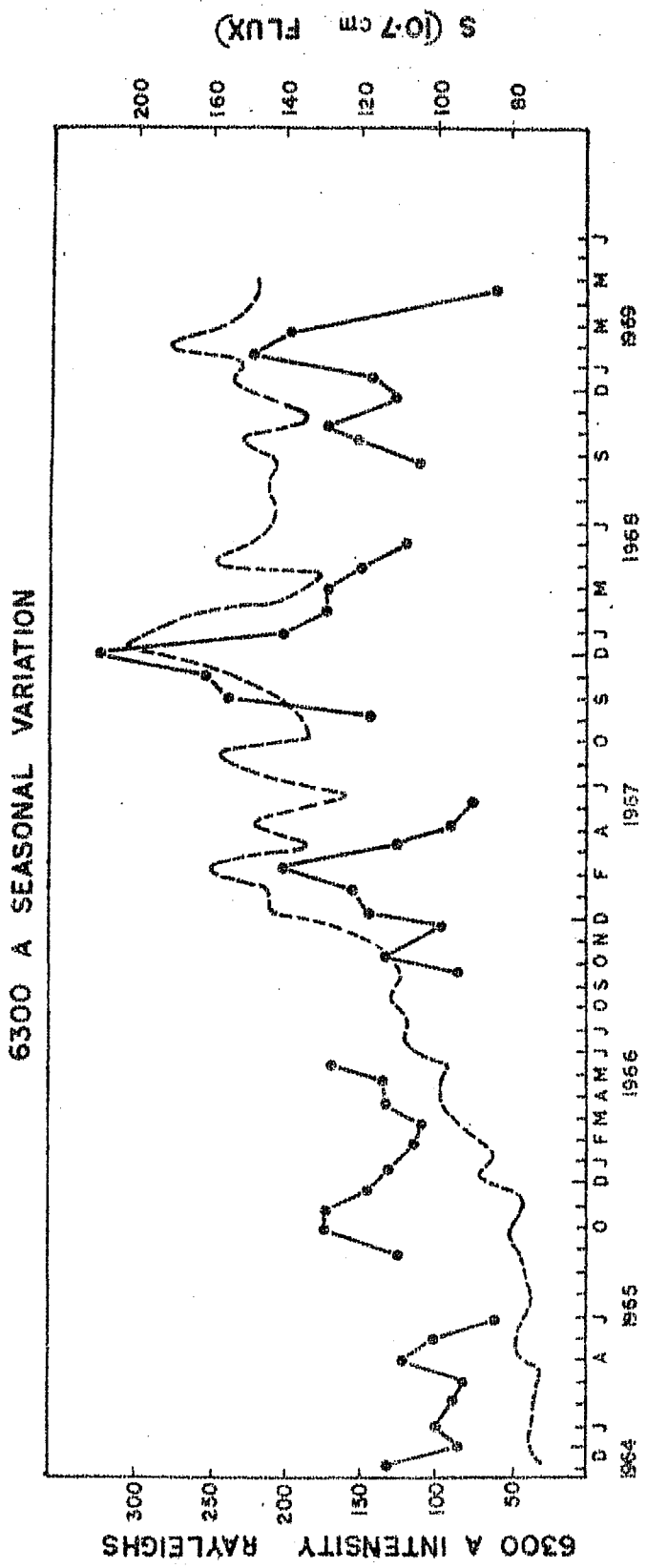

FIGURE 6.8 6300 Å seasonal variation during 1964–69.

6.2.6 Barbier's formula:

Barbier's formula

$$Q_{6300} = A + B(f_oF_2)^2 \exp\left\{-(h'F-200)/H\right\}$$

is found to be valid at Mt. Abu. This formula relates the airglow quantal emission Q_{6300} to the ionospheric parameters h'F and f_oF_2 and the scale height of O_2. 6300 A intensities on 86 nights covering the period from November 1966 to January 1968 were analysed. The 6300 A data were obtained from the RED photometer which was looking towards zenith in that period. Ahmedabad ionosonde data of f_oF_2 and h'F for the hours when airglow observations were taken at Abu were used for the calculations. The least square line which best fits the airglow intensity versus the function on the right of the above equation was found for each night; and the slope B and the intercept A were determined. The average correlation coefficient between I_{6300}, and Q_{6300} the observed and calculated quantal emissions for 86 nights was found to be 0.94. Only those nights in which observations were available for more than 5 hours are taken into consideration. The histogram of the correlation coefficients is given in Figure 6.9.

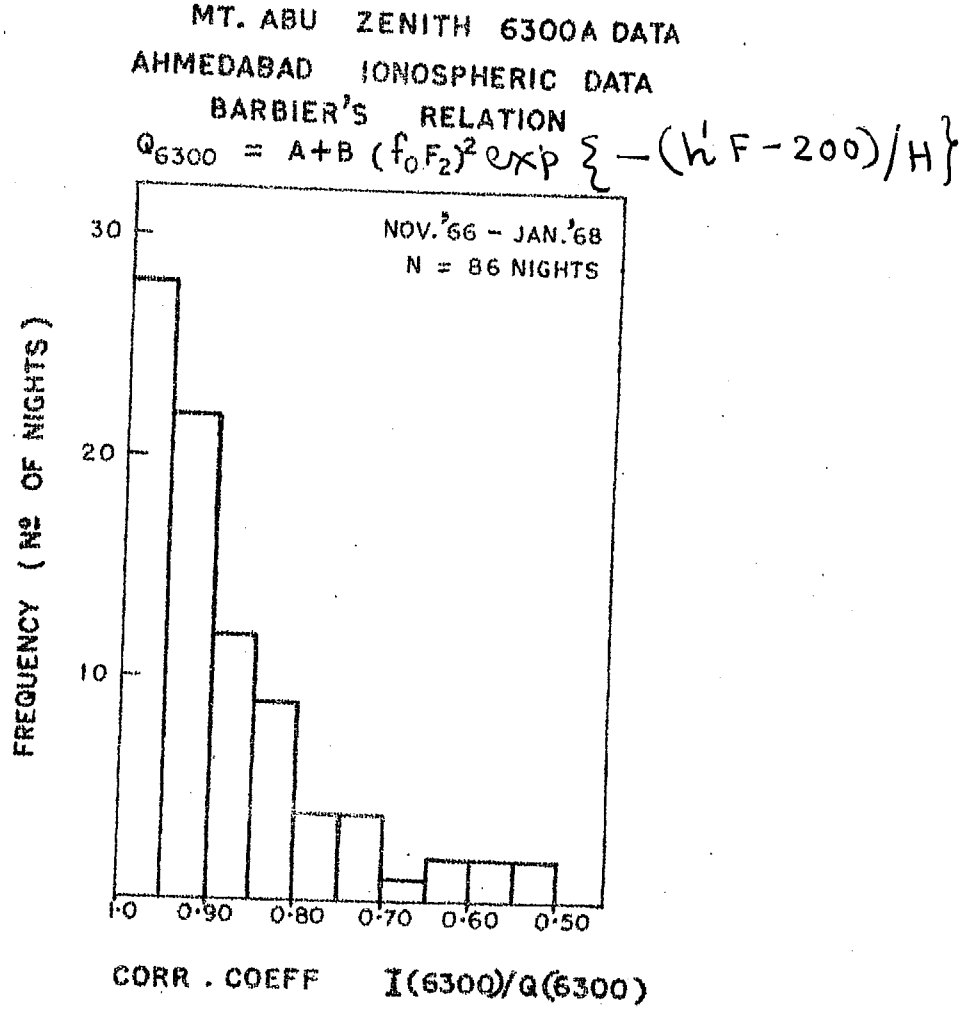

FIGURE 6.9 Histogram of the correlation coefficients between the observed 6300 Å intensity (I_{6300}) at Mt.Abu zenith and Q_{6300} the intensity determined from the ionospheric parameters at Ahmedabad.

Similar calculations were also made for the above period for the 6300 A data obtained with the pole photometer, and in this case, the ionospheric data were those obtained at Delhi. Also on the scanning nights from Mt. Abu, the data of 40°S zenith angle which relates to the ionospheric F layer of Ahmedabad, and 60°-70° zenith angle data which relates to Delhi ionospheric F layer data were also analysed. On all these occasions, it is found that Barbier's formula fits reasonably well with Q_{6300} determined from ionospheric parameters and I_{6300} obtained from observations.

In Figure 6.10, the nocturnal average values of the intensity of 6300 A emission for different lunations are plotted for the period November 1966 to June 1967. The photometer looking at the zenith of Mt.Abu and the other looking at 65° zenith angle (poleward) were operating simultaneously in this period. To compare the ionospheric parameter f_0F_2, monthly median values at Ahmedabad and Delhi are plotted. By the side of this graph h'F values (monthly median) of Ahmedabad and Delhi are also plotted. It is interesting to note that 6300 A intensities at Ahmedabad are more than those at Delhi in all the lunations. Also f_0F_2 values at Ahmedabad were larger than those at Delhi and h'F values are smaller at Ahmedabad than at Delhi. This is all in agreement with Barbier's relation.

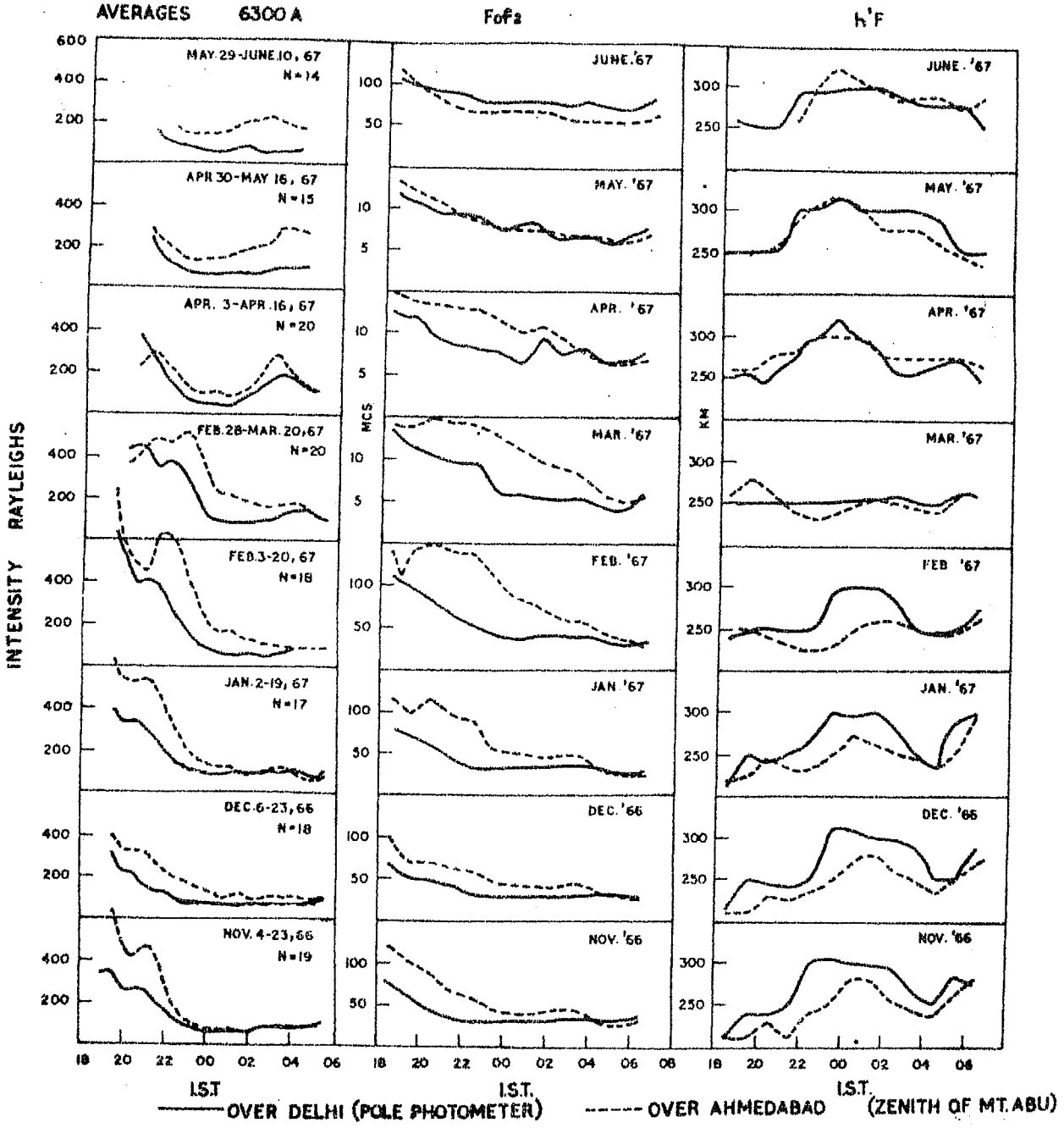

FIGURE 6.10 Average nocturnal intensity values of 6300 A at zenith and poleward directions of Mt. Abu and monthly median values of $f F_2$ and h'F in different lunations at Ahmedabad[2] and Delhi during November 1966 to June 1967.

In Table 6-I the constants A and B obtained for the Red photometer 6300 A data at Mt.Abu, Ionospheric data at Ahmedabad are given. It is seen from this table that A and B have variations from month to month. The seasonal variation of A is not similar to the seasonal variation of OH which shows that the term A is not entirely due to the OH (9-3) contamination in 6300 A observations. In general, the values of B are more in the winter months than in summer. This seasonal variation of B is quite unlike the temperature variations of neutral gas concentrations in the F region as noted by PETERSON et al. (1966). The A term may be due to

$$O(^3P) + N(^2D) \longrightarrow N(^4S) + O(^1D)$$

or $$O(^3P) + e \longrightarrow O(^1D) + e$$

Evidence is available for both these mechanisms. The reactions

$$NO^+ + e \longrightarrow O(^3P) + N(^2D)$$

$$N(^2D) \longrightarrow N(^4S) + h\nu \ (5200\ A)$$

are known to occur at low latitudes (WEILL et al.,1968). Also fluxes of energetic electrons are possibly present in the night time F region at low latitudes (KNUDSEN and SHARP, 1968).

TABLE 6-I

Barbier's A and B coefficients (Red Photometer data)

Lunation period	A	Error in A	B	Error in B	Correlation coefficient I_{6300}/Q_{6300}
Nov 1966	73	24	5.7	0.6	0.95
Dec 1966	58	19	11.0	1.3	0.94
Jan 1967	73	19	12.2	0.8	0.98
Feb 1967	89	38	5.9	0.9	0.92
Mar 1967	134	34	2.8	0.5	0.90
Apr 1967	59	31	5.0	0.9	0.89
May 1967	131	22	12.1	2.1	0.92
Oct-Nov 1967	111	23	3.8	0.4	0.96
Nov-Dec 1967	93	16	5.6	0.4	0.98
Dec-Jan 1967	96	31	7.2	0.7	0.96

A similar conclusion regarding A and B coefficients was reached by BROWN (1969) from Haleakala airglow data. However, an interesting observation by PETERSON and VANZANDT (1969) is worth mentioning. They say that when very narrow filters were used for making 6300 A intensity observations at Jicamarca observatory, Peru, the A term in Barbier's formula almost completely vanished. This indicated that at that place 6300 A emission was almost entirely due to dissociative recombination. It is very necessary to get 6300 A intensity data with very narrow filters.

6.2.7 Behaviour of 6300 A during Spread-F conditions:

The scattered reflections, either diffuse or duplicate traces on ionograms are called spread F echoes. The occurrence of spread F at different stations and their possible causes have been considered by various authors. At Ahmedabad, spread-F is found to be very variable. From a large amount of data, RASTOGI and KULKARNI (1969) have investigated the frequency of occurrence of spread-F during one complete solar cycle (1954-65) and they noted that spread F at Ahmedabad and other low latitudes stations is most frequent when the layer is descending. VAN ZANDT and PETERSON (1968) concluded that 6300 A structure is mainly due to changes in h'F and to a smaller extent to

changes in critical frequency. KING (1970) noted that from the 6300 A airglow scanning observations, the geometry of the large tilted surfaces of ionization (which are possibly the cause of spread F echos) can be investigated.

The airglow observations made with a narrow field (5^{o} or less) photometer will help to understand the behaviour of the ionosphere during spread F conditions.

Figure 6.11 shows observations of 6300 A with the pole photometer on a few nights when spread F was seen on the Delhi ionograms. Figure 6.12 shows a few nights 6300 A observations from the scanning photometer directed to 40^{o}S zenith angle or at zenith of Mt.Abu, during which spread F occurred at Ahmedabad. Whenever data of h'F and $f_{o}F_{2}$ were available, they are also plotted. It was noted that at Delhi, spread-F was observed while h'F was increasing on a few occasions, while it was decreasing on a few other occasions (see Figure 6.12).

However, on most of the occasions height variations were in anti-relation with 6300 A intensity variations. On many occasions, when spread F started at Ahmedabad, 6300 A intensities increased and the intensity of 6300 A was in anti-relation with the height variations. As the occasions

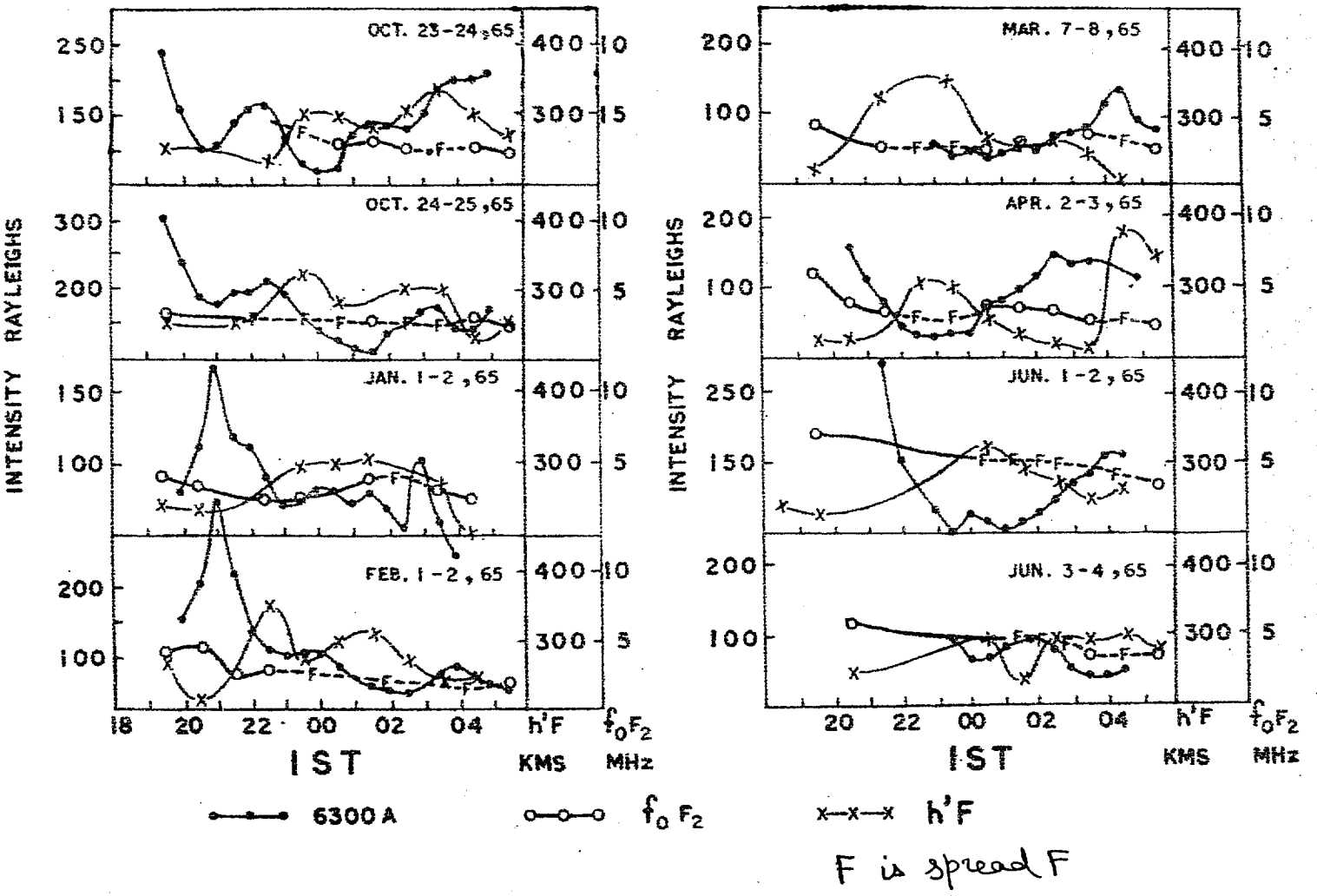

FIGURE 6.11 6300 A observations on a few nights when spread F was seen on the Delhi ionogram.

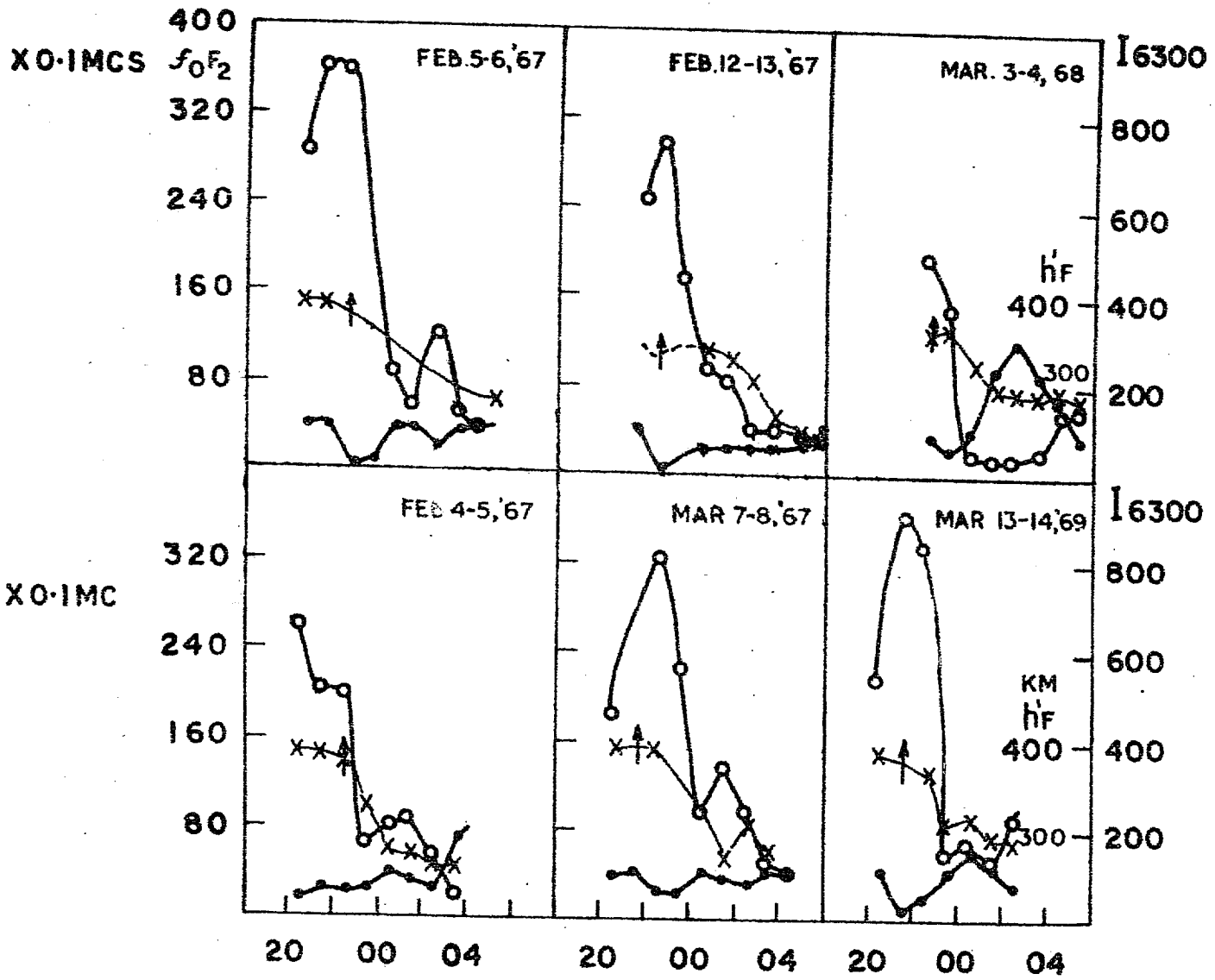

FIGURE 6.12 6300 A observation on a few nights when spread F was seen on the Ahmedabad ionogram.

during which simultaneous observations were available were few, further co-ordinated observations are required to study the behaviour of 6300 A during spread-F conditions.

6.3 6300 A Enhancements:

6.3.1 Introduction:

In addition to the normal post twilight decay and pre-dawn enhancement, there are often peaks of intensity in 6300 A nocturnal variation in the course of a night. Figure 6.13 shows a histogram of the number of such enhancements in each hour during the night, based on 714 nights of observations taken with the Pole photometer during 1964-69. The figure shows that statistically more enhancements occur in the post midnight period, often around 0300-0500 IST, compared to the pre-midnight period.

Comparing enhancements in two directions of observation, poleward (29^{o}N geographic) and at zenith (24.6^{o}N geographic) during January 1967 and April 1967 (Figures 6.14 and 6.15) it is found that the zenith enhancements are stronger. Both pre-midnight and post-midnight enhancements have been studied using lunation average curves and also curves of individual nights. The latter show up the characteristics more clearly.

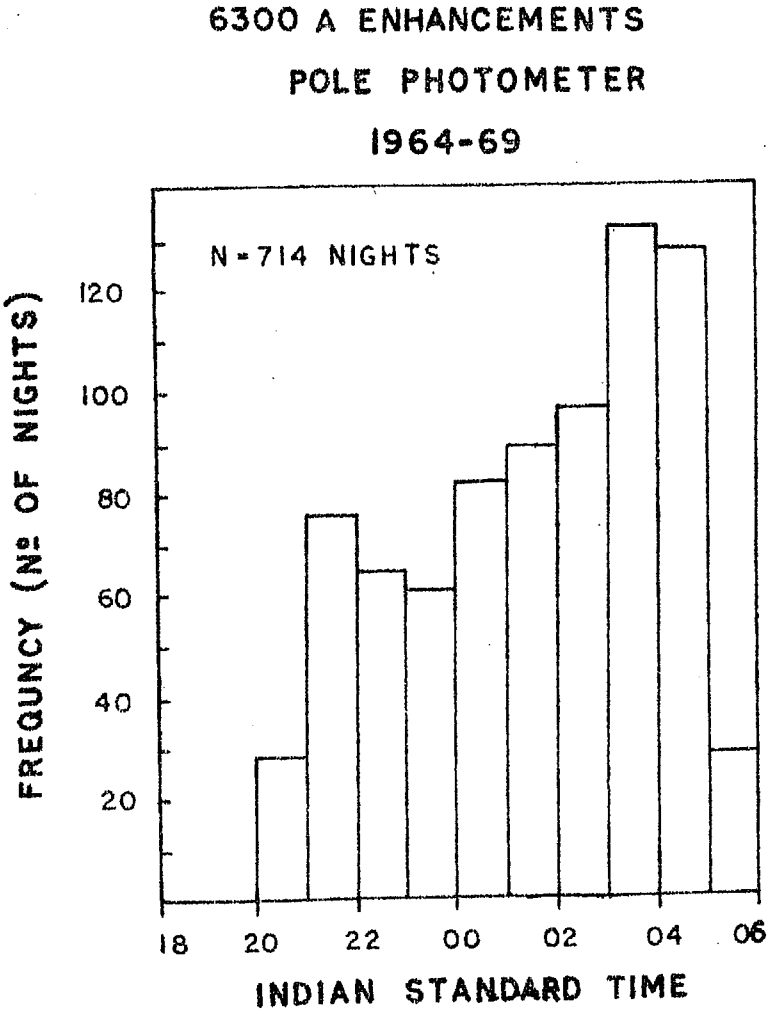

FIGURE 6.13 Histogram of the 6300 A airglow enhancements observed in the nocturnal variation during 1964-69. (The enhancement is defined as an increase in intensity following a decrease after some time).

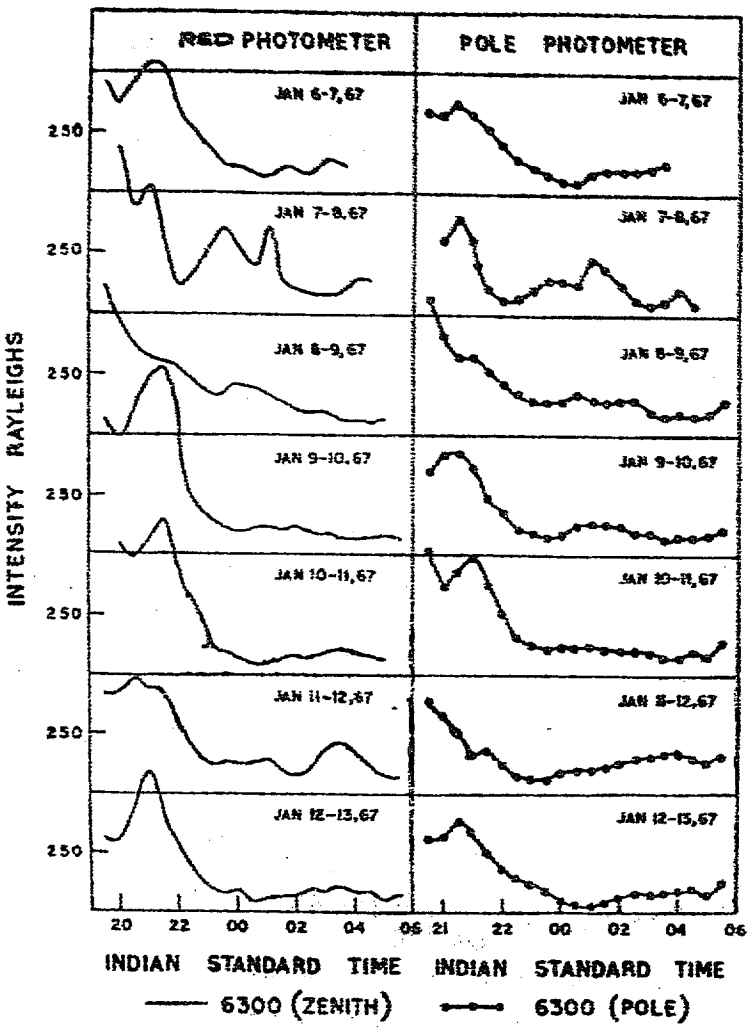

FIGURE 6.14 Comparison of the airglow 6300 A enhancements in two directions(zenith 24.6°N geographic;and poleward 29°N geographic)in January 1967.

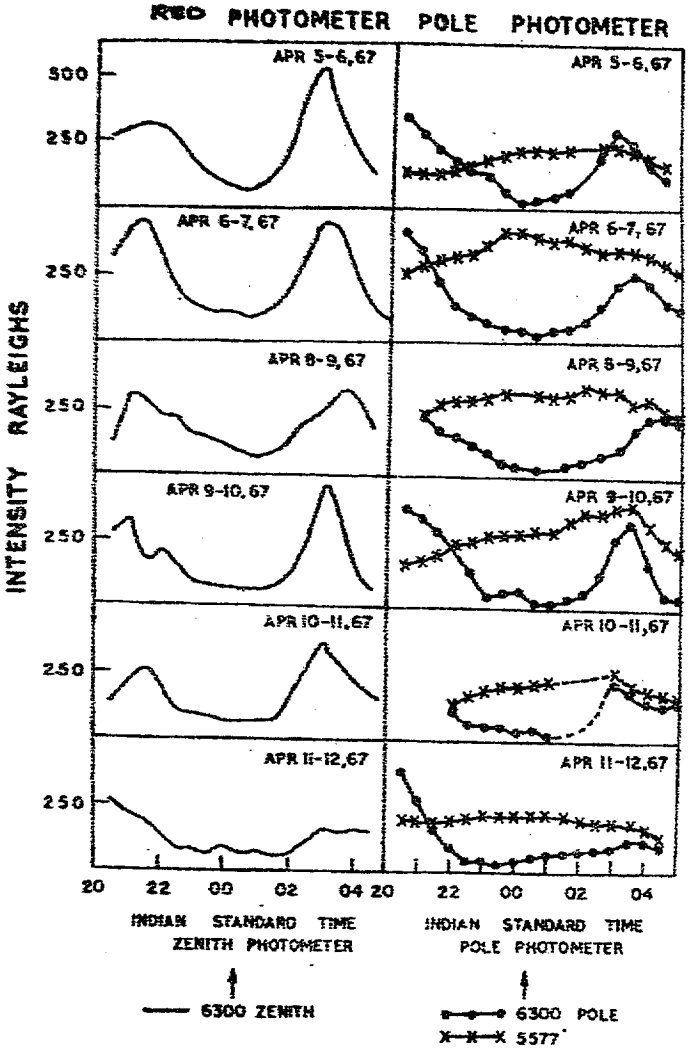

FIGURE 6.15 Comparison of the airglow 6300 A enhancements in two directions (zenith 24.6°N geographic; and poleward 29°N geographic) in April 1967.

6.3.2 Pre-midnight enhancements:

Superposed on the post twilight decay, an increase in intensity was observed for some hours on many nights in 6300 A intensities. The number of nights on which pre-midnight enhancement was observed and the total number of nights of observation in each lunation at Mt. Abu are plotted in Figure 6.16. as monthly histograms in each of the years 1964-1969. The composite histogram of all the years is given in Figure 6.17. Out of 391 nights of observation in 1964-69, this enhancement was observed on 231 nights. The following conclusions can be drawn regarding the pre-midnight enhancement at Mt. Abu.

1) The pre-midnight enhancement is more frequent in winter months than in summer. In high activity years, however, it is observed on a few occasions in the summer months also(See Figures 6.14 and 6.15). It occurs more frequently at zenith and at latitudes south of Mt.Abu. Figure 6.18 shows isophote maps of a few nights obtained with the scanning photometer. The enhancement occurs at all the southern latitudes as seen from Mt.Abu with the scanning photometer. Figure 6.19 shows the intensities at different latitudes from 17^{o}N to 32^{o}N(geographic)obtained with Mt.Abu

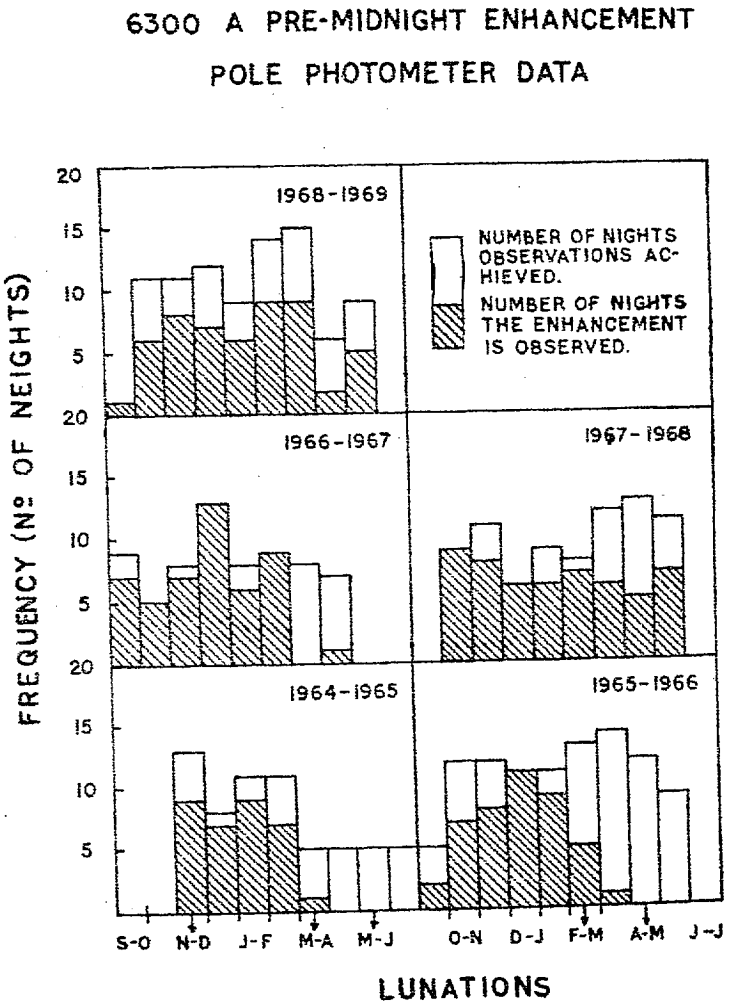

FIGURE 6.16 Histograms of the occasions when premidnight enhancement was observed in each of the lunations during 1964-69.

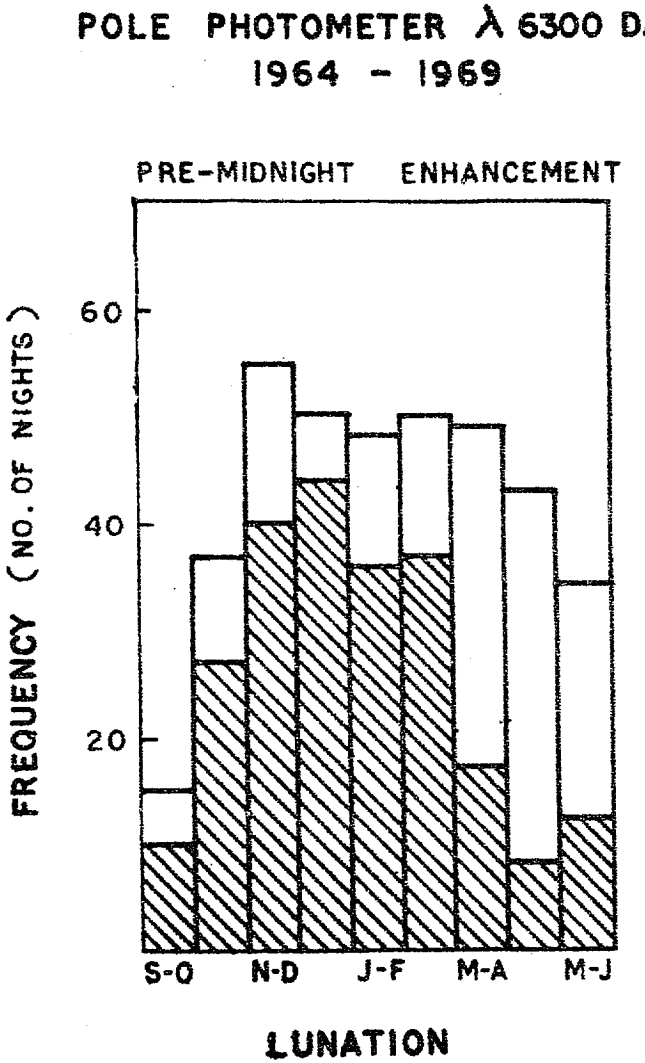

FIGURE 6.17 Composite histogram of the all the months in 1964-69.

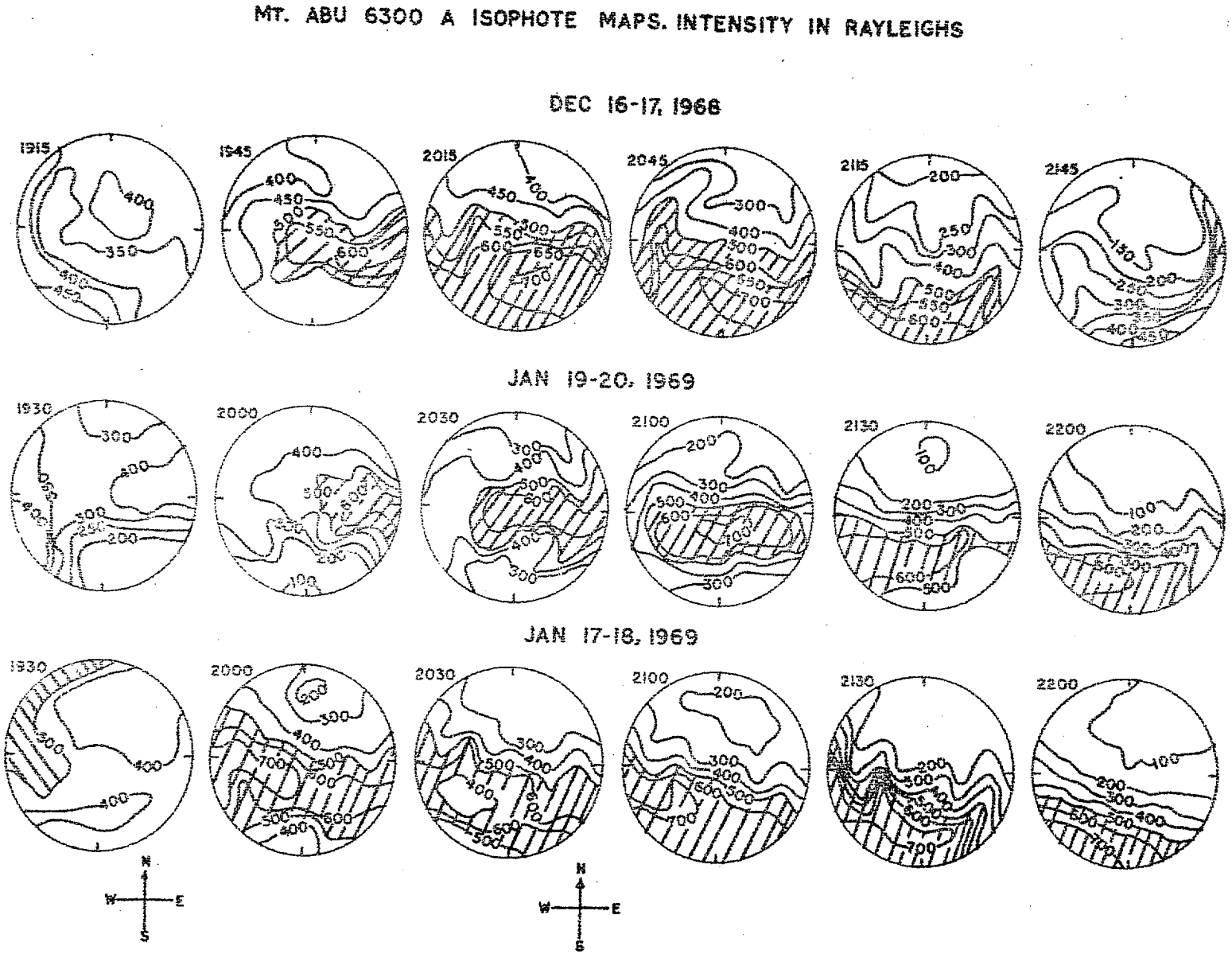

FIGURE 6.18 Isophote maps of 6300 Å on a few nights during the hours of the pre-midnight enhancement.

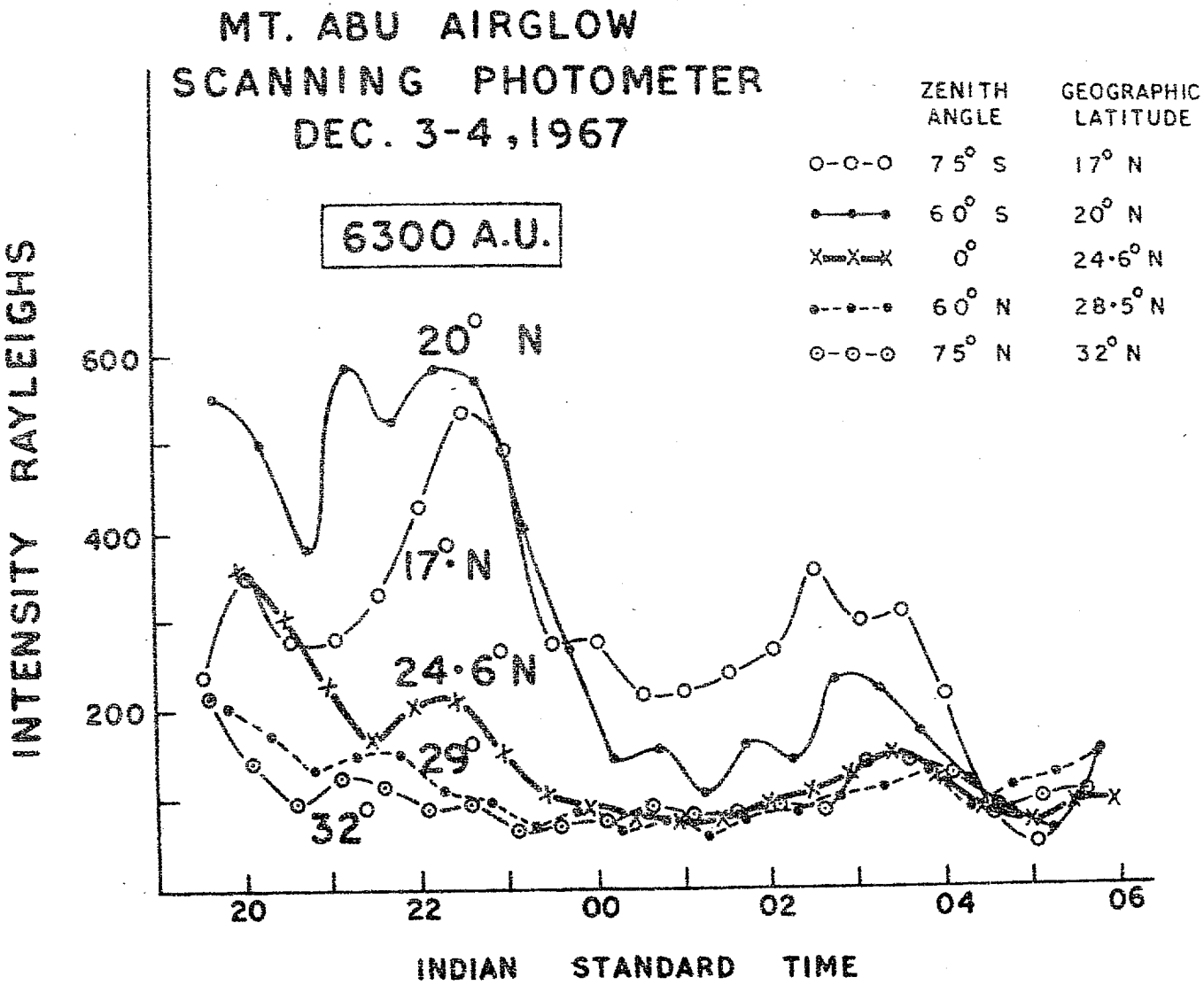

FIGURE 6.19 Nocturnal variation of 6300 A at different latitudes (17°N-32°N geographic).

scanning photometer and converted to local zenith intensities on a typical night December 3-4, 1967. This night is presented as an example out of the data of many nights taken from Mt. Abu.

2) The pre-midnight enhancement is more intense at the zenith over Abu than at 65°N zenith angle ie., towards pole star. Both the zenith and poleward data are plotted for a few nights in Figures 6.14 and 6.15. From Figure 6.14 it is seen that in winter months 5577 A also shows an enhancement corresponding to the increase in 6300 A on many nights.

6.3.3 Correlation of pre-midnight enhancement of 6300 A with the changes in electron density profiles of the F region of the ionosphere:

A) Pre-midnight enhancement : Electron content (N_T) in the ionosphere:

The pre-midnight enhancement is always associated with an increase in total electron content (N_T) up to h_mF_2. Figure 6.20 shows the time variations of 6300 A emission

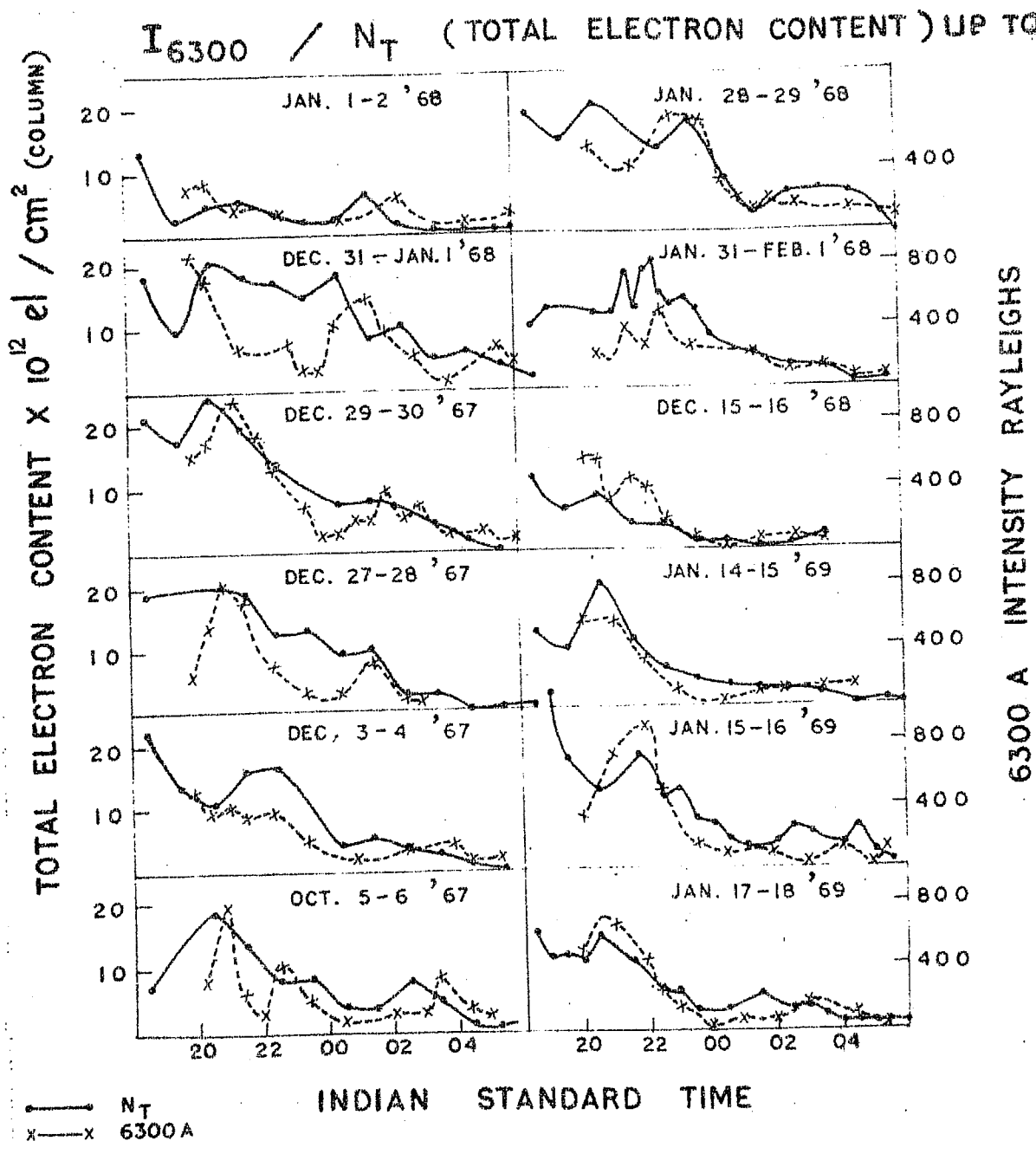

FIGURE 6.20 6300 Å intensity and electron content (N_T) up to h_mF_2 in the ionosphere on a few nights.

and the electron content up to h_mF_2 in the ionosphere on 12 nights on which the pre-midnight enhancement was pronounced. The airglow data were taken from the scanning photometer at 40^oS zenith angle and the ionospheric data from Ahmedabad ionasonde observations. The ionospheric electron content was determined from true height analysis. It is seen from Figure 6.20 that the pre-midnight enhancement is associated with an increase in electron content (N_T up to h_mF_2).

B) Pre-midnight enhancement: Vertical drifts in the ionosphere.

As noted above in Figure 6.20 the pre-midnight enhancement is always associated with increase in N_T the electron content up to h_mF_2. Downward vertical drifts of plasma which occur some time after sun-set can bring down more electrons causing increase in the electron content up to h_mF_2 which then recombine and give more 6300 A. In Figure 6.21 the electron density profiles (N(h) profiles) on a few nights are plotted during the hours when the pre-midnight enhancement occurred. The N(h) profiles were obtained from the ionograms at Ahmedabad by true height analysis. The downward movement of the electron density profiles and also of h_mF_2 during the time of this enhancement are seen from these N(h) profiles.

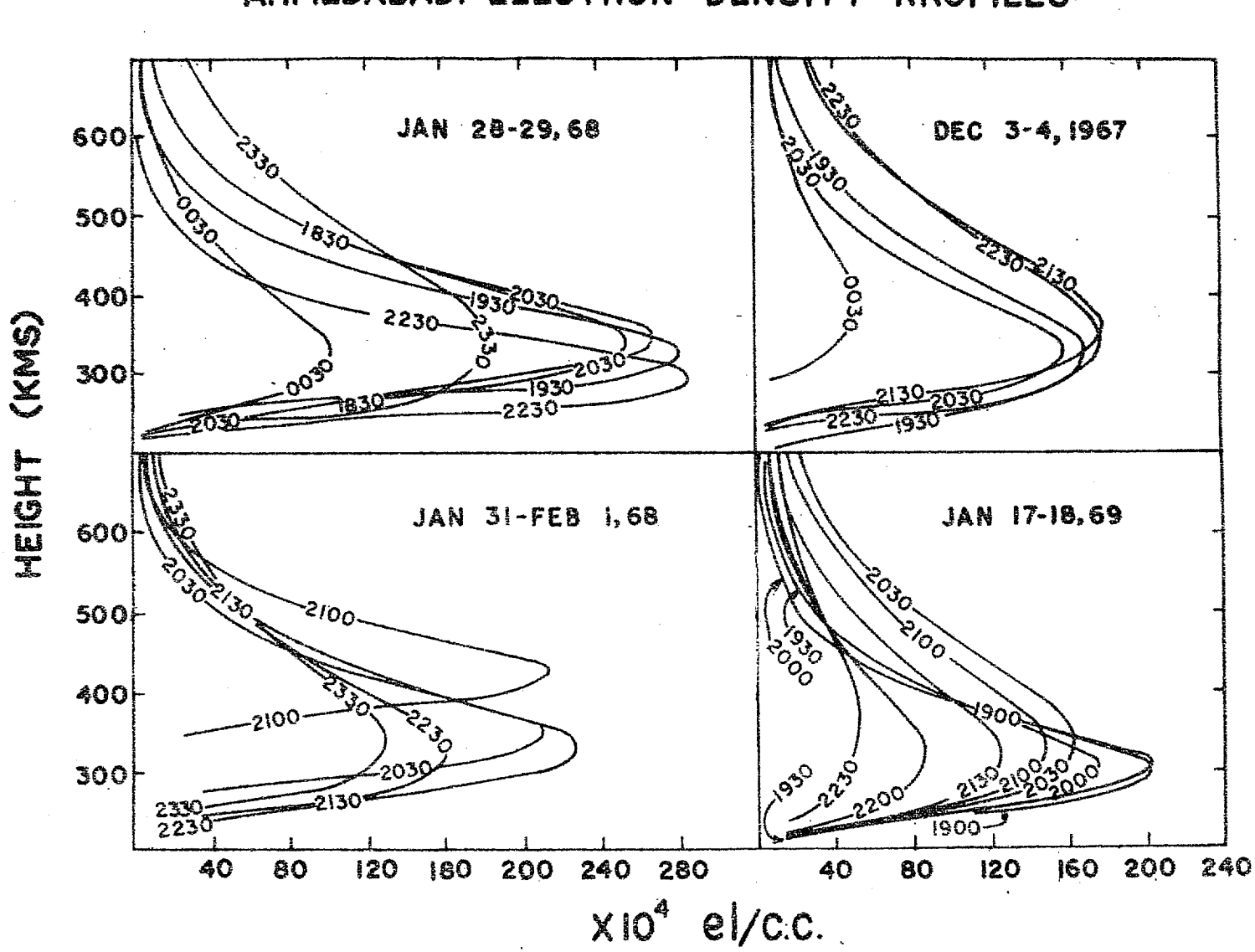

FIGURE 6.21 Electron density profiles of a few nights (N(h) profiles) at Ahmedabad during the hours when pre-midnight enhancement in 6300 A was observed.

From the electron density profiles, assuming the temperature variations as given by CIRA (1965) model atmosphere, following the procedure of solving the continuity equation as given by SHIMAZAKI (1964, 1966) the vertical drift velocities can be calculated. This procedure takes into account, ambipolar diffusion and associated velocity of the ionised gas V_D, velocity due to temperature changes V_T, and the vertical electromagnetic drift velocity ω. On many nights on which the pre-midnight enhancement occurred, the vertical drift velocities were calculated taking all the relevant data required for the procedure given by Shimazaki. The data of a few nights are plotted in Figure 6.22. It is noted that the vertical drift velocities are more negative (downward) at the time of the pre-midnight enhancement.

C) Pre-midnight enhancement in low latitudes: Height variations of the F_2 region at the magnetic equator (Thumba).

From Figure 6.19 it is seen that the pre-midnight enhancement of 6300 Å airglow is quite pronounced and occurs more often towards the south of Mt. Abu (maximum intensity is around 20°N geographic). From the ionospheric data of Thumba (8°N geographic) India, an ionospheric station near the magnetic equator, the h'F and h_pF_2 values reach a very

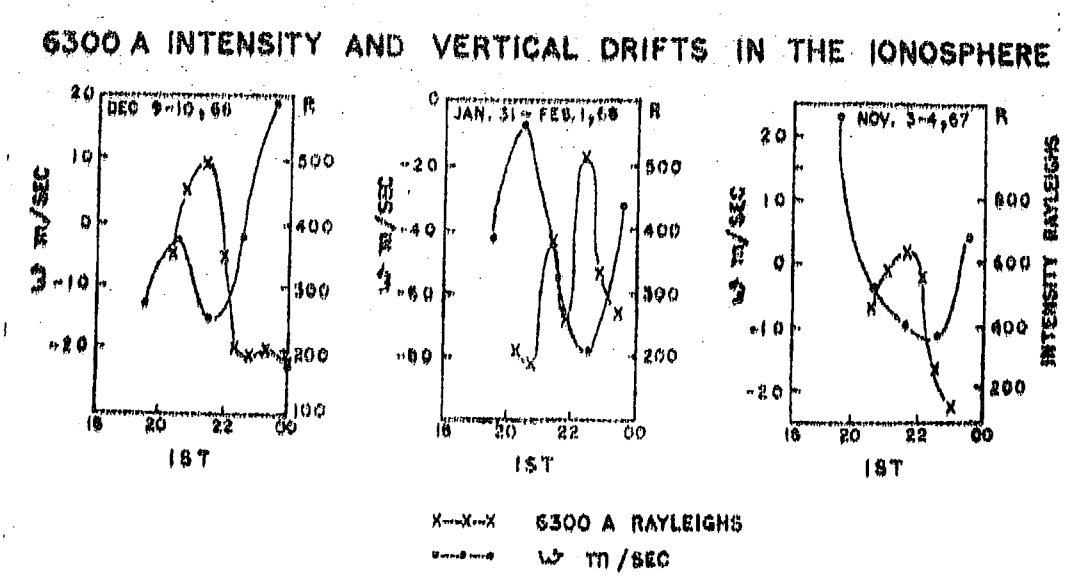

FIGURE 6.22 6300 A intensity and vertical drift (ω) in the ionosphere.

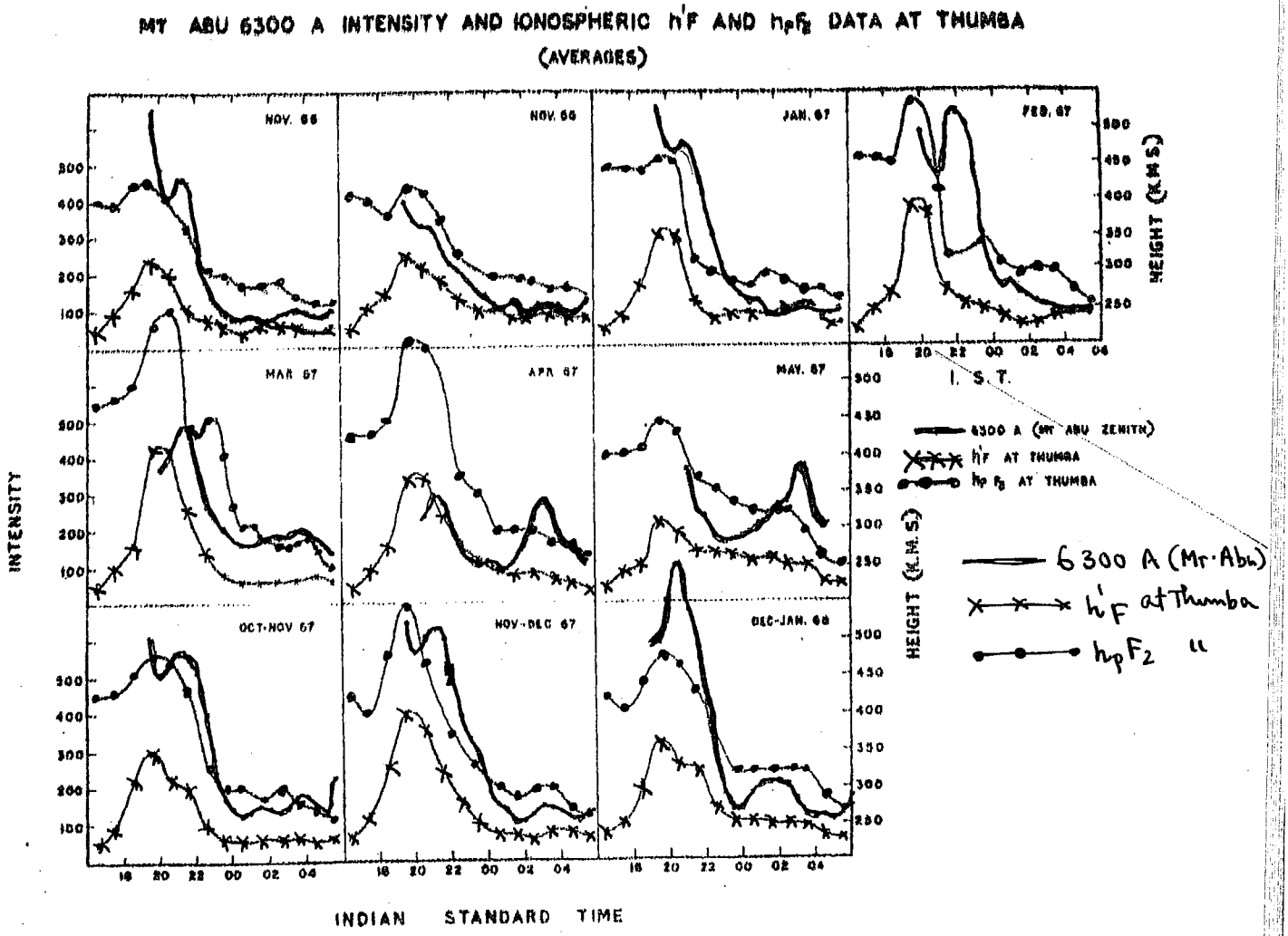

FIGURE 6.23 Mt. Abu average nocturnal variation of 6300 A intensity and the ionospheric parameters h'F and h_pF_2 at the magnetic equator (Thumba).

high value at about 17-20 hours IST. In the Figure 6.23 the monthly average values of h'F and h_pF_2 at Thumba obtained from the C-4 recorder and the lunation average values of 6300 A zenith observations at Mt.Abu are plotted. Also on a few individual nights the same parameters are plotted in Figure 6.24. It may be mentioned that increase of h'F at Thumba in evening hours is inconspicuous in the summer months. The pre-midnight enhancement is also not observed prominently on those occasions.

It may be said that as the F region at the magnetic equator rises in the evening hours, there can be diffusion of electrons along the field lines of force which diffuse and descend at higher latitudes. After the reversal of the field, vertical downward movements increase 6300 A, as the electrons descend to the favourable height of 6300 A emission, which then appears as an enhancement superposed on the post twilight decay. However, the magnitude of the enhancement depends on the rate of post twilight decay and the vertical drift velocities.

This particular increase of electron content in the evening hours at low latitudes is responsible for more pronounced enhancement of 6300 A in the southern skies of Mt. Abu.

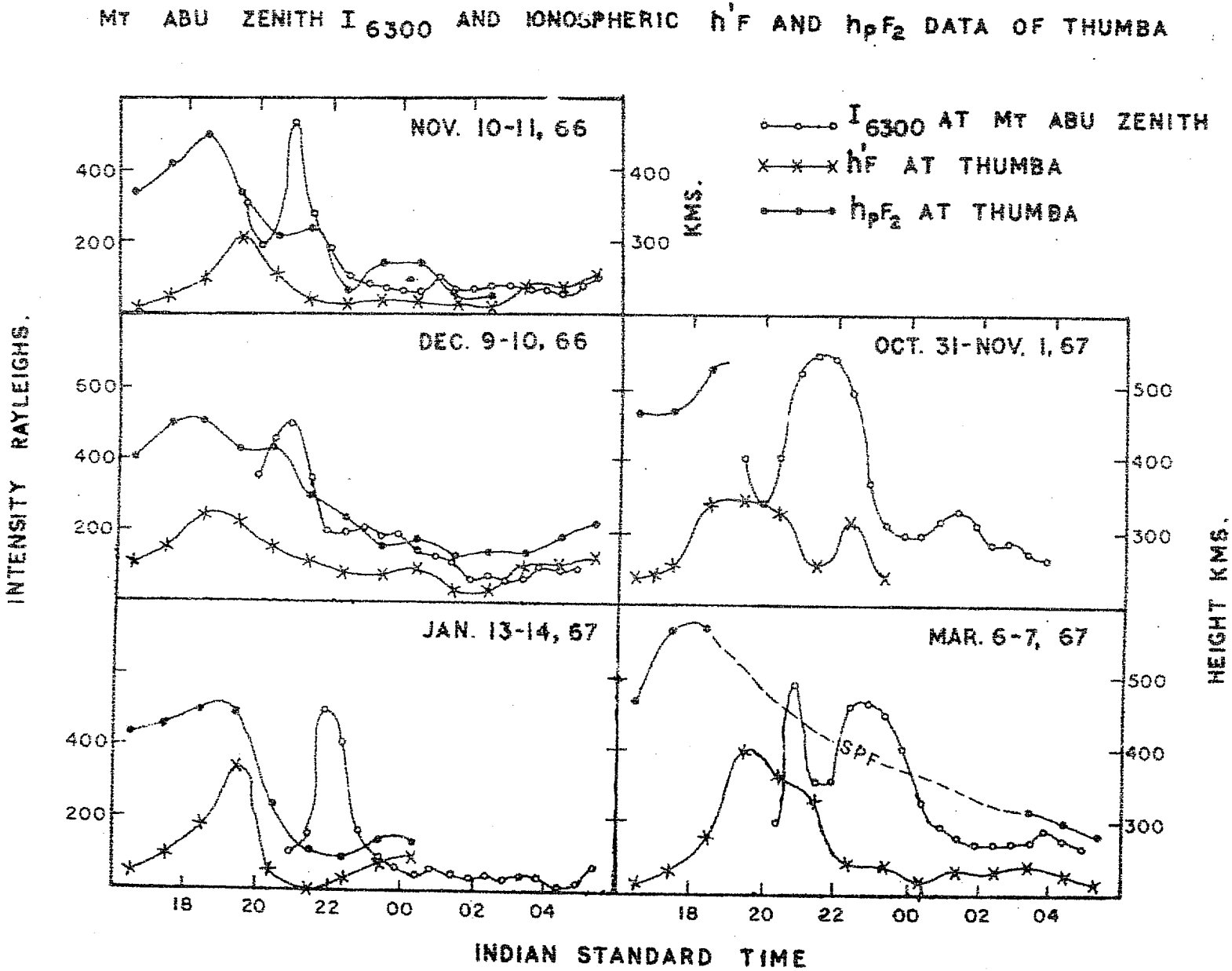

FIGURE 6.24 Mt.Abu zenith 6300 Å intensity and the ionospheric parameters h'F and h_pF_2 at the magnetic equator (Thumba) on a few nights.

6.3.4 Post-midnight enhancements:

This enhancement has been studied from Mt. Abu and Haleakala (Hawaii) data by PAL and KULKARNI (1968). They observed at Mt. Abu a hump of intensity at about 0430 IST on many nights of observation in the year 1965. They offered an explanation for this enhancement that vertical downward movements of the ionisation in the F region were the cause of this increase. The following gives additional information about this post-midnight enhancement from the data from 1964-69.

1) The post-midnight enhancement is seen in all the years from 1964-69. The histogram showing the number of nights this enhancement was seen against the number of nights of observation at Mt. Abu during each of the lunations in the years 1964-69 is given in Figure 6.25. The composite histogram of the lunations in all the years combined is given in Figure 6.26. Out of 377 nights of data, on 306 nights (81%) this enhancement was observed. There is a high probability of its occurrence in all the years in both low (1964-65) and high (1967-68) solar active years, and on all the nights in the year.

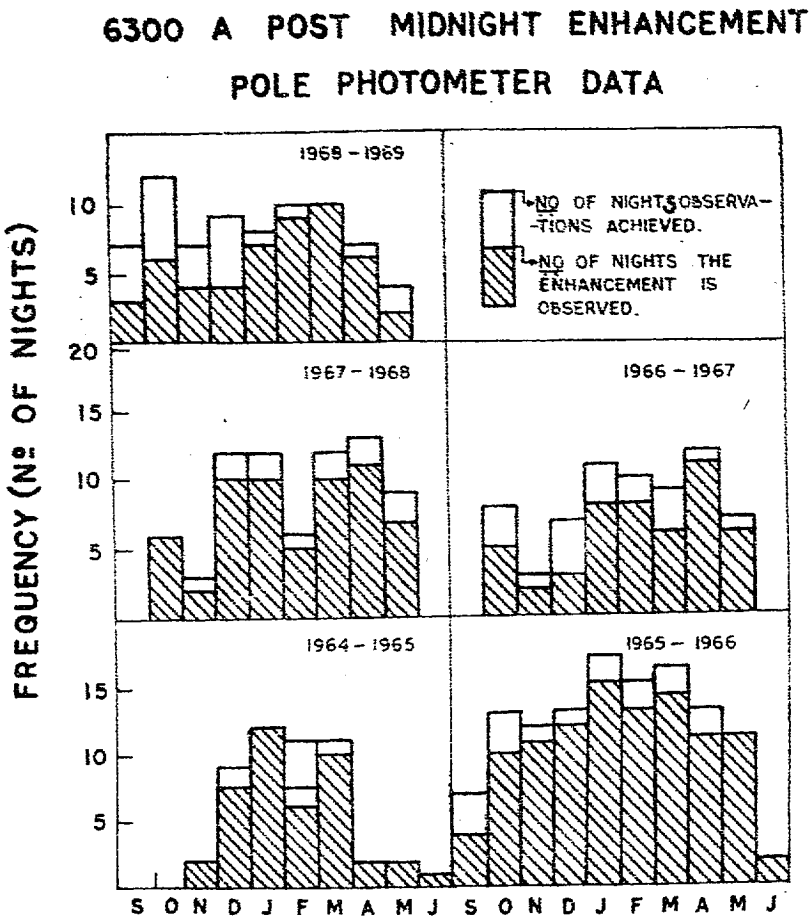

FIGURE 6.25 Histograms showing the number of nights the post midnight enhancement was seen against the number of nights of observations taken at Mt. Abu in different lunations during 1964-69.

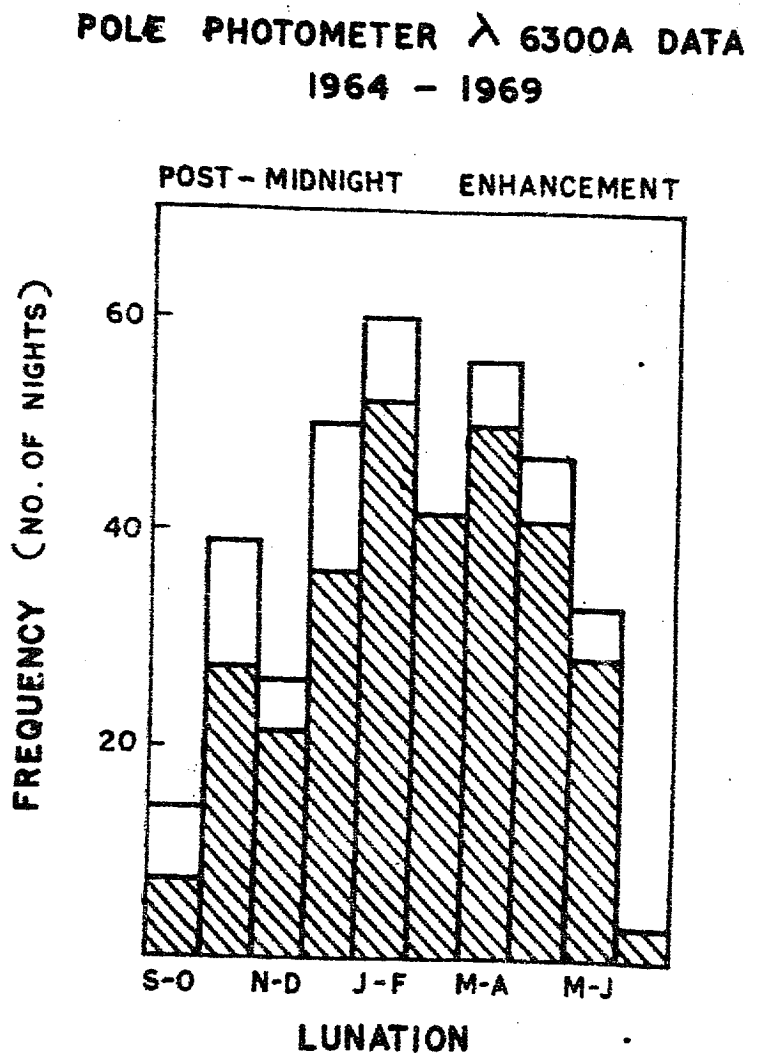

FIGURE 6.26 Composite histogram showing the number of nights the post midnight enhancement was seen in all the years from 1964-69.

2) The magnitude of this enhancement is large in summer months as compared to winter months. From Figure 6.14 and 6.15, this point is clearly seen. In the same figures, the 6300 Å nocturnal variation at zenith and poleward direction are compared (poleward observations are converted to local zenith). It shows that this enhancement is stronger at the zenith of Mt. Abu compared to that at 65°N zenith angle (29°N geographic) of Mt. Abu. 5577 Å does not show any corresponding enhancement to this 6300 Å enhancement.

3) This enhancement is seen at all the geographic latitudes from 17°N to 32°N with varying magnitudes. It is most intense at nearly 23°N geographic latitude. Figure 6.19 A shows the intensity variation at different latitudes from 17°N to 32°N (geographic) obtained from Mt.Abu scanning photometer on typical nights December 3-4 1967 and April 18-19, 1968.

4) The time of occurrence of this enhancement varies from night to night although around 0400 IST is the most common time. No solar activity control is seen on the time of occurrence of this enhancement.

6.3.5 Correlation of the post-midnight enhancement with changes in the electron density profiles of the F_2 region.

As a typical example of a post midnight increase of 6300 Å intensity, December 31-January 1, 1968 night may be

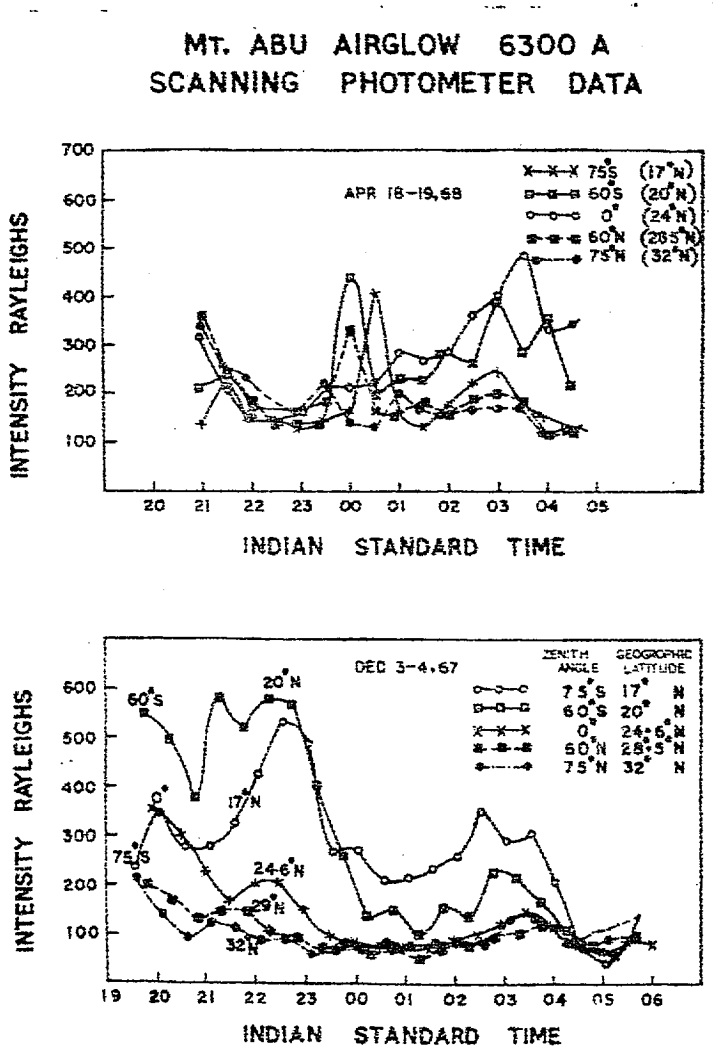

FIGURE 6.19 A Nocturnal variation of 6300 Å at different latitudes on April 18-19, 1968 and Dec.3-4,1967.

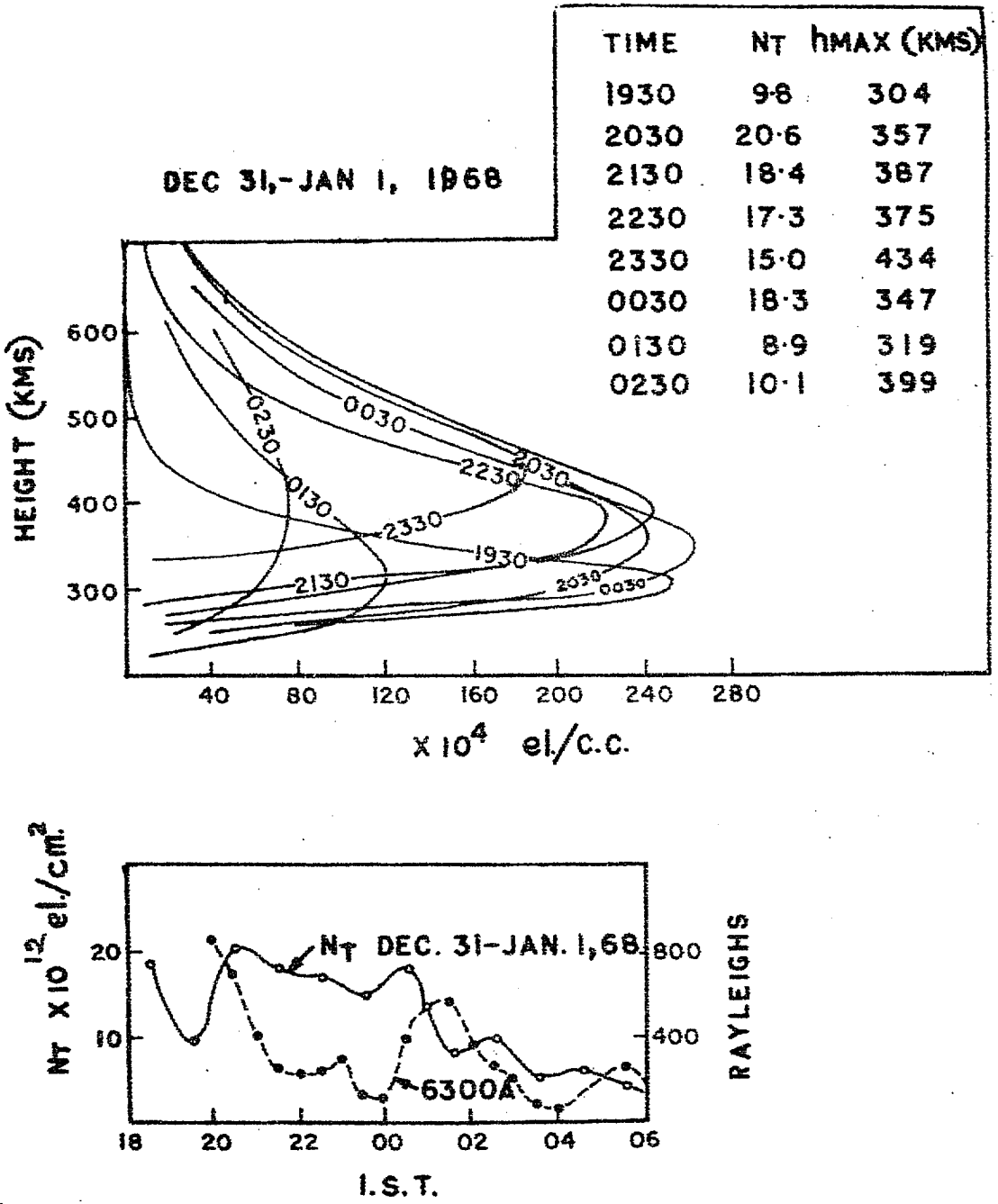

FIGURE 6.27 Electron density profiles (N(h)profiles) on December 31-January 1, 1968.

considered. Detailed N(h) profiles given in the Figure 6.27 showed that the electron content was mostly confined to the higher heights till midnight. After midnight electrons drifted downwards and 6300 A emission started increasing, reaching a maximum intensity around 0130 IST. It is also noted that the airglow enhancement occurred when the electron content decreased rapidly as was pointed by BROWN and STEIGER (1967).

Thus the vertical downward movements of ionisation in the ionosphere are the main cause of airglow 6300 A enhancements in low latitudes.

6.4 Correlation of 6300 A intensity and the electron content in the ionosphere -- Height of 6300 A emission.

To test whether the total electron content in the ionosphere above 200 km was responsible for the 6300 A emission the correlation coefficients of the electron content in the slab 200 km to h_mF_2 and the 6300 A intensity on many nights were found. All half hourly values of observations in a night are considered for this analysis. Also we calculated the electron content in the slabs defined by 200 km and the height h_2 where h_2 was started from 300 km and increased in steps of 20 km up to 400 km. In each case the electron

content between h_1(200 km) and h_2 was found considering all the half hourly observations. A graph of the correlation coefficient between $N(h_2 - 200)$ and the intensity of 6300 Å and the height h_2 is plotted in the Figure 6.28. The last height point on the curve refers to h_mF_2.

On each of these nights the correlation coefficients with N_T the electron content upto h_mF_2 is smaller than the correlation coefficient with h_2 between 300 and 400 km. This shows that the electron content above 400 km is not important to determine the 6300 Å emission rate. The positive correlation reaches its maximum value when h_2 lies between 300 and 400 km with some difference from night to night. Thus the maximum emission of 6300 Å is between 300 and 400 km.

6.5 6300 Å isophote maps.

6.5.1 Introduction:

From the observations with the scanning photometer described in Chapter I, isophote maps of 6300 Å have been prepared after reducing the data by the method described in Chapter III. Figure 6.29 gives some examples of the isophote maps.

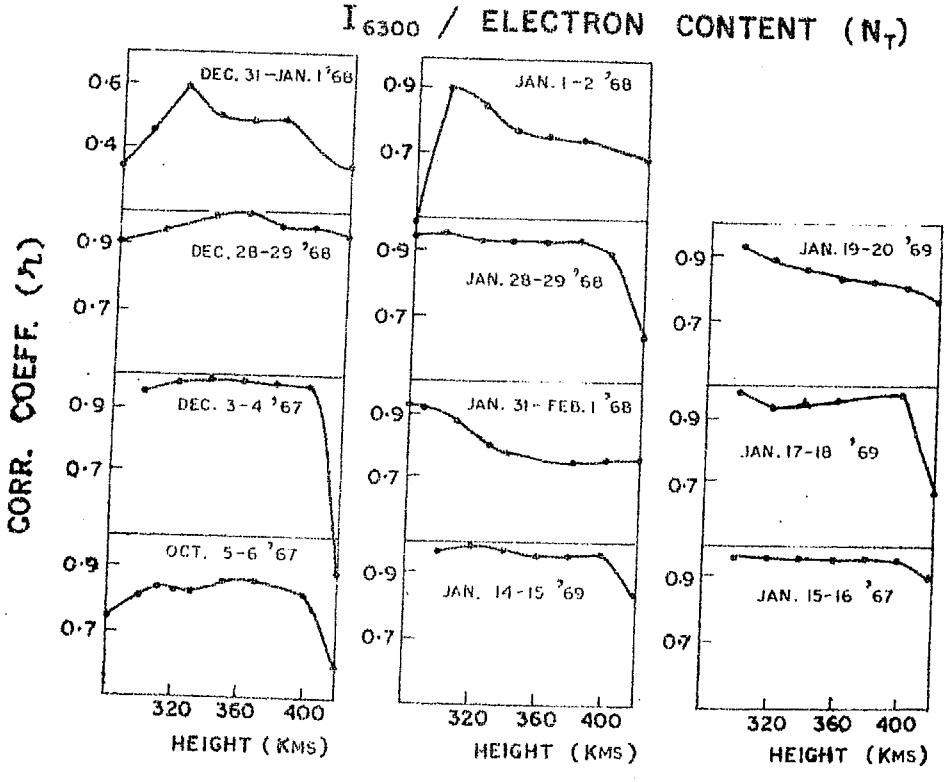

FIGURE 6.28 Correlation coefficients of I_{6300} and total electron content at different heights on a few nights.

The maps are classified roughly into two types in the same way as was done by STEIGER et al.(1966).

(1) Maps that show a patchy (or spotty) character with some of the isolines making closed loops as in the Figure 6.29 A, and

(2) Maps that show somewhat 'aligned' character with the isophotes roughly linear and parallel to each other as in the Figure 6.29 B. It should be made clear here that this alignment is not due to twilight effect which will be in north-south direction.

The spotty or patchy character is often associated with localised tropical enhancements discussed in section 6.3. Aligned isophote maps could occur at any time of the night. When the isophotes were aligned, the direction of alignment in the vicinity of the zenith was determined, the direction being specified as the direction of the gradient of airglow intensity as was defined by STEIGER et al. (1966). Our observations were limited to measurements at different altitudes and $22\frac{1}{2}^{o}$ azimuth angle only. Hence a rough estimate whether the alignment is south-west (Figure 6.29 C) or north-west (Figure 6.29 D) or south (Figure 6.29 B) could be made within $22\frac{1}{2}^{o}$ azimuth angle.

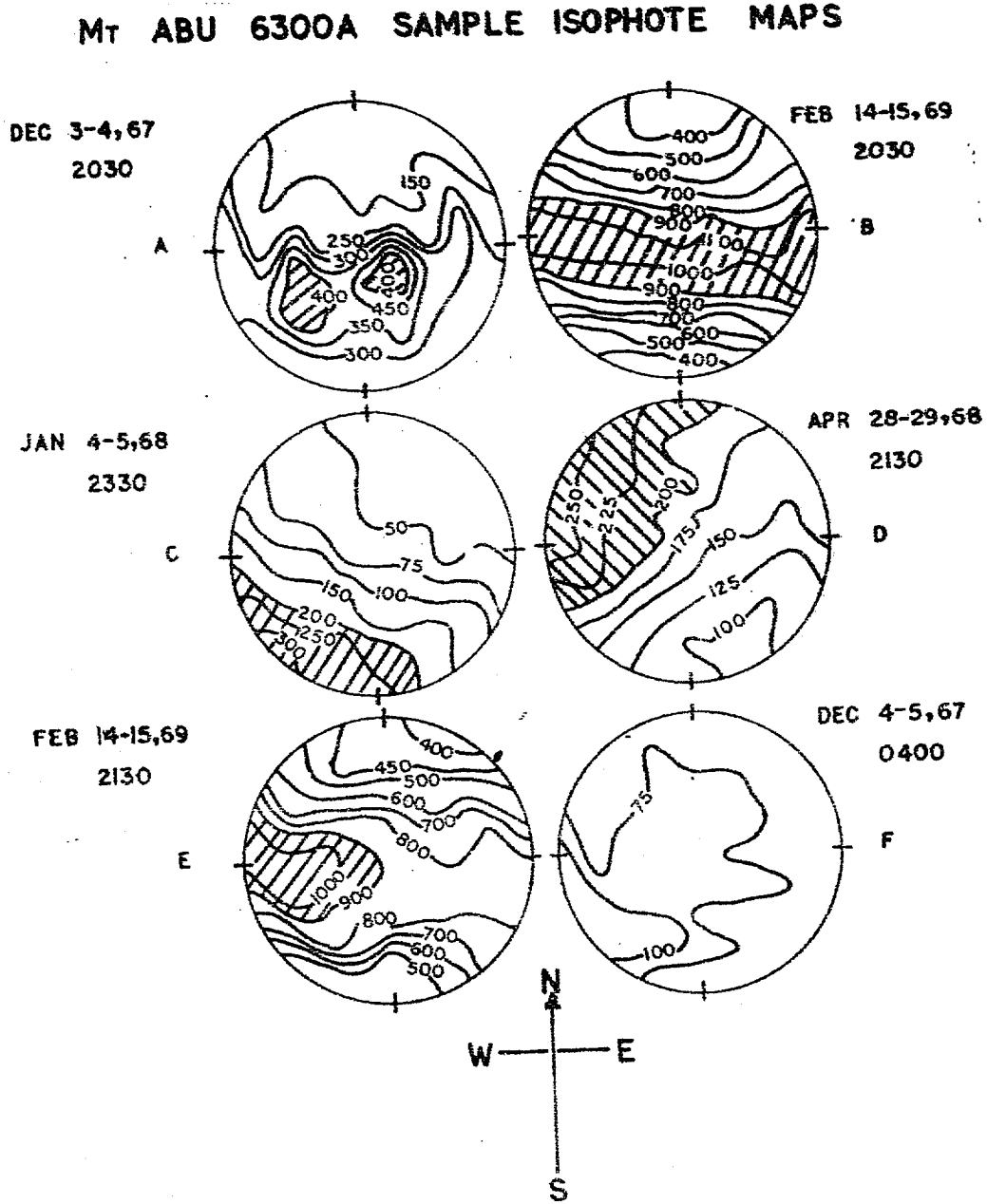

FIGURE 6.29 Mt. Abu 6300 A sample isophote maps.

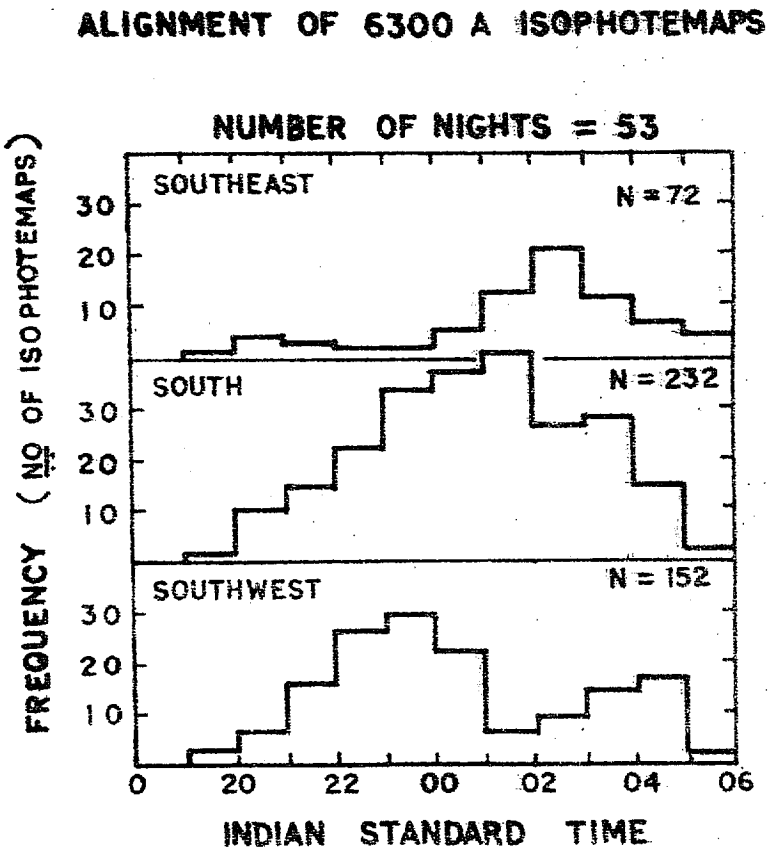

FIGURE 6.30 Histograms of the aligned maps in the directions south-east, south, and south-west.

6.5.2. 6300 Å aligned isophote maps:

The analysis of the isophote maps of 53 nights of the 130 nights data taken at Mt.Abu during 1967-69 showed that out of 840 isophote maps 475 were of the aligned type. Out of the rest, some were patchy (Figure 6.29 A) and a few of them were more or less uniform (Figure 6.29 F). The last one occurred during the early morning hours.

From the aligned maps, histograms are prepared and plotted in Figure 6.30 to see the predominent approximate direction of alignment during different hours. It is seen that out of 152 south-west aligned maps, a greater number occurred before midnight. Out of 72 south-east aligned maps, the greatest number occurred after midnight and out of 232 south aligned maps most of them were spread between 2100 and 0400 hours. There were a few maps (19) which were partly aligned towards west (see Figure 6.29 E) in the beginning of the night. In total, there are more south and south-west aligned isophote maps. With time, these aligned maps move south or south-west with a velocity of approximately 200 m/sec. In Figure 6.31 the isochrones of a few nights are plotted to know the velocity of movement.

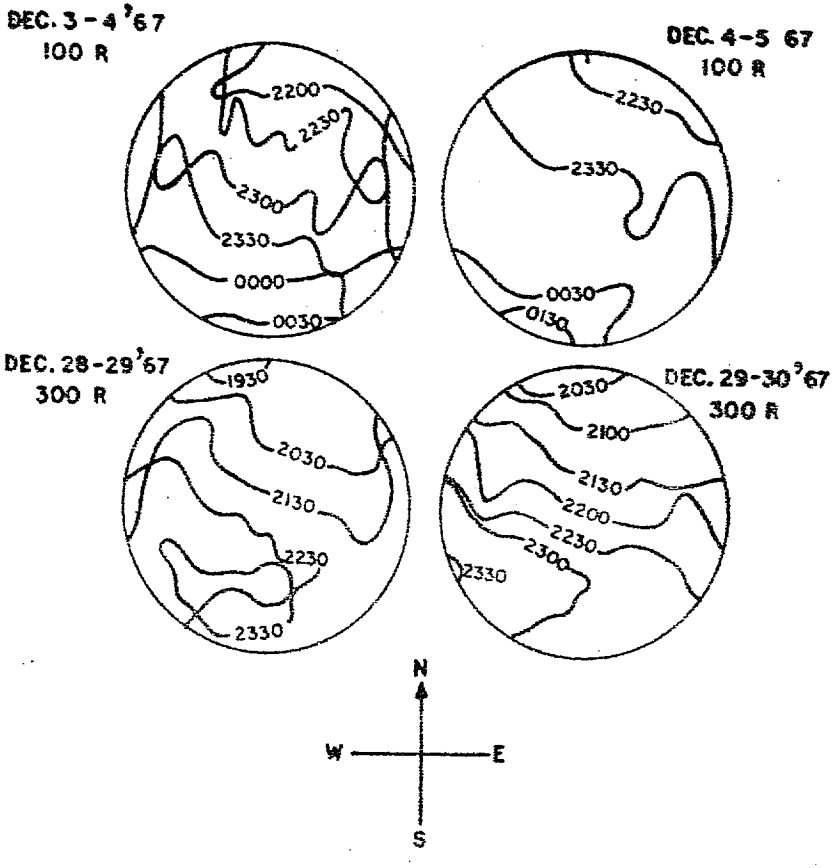

FIGURE 6.31 Isochrones of 6300 A on a few nights.

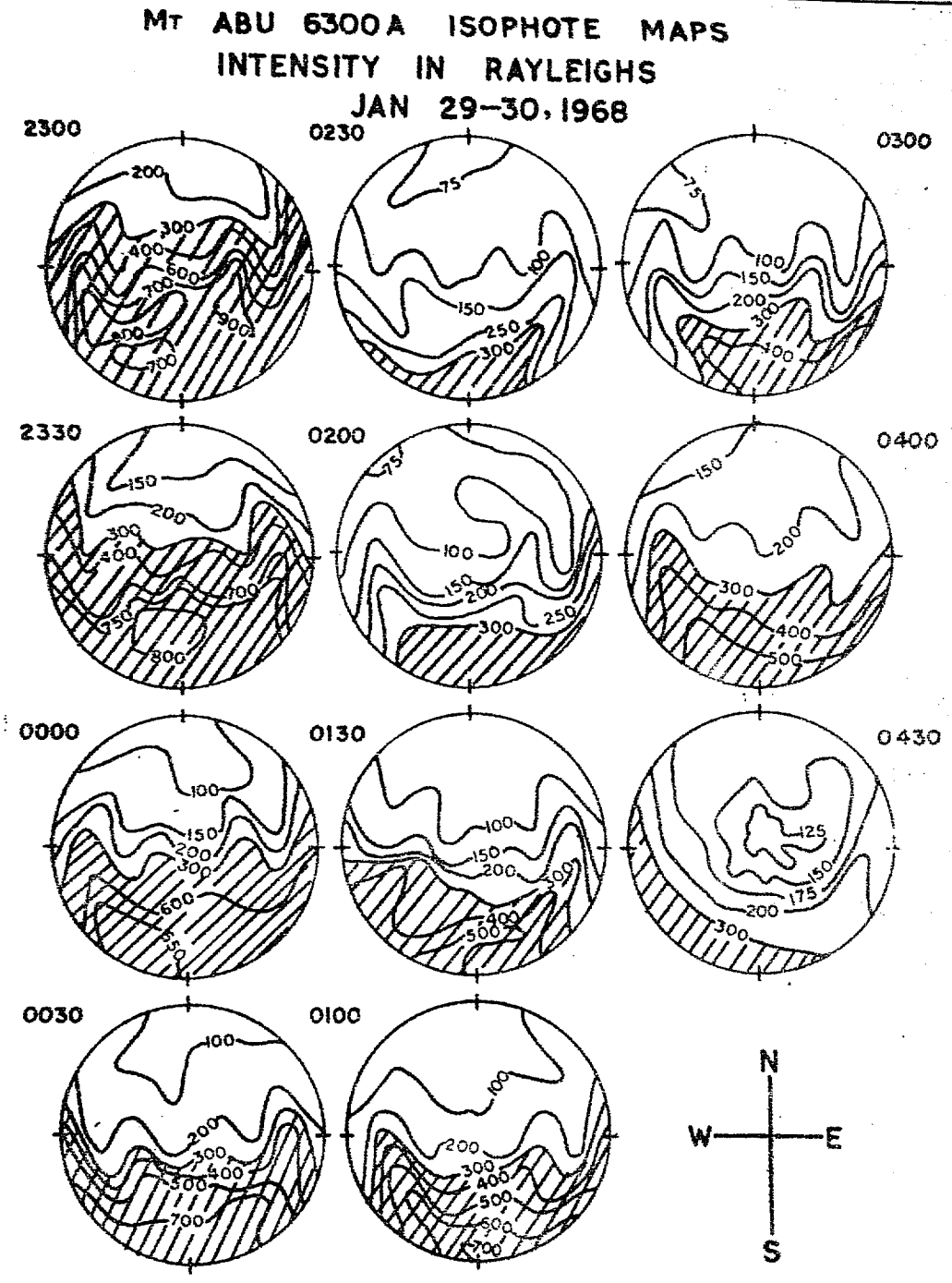

FIGURE 6.32 6300 A isophote maps on Jan.29-30,1968 showing the southward movement. A sinusoidal manifestation in the east-west movement is also seen.

Further, it may be mentioned in addition to southward movement on a few hours of some nights an east-west movement in the isophotes as a sinusoidal wave was observed. This is identified by seeing the crests which change their position in the successive isophote maps. In Figure 6.32, the isophote maps of one night are shown where the sinusoidal movement is seen in east-west direction. Although such movements are not regularly observed, they are observed on a few nights the velocity of movement being approximately 200 m/sec. It is suggested that travelling ionospheric disturbances are the cause of such a sinusoidal manifestation in the east-west movement. Further study with fast scanning will help in understanding such phenomena.

6.5.3 Southward movement of 6300 Å isophotes and the decay phase of the equatorial anomaly:

The movement of 6300 Å isophotes towards south during night is consistent with the concept of the geomagnetic control of the F region of the ionosphere and the associated 6300 Å emission region of the equatorial anomaly (APPLETON, 1954; BARBIER et al., 1962; STEIGER et al., 1966).

In the equatorial region, the electron density of the F_2 layer is enhanced in two zones centered at about $\pm 30^{\circ}$ dip and there is a minimum near the dip equator around local noon. This is called the equatorial F_2 region anomaly.

This anomaly is absent at sunrise, builds up in the forenoon and persists during the day. At solar minimum, the anomaly decays rapidly after sunset.(RASTOGI, 1959). At solar maximum, it persists or is even enhanced after sunset and decays around midnight. SANATANI (1966) has shown the detailed morphology of the equatorial anomaly from a large amount of data covering two solar cycles (1945-1963). In high sunspot years, in the months of March, September and December, the subtropical peak of F region ionisation is maximum around 2100 hours LMT at 34° dip and this peak stays over $34^{\circ} \pm 2^{\circ}$ dip from 1500 hours to 0100 hours LMT and later moves back towards the equator. Of course these variations are only average since the anomaly is variable from day to day, particularly at night.

KING (1968) has shown many points of similarity between the movement and morphology of the intertropical arcs described by Barbier and his co-workers and the crests of the equatorial anomaly during both disturbed and quiet conditions. WEILL (1967) has drawn attention to the relationship between measured airglow intensities and ionospheric equatorial anomaly parameters. ROACH (1968) has emphasised the intimate association of the optical phenomena of 6300 A emission and the ionospheric anomaly.

6300 A observations from Mt. Abu (dip 34°N) are very significant for understanding the decay phase of the equatorial anomaly, as Mt. Abu/Ahmedabad(34°Ndip) are at the subtropical peak of the equatorial anomaly. We have observed the intertropical arc on many nights and studied its behaviour in detail on a number of occasions. Figure 6.33 is a plot of the intensities at different azimuths and at 75° zenith angle on a few nights. The data of one night in each lunation are presented to show the behaviour of the tropical arc and its movement. It is noticed that the arc was seen on most of the nights in the years 1967-69, and as the night advanced, the arc closed and moved towards the magnetic equator. It is seen from Figure 6.33 that the rate at which the arc closed from east and west and moved towards the equator was different in different months; also it was different on magnetically disturbed days (December 29-30,1968). The intensity of the arc was different even on successive nights. To study the intensity variation and the movement of the anomaly, meridonal observations (N-S) at all the zenith angles 75°, 70°, 60°, 40° and zenith at different hours were made on many nights.

In Figures 6.34 A and B a few nights observations of the meridonal scanning are plotted and the isophote lines are plotted. The occurrence of maximum intensity around 30°dip

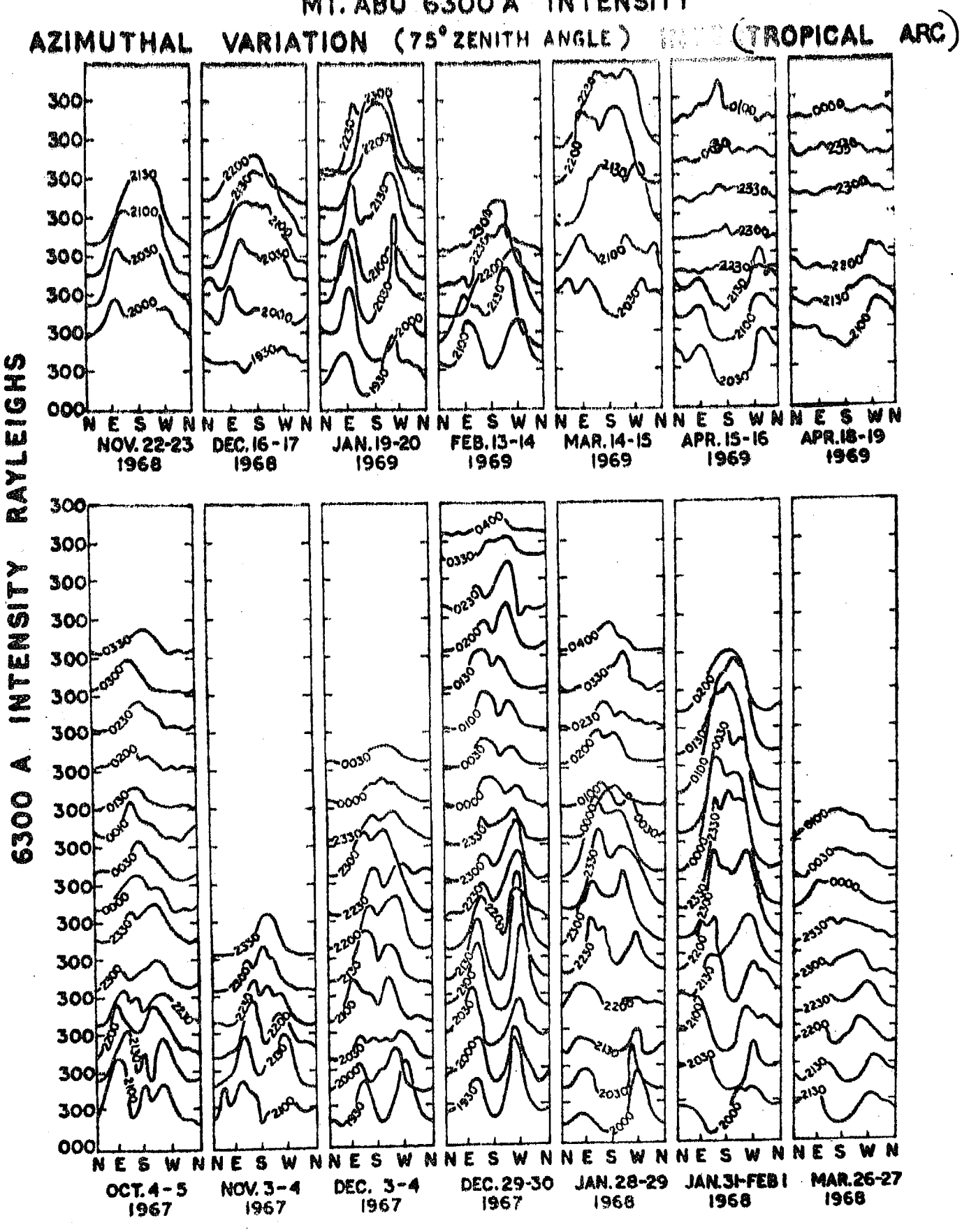

FIGURE 6.33 6300 A azimuthal variation at 75°zenith angle of Mt.Abu on a few nights showing the east-west oriented arc in the beginning of the night. The arc closed towards south as the night progressed.

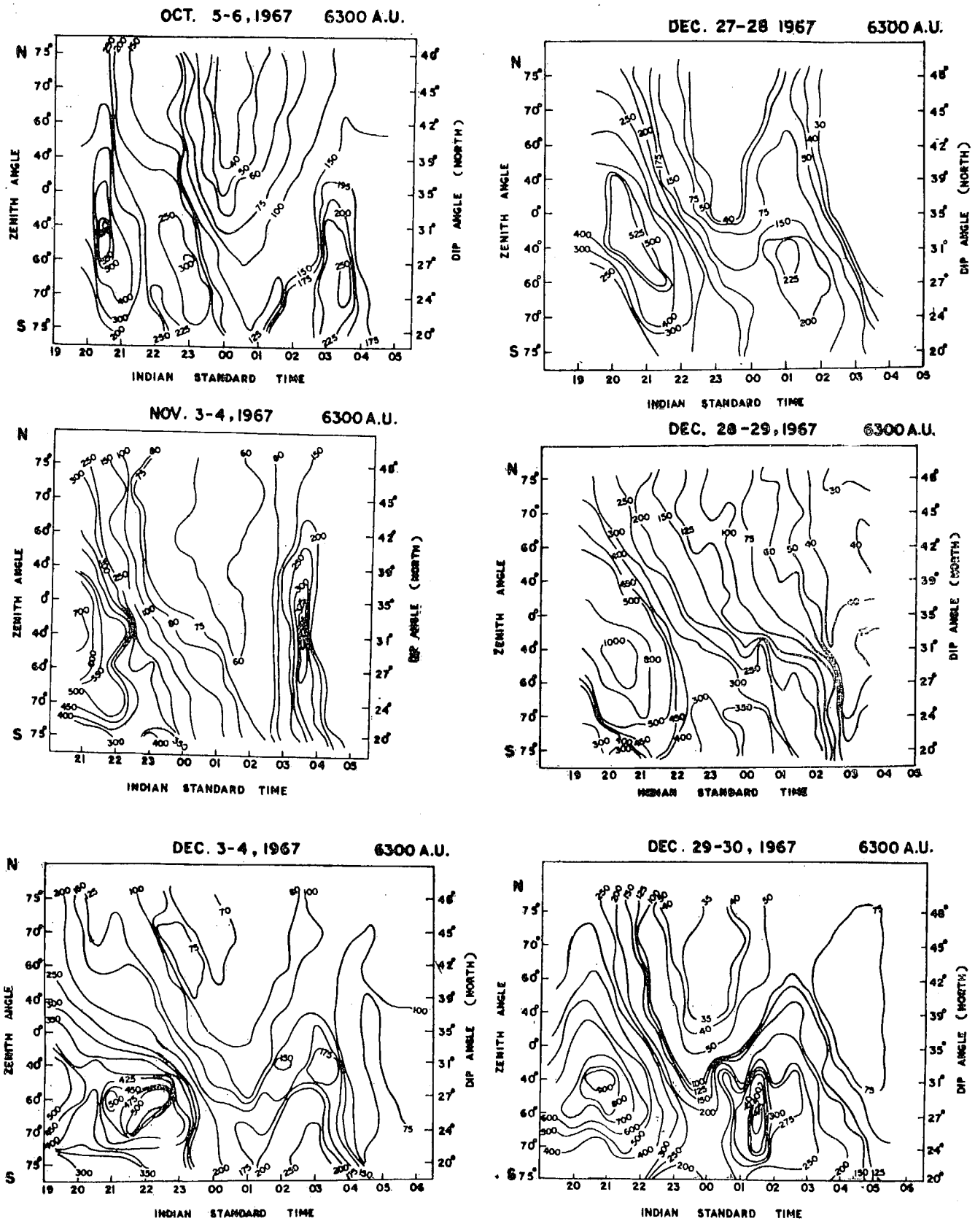

Fig. 6.34 A Meridonal Scanning of 6300 A observations at zenith angles 75°, 70°, 60°, 40°, 0°, plotted as isophotes

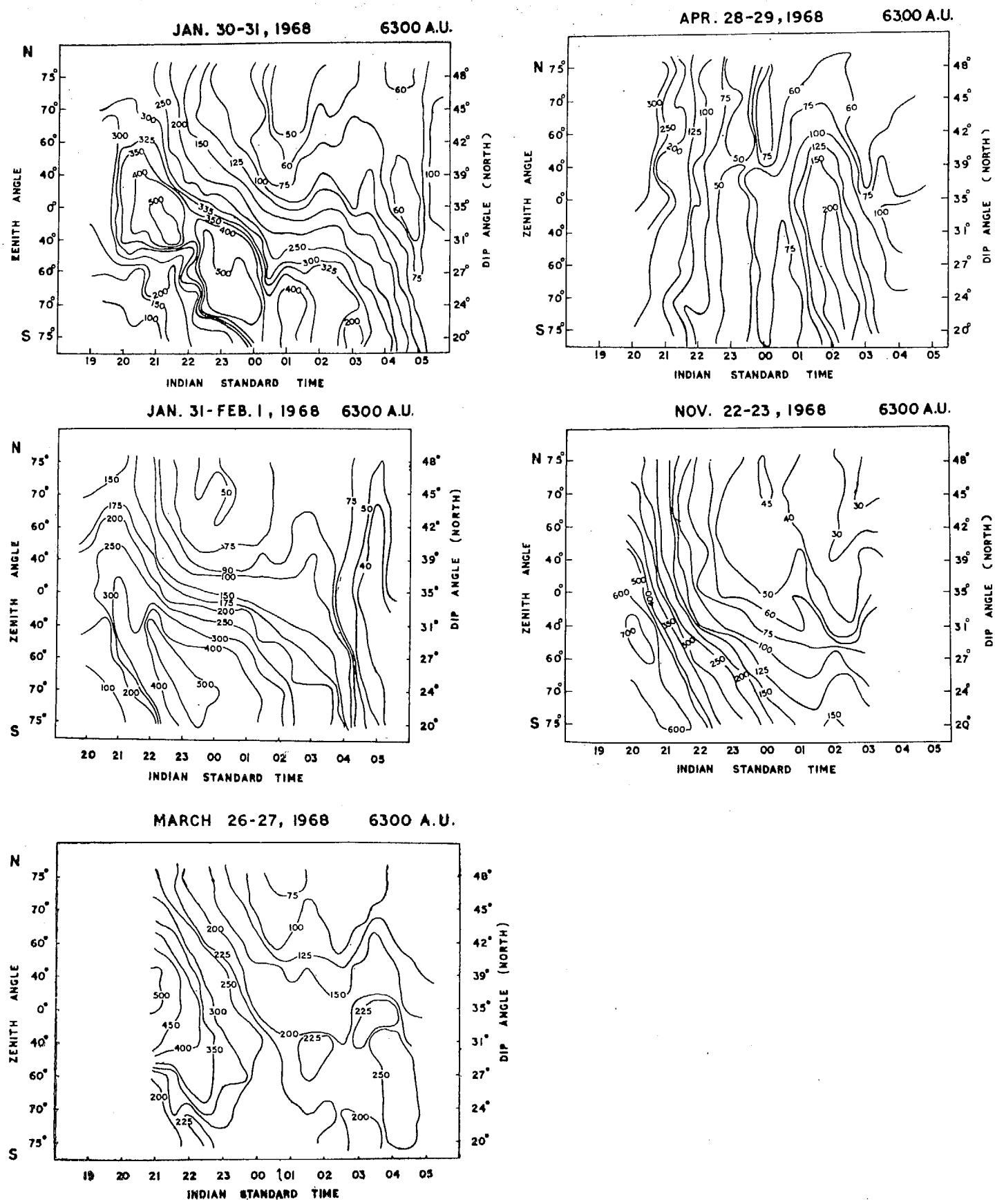

Fig. 6.34 b Meridonal Scanning of 6300 A at 75°, 70°, 60°, 40°, 0° Zenith angles plotted as isophotos

in the beginning of the night and its movement towards the south of Mt. Abu is seen on all the nights, the rate at which it moves is different from night to night. The location of the isophotes of maximum intensity in the beginning of the night is different in different months. However, in December and January, the maximum intensity was located up to midnight towards the south-west, and later it moved towards south and south-east. This behaviour in high active period is consistent with the behaviour of the equatorial anomaly movement discussed by SANATANI (1966).

The results of solving the continuity equation are given by HANSON and MOFFETT (1966). They show with a downward drift velocity (ie. a westward electric field), the vector plot of electron fluxes that are associated with the electron concentration profiles. An 'invert fountain' is created. Ionization from higher latitudes flows along the field lines towards the equator and eventually recombines at low altitudes near the F_2 peak. On the field lines above 450 km, the plasma flux is towards the equator, while below it, it is downwards near the equator. The reason for this behaviour is that as the plasma tube drifts downwards, the particle concentration over the equator must increase if diffusive equilibrium tends to be maintained. Thus most of the photoproduction above 450 km is transported to the equator

in this manner for eventual recombination. Thus the principal effect of downward vertical drift is to replace the Appleton peaks with an equatorial ionization enhancement.(HANSON and MOFFETT, 1966).

VANZANDT and PETERSON (1968) explained the equatorward movement during the night of both the peaks of the anomaly and the nightglow enhancements with the increase in ionisation by the downward drifts and 'inverse fountain effect'. At the dip equator the F_2 layer starts at a higher level and so takes more time to move down into the region of high recombination. Thus the 6300 A behaviour at equator showing midnight maximum can be explained with the above two processes. VANZANDT and PETERSON (1968) suggested a model for the nightglow enhancements and the equatorial anomaly that f_oF_2 is enhanced every where in an east-west band and that the enhancement occurs in this band. This enhancement is usually homogeneous and much weaker than what is observed. Then the F_2 layer moves downwards either over the whole east-west band or in narrow north-south ridges causing associated night airglow enhancements. Further measurements with fast scanning, simultaneous observations from two or three locations within the equatorial belt will help towards a fuller understanding of the decay phase of the equatorial anomaly.

6.6 Covariation of 6300 A and 5577 A emissions in tropical night airglow and the emission of 5577 A from the F region:

The months of the year are grouped according to season as -

a) D-months .. November, December, January and February.

b) E-months .. March, April, September and October.

c) J-months .. May, June, July and August.

The night airglow observations made in the poleward direction at Mt. Abu indicate in general an absence of covariation between 6300 A and 5577 A emissions in E and J months.

Observations in June are very few and there are no observations in July and August due to the monsoon at Mt.Abu. Statistically in E and J months, 5577 A emission shows a maximum around midnight. On the other hand, on most of the nights, 6300 A shows a minimum around midnight. A close examination of all the data (1964-1968) taken in the poleward direction (65°zenith angle) showed that in the D months on a number of occasions both red and green lines showed a covariation. In Figure 6.35, the histogram of the

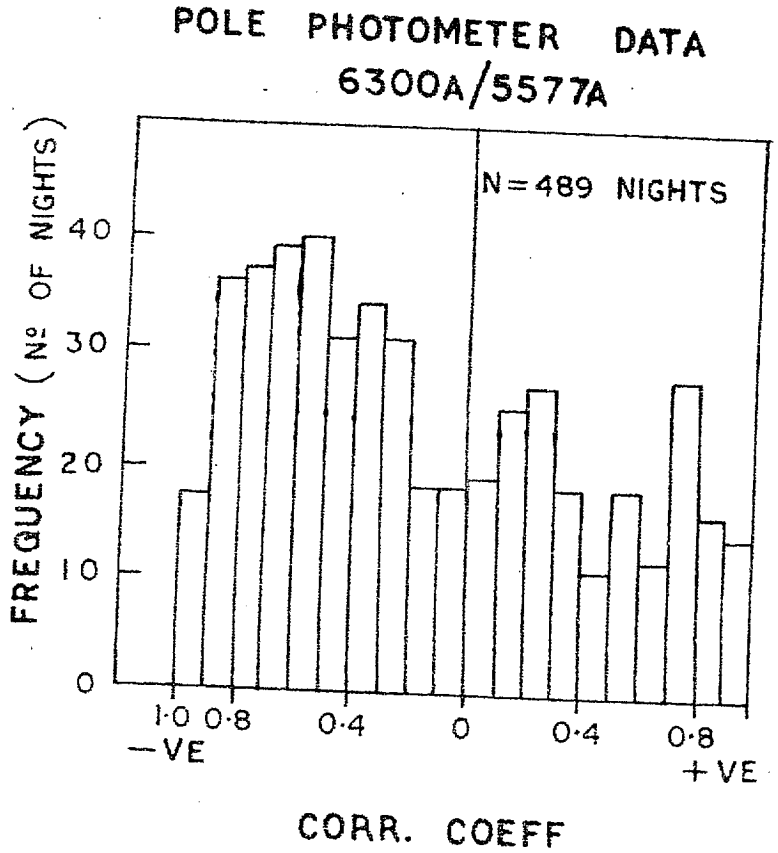

FIGURE 6.35 Histogram of the correlation coefficients of 6300 A and 5577 A. Pole photometer data of 489 nights during 1964-68 is considered.

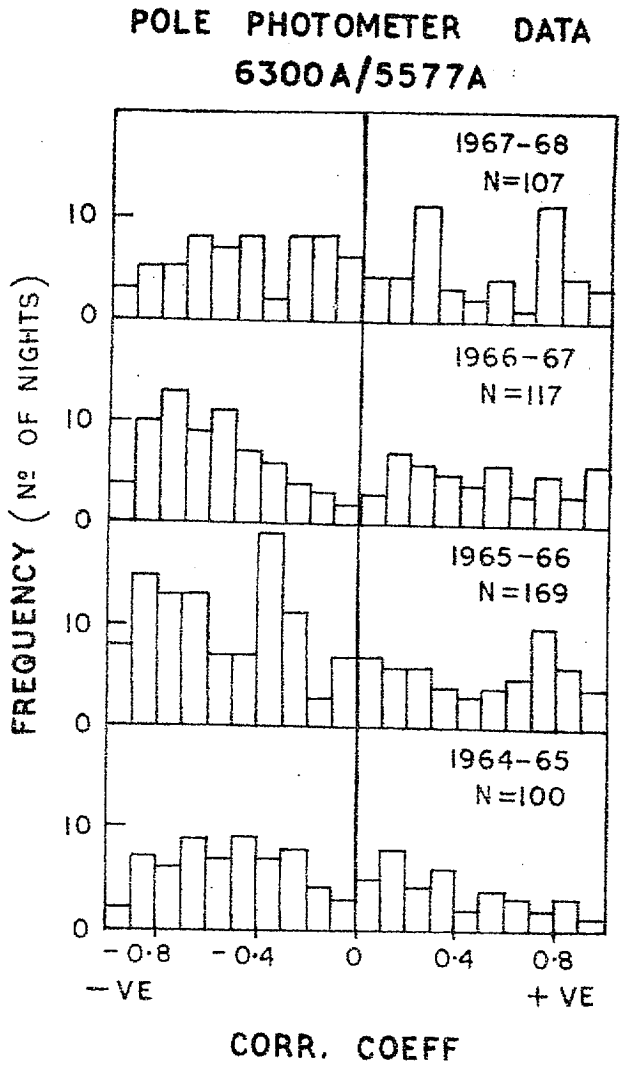

FIGURE 6.36 Histograms of the correlation coefficients between 6300 A and 5577 A in the each of the years during 1964-69.

correlation coefficients of the individual nights between 6300 A and 5577 A are shown, using the data of all the nights in 1964-1968. It shows that although the occasions when negative correlation was more common, there are many occasions when there was a positive correlation. Figure 6.36 shows the histogram of the correlation coefficients of the individual nights in different years. Figure 6.37 shows the histogram of the total number of nights which showed positive and negative correlations in October, November-December, January and April. The negative correlation is particularly pronounced in October-November and in April..

The nocturnal variation on a few nights when these two emissions show an anticovariation are shown in the Figure 6.38. Figure 6.39 shows a few occasions when these two emissions covaried through out the night. It is interesting to note that the pre-midnight enhancements which were discussed in section 6.3 are present in both 6300 A and 5577 A. This shows that there is a significant contribution to 5577 A from O_2^+ reaction in the F region.

A similar study of the scanning photometer data showed that the correlation coefficient between 6300 A and 5577 A is more positive on a greater number of observations in latitudes south of Mt. Abu (34°N to 20°N dip) compared to

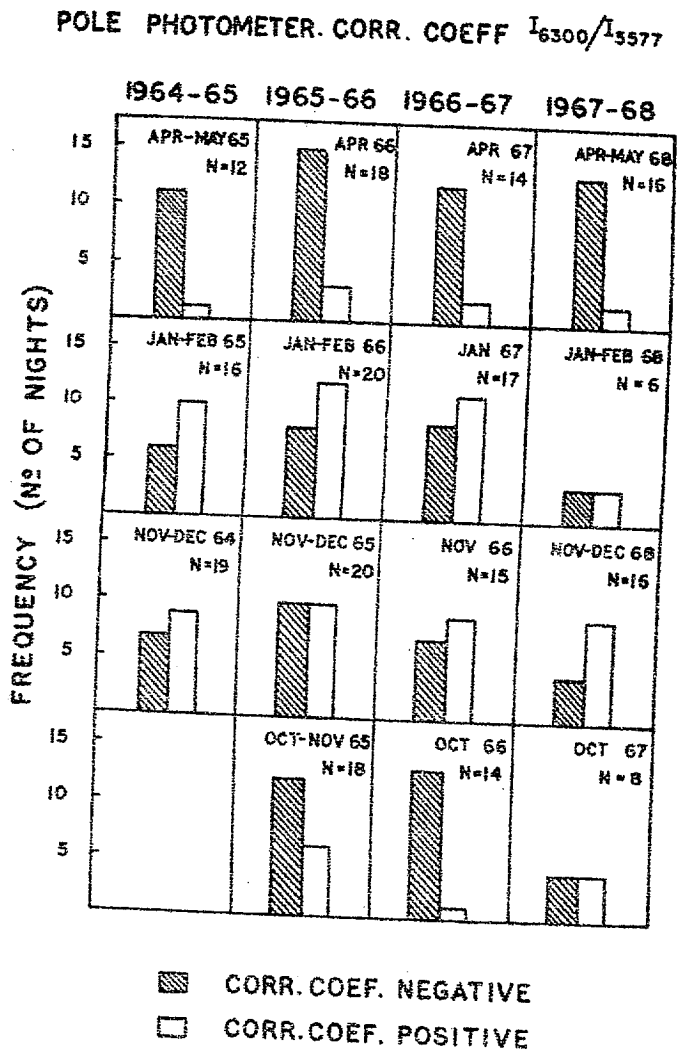

FIGURE 6.37 Histogram of the correlation coefficients between 6300 A and 5577 A showing positive and negative correlation in the months Oct, Nov, Dec, Jan Feb, April and May months in each of the years.

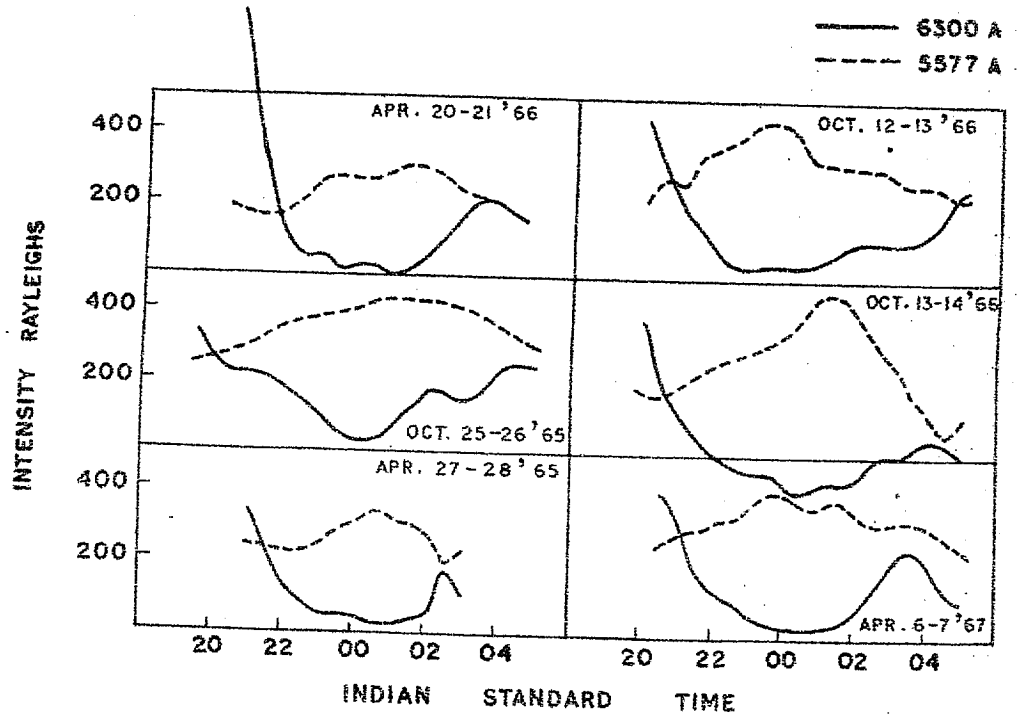

FIGURE 6.38 Nocturnal variation of 6300 A and 5577 A on a few nights showing anticovariation.

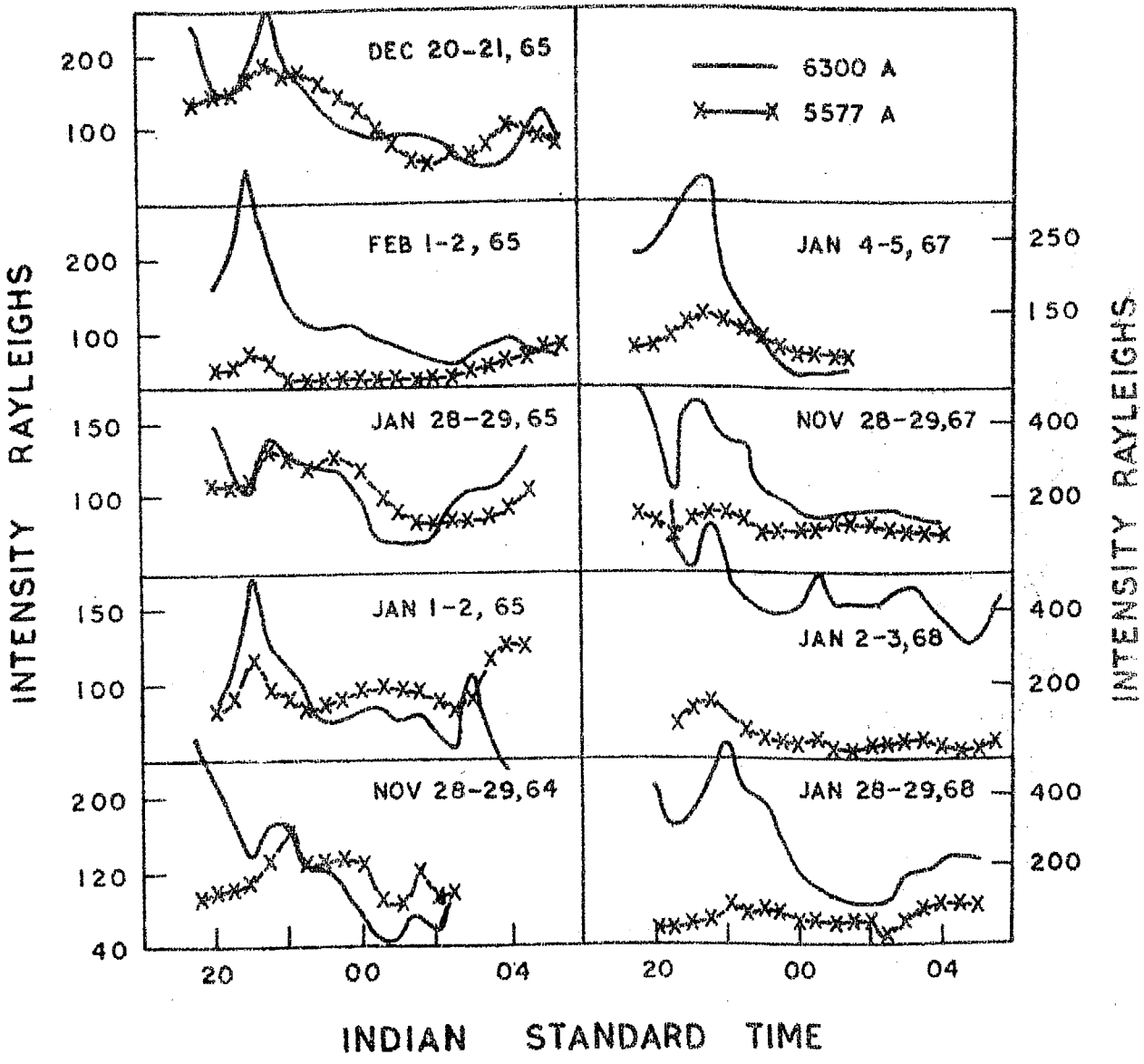

FIGURE 6.39 Nocturnal variation of 6300 A and 5577 A on a few nights showing covariation.

latitudes north of Mt.Abu (34°N to 48°N dip). The correlation coefficients between 6300 A and 5577 A for the latitudes that could be covered from Mt. Abu on a few nights are plotted in Figure 6.40. Histograms are plotted in Figure 6.41 showing the correlation that is observed on 46 nights from the scanning photometer pointed towards different zenith angles. The large frequency of high positive correlations when observations are made towards the south may be noted. In Figure 6.42 is shown the isophote maps of October 5-6, 1967, in which the variations of 5577 A and 6300 A are independent. In Figure 6.43 the isophotes of January 31-February 1, 1968 and December 28-29, 1967 are shown which show close similarity for many hours between 6300 A and 5577 A emissions. This shows that on such occasions which occur in the winter months a major contribution of 5577 A emission comes from F-region.

Such occasions when peak-to-peak covariation is observed in 6300 A and 5577 A emissions are frequent in D months and are more pronounced in south latitudes (20° to 34°N dip)of Mt. Abu than in northern latitudes (34° to 48°Ndip).

When the 5577 A and 6300 A emissions co-vary, the 100 km component is steady or varies in the same way as the F region component. In other months when covariation is not

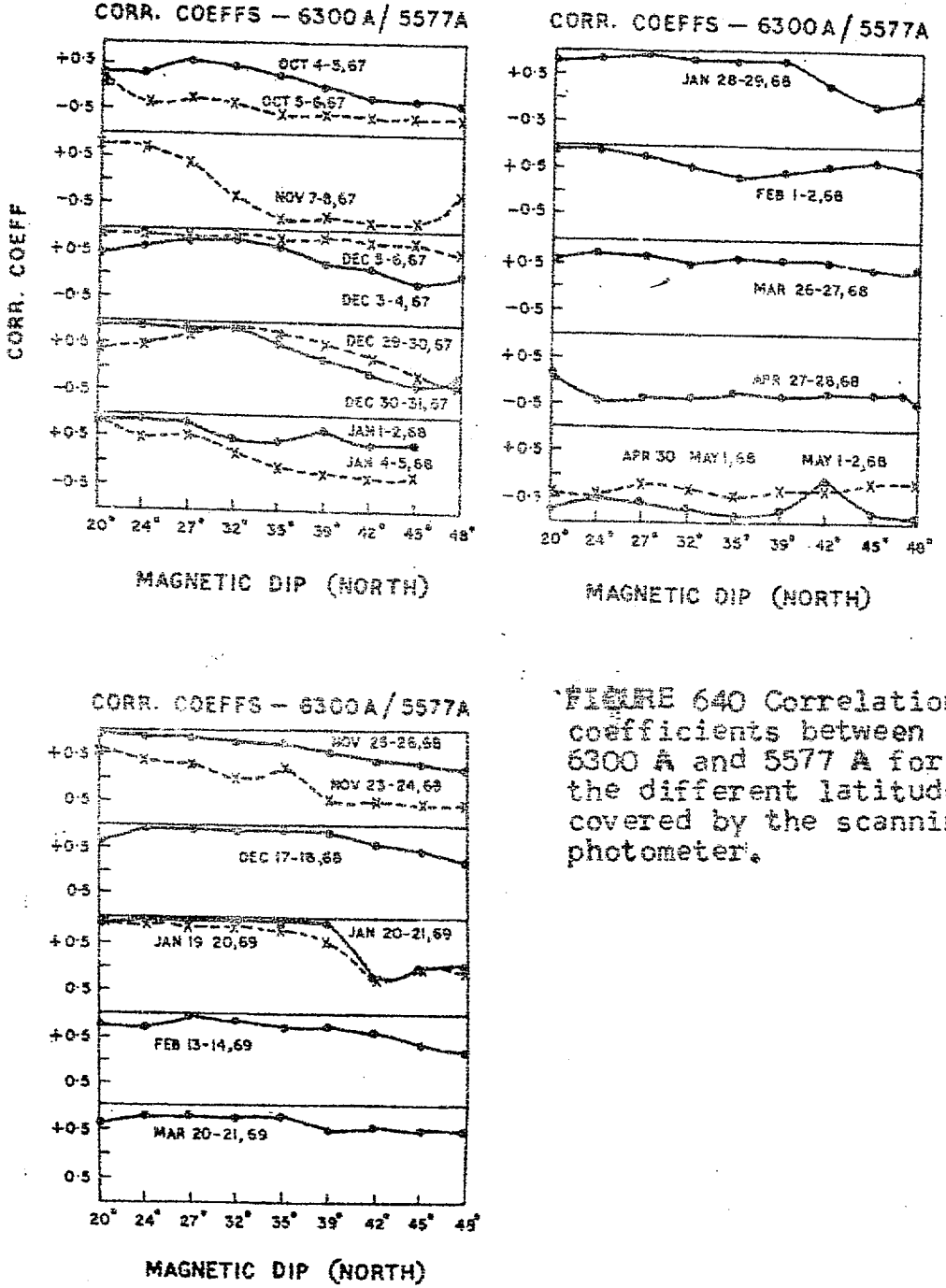

FIGURE 6.40 Correlation coefficients between 6300 A and 5577 A for the different latitudes covered by the scanning photometer.

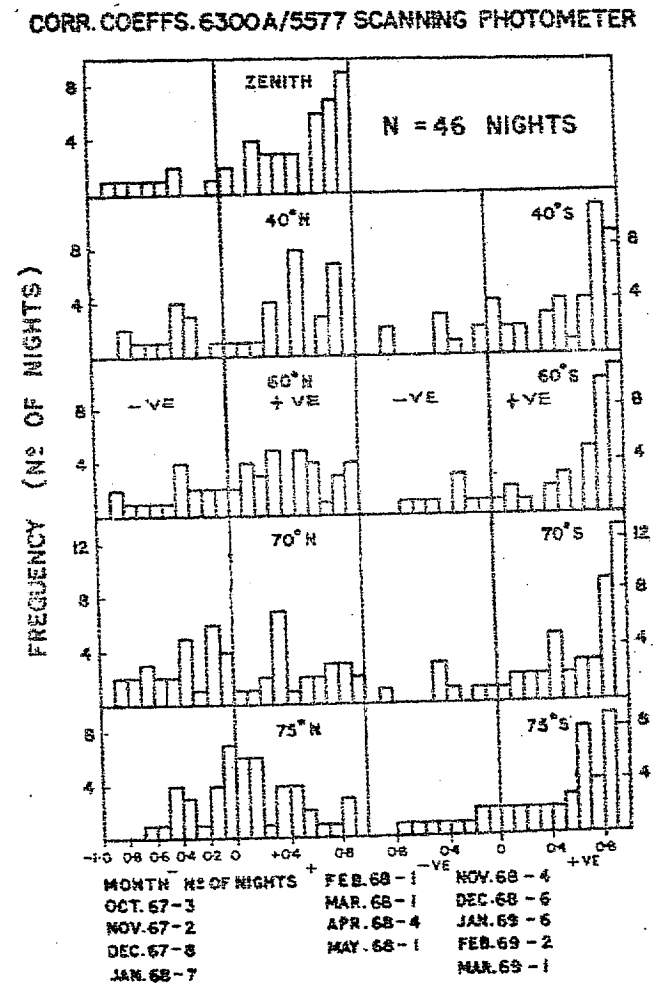

FIGURE 6.40 Histograms of the correlation coefficients of 6300 A and 5577 A for the different latitudes.

MT. ABU 6300 A ISOPHOTEMAPS. INTENSITY IN RAYLEIGHS. OCT. 5-6, 67.

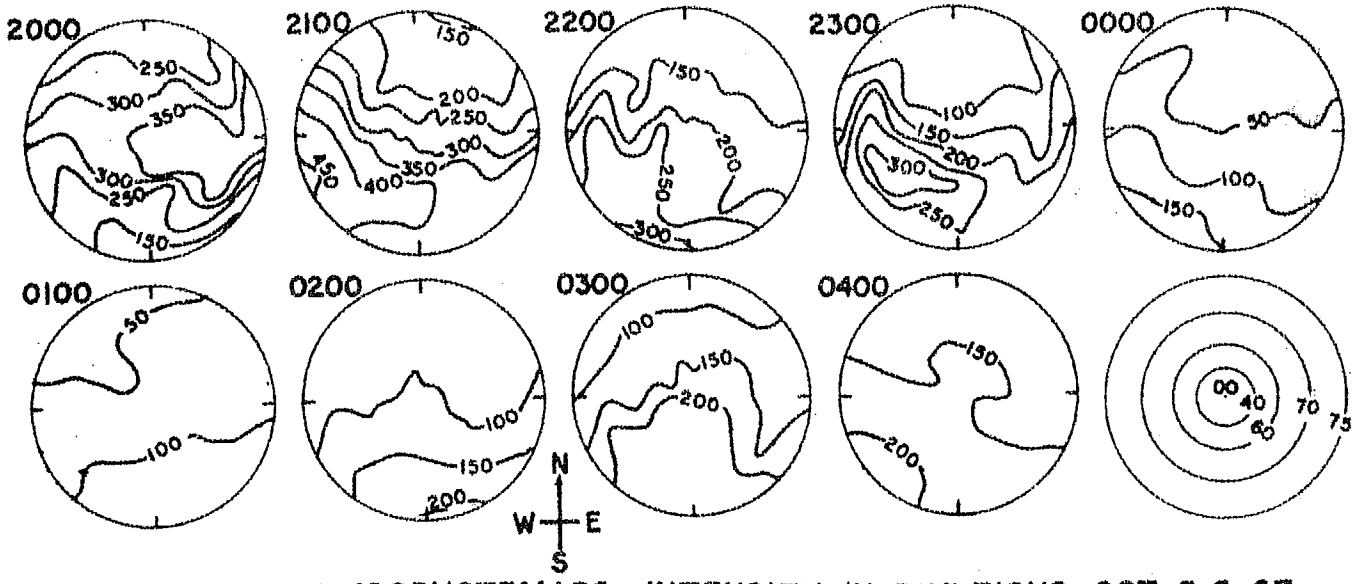

MT. ABU 5577 A ISOPHOTEMAPS. INTENSITY IN RAYLEIGHS. OCT. 5-6, 67.

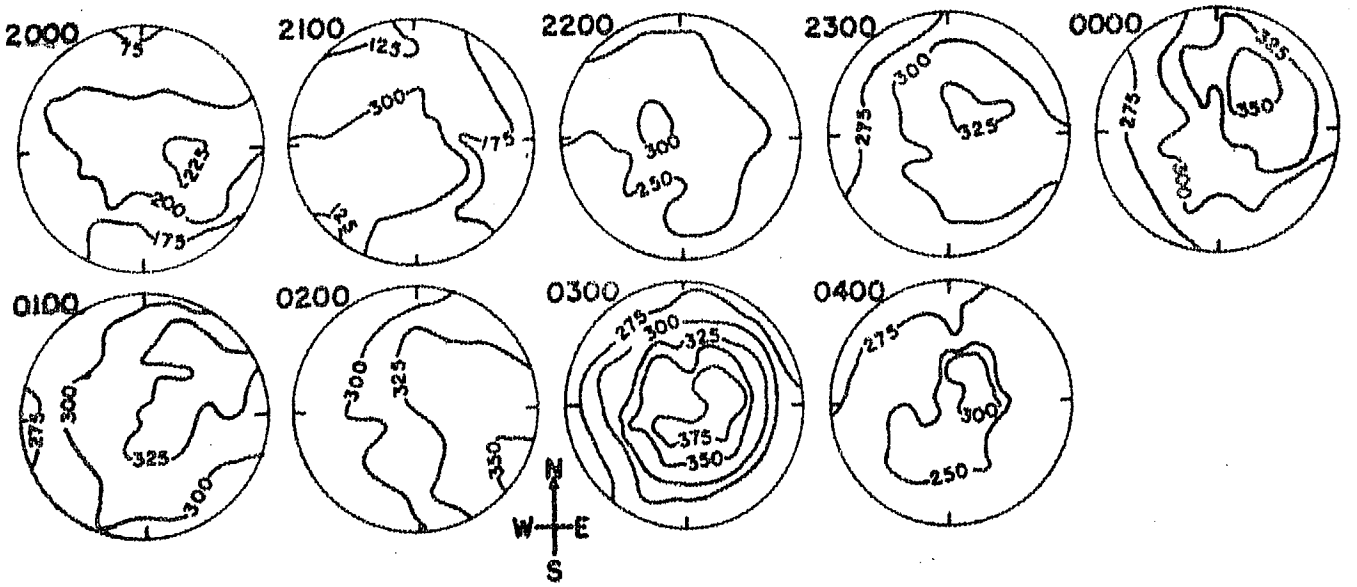

FIGURE 6.42 Isophote maps of 6300 A and 5577 A showing independent variation on October 5-6, 1967.

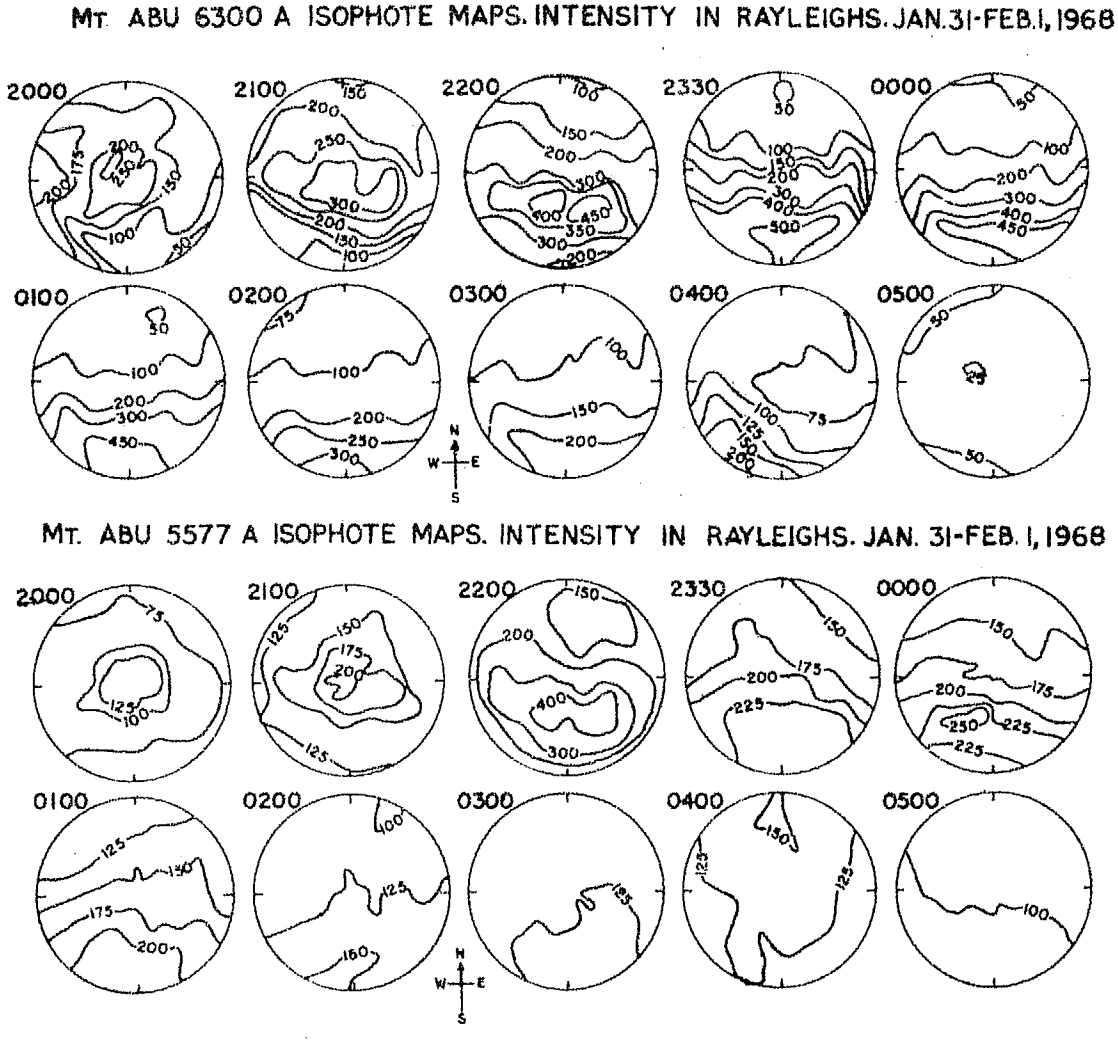

FIGURE 6.43 A Isophote maps of 6300 A and 5577 A on January 31-February 1, 1968 showing close similarity in their nocturnal variations.

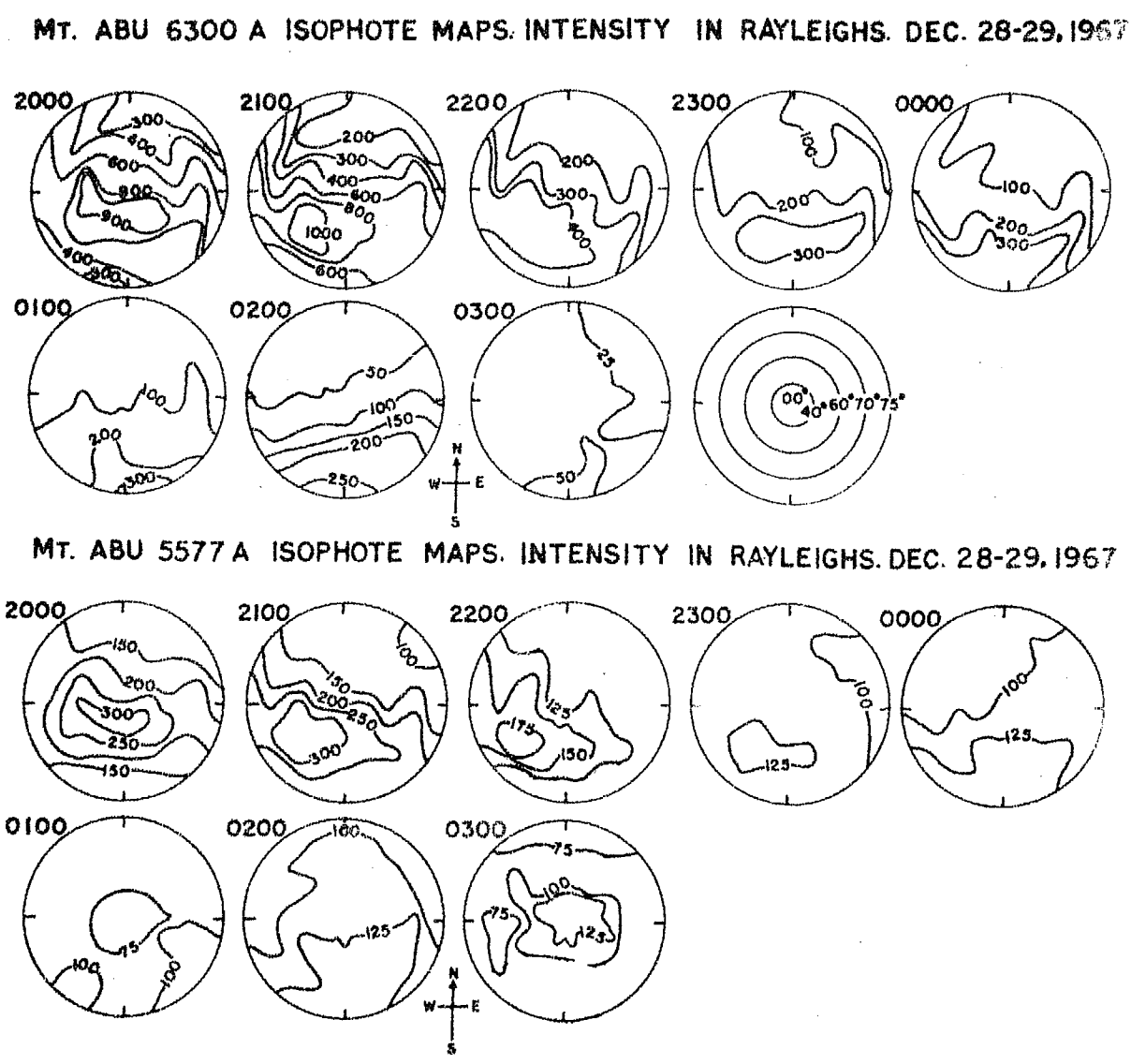

FIGURE 6.43 B Isophote maps of 6300 A and 5577 A on December 28-29, 1967 showing close similarity in their nocturnal variations.

seen, it is to be presumed that the F region component of 5577 A is masked by the strong component from the 100 km region.

6.6.1 Barbier's relation for 5577 A emission:

On occasions when there is a high positive correlation between 6300 A and 5577 A, it is found that Barbier's relation using ionospheric parameters for 6300 A emission can also be used for 5577 A emission. The observations on some clear nights made with the scanning photometer towards 40^{o}S zenith angle are plotted in Figure 6.44. The correlation coefficients(η) between 6300 A and 5577 A on these nights were found to be high and positive. Also in the same graph, f_0F_2 and h'F are plotted. Barbier's relation is fitted for both 6300 A and 5577 A. This relation fits reasonably well for both 6300 A and 5577 A emissions. Figure 6.45 gives the I_{6300} vs. Q_{6300} and I_{5577} vs. Q_{5577} plots, where I denotes the observed and Q the calculated intensities using Barbier's relation. The constant term in Q_{5577} relation gives the contribution from the 100 km region and other unresolved contributions. This when subtracted from the observed intensity gives the F region component of 5577 A.

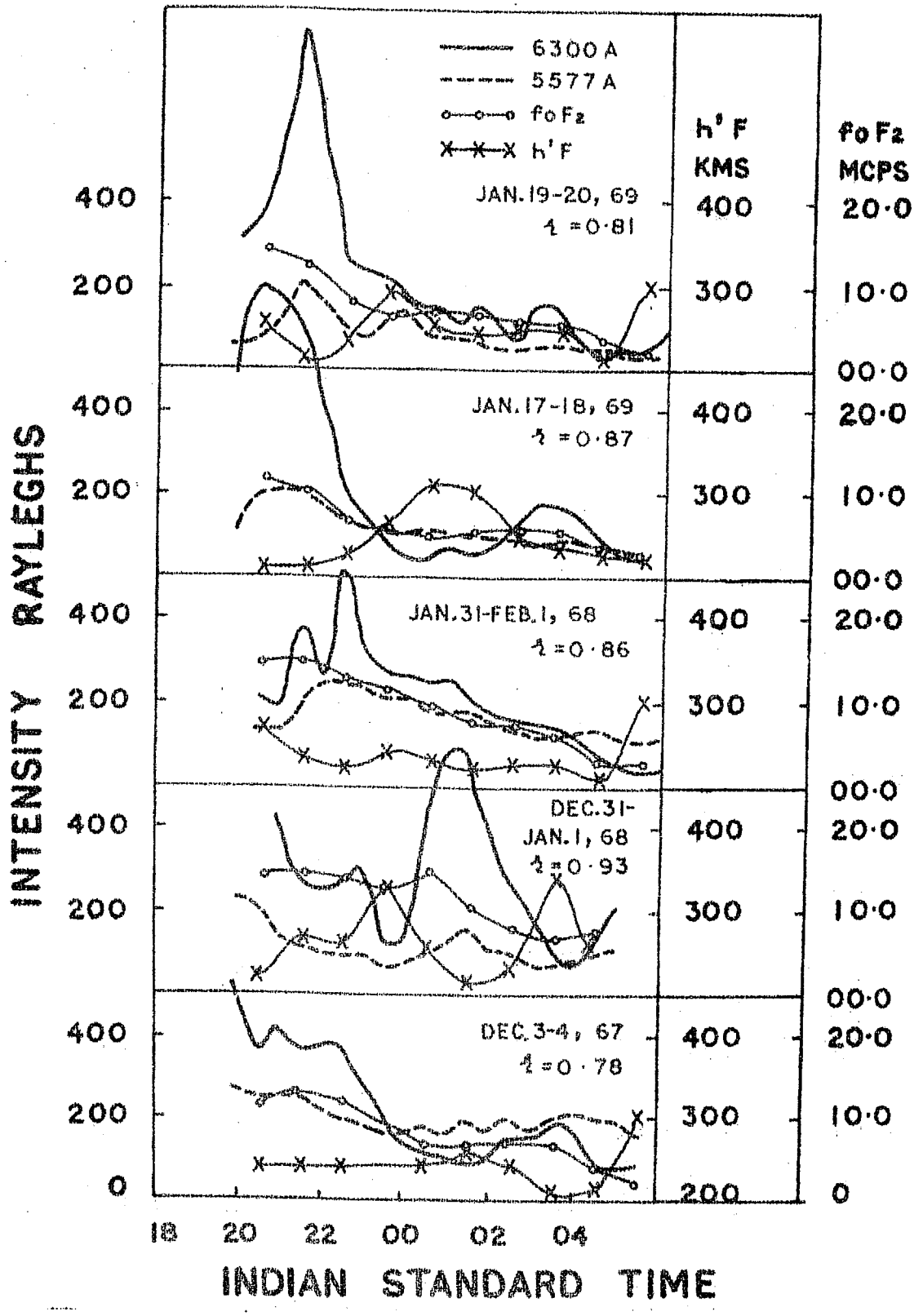

FIGURE 6.44 Nocturnal variation of 6300 A and 5577 A at 40°S zenith angle of Mt.Abu on a few nights showing a high positive correlation. f_0F_2 and h'F of Ahmedabad on those nights are also plotted.

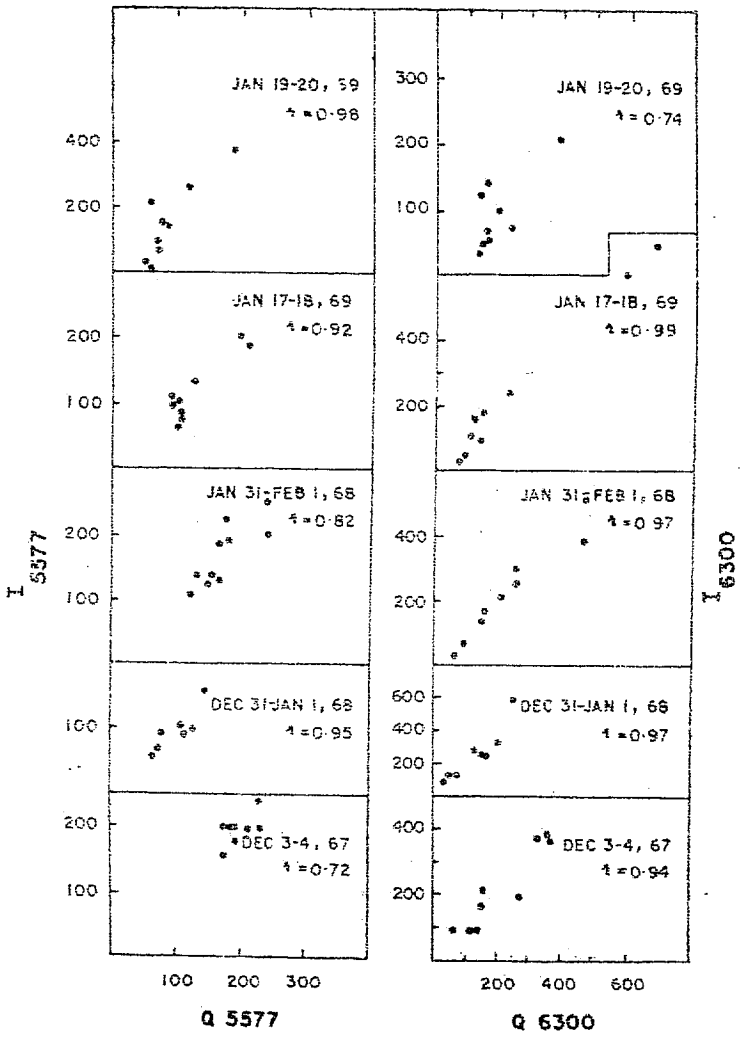

FIGURE 6.45 Barbier's relation for 6300 A and 5577 A .

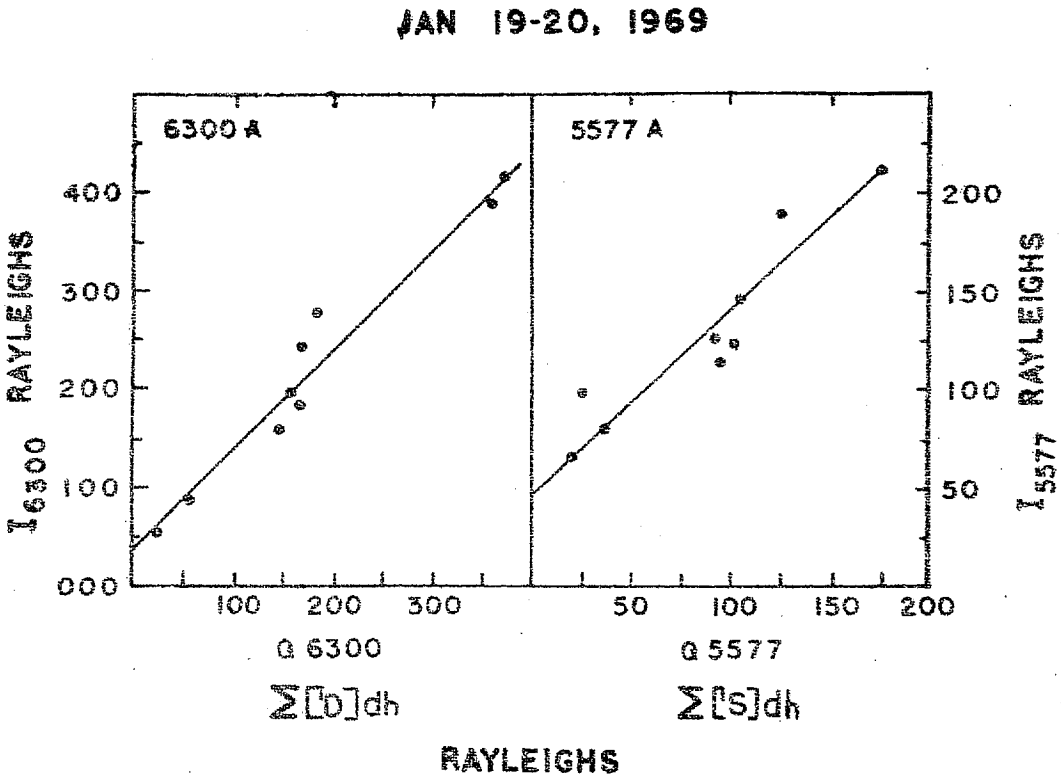

FIGURE 6.46 Comparison of the observed 6300 A and 5577 A intensities and calculated from the N(h) profiles using the expressions given by Peterson et al.

6.6.2 Calculations of 6300 A and 5577 A intensities from N(h) profiles:

In the following, a summary is given of the theoretical expressions for the F region night airglow emissions of atomic oxygen 6300 (^1D) and 5577 (^1S). With these expressions, using the electron density profiles obtained from the ionograms at Ahmedabad, the intensities of 6300 A and 5577 A were determined on a few nights when these two emissions showed a high positive correlation. They were compared with the ground based observations made with the scanning photometer at 40°S zenith angle of Mt. Abu.

The emission rate ϵ_λ of a line of wavelength λ from level (^1D or ^1S) is given by the product of the transition coefficient A_λ and the concentration $[i]$ of atoms in the level i.

$$\epsilon_\lambda = A_\lambda [i] \qquad (1)$$

Expressions for the $\epsilon_\lambda(h)$ can be derived by solving the continuity equations for the populations of the ^1D or ^1S levels.

$$\frac{\partial [i]}{\partial t} = P_i(h) - L_i(h) - \text{div}([i]\ V_i) \qquad (2)$$

where P_i is the production of atoms in level i.

L_i is the loss rate of i. and div ($[i]$ V_i) is the divergence. The quantity that can be compared with the observations made by ground based airglow observations is Q_λ the integrated emission rate in the vertical direction.

$$Q_\lambda \text{ (rayleighs)} = 10^{-6} \int_0^\infty \epsilon_\lambda(h)\, dh$$

$$10^{-6}\, A_\lambda \int_0^\infty [i]\, dh \qquad (3)$$

where h is the height above ground in cm. The factor 10^{-6} converts the integrated emission rate from photons cm^{-2}(column) sec^{-1} to rayleighs. (The integral can be taken between the heights 200 km to 500 km).

PETERSON et al.(1966) have given the following expressions for $[i]$, for $[^1S]$ and $[^1D]$ after solving the continuity equations.

$$[^1S] = \frac{k_S}{A_S} \cdot \frac{\beta_1 N_e}{1 + (\beta_1/\alpha_1 N_e)(1 + a)} \qquad (4)$$

$$[^1D] = \frac{k_D}{A_D} \frac{\beta_1 N_e}{1 + (\beta_1/\alpha_1 N_e)(1 + a)} \cdot \frac{1}{1 + d_D/A_D} \qquad (5)$$

where $a = \frac{\beta_2}{\beta_1} \quad \frac{\alpha_1}{\alpha_2}$ and

$$\beta_1 = \gamma_1 [O_2] \; ; \; \beta_2 = \gamma_2 [N_2]$$

α_1, α_2, γ_1, γ_2 are the rate coefficients of the reactions.

$$O_2^+ + e \longrightarrow O + O + 6.96 \text{ ev} \qquad (\alpha_1)$$

$$NO^+ + e \longrightarrow N + O + 2.76 \text{ ev} \qquad (\alpha_2)$$

$$O^+ + O_2 \longrightarrow O_2^+ + O + 1.53 \text{ ev} \qquad (\gamma_1)$$

$$O^+ + N_2 \longrightarrow NO^+ + N + 1.09 \text{ ev} \qquad (\gamma_2)$$

A_S and A_D are the Einstein transition coefficients for S and D levels of atomic oxygen.

k_S and k_D are the number of excitations per recombination.

d_D is the collisional deactivation coefficient.

N_e is the electron density at any height.

The integrated emission rate can be calculated from equation (3).

From the ionograms obtained at Ahmedabad using the true height analysis the electron density at each 10 km level was determined and the electron density profiles were obtained. The particle concentrations of O, O_2, N_2 and their distribution with height and the temperature distribution are taken from CIRA model atmosphere taking the appropriate value of solar flux. The rate coefficients and other constants were taken from PETERSON and STEIGER (1966). The integrated emission rates of 6300 A and 5577 A were calculated on a few occasions. The ground observations made with the scanning photometer towards 40°S from the zenith of Mt. Abu are used on nights when the correlation coefficients between 6300 A and 5577 A were high and positive. The data of some of these nights are plotted in the Figure 6.45.

In Figure 6.46 the plot of $Q_{6300} = \sum \left[{}^1D\right] .dh$ determined from equation (5) and the observed I_{6300} is shown for the night January 19-20, 1969. In the same graph $Q_{5577} = \sum \left[{}^1S\right] .dh$ determined from equation (4) and the observed I_{5577} are also plotted. It is seen from this graph that the theoretical expressions given by PETERSON et, al. reasonably account for the F region contribution of 6300 A and 5577 A, considering that there are uncertainties in the assumed values of the coefficients and in the calculated electron density profiles.

.....

CHAPTER VII

SUMMARY AND CONCLUSIONS

The material presented in the previous chapters is summarised in the following, giving the main observational results of night airglow made at Mt. Abu and the conclusions.

CHAPTER I: Brief review of night airglow work in low latitudes: Experimental set up at Mt. Abu.

Using two fixed photometers, night airglow observations of 6300 A, 5893 A, Na and 5577 A (OI) emissions and of two hydroxyl bands OH (7-2) (band origin 6862 A), and OH (8-3) (band origin 7272 A) were taken on all clear moonless nights at Mt.Abu from 1966-69. With an automatic all sky scanning photometer, observations in the same spectral regions were also taken on many nights.

CHAPTER II: The extinction coefficient (τ_λ) of the atmosphere:

For measuring the extinction coefficient (τ_λ) of the atmosphere which affects the airglow calculations, two separate photometers (named as Extinction photometers) were constructed for measuring extinction coefficients (τ_λ)

at the wavelengths 6080 A, 5750 A and 5360 A where there are no airglow emissions. From the measurement of the star intensities at different zenith angles, values of τ were determined. The interpolated τ values at all the necessary wavelengths obtained from the above measurements were used in the reduction of the night airglow observations.

It is observed that τ varies from day to day. The average monthly variation of τ from October to January is small. It is rather large and random in April to June; due to strong dustly winds and dust storms arriving at the airglow station from the desert area. It is observed that on 70% of the occasions, τ decreased with increasing wavelength, and on the rest of the occasions, τ had different types of variations. The different types of variation can be attributed to the varying sizes of the aerosol particles present in the atmosphere. It was concluded that at Mt. Abu, particles of radii 0.4 μ to 0.5 μ are most common.

CHAPTER III: Reduction of airglow observations into absolute units - Correction of OH contamination in night airglow intensities of emission lines.

Night airglow observations of 6300 A, 5893 A and 5577 A emissions were taken and reduced to absolute units by the two colour method described by Roach and Meinel. Filters

centered at 6080 A, 5750 A, 5350 A and 5300 A are used for estimating the background intensity. The formula and procedure given by Kulkarni and Sanders were used for reducing the observed data to absolute units, using a radioactive C^{14} source for calibration.

The two colour method is extended to measure the intensities of OH (7-2) and OH (8-3) bands taking into consideration the relative intensities of the rotational lines in the band. The background filter is centered at 6080 A.

The objections raised by Blacker and Gadsden to the above procedure of reduction were examined taking into consideration the photomultiplier response, filter transmissions and radiances of C^{14} source. It was noted that for all the moderately narrow filters ($\sim$ 50 A half width) it is adequate to take into account the average photomultiplier response and C^{14} source radiance, instead of making detailed integration over the photomultiplier response and the filter transmission curves of the filters.

One of the important factors in ascertaining the intensities accurately is the ratio of the background intensity at the peak wavelength of the line filter to that at the peak transmission of the background filter. Total background intensities at 6080 A, 5750 A and 5360 A were measured and the necessary ratios were determined.

From the measured intensities of the two OH bands OH (7-2) and OH (8-3) an estimate of OH (9-3) contamination in 6300 A observations was made, and similarly OH (8-2) contamination in 5893 A observations. Thus, the OH contamination was accounted for in the estimation of the intensities of the emission lines.

Also, with the simultaneous observations of 6300 A with three different filters of different transmissions, and solving the simultaneous equations, 6300 A intensities (without OH contamination), and OH (9-3) intensities were estimated.

CHAPTER IV: Studies of 5577 A and 5890-96 A emissions:

A statistical analysis in the case of the intensity of 5577 A (Q) emission showed a normal distribution with $\sqrt{3Q}$ or Log_{10} Q.

The nocturnal variation of 5577 A shows in general a maximum in intensity during a night. It is noted that out of 352 nights, 200 nights (57%) showed a maximum around midnight, 63 nights (18%) showed a maximum before midnight and 89 nights (25%) showed a maximum after midnight. The seasonal variation of 5577 A shows two maxima of intensity one in October and the other in April. The range of variation is more in October and April months compared to those in the other months. The isophote maps of 5577 A show a similar behaviour showing

midnight maximum in October and April months at all the latitudes ($\pm$ 3° of Mt. Abu zenith) covered by the scanning photometer. The average intensities of 5577 A show the solar activity effect over the 11 year cycle. There seems to be an intensity maximum in 5577 A in south of Mt. Abu in the month of January; and slightly later in the case of 5893 A.

5893 A shows two types of intensity variations; i) continuously increasing in the course of the night; or ii) decreasing in the night. The isophote maps show a cell structure, the cells forming and expanding resulting in the continuous increasing type of variation, contracting and condensing in the decreasing type of variation.

5893 A also shows a somewhat similar seasonal behaviour as that of 5577 A. However, no solar activity control is seen. It is interpreted that the 5893 A emission height is slightly above OH emission height and thus nearer to 5577 A emission height and the variations of concentrations of atomic oxygen at these heights are reflected in their long term variations.

There is no obvious correlation between 5577 A and 5893 A emissions. However, if vertical downward movements of atomic oxygen take place 5577 A and 5893 A may show an increase in intensity with time differences in their maxima; the 5577 A leading the 5893 A.

There is no conspicuous effect of R_Z or K_p in 5577 A intensity. An increase in intensity of 5577 A is observed at Mt. Abu, following solar flares and magnetic storms. Other airglow emissions viz. 6300 A and 5893 A do not appreciably enhance following the solar flares, and magnetic storms.

CHAPTER V: Study of OH bands in night airglow:

It is observed that OH (7-2) and OH (8-3) bands show similar time variations. There is a very high positive correlation between the intensities of these two bands. Most frequent values of the intensities of OH (8-3) and OH (7-2) are between 300-500 R and 200-400 R and an average ratio of these two band intensities is 1.2 to 1.3. It is noted that the nocturnal variation of the ratio of OH (8-3) to OH (7-2) intensity increases during the early party of the night and then show a decrease on many occasions. There are considerable fluctuations in the ratio during the course of a night which may be due to temperature fluctuations.

The OH intensity exhibits different types of night time variation. The type of variation with constant intensity throughout the night is seldom seen at Mt, Abu. Type B (showing a minimum intensity around midnight and again another decrease in the early morning hours) is more frequent here.

Thus it appears that ozone-hydrogen reaction is the main reaction responsible for the nocturnal variation of OH at Mt. Abu. It is noted that solar flares or magnetic storms do not cause the different types of variations observed in OH. It is possible that the initial value of oxygen atoms which determine the ozone density in the beginning of the night is responsible for the type of variation observed in OH.

The times of occurrences of maximum intensity of OH glow from November-March nearly coincide with the minimum zenith angle (transit times) of the celestial X-ray source Tau X-1, ($\alpha = 5^h\ 31^m$; $\delta = +21^o59'$). The effect of other celestial X-ray sources is also seen in the months of April and May. The positions of maximum intensity and their movement with the position of the celestial sources are seen clearly in the OH isophote maps. It is interpreted that due to the increased ionisation in the mesosphere due to the X-rays from these celestial X-ray sources, ozone and or hydrogen also increase and thus OH intensities are enhanced during the transit times of the celestial X-ray sources.

It is seen that generally there is a high positive correlation between OH and Na emissions. The observed covariability of the OH and Na emissions in the night sky might follow as a consequence of the fact that they primarily represent in their intensities the nocturnal variation of O_3 and O at the common levels of origin.

A comparison of the seasonal variation of OH and 5577 A emissions showed more or less opposite behaviour. The minimum intensity is observed in April and a maximum in November/December months. It is probable that the atomic oxygen descends to lower heights in the winter and thus the formation of O_3 and the intensities of OH are greater in those months.

A study of night time variations on individual nights of OH and 5577 A has showed no similar behaviour. However, there are a few occasions when maxima in 5577 A and OH are seen with a time lag. It is interpreted that if atomic oxygen, which is important in determining the excitation rate of all these emissions (5577 A, OH and 5893 A), comes down due to vertical eddy transport such maxima can be understood.

CHAPTER VI: F region night airglow emissions of atomic oxygen:

6300 A emission at Mt. Abu shows significant temporal changes. A post twilight decay in intensity is observed in all the months in both low and high active years. Around midnight 6300 A emission attains its minimum value and this minimum is different in low and high active periods being more in high active periods.

A pre-dawn enhancement in 6300 A is seen in all months in both low and high active periods and starts just after midnight on many summer nights and much later in winter nights. Cole's hypothesis (that the photoelectrons from the conjugate sunlit point are transported along the magnetic lines of force) explains some enhancements in winter months only. On other occasions, especially in summer months when the enhancements are more pronounced the vertical movements of electrons in the ionosphere can explain such enhancements.

It is noted that year to year seasonal variation of 6300 A runs parallel to the solar flux variation at 10.7 cm wavelength.

Barbier's formula which relates 6300 A intensity and the ionospheric parameters f_oF_2 and h'F is found to be valid on all occasions at Mt. Abu - Ahmedabad/Delhi. Even during spread F condition the height variations of F region are in antirelation with 6300 A intensities.

Superposed on the post twilight decay an increase in intensity was observed for some hours on many nights in 6300 A emission. Out of 391 nights, on 231 nights this pre-midnight enhancement was observed during 1964-69. It is more frequent in winter months than in summer. It occurs more

frequently at the zenith of Mt. Abu and at all southern latitudes. 5577 A also shows a slight enhancement corresponding to the increase in 6300 A.

The pre-midnight enhancement is always associated with an increase in total electron content (N_T) upto h_mF_2. Downward vertical drifts of plasma which occur after sunset can bring down more electrons causing increase in the electron content (N_T) which then recombine and give more 6300 A. Downward movement of the electron density profiles are noted at the time of this enhancement. It is also noted that the calculated vertical drift velocities are more negative (downwards) at that time.

h'F and h_pF_2 values at the magnetic equator reach a very high value in the evening hours at about 17-20 hours. It may be said that as the F region goes to high heights in the evening hours there can be diffusion of electrons along the field lines. After field reversal, vertical downward movements of electron density at other low latitudes increase 6300 A due to the electrons drifting to the favourable height of 6300 A emission which appears as an enhancement on the post twilight decay. This explanation favours the observations that the pre-midnight enhancement is more frequent and intense in the southern latitudes of Mt.Abu. However, the magnitude of the enhancement depends on the rate of post twilight decay and the vertical drift velocities.

The post-midnight enhancement occurred on 306 nights out of 377 nights (81%) of observation. The magnitude of this enhancement is large in summer months compared to winter months. It is stronger in intensity at the zenith compared to poleward direction. It is seen at all the geographic latitudes covered by the scanning photometer. The time of occurrence of this enhancement is not controlled by solar activity.

Detailed N(h) profiles showed that the downward drift of electrons cause this enhancement. Thus vertical movements of the ionisation in the ionosphere are the main cause of the airglow 6300 A enhancements in low latitudes.

The electron content in the ionosphere and 6300 A intensity showed that the correlation is maximum some where between 300-400 km which should be the height of maximum emission of 6300 A.

6300 A isophotes at Mt. Abu are classified into two types, maps with patchy structure and maps that show aligned character. The analysis of 53 nights showed that out of 840 isophotes maps 475 were aligned. The patchy or spotty maps occurred during the time of airglow enhancements. Many of of the aligned maps were aligned in south direction and occurred during 21-03 hours IST of the night; the velocity of movement being $\sim$ 200 m/sec.

On many nights, an east-west oriented arc was seen in the beginning of the night at Mt.Abu and the arc closed to south as the night progressed, and moved to south with a velocity $\sim$200 m/sec. The magnitude and the rate of movement and closing of the arc in the south are different on different nights, months and solar activity. The movement of the arc to south is consistent with the movement of the crests of the equatorial anomaly.

The poleward observations showed in general an absence of covariation between 6300 A and 5577 A in E and J months, while on most of the nights in D months they showed a covariation. A study of the correlation between these two lines at the different latitudes covered by the scanning photometer showed that a greater number of observations in latitudes south of Mt.Abu (34^{o}- 24^{o}N dip)showed positive correlation between 6300 A/5577 A than latitudes north of Mt.Abu (34^{o} - 48^{o}N dip). When these emissions covary, the variations in the F-region component of 5577 A are reflected pronouncedly in the ground observations the 100 km component remaining steady.

On these occasions Barbier's relation fits reasonably well even in the case of 5577 A, the constant term in that equation representing the contribution from 100 km level. From the expressions of Peterson et al.(1966) the emission rates of 6300 A and 5577 A from F region are calculated, using the deduced N(h) profiles and are compared with the ground observation It is found that the agreement is reasonably good.

....o....

REFERENCES

Abadie, P., Vassy, A. and Vassy, E.	1945	Ann.Geophys., 1,189.
Abadie, P., Vassy, A. and Vassy, E.	1949	Ann.Geophys., 5, 157.
Allen, C.W.	1963 a	Astrophysical Quantities, Athlone Press, University of London, P.122.
Allen, C.W.	1963 b	Astrophysical Quantities, Athlone Press, University of London, p.120.
Ananthakrishnan, S. and Ramanathan, K.R.	1969	Nature (London), 223, 488.
Ananthakrishnan,S., Chakravarty, S.C. and Ramanathan, K.R.	1970	Proc. Indian Aca.of Sci., LXXI(2), 69.
Angreji, P.D.	1961	Proc. IGY Symp., Vol.II, Feb.1961, New Delhi,pp.112-118.
Angreji, P.D.	1967	Ph.D.Thesis, Gujarat University, Ahmedabad, India.
Angreji, P.D.	1969	Proc. III Int.Symp.Equat. Aeronomy, Ahmedabad, India pp.424-430.
Appleton, E.V.	1954	J.Atmos.Terrs.Phys.,5, 348.
Armstrong, E.B.	1956	The Airglow and the Aurorae, (E.B.Armstrong and A.Dalgarno eds.) Pergamon Press, London, pp.63-66.
Arp., H.C.	1958	Astrophys.J., 63, 58.
Ashburn, E.V.	1954	J.Atmosph.Terr.Phys.,5,83.
Babcock, H.W.	1923	Astrophys, J., 57, 209.

Babcock, H.W.	1939	Pub.A.S.P., 51, 47.
Ballii , J. and Venkateswaran, S.V.	1962	J.Atmos. Sci., 19, 426.
Ballii , J. and Venkateswaran, S.V.	1963	J.Atmos. Sci., 20, 1.
Bappu, M.K.V.	1950	Astrophys. J., 111, 201.
Barbier, D.	1944	Ann.Geophys., 1, 144.
Barbier, D., Dufay, J. and Williams,D.R.	1951	Ann. Astrophys., 14, 399.
Barbier, D.	1954 a	Ann. Astrophys., 17, 97.
Barbier, D.	1954 b	Compt.Rand., 238, 770.
Barbier, D., Dufay, J. and Williams, D.R.	1954	Proc.Conference on Auroral Physics. (N.C.Gerdon, T.J.Keneshea and R.J.Donaldson eds.) pp.137-183, Geophysical Research paper No.30,(AFCRC).
Barbier, D.	1955	Ann. Geophys., 11, 181.
Barbier, D.	1956	The Airglow and the Aurorae (E.B.Armstrong and A.Dalgarno eds.),pp.9-19,Pergamon Press, London.
Barbier, D.	1957 a	C.R. Acad.Sci., Paris, 244,1809.
Barbier, D.	1957 b	C.R. Acad.Sci., Paris, 244,2077
Barbier, D.	1957 c	C.R. Acad.Sci., Paris, 245,1559.
Barbier, D. and Glaume, J.	1957	Ann. Geophys., 13, 317.
Barbier, D.	1958	Ann. Geophys., 14, 334.
Barbier, D.	1959	Ann. Geophys., 15, 179 and 412.
Barbier, D. and Christophe-Glaume, J.	1959	Ann. Geophys., 15, 266.
Barbier, D.	1960	Ann. Geophys., 16, 544.

Barbier, D. and Christophe-Glaume, J.	1960	Ann. Geophys., 20, 22.
Barbier, D.	1961	Ann. Geophys., 17, 3.
Barbier, D., Weill, G.M. and Glaume, J.	1961	Ann. Geophys., 17, 305.
Barbier, D. and Glaume, J.	1962	Planet. Space Sci., 9, 133.
Barbier, D., Roach, F.E. and Steiger, W.R.	1962	J.Res.Nat. Bur.Stand., 66D,145.
Barbier, D.	1963	Geophysics, the earth's environment, (C.Dewitt, J.Hieblot and A.Lebean eds.) New York.
Barbier, D.	1964	Ann. Geophys. 20, 22.
Barbier, D.	1965	Ann. Geophys., 21, 228.
Barbier, D.	1967	Int. Dictionary of Geophysics, Vol.II, (K.Runcorn ed.) Pergamon Press, New York, pp.1112-1115.
Barth, C.A.	1964	Ann. Geophys., 20, 182.
Barth, C.A.	1967	Int. Dictionary of Geophysics, (K.Runcorn ed.), Vol.II, Pergamon Press, New York, p.1110.
Bates, D.R.	1946	Monthly Notices, Roy. Astron.Soc., 106, 509.
Bates, D.R.and Nicolet, M.	1950	J. Geophys., Res., 55, 301.
Bates, D.R.	1960	Physics of the Upper Atmosphere, (J.A. Ratcliff ed.) Academic Press, New York, pp.219-267.
Benedict, W.D., Plyler, R.K. and Humphreys, C.J.	1953	J. Chem. Phys., 21, 389.

Berg, O.E., Koomen, M., Meredith, L.H. and Scolnik, R.	1956	J. Geophys.Res., 61, 302.
Bernard, R.	1938 a	Z.Physik, 110, 291.
Bernard, R.	1938 b	C.R. Acad. Sci., 206, 928.
Bernard, R.	1938 c	Nature, 141, 788.
Berthier, P.	1954	Compt. Rand., 238, 263.
Berthier, P.	1956	Ann. Geophys., 12, 113.
Blackwell, D.E., Ingham, M.F. and Rundle, H.N.	1960	Astrophy.J., 131, 15.
Blacker, H.V. and Gadsden, M.	1966	Planet.Space Sci., 14, 921.
Brenton, J.G. and Silverman, S.M.	1970	Planet. Space Sci.,18, 641.
Brown, W.E. and Steiger, W.R.	1967	Nature,(London), 216, 47.
Brown, W.E.	1969	Ph.D. Dissertation, University of Hawaii, Hawaii.
Cabannes, J., Dufay, J. and Gauzit, J.	1938	C.R. Acad. Sci., 206, 870.
Cabannes, J., Dufay, J. and Dufay, M.	1950	C.R. Acad.Sci.,Paris, 230, 123.
Cabannes, J. and Dufay, J.	1956	The Aurora and the Airglow (E.B.Armstrong and A. Dalgarno eds.), Oxford, Pergamon Press, London. pp. 73-85.
Carlson, H.C. and Weill, G.M.	1967	Ann. Geophys., 23, 569.
Carlson, H.C.	1967	Aurora and Airglow, (B.M.McCormac ed.), p.643, Reinhold Co., New York,

Carmen, E.H., Kilfoyle, B.P. and Gibson-Wilde, B.C.	1964	J.Geophys.Res., 69, 4725.
Chamberlain, J.W. and Oliver, N.J.	1953	Phys.Rev., 90, 1118.
Chamberlain, J.W.	1958	Astrophys. J., 127, 54.
Chamberlain, J.W. and Smith, C.A.	1959	J. Geophys.Res., 64, 611.
Chamberlain, J.W.	1961 a	Physics of the Aurora and Airglow,Academic Press, New York, pp.345-376. and 486-565.
Chamberlain, J.W.	1961 b	Physics of the Aurora and Airglow, Academic Press, New York, p.490.
Chamberlain, J.W.	1961 c	Physics of the Aurora and Airglow, Academic Press, New York, p.556.
Chamberlain, J.W.	1961 d	Ibid. pp.55-61 and p.492-496.
Chamberlain, J.W.	1961 e	Ibid. p.359-360, p.504-520, p.564-566
Chamberlain, J.W.	1961 f	Ibid. p.517
Chamberlain, J.W.	1961 g	Ibid. p.359.
Chamberlain, J.W.	1961 h	Ibid. p.55-61.
Chapman, S.	1931	Proc.Roy.Soc.(London),A 132, 353.
Chapman, S.	1939	Astrophys. J., 90, 309.
Chapman, S.	1967	Aurora and Airglow (B.M.McCormac ed.), Reinhold Co., New York, pp.24-25.
Chiplonkar, M.W.	1950	Bull.Astron.Inst. Czechoslovakia, 2, 79.
Chiplonkar, M.W. and Kulkarni, P.V.	1958	Indian J.Meteo.Geophys., 9, 133.
Chiplonkar, M.W. and Kulkarni, P.V.	1960	J. Uni. Poona,(Sci & Tech.Sec.), 18, 1.

Chiplonkar, M.W. and Agashe, V.V.	1961	Ann. Geophys., 17, 231.
Chiplonkar, M.W., Kulkarni, P.V. and Agashe, V.V.	1961	Bull. Astr. Inst.(Czechoslovakia), 12, 18.
Chiplonkar, M.W., Agashe, V.V. and Tillu, A.D.	1966	Ind. Journ.Met. Geophys.,17, 95.
Chiplonkar, M.W. and Tillu, A.D.	1967	Indian J. Pure and Appl. Phys., 5(3), 87.
Chiplonkar, M.W. and Tillu, A.D.	1970	Ann. Geophys., 26, 213.
Christophe Glaume, J.	1965	Ann. Geophys., 21, 1.
Chvostikov, I. and Lebedev, A.	1935	Compt. Rend,(U.S.S.R.),1, 118.
CIRA	1965	Cospar International Reference Atmosphere, North-Holland Pub. Co., Amsterdam, 1965.
Cogger, L.L. and Shepherd, G.G.	1969	Planet. Space Sci., 17, 1857.
Cole, K.D.	1965	Ann. Geophys., 21, 156.
Cooper, H.W., Gulledge, I.S., Koomen, M. and Packer, D.M.	1960	J. Geophys. Res., 65, 2484.
Dachs, J., Haug, U. and Pfleiderer, J.	1966	J.Atmosph.Terr.Phys., 28, 637.
Dalgarno, A.	1963	Planet. Space Sci., 10, 19.
Dandekar, B.S.	1961	Ph.D. Thesis,Gujarat University, Ahmedabad,(India).
Dandekar, B.S., Bhonsle, R.V. and Ramanathan, K.R.	1961	Ann. IGY., 11, 123.
Dandekar, B.S. and Silverman, S.M.	1964	Planet. Space Sci., 12, 867.

Davis, D.N.	1951	J.Geophys. Res., 56, 567.
Davis, D.N. and Smith, L.L.	1964	Geophys. Research Report No.10.
Davies, W.O. and McCormac, B.M.	1967	~~The~~ Aurora and ~~the~~ Airglow (B.M.McCormac ed.), Reinhold Co. pp. 374.
Delesemme, A. and Delesemme, D.	1960	Ann. Geophys., 16, 507.
Dessens, H.	1947 a	Ann. Geophys., 2, 68.
Dessens, H.	1947 b	Ann. Geophys. 3, 68.
Donahue, T.M.	1967	Int. Dictionary of Geophys. Vol. II, (K.Runcorn ed.), Pergamon Press, New York, pp.1417-1426.
Duboin, M.L., Lejeune, G., Pettit, M. and Weill, G.M.	1968	J.Atmosph.Terr.Phys., 30, 299.
Dufay, J. and Tcheng Mao-Lin	1946	Ann. Geophys., 2, 189.
Dufay, J. and Tcheng Mao-Lin	1947	Ann. Geophys. 3, 153.
Dufay, J. and Dufay, M.	1951	C.R. Acad.Sci., Paris, 232, 426.
Dufay, J., Berthier, P. and Morignat, B.	1953	Compt. Rand., 237, 828.
Dufay, J. and Tcheng Mao-Lin	1955	Ann. Geophys., 11, 387.
Duncan, R.A.	1960	J.Atmos.Terr.Phys., 18, 89.
Elsasser, H. and Siedentopf, H.	1956 a	J.Atmos.Terr.Phys., 8, 222.
Elsasser, H. and Siedentopf, H.	1956 b	The Airglow and The Aurora (E.B.Armstrong and A.Dalgarno eds.) Pergamon Press, London, pp.27-28.

Elvey, C.T. and Farnsworth, A.H.	1942	Astrophys. J., 96, 451.
Elvey, C.T.	1943	Astrophys. J., 97, 65.
Elvey, C.T.	1950	Astrophys. J., 111, 432.
Fishkova, L.M. and Markova, G.V.	1961	Aurora and Airglow (Moscow), No.6, 17.
Fishkova, L.M.	1962	Aurora and Airglow (Moscow), No.9, 57.
Fontheim, E.G., Beutler, A.E. and Nagy, A.F.	1968	Ann. Geophys., 24, 489.
Gadsden, M.	1967	The Aurora and Airglow (B.M.McCormac ed.), Reinhold Pub.Co., pp.109-122 and pp.305-314, New York.
Garvin, D., Broida, H.P. and Kistkowski, J.J.	1960	J. Chem. Phys., 32, 880.
Ghosh, S.N.	1943	Proc. Nat. Inst. Sci.(India), 9, 301.
Gotz, F.W.P.	1944	Verhandl. Schweiz. Natarforsch Ges., p.88.
Greer, R.G.H. and Best, G.T.	1967	Planet. Space Sci., 15, 1857.
Gulledge, I.S., Packer, D.M. and Tilford, S.G.	1966	Trans. Am.Geophys. Union, 47, 74.
Gulledge, I.S., Packer, D.M., Tilford, S.G. and Vanderslice, J.T.	1968	J. Geophys. Res., 73, 5533.
Gush, H.P. and Vallance Jones, A.	1955	J. Atmosph. Terr. Phys., 7, 285.
Gush, H.P. and Buijs, H.L.	1964	Can. J. Phys., 42, 1037.

Guttaman, A.	1968	Appl. Opt., 7, 2377.
Hanson, W.B. and Moffett, R.S.	1966	J. Geophys. Res., 71, 5559.
Harrison, A.W. and Vallance Jones, A.	1957	J. Atmos. Terr. Phys., 11, 192.
Heaps, H.S. and Herzberg, G.	1952	Z. Phys., 133, 48.
Heppner, J.P. and Meredith, L.H.	1958	J. Geophys. Res., 63, 51.
Hernandez, G.J. and Silverman, S.M.	1964	Planet. Space Sci., 12, 97.
Herzberg,G.	1950	"Spectra of Diatomic Molecules" D. Van Nostrand, New York, Vol. I, p.208.
Herzberg, G.	1951	J. Roy. Astron. Sco., Canada, 45, 100.
Hesstvedt, E.	1968 a	Geofysiske Publikasjoner Geophysica Norvegica, 27 (4), 1.
Hesstvedt, E.	1968 b	Atmospheric emissions (B.M.McCormac and A.Omholt eds.)pp.501., Van Nostrand, Reinhold Co.,New York.
Honl, H. and London, F.	1925	Z. Phys., 33, 803.
Hunten, D.M., Roach, F.E. and Chamberlain, J.W.	1956	J. Atmos. Terr. Phys., 8, 345.
Huruhata, M.	1950	Rep. Ionosph. Res., Japan, 4, 137.
Huruhata, M.	1953	Ann. Tokyo Ast. Obs., (2), 3, 165.
Huruhata, M., Tanabe, H. and Nakamura, T.	1955	Rep. Ionosph. Res., Japan, 9, 136.
Huruhata, M., Tanabe, H. and Nakamura, T.	1956	The Airglow and the Aurorae (E.B.Armstrong and A. Dalgarno ed.), Pergamon Press, London, pp.20-26.

Huruhata, M., Nakamura, T. and Tanabe, H.	1957	Tokyo Astronomical Bulletin, Second Series No.94, 1005.
Huruhata, M., Nakamura, T., Nakamura, J. and Nakamura, M.	1962	Proc. 4th Int. Symp. Space Sci. and Tech., Japan, p.459.
Huruhata, M., Nakamura, T. and Tanabe, H.	1966	Rep. Ionos.Space Res., Japan, 20, 223.
Irvine,W.M. and Peterson, F.W.	1970	J. Atmos.Sci., 27, 62.
Johnson, H.L. and Morgan, M.W.	1951	Astrophys. J,, 114, 522.
Johnson, H.L.	1963	Basic Astronomical data(K.Strand ed.) p.204, Vol.3 of Stars and Stellar Systems, University of Chicago Press.
Karandikar, R.V.	1933	Indian J. Phys,, 8, 547.
Karandikar, R.V.	1934	Indian J. Phys., 9, 245.
Karimov, M.G.	1947	Ast. Zhur., 24, 114.
Karimov , M.G.	1952	Ast.Zhur., 29, 472.
King, J.W.	1968	J. Atmos.Terr, Phys., 30, 391.
King, G.A.M.	1970	J. Atmos. Terr.Phys., 32, 209.
Knudsen, W.C. and Sharp, G.W.	1968	J. Geophys. Res., 73, 6275.
Koomen, M., Scolnik, R. and Tousey, R.	1956	J. Geophys. Res., 61, 304.
Krassovsky, V.I.	1949	Doklady Akad. Nauk., S.S.S.R., 66, 53.
Krassovsky, V.I.	1955	The Airglow and the Aurora, (E.B.Armstrong and A.Dalgarno eds.) Pergamon Press, New York, pp. 197-200.

Krassovsky, V.I.	1958	Ann. Geophys., 14, 35, 395-413.
Krassovsky, V.I., Shefov, N.N. and Yarin, V.I.	1962 a	Atlas of Airglow spectrum, 3000-12, 400, Institute of Physics of the Atmosphere, USSR, Academy of Science, MOSCOW.
Krassovsky, V.I., Shefov, N.N. and Yarin, V.I.	1962 b	Planet. Space Sci., 9, 883.
Krassovsky, V.I.	1963	Planet. Space Sci., 10, 7.
Krassovsky, V.I. and Shefov, N.N.	1965	Space Sci.Rev., 4, 176.
Kron, G.E.	1950	Publ.Ast. Soc., Pacif.,62, 264.
Kulkarni, P.V.	1958	Ph.D. Thesis, University of Poona, Poona, India.
Kulkarni, P.V. and Sanders,C.L.	1964	Planet. Space Sci., 12, 189.
Kulkarni, P.V.	1965	Ann. Geophys., 21, 58.
Kulkarni, P.V. and Steiger, W.R.	1967	Ann. Geophys. 23, 125.
Kulkarni, P.V.	1969	Proc. III.Internat.Symp.Equat. Aeronomy (Ahmedabad, India), pp.413-414.
Kvifte, G.	1959 a	Geophys. Publ., 20, No.12. 1-15
Kvifte, G.	1959 b	J.Atmos.Terr. Phys., 16, 252.
Kvifte, G.	1960	Planet. Space Sci., 5, 153.
Lagos, P., Bellew, W. and Silverman, S.M.	1963	J.Atmos. Terr. Phys., 25, 281.
Lagos, C.P.	1968	Atmospheric Emissions,(B.M.McCormac and A.Omholt eds.), Van Nostrand Reinhold Co., New York, p.519.
Lytle, E.A. and Hampson, J.	1964	Nature, 202, 76.

Manring, E.R. and Pettit, H.B.	1957	"The threshold of space" (M. Zelikoff. ed). Pergamon Press, New York, pp.58-64.
Manring, E.R. and Pettit, H.B.	1958 a	J. Geophys. Res., 63, 39.
Manring, E.R. and Pettit, H.B.	1958 b	Ann.Geophys., 14, 506.
Massey, H.S.W. and Boyd, L.F.	1958	The Upper Atmosphere, pp.150-175, Philosophical Library, New York.
McCormac, B.M.	1967	The airglow and the aurora, (B.M.McCormac ed.), Reinhold Pub. Co., p. 1.
McLennan, J.C. and Shrum, G.M.	1924	Proc. Roy. Soc., A106, 138. (London)
McLennan, J.C., McLeod, J.H. and Ireton, H. J.C	1928	Transact. Roy. Soc., ~~London~~, Canada Sec. III, 22, 397.
McPherson, D.H. and Vallance Jones, A.	1960	J. Atmos. Terr. Phys., 17, 302.
Meinel, A.B.	1950 a	Astrophys. J., 111, 555.
Meinel, A.B.	1950 b	Astrophys. J., 112, 120.
Mitra, S.K.	1945	Observatory, 66, 13.
Mitra, S.K.	1952	The Upper Atmosphere, pp.485-548, The Asiatic Society, 1 Park Street, Calcutta-16. India
Moroz, V.I.	1960	Soviet Astron. J., 4, 118.
Nagata, T. and Ogawa, T.	1964	Rep. Ionos. Space Res., Japan, 18, 394.
Nakamura, J.	1957	J. Geophys. Res., 62, 487.
Nakamura, J.	1959	Rep. Iono. Space Res., Japan, 12, 419.
Nakamura, T.	1961	Rep. Ionos.Space Res., Japan, 15, 245.
Nakamura, M.	1961	Rep. Ionos. Space Res., Japan, 15, 346.

Nichol, D.G.	1970	Planet. Space Sci., 18, 1335.
Nicolet, M.	1954	Phys. Rev., 93, 633.
Noxon, J.F., Harrison, A.W. and Vallance Jones, A.	1959	J. Atmos. Terr. Phys., 16, 246.
O'Brien, B.J., Allum, F.R. and Goldwire, H.C.	1965	J. Geophys. Res., 70, 161.
Okuda, M.	1965	Rep. Ionos. Space Res., Japan, 19(4), 470.
Okuda, M.	1966	Rep. Ionos. Space Res., Japan, 20(3), 304.
Packer, D.M.	1961	Ann. Geophys., 17, 67.
Pal, S.R.	1968	Ph.D. Thesis, Gujarat University, Ahmedabad, India.
Pal, S.R. and Kulkarni, P.V.	1968	Ann. Geophys., 24, 399.
Pavlova, E.N., Rodionov, S.F., Sominiskii, M.S. and Fishkova, L.M.	1950	Doklady Akad. Nauk. S.S.S.R, 73, 69.
Peterson, V.L., Van Zandt, T.E. and Norton, R.B.	1966	J. Geophys. Res., 71, 2255.
Peterson, V.L. and Steiger, W.R.	1966	J. Geophys. Res., 71, 2267.
Peterson, V.L.	1968	Ann. Geophys., 24, 101.
Peterson, V.L. and Van Zandt, T.E.	1969	Planet. Space Sci., 17, 1725.
Pettit, H.B., Roach, F.E., St.Amand, P. and Williams, D.R.	1954	Ann. Geophys., 10, 326.
Potter, A.E. and Del Duca, B.S.	1960	J. Geophys. Res., 65, 3915.

Ramanathan, K.R.	1932	Indian J. Phys., 7, 405.
Rastogi, R.G.	1959	J. Geophys. Res., 64, 727.
Rastogi, R.G. and Kulkarni, P.P.	1969	Ann. Geophys., 25, 577.
Rayleigh, Lord	1922	Proc. Roy. Soc. (London), A100, 367.
Rayleigh, Lord	1928	Proc. Roy. Soc. (London),A119, 11.
Rayleigh, Lord	1929	Proc. Roy. Soc. (London), A124, 395.
Rayleigh, Lord. and Spencer Jones,H.	1935	Proc. Roy.Soc. (London), A151, 22.
Roach, F.E. and Barbier, D.	1950	Ann. Geophys., 31, 7.
Roach, F.E., Pettit, H.B. and Williams,D.R.	1950	J. Geophys. Res., 55, 183.
Roach, F.E. and Pettit, H.B.	1951	J. Geophys. Res., 56, 325.
Roach, F.E. and Pettit, H.B.	1952	Mem. Soc. Roy. Sci. Leige, 12, pts. 1-2, 13-42.
Roach, F.E., Pettit, H.B., Williams,D.R. St.Amand, P. and Davis, D.N.	1953	Ann. Astrophys. 16, 185.
Roach,F.E., Williams, D.R., St.Amand, P., Pettit, H.B. and Weldon, R.G.	1954	Ann. Astrophys., 17, 172.
Roach, F.E.	1955	Ann. Geophys., 11, 100 and 214.
Roach, F.E. and Meinel,A.B.	1955	Astrophys. J., 122, 530.
Roach, F.E., Megill, L.R., Rees, M.H. and Marovich, E.	1958 a	J. Atmos. Terr. Phys., 12, 171.

Roach, F.E., Tandberg-Hanssen, E. and Megill, L.R.	1958 b	J.Atmos.Terr.Phys., 13, 113 and 122.
Roach, F.E.	1959	Proc. Inst.Radio Engrs., 47, 267.
Roach, F.E.	1963 a	Adv. in Electronics, 18, 1, Academic Press, New York.
Roach, F.E.	1963 b	IQSY Instructional Manual No.5, IQSY Secretariat, London, Part-1.
Roach, F.E.	1964	Space Sci. Reviews, 3, 512.
Roach, F.E.	1964	Technical Report H I G-64-15 Hawaii Institute of Geophysics, Honolulu.
Roach, F.E. and Smith, L.L.	1967	Aurora and Airglow, (B.M.McCormac ed.),Reinhold Co., New York, p.29-39.
Roach, F.E.	1968	Atmospheric Emissions, (B.M.McCormac and A.Omholt eds.), Reinhold Co., New York, p.439-447.
Roach, F.E., Smith, L.L. and McKennan, J.R.	1969	Annals of IQSY, Vol.4, MIT Press, Cambridge, Mass. P.375-387.
Rodionov, S.F. and Pavlova, E.N.	1949	Doklady Akad. Nank. U.S.S.R., 65, 831.
Rosenberg, N. and Zimmerman, S.P.	1967	Planet. Space Sci., 15, 863.
Sato, T.	1966	Rep. Ions. Space Res., Japan, 20, 150.
Sato, T.	1968	J. Geophys. Res., 73, 6225.
Sanatani, S.	1966	Ph.D. Thesis, Chapter VII, Gujarat University, Ahmedabad, India.
Sandford, B.P.	1964	J.Atmos.Terr.Phys., 26, 749.
Saito, Bun-ichi	1962	The Antartic Record No.14, 1128-1130 Ministry of Education, Tokyo, Japan.

Satya Prakash and Subbaraya, B.H.	1967	The Rev. Sci. Inst., 38, 1132.
Shefov, N.N.	1959	Spectral, Electrophotometrical and Radar Researches of Aurorae and Airglow, No.1, pp.25-29. Publ.House,Academy of Sciences, USSR, Moscow.
Shefov, N.N.	1961 a	Aurora and Airglow (Moscow), No.5, 5.
Shefov, N.N.	1961 b	Aurora and Airglow (Moscow), No.6, 21.
Shefov, N.N.	1969	Planet. Space Sci., 17, 797.
Shklovsky, I.S.	1950	Dokl. Akad. Nauk. SSSR, 75, 789.
Shimazaki, T.	1964	J. Geophys. Res., 69, 2781.
Shimazaki, T.	1966	J. Geophys. Res., 71, 3177.
Silverman, S.M. and Casaverde, M.	1961	J. Geophys. Res., 66, 323.
Silverman, S.M.	1962	J. Phys. Soc., Japan, 17, Suppl. A-I, 205.
Silverman, S.M.	1964	Planet.Space Sci., 12, 247.
Silverman, S.M.	1965	Airforce Surveys in Geophys. AFCRL 65-280.
Silverman, S.M. and Bellew, W.F.	1965	Proc. II Internat.Symp.Equat. Aeronomy,(Sao Paulo),1965,p.360.
Silverman, S.M., Hernandez, G.J., Carrigan,A. and Markham, T.	1965	Airglow and Aurorae, Chapter 13, Hand of Geophysics,(S.Valley ed.), McGrew Hill, New York.
Silverman,S.M.	1968	"Atmospheric Emissions", (B.M.McCormac and A.Omholt eds.) Van Nostrand Reinhold Co., New York, pp.383-397.
Silverman, S.M.	1970	Space Sci. Rev., 11, 341.

Slipher, V.M.	1919	Astrophys. J., 49, 266.
Slipher, V.M.	1929	Pub.Astronom.Soc. Pacific., 41, 262.
Slipher, V.M.	1933	Mon. Not. Roy. Astron. Soc., 93, 657.
Smith, L.L. and Alexander, R.B.	1963	IQSY Instructional Manual No.5, IQSY Secretariat, London Part 1.
Smith, L.L. and Steiger, W.R.	1968	J. Geophys. Res., 73, 2531.
Smith, L.L.	1969	J. Geophys.Res., 74, 3042.
Smith, R.W.	1969	Planet.Space Sci., 17, 879.
Spencer, N.W., Boggess, R.L. and Tacusch, D.R.	1964	J. Geophysics.Res.,69, 1367.
St.Amand, P.	1955	Ann. Geophys.,11, 450.
St.Amand, P., Pettit, H.B., Roach, F.E. and Williams, D.R.	1955	J. Atmos. Terr.Phys., 6, 189.
Stebbins, J., Whitford, A.E. and Swings, P.	1944	Phy.Rev., 66, 225.
Stebbins, J., Whitford, A.E. and Swings, P.	1945	Astrophys. J., 101, 39.
Steiger, W.R., Brown, W.E. and Roach, F.E.	1966	J. Geophys. Res., 71, 2846.
Steiger, W.R.	1967	Aurora and Airglow, (B.M.McCormac ed.),Reinnold Co., New York, pp.419-433.
Tarasova, T.M.	1963	Space Research III (W.Priester ed.), North Holland Publ.Co.,Amsterdam, p.162.

Thomas, L.	1968	Atmospheric Emissions, (B.M.McCormac and A.Omholt eds.), Reinhold Co., New York, pp.423-435.
Tillu, A.D.	1966	Ph.D. Thesis, Poona University, Chapter II, page 177.
Tohmatsu, T.	1958	Rep. Ionos. Res., Japan, 12, 253.
Tohmatsu, T. and Nagata, T.	1963	Planet.Space Sci., 10, 103.
Tousey, R.	1958	Ann. Geophys., 14, 186.
Van de Hulst	1957	Light Scattering by Small Particles, John Willy & Sons Inc., New York, p.414.
Van Zandt, T.E. and Peterson, V.L.	1968	Ann. Geophys., 24, 747.
Van Zandt, T.E. and Peterson, V.L.	1968	Trans. Am. Geophys.Un., 49, 159.
Van Zandt, T.E.	1969	Proc. III Int.Symp. Equat. Aeronomy, Ahmedabad (India), pp.436-438.
Vassy, A. and Vassy, E.	1939	J. Phys., 10, 75, 403 and 459.
Wallace, L.	1960	J. Geophys.Res., 65, 921.
Wallace, L.	1961	J.Atmos.Terr.Phys., 20, 85.
Wallace , L.	1962	J. Atmos. Sci., 19 , 1.
Wallace , L.	1967	Int.Dictionary of Geophysics, Vol.II, (K.Runcorn ed.), Pergamon Press, New York, pp.1088-1094.
Weill, G.M. and Christophe-Glaume,J.	1965	Proc. II International Symp. Equat.Aeronomy (Sao Paulo), 1965, p.359.
Weill, G.M.	1967	Aurora and Airglow (B.M.McCormac ed.) Reinhold Co., New York, pp.407-418.

Weill, G.M. and Christophe-Glaume, J.	1967	Ann. Geophys., 23, 317.
Weill, G.M., Fehrenbach, M., Morguleff, N. and Christophe-Glaume, J.	1968	Ann. Geophys., 24, 109.
Weinberg, J.L.	1964	Ann. Astrophys., 27, 718.
Yarin, V.I.	1962	Aurora and Airglow (Moscow), No.9, 10.

. . . . . .
. . . . .
. . .
.